The Assessment and Prediction of Reinforcing Steel Corrosion on the Dickson Bridge

by

Rossella Fazio

Department of Civil Engineering and Applied Mechanics

McGill University

Montreal, Canada

March 1999

A THESIS SUBMITTED TO THE FACULTY OF GRADUATE STUDIES AND RESEARCH IN PARTIAL FULFILMENT OF THE REQUIREMENTS OF THE DEGREE OF MASTER OF ENGINEERING

0-612-50605-3

Canada

The Assessment and Prediction of Reinforcing Steel Corrosion on the Dickson Bridge

To my Father

With Love.
Rossella Fazio

Abstract

Many concrete structures built in the 1960s and 1970s are now showing significant signs of deterioration. The Dickson Bridge, constructed in 1959, was decommissioned by the City of Montreal in 1994 due to extensive deterioration of the bridge deck. A collaborative research investigation was carried out in 1997-8 on the bridge to: (a) assess the corrosion induced damage in the concrete deck, (b) identify the causes of the observed deterioration, and (c) investigate suitable test techniques for predicting corrosion. The results of this collaborative research program between McGill University and The Queen's University of Belfast, Northern Ireland, and some industrial partners, are presented in this thesis.

A range of test methods related to the mechanisms causing corrosion, or to the concrete properties indicative of the probability of corrosion was used. Considering all the data available, it was concluded that the bridge deck was in a critical condition and the corrosion process of the reinforcing steel was mainly due to the high level of chloride content in the concrete. Both methods (measuring damage, and measuring material properties and exposure parameters) were used to predict the corrosion rate of the reinforcing steel. Overall, the measurement of the corrosion potential was of important significance, however, to improve the assessment of the likelihood of corrosion, it was advantageous in combining this technique with a survey of the delamination, concrete cover thickness and chloride profiles. The in-situ chloride migration coefficients were the most significant in predicting the corrosion rate values especially for the east side of the bridge. The new in-situ chloride migration test, developed at The Queen's University of Belfast, is a useful tool to assess and predict the durability of a reinforced concrete structure. The results showed that the concrete compressive strength testing needs to be complemented by the evaluation of the diffusivity, permeability, and resistivity of the concrete to provide an improved estimate of the durability of the system.

The findings of the analysis affirm the fact that it is the material properties and the exposure parameters which control the susceptibility of the concrete to deterioration, and it is the damage that is measured with all other methods. When a structure is at an earlier stage in the deterioration process, measuring the material properties and the exposure parameters is more useful in monitoring and maintaining the structure, while at a later stage the damage can only be assessed.

Sommaire

Plusieurs charpentes en béton construites dans les années 60 et 70 sont actuellement très détériorées. Par exemple, le viaduc Dickson, construit en 1959, a été déclaré désuet par la Ville de Montréal en 1994 à cause de la détérioration excessive de son tablier, principalement causée par la corrosion des armatures en acier. Un projet de recherche a été réalisé en 1997-8 sur cet ouvrage avec comme objectifs principaux de: (a) évaluer les dommages dus à la corrosion dans le tablier, (b) identifier les causes de ces dommages, et (c) explorer certaines techniques de mesures de prédiction de la corrosion. Cette thèse résume les résultats de cette recherche menée à l'Université McGill en collaboration avec l'Université Queen's de Belfast, Irlande du Nord, ainsi que certains partenaires industriels locaux.

Plusieurs méthodes d'essais on été utilisées, lesquelles peuvent être classifiées en deux catégories, soit les techniques d'évaluation des mécanismes causant la corrosion et la mesure des propriétés du béton indicatives des risques de corrosion. L'ensemble des données recueillies permettent de confirmer la condition critique du tablier du viaduc due principalement à la concentration excessive d'ions chlorure dans le béton alimentant le processus de corrosion des armatures en acier. Les deux catégories de mesures utilisées (mesure des dommages et mesure des propriétés du béton et des paramètres d'exposition) ont servi à prédire le taux de corrosion de l'armature. La mesure du potentiel de corrosion est celle qui s'est avérée la plus concluante, mais il est possible d'améliorer sa fiabilité en la combinant avec une évaluation de la délamination des armatures, de la couverture de béton et des profils en ions chlorure. Les coefficients de migration des ions chlorures sont l'indicateur le plus significatif du taux de corrosion, surtout pour la partie est du tablier. Une nouvelle technique de mesure de migration des ions chlorure, développée à l'Université Queen's de Belfast, s'est avérée utile et fiable pour prédire la durabilité du tablier détérioré par corrosion des armatures. Les résultats indiquent qu'ils est nécessaire de combiner les essais de résistance en compression du béton à des mesures de diffusibilité, perméabilité, et résistivité afin d'améliorer la fiabilité des prédictions de durabilité.

L'étude confirme que les propriétés du béton et les paramètres d'exposition contrôlent sa susceptibilité à l'endommagement par corrosion, alors que les autres techniques de mesure évaluent directement l'endommagement comme tel. Ainsi, pour un ouvrage relativement jeune et peu détérioré en apparence, la mesure des propriétés du béton et des paramètres d'exposition est

tout indiquée comme activité de maintenance préventive, alors que les dommages peuvent seulement être mesurés a posteriori.

Acknowledgements

Table of Contents

List of Symbols

a	Atomic weight.
A	Constant, that is the intercept derived from the calibration graph.
A	Surface area of steel bar.
A	Transmission area (In-situ chloride migration test).
A_{anode}	Anodic surface area.
$A_{cathode}$	Cathodic surface area.
B	Stern-Geary constant.
B	Constant, that is the slope derived from the calibration graph.
c	Calibration factor dependent on the geometry of the specimen and the applied pressure used with the Autoclam Permeability System.
C	Source chloride concentration (Equation (3.28)).
$[C]_b$	Concentration of reduced species (in the bulk electrolyte).
C_c	Concentration of the standardizing (calibration) solution.
C_{cl}	Concentration of the unknown solution.
CD	Cook's Distance.
C_i	Initial chloride concentration of the concrete.
COV	Coefficient of variance.
$Cover$	Variable representing the measured concrete cover thickness values.
CR	Variable representing corrosion rate.
C_s	Chloride concentration of the concrete surface.
$C(x,t)$	Denotes the chloride profile, i.e. the chloride concentration of the concrete versus the distance x from the exposed surface at time t, since the chloride exposure started.
D	Effective diffusion coefficient (Equation (3.16)).
D	Chloride diffusion coefficient of concrete (Equation (3.28)).
D_a	Variable representing the apparent chloride diffusion coefficient values.
dc/dx	Concentration gradient through the specimen.
dc/dt	Steady state migration rate of chloride ions.
$Delam$	Variable representing the measured delamination values.
D_{mig}	Variable representing the in-situ chloride migration coefficient values.
DOF	Degrees of freedom.
D_{rb}	Diameter of the rebar.

D_s	Steady-state chloride diffusion coefficient.
e	Residual.
e^-	Free electron.
$erf(z)$	Error function.
$erfc(z)$	Error function compliment.
F	Faraday's constant.
F	F-ratio.
i_a	Anodic current density ($i_{dissolution}$).
i_c	Cathodic current density ($i_{deposition}$).
$i_{c'}$	Critical current density.
i_{corr}	Corrosion current density.
i_L	Limiting current density.
i_{max}	Maximum current density.
i_o	Exchange current density.
i_p	Passive current density.
IR_{drop}	Potential difference between the electrodes through the electrolyte.
i_1	Current density at point 1.
I	Low frequency alternating current passed between the oute:" electrodes of the Wenner probe.
I_{anode}	Overall anodic current.
$I_{cathode}$	Overall cathodic current.
I_{corr}	Corrosion current.
J	Ion flux entering solution B (Equation (3.16)).
J	Unidirectional flux of chloride ions (Equation (3.28)).
k	A constant which is a function of the material properties and the environmental conditions.
k	Mass transfer coefficient.
K	Kelvin.
k_w	Variable representing the coefficient of permeability values.
L	Distance between electrodes (In-situ chloride migration test).
L	Length of the polarized working electrode (rebar).
LCL	Lower control limits.
$LogCR$	Variable representing the logarithm of the corrosion rate values.
$LogD_a$	Variable representing the logarithm of the apparent chloride diffusion coefficient values.

$LogD_{mig}$	Variable representing the logarithm of the in-situ chloride migration coefficient values.
$Logk_w$	Variable representing the logarithm of the coefficient of permeability values.
$Log\rho$	Variable representing the logarithm of the resistivity values.
m	Mass in the reaction.
mol	Mole
MS	Mean squares.
n	Number of electrons (e^-) transferred during corrosion reaction.
n	Number of electrons transferred in the reduction (Equation (3.8)).
n	Number of equivalents exchanged (Equation (3.14).
N or n	Number of observations.
P_{O2}	Partial pressure of oxygen.
ppm	Parts per million.
(Products)	Concentration of reduced species.
q	Rate of flow for the steady state.
q	Y-intercept of the regression analysis of the transformed variables, that is y values obtained against depth, x (Equation 3.21).
Q_1	Lower hinge or first quartile (approximately equivalent to the 25th percentile).
Q_3	Upper hinge or third quartile (approximately equivalent to the 75th percentile).
R	Gas constant.
R	Pearson correlation coefficient.
R_e	Internal electrolytic (concrete) resistance.
R_e	Ohmic or uncompensated resistance.
(Reactants)	Concentration of oxidized species.
RH	Relative humidity.
R_m	External metallic resistance.
R_p	Polarization resistance.
R^2	Coefficient of determination or correlation coefficient.
s	Electrode spacing of the Wenner probe.
S	The change in electrode potential per ten-fold change in concentration (electrode slope).
SSE	Error sum of squares.
Str	Variable representing the measured concrete compression strength values.
t	Exposure time.
T	Absolute temperature (K).
UCL	Upper control limits.

V	Volume of collecting cell (In-situ chloride migration test).
x	Depth from the concrete top surface.
X	Carbonation depth.
X_i	Independent / regressor variable.
$\overline{X}$ or μ	Mean.
y	Transformed variable in Equation (3.21).
y'	Mean of Y.
Y	Dependent / response variable.
Z	Valency of chloride ions (-1).
α	Level of significance.
α	Slope of the regression analysis of the transformed variables, that is y values obtained against depth, x (Equation 3.21).
β_a	Anodic Tafel constant.
β_c	Cathodic Tafel constant.
β_o	Point of intersection of a line with $y = 0$.
β_l	Slope of a line.
$\beta_l, \ldots, \beta_k$	Constants referred to as regression coefficients (multipliers).
$\partial c / \partial t$	Change in concentration with time.
ΔE	Potential differnce between the electrodes (In-situ chloride migration test).
$\Delta\phi$	Potential change.
$\Delta\phi$	Difference between the observed potentials in the standardizing and the sample solutions.
Δi	Current density change.
ΔG	Free energy difference necessary to transform the metal oxide into a processed metal.
ΔG^{*}	Activation free energy barrier between the metal and its corrosion products.
ΔG^{o}	Standard free energy difference.
ΔV	Voltage drop measured between the inner electrodes of the Wenner probe.
ϕ_{corr}	Variable representing corrosion potential.
ϕ_N	Nernst potential.
$\phi_N{}^{o}$	Standard Nernst potential.
$\phi_{N(anodic)}$	Anodic potential.
$\phi_{N(cathode)}$	Cathodic potential.
ϕ_{oc}	Open circuit potential.

ϕ_{pp}	Passive potential.
ϕ_{tp}	Transpassive potential.
ϕ_1, ϕ_2	Potential at points 1 and 2 respectively.
η	Overpotential; polarization.
η_a	Anodic polarization.
η_c	Cathodic polarization.
ρ	Variable representing the apparent electrical resistivity values.
σ	Standard deviation.
σ^2	Variance.
υ_1	*DOF* of the numerator.
υ_2	*DOF* of the denominator.
ω	Benchmark model in a significance test.
Ω	Model being tested in a significance test.
Ω	Ohm.
^oC	Degrees Celsius.
%Cl	Variable representing the chloride content at the steel level.
%Chl	Percentage of chlorides (acid-soluble) by weight of concrete.

List of Figures

List of Tables

1 Introduction

1.1 Infrastructure and Society

In developed countries, steel reinforced concrete constitute a major versatile, economical and successful constructional material and has contributed significantly to the society's infrastructure, which is an umbrella of the society's public works. It creates the foundation for a healthy economy and high standard of living. It ensures modern-day conveniences and supports a climate favorable to jobs and employment growth. It is a public asset often taken for granted, yet what would life be like without basic essentials such as bridges, highways and roads[1]. The bridge structure is one of the most integral components in any transportation network. Canada is a young nation, but its bridges and other infrastructure are ageing, confronting the traveling public and the engineering community with problems and concerns about maintenance and rehabilitation. Maintenance and repair of bridges has become a constant and major concern of public works officials[2].

1.2 Brief History

As a result of the inherent protective characteristics of the concrete, reinforcement corrosion does not normally occur, provided that the surrounding concrete is of suitable quality and is properly designed for the intended environmental exposure. Nevertheless, corrosion can result if the above criteria are not fulfilled or if other factors are not as anticipated or have changed during the life of the structure. Design of concrete structures based on the material strength rather than on durability, the growing use of deicing salts, and the construction in increasing aggressive environments are some of the factors that have led to the surge of concrete structures experiencing reinforcement corrosion in recent decades[3]. When salts penetrate the concrete and reaches the level of steel rebars, corrosion becomes active. Rust occupies a volume several times larger than that of the iron from which it is formed, developing pressures as large as 5000 psi within the concrete. This pressure causes cracking and spalling. Ultimately, failure occurs due to cracking and spalling of the concrete, and major repair or replacement of the system is needed. With

concrete of suitable quality, corrosion of steel can be prevented, providing that the structure is properly designed for the intended environmental exposure.

Structural collapses of reinforced concrete structures due to corrosion are rare. Two multistorey parking structures in North America have collapsed due to deicing salt induced corrosion. A post-tensioned concrete bridge collapsed in Wales because of corrosion due to deicing salt attack on the strands[4], and so did one in Belgium. Concrete damage usually has to be well advanced before a reinforced concrete structure is at risk. The most common problem caused by corrosion is the spalling of concrete cover, which can be very dangerous. For example, a piece of concrete cover can spall and fall off a bridge deck causing deaths or injuries of motorists or pedestrians on the roads under the bridges or the overpasses, as it happened at the Sources Interchange in Montreal in 1997. It is noteworthy that every level of government has spent and will be spending an enormous amount of money to maintain the structures suffering from premature deterioration.

1.2.1   Importance of Corrosion to Society

Infrastructure must be planned, financed, constructed, operated, and maintained. Unless all of these engineering and management functions are fulfilled properly, either the systems will not fully meet the intended need, or they will be too costly[5]. The problem of the concrete infrastructure degradation due to rebar corrosion is particularly serious with major economic implications. Within Europe and North America, it has been estimated that around 50% of the national wealth of most countries is invested in their infrastructure. Therefore, the degree and rate of degradation of the built environment is of enormous economic, technical and competitive importance. As a matter of fact, 50% of the expenditure in the construction industry is incurred on repair, maintenance and remediation. Therefore, it is evident that even marginal savings could result in the release of substantial funds. It is becoming increasingly apparent that the steel reinforced concrete infrastructure of North America and many other regions is suffering premature degradation, and the economic implications of this problem are alarming[5]. Deterioration of infrastructure is occurring at a continually increasing rate around the world. The principal cause of the degradation of structures such as bridges and parking garages is corrosion damage to the reinforcing steel, which is embedded in the concrete. In turn, this corrosion damage is largely related to the use of de-icing salts.

In Canada, with the large scale use of de-icing salts dictated by the cold climate, the situation is serious. Canada's concrete infrastructure, of which significant portion is near the end of its design life, has a replacement value of over half a trillion dollars[6]. Lack of consideration of durability and performance in the initial design, and deficiencies and lack of maintenance have resulted in repair and rehabilitation costs for Canada's infrastructure, estimated at well over $200 billion. The cost of rehabilitation due to corrosion of reinforcing steel alone is $30 billion per year for Canada[6].

The deterioration of concrete bridges in the United States is a monumental problem. The seriousness of the deterioration was first noted in the early 1960s and since than it has grown. The financial consequences of the problem associated with the corrosion of the reinforcing steel in concrete bridges was recognized in the early 1970s. The Federal Highway Administration (FHWA) estimated the cost of bridge deck repairs at $70 million per year in 1973. By 1975, the estimate for bridge deck repairs was increased to $200 million per year. In 1981, a report published by the US General Accounting Office[7] covering some 514,000 of the nation's 566,000 bridges estimated the rehabilitation / replacement costs at $33.2 billion. About one-half was due to the corrosion of steel in concrete. The problem has been steadily growing in magnitude; more recent projections presented by the Strategic Highway Research Program Research Plans estimate the liability of corrosion-induced deterioration in bridges at $20 billion, increasing by a rate of $500 million annually[8].

In the United Kingdom alone, it is estimated that repairs to damaged concrete cost over £500 million (CND$1 trillion) each year[9]. The statistics for Europe, the Asian Pacific countries and Australia are similar. Hence, the corrosion of reinforcing steel in concrete is a major problem facing civil engineers today as they maintain an ageing infrastructure. In summary, premature deterioration of concrete structures is a multibillion dollar problem in all countries around the world. Presently, more concrete structures are suffering from durability problems than was the case fifty years ago. Consequently, the inherited problems of corrosion in existing concrete structures are likely to increase as the 21st century approaches. Hence, the ability to assess the severity of corrosion in existing structures for maintenance and inspection scheduling and the use of corrosion data for predicting the remaining service life is becoming increasingly important.

1.3 Loss of Performance with Time

Concrete bridges are designed to provide satisfactory service over a long period of time. The life of any bridge depends on the preservation of the physical integrity of its components. Whilst bridges are generally required to have a design life of over 75 years, a number are suffering durability problems at a fraction of this age. The safety, the serviceability and the appearance of a structure determine the performance of the structure. The primary concern in practice is to ensure a satisfactory performance over a sufficiently long period of time. The performance over time, whether due to initial good quality, or to repeated repair of not-so-good structure, is termed the service life of the structure[10].

The relationship between concrete performance and time has been described graphically by Sommerville[11] (Figure 1-1).
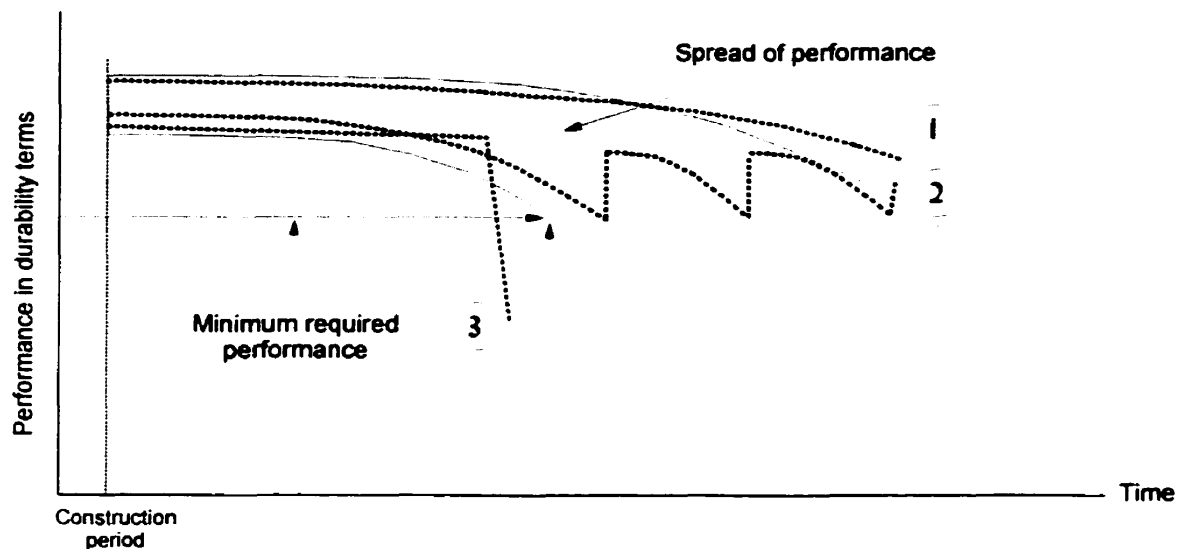
Figure 1-1: *Loss of performance with time*[11]

The performance depicted in curve 3 follows a high rate of deterioration and failure occurs suddenly and catastrophically. Negligible deterioration, indicated by curve 1, may not be achievable and requires high initial expenditure. Consequently, most concrete follows a pattern similar to curve 2 in which there is significant deterioration with time, but intermittent maintenance changes the performance level, or alters the rate of deterioration. Hence, continuous monitoring of the condition of structures on site is necessary to determine the state of health of a structure upon completion and regularly during its life by further routine tests.

4

1.4   Impact of Corrosion

Evaluation of corrosion activity of steel in reinforced concrete field structures is not an easy task because the steel is not visible, the concrete has a high resistivity and the structures are in use. There have been active efforts to determine the corrosion rates and other factors such as permeability to the ingress of chloride as well as other concrete properties that could affect performance. A monitoring system could be embedded in the concrete structure during construction, or after a repair so that the condition could be assessed at any time during its useful service. However, most probably the monitoring system would be located where deterioration is not most severe and there is no guarantee that it would be durable as long as the structure, and that it will continue to provide reliable readings throughout its life. For these reasons, intermittent monitoring, using appropriate in-situ tests, represents the only practicable way forward at present[12].

The primary cause for the deterioration of reinforced concrete bridge components is corrosion of reinforcing steel due to the presence of soluble chlorides from deicing chemicals. It is generally agreed that life-cycle cost analyses of viable alternatives are necessary in order to develop rational strategies for the repair, rehabilitation, and replacement of concrete bridge components. This, in turn, necessitates the acquisition of reliable information on the level and rate of deterioration[13]. Research centers all over the world have started addressing the issue of durability of reinforced concrete structures in codes with much emphasis on the protection provided to the reinforcing steel. Many approaches are intended to enhance the durability of concrete structures, however, little effort was made to incorporate regular inspections and condition surveys which could be used to monitor durability on site[10, 14]. When testing and evaluating the quality of concrete structural elements, it is often presumed that the concrete within one member is uniform in composition and properties. However, during placing and compacting of the fresh concrete, the surface layer often contains more water, fines and air than the core concrete. Hence the composition and properties of the surface layer of the concrete (covercrete) differ considerably from those of the core (heartcrete)[15]. Furthermore, during the service life of the structure, the surface layer is usually subjected to more severe environmental attacks than the core concrete. Hence, serious misjudgments occur if the results from laboratory tests are used for linear extrapolations of the corrosion phenomenon for real structures[14,15].

1.4.1 Bridge Maintenance

Structures will still continue to be built in corrosive environments. Therefore, the need for in-situ techniques to deal with the resulting problems is of considerable importance. Structures need to be monitored as it cannot be assumed that it is performing well by simply looking at the structure and taking precautions once the damage is visible. The damage needs to be predicted and suitable testing techniques need to be used to develop proper maintenance techniques. Bridge maintenance is an especially important need since the safety of bridges is always of concern. A national bridge inspection program is essential. Many components of today's bridges have reached middle and old age. But over the years, with resources largely directed by economic and political forces toward expansion and growth, maintenance often shrunk to little more than repairs on as needed basis. It was, and often still is, difficult to argue the real need for maintenance for bridges whose very presence personifies strength and performance; in most cases, the bridges have been performing well for years. Too often, growing hazards went undetected[16]. Bridge inspection is a key aspect to preventive maintenance and to proper running of any bridge management system, as this is the only means by which the condition of the bridge is determined. In achieving this goal, assessments are made and records are kept of the physical condition of every bridge. The inspection process for each bridge should be scheduled such that no bridge is inspected later than a specified interval of time.

1.5 Dickson Bridge Research Program

Many concrete structures built in the 1960s and 1970s are now showing significant signs of deterioration. In order to understand the mechanisms at work in natural degradation of the concrete, it is essential to study existing structures. Selected structures must be those which have been exposed to a representative environment, over a period of time long enough to involve the development of any secondary mechanisms, which may not be obvious at early ages. On the other hand, selected structures must not have suffered from damage so severe, that it becomes impossible to identify the early mechanisms behind the onset of the degradation. The Dickson Bridge is a typical example. The background and the scope of the entire research program are discussed emphasizing the objectives of the present thesis.

1.5.1 Background

Construction of the Dickson bridge was completed in 1959 at a cost of under a million dollars in a heavily industrial zone as a grade separation over the CN (Canadian National) rail tracks in the east end of Montreal (Figure 1-2).

The bridge consists of three sections, with the north and south sections consisting of reinforced concrete deck on concrete beams and girders on concrete column piers and the central section consisting of reinforced concrete deck on steel girders on steel column piers (Figure 1-3). The bridge superstructure, 366 m long by 27 m wide, consists basically of a 150 mm thick heavily reinforced concrete deck over continuous heavily reinforced concrete beams, 1500 mm x 1200 mm in section, over spans of 12 to 18 meters (Figure 1-4), except for the central three spans over the CN railway tracks, where the deck is supported on steel girders[17].

Figure 1-2: *Dickson bridge over CN rail tracks*
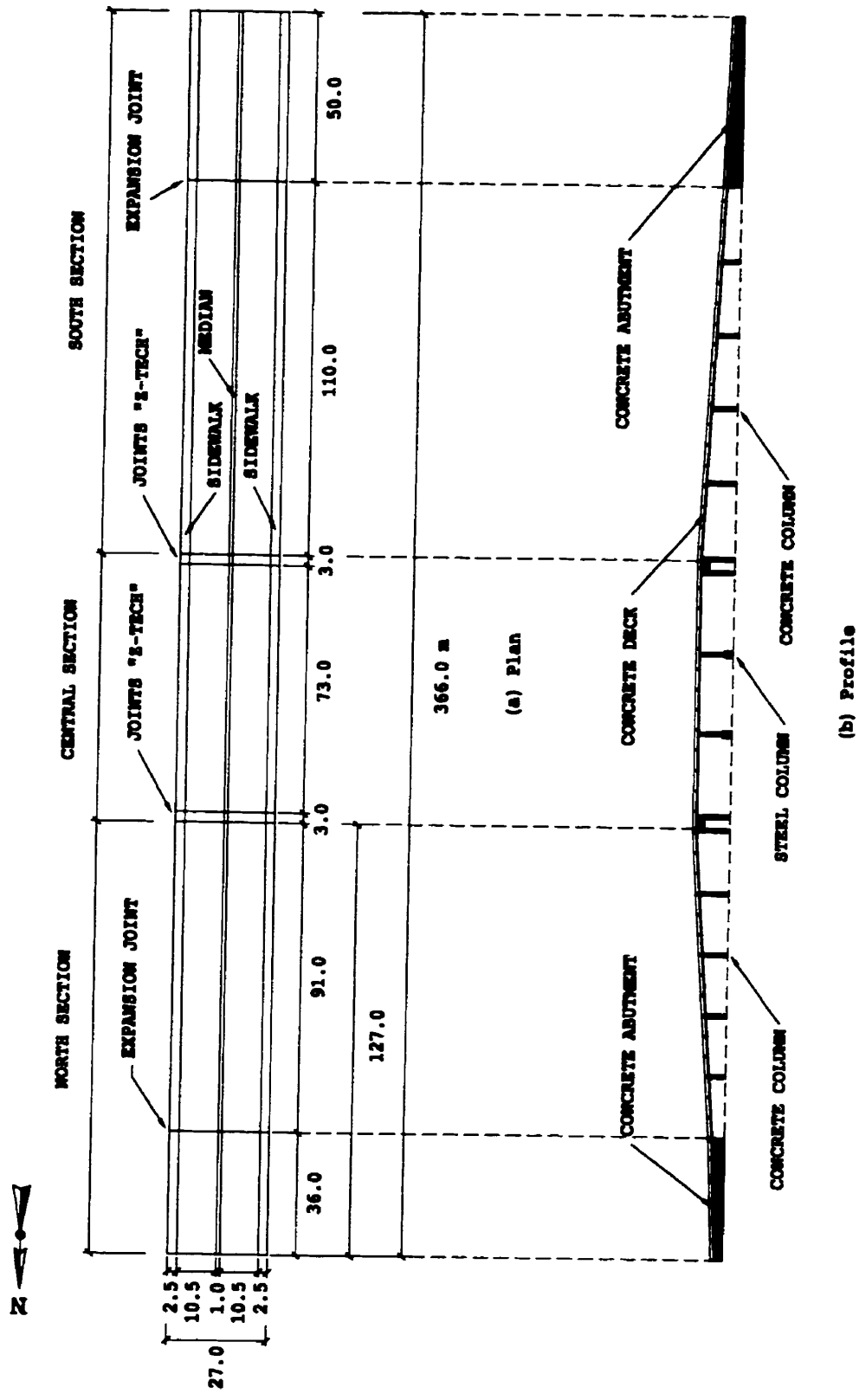
Figure 1-3: *Schematic of Dickson Bridge*

8

Figure 1-4: *Substructure of northern part of bridge*

1.5.2   Research Program

In 1988, the City undertook a detailed program to inspect and evaluate its transportation infrastructure, including the deck of the Dickson Bridge, which was found to be severely delaminated, with chloride ion contents well above the permissible limits with deficient air content not suitable for the ambient exposure conditions. As a temporary solution, the bridge rating was reduced to 3 metric tons and the two outside lanes were thickened with a heavily reinforced concrete overlay to be used as controlled truck lanes. Consequently, because of safety concerns, the bridge was decommissioned in 1994 by the City of Montreal and a detour was built to accommodate the Dickson street and the railway traffic, however, the CN Rail reduced the number of trains to about one or two per day and then stopped the railway traffic completely[17].

Realizing that there was no longer the need for the bridge, the City decided to demolish the bridge, however, due to the lack of funds, the bridge continued to exist for some time. McGill University, along with some industrial partners, and Le Centre des Études et Recherche en Infrastructure Urbaine (CERIU) approached the City to let them use the bridge for research and development purposes providing an excellent opportunity for a useful joint industry-university research program to be undertaken. The Queen's University of Belfast was invited to join the

9

research team because of its expertise in the development of in-situ testing techniques such as the Autoclam Permeability System and the In-situ Chloride Migration Test.

A summary of the proposed program determined among the various partners at meetings organized by McGill University and CERIU is as follows[18]:

- Surface protection and repair techniques:

  - Repair and rehabilitation of deteriorated surfaces using fibre-reinforced and normal, and high performance concretes, and shotcrete;

  - Encapsulation of structural elements and injection repair of cracks;

- Use and evaluation of composite materials as reinforcement and for deck repairs;

- Evaluation of structural capacity of the deck and the bridge through physical testing and nonlinear computer analyses;

- Evaluation of permeability and carbonation of the deck and examination of desalination and realkanization techniques;

- General condition survey of the bridge utilizing existing and some selected new tests;

- Creation of a detailed data bank of the parameters which influence the corrosion process for development of probabilistic models for the various phenomena and the development of techniques for reliability-based durability design methods to provide protection against corrosion and assessment of service life;

- Evaluation of membranes and other repair techniques (involving polymer concrete, etc...) for their ability to bridge cracks; and

- Laboratory and field investigations to determine the influence of the rate and extent of corrosion on bond characteristics between the reinforcing steel and concrete.

1.5.3 Objectives and Scope of Thesis

Given the substantial length and area of the overpass, it was decided to concentrate on the northern part of the bridge deck for this research program (Figure 1-3). It is noted that hereafter when the word 'entire' bridge deck is mentioned, it is understood that it is the northern part of the bridge (127 meters) and not the entire length (366 m) of the bridge deck.

Corrosion in its initial stages, is not detrimental to the structure, however, after initiation, the rate of progress is of importance, and it depends on the concrete properties. Researchers tend to study durability of reinforced concrete structures from two very disparate, standpoints: (a) using the results from permeability tests, diffusivity and resistivity tests, and (b) by monitoring the state of the rebar surface using tests such as linear polarization or half-cell potential. Unfortunately, the latter techniques yield no information on the properties of the concrete in the vicinity of the rebar[19]. It is surprising that little concerted effort has been undertaken to link these two aspects of durability. Cover-zone properties (permeability, diffusivity and resistivity), and the state of the rebar surface can only be determined by monitoring these parameters on site, all of which influence reinforced concrete durability. Taking this into account, the primary objectives of the present research program were as follows:

* To conduct an examination of the corrosion of the reinforcing steel in the Dickson Bridge deck by measuring the corrosion rate;

* To assess the corrosion induced damage in the concrete deck to determine the existing "state of health" of the deck and to identify the causes of the observed deterioration; and

* To identify suitable test techniques for predicting corrosion by investigating those parameters of the cover-zone concrete which are instrumental in initiating and sustaining corrosion, with particular interest in the role played by the environment in the vicinity of the rebar.

The organization of the thesis is illustrated by the flowchart in Figure 1-5. The following chapter explores the stages of the corrosion process of reinforcing steel in concrete. The first requirement, when addressing a deterioration problem is to quantify it. Chapter 3, therefore, discusses the testing procedures and the techniques available to assess the causes and extent of the corrosion damage in a structure. Chapter 4 is concerned with the test program undertaken on the north part of the Dickson Bridge deck where details of the test techniques and the calculations of the appropriate parameters under investigation are outlined. Chapter 5 presents the experimental results and states the present condition of the bridge deck. Chapter 6 discusses the experimental results and details of the multivariate statistical analysis, that is the prediction of corrosion rate using "Assessment" and "Prediction" methods. In-situ tests that are able to detect the damage and the susceptibility to corrosion are investigated. The results are analyzed keeping in mind that it is important to monitor the damage of a structure to take action on a short-term basis, but most importantly it is essential to predict the corrosion rate to undertake preventive measures which will be beneficial to the structure in the long run. The results discussed in Chapters 4 to 6 are summarized in Chapter 7 and appropriate conclusions and recommendations are drawn.

THE ASSESSMENT AND PREDICTION OF REINFORCING STEEL CORROSION ON THE DICKSON BRIDGE

Background | Objectives

Review

Experimental

CHAPTER 1

| Corrosion of Reinforcing Steel embedded in Concrete CHAPTER 2 | Measurement of Corrosion and Influencing Factors CHAPTER 3 | Experimental Program and Calculation of Parameters CHAPTER 4 | Presentation of Experimental Results CHAPTER 5 |

— Corrosion model:
- Initiation stage
- Propagation stage

— Monitoring corrosion activity
— Measurement of resistivity and permeation properties

— Test program:
- Half-cell potential survey
- Covermeter survey
- Delamination survey
- Resistivity of concrete
- Linear polarization resistance test
- In-situ chloride migration test
- Chloride profiling
- Autoclam permeability system
- Water absorption test
- Concrete compressive strength
- Carbonation depth

— Field test results: condition of bridge deck

Analysis and Reliability of Results to Assess/Predict Corrosion of the Dickson Bridge Deck CHAPTER 6

— Variation of test results
— Prediction of corrosion rate using multiple linear regression analysis

Conclusions and Recommendations CHAPTER 7

Figure 1-5: *Organization flowchart of thesis contents*

2 Corrosion of Reinforcing Steel Embedded in Concrete

2.1 Introduction

Corrosion of reinforcing bars is one of the main causes which induces an early deterioration of concrete structures, reducing their service life and consequently their residual life[20]. Good quality concrete provides excellent protection for steel reinforcement. Steel does not corrode immediately after embedment. Chemical protection is provided by the concrete's high alkalinity, and physical protection is afforded by the concrete acting as a barrier to the access of aggressive species. However, despite these inherent protective qualities, corrosion of steel reinforcement has become the most common cause of failure in concrete structures[21].

The service life of a concrete structure is defined from the time of erection of the structure until the maximum tolerated extent of deterioration, in this case corrosion, which obviously depends on the particular purpose of the structure. A model to describe this corrosion process was proposed by Tuutti[22] which is illustrated in Figure 2-1.
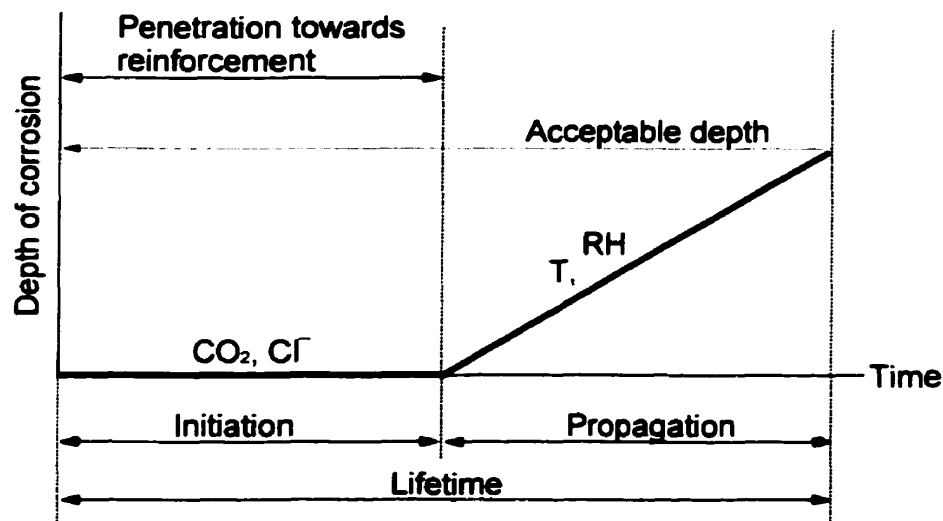
Figure 2-1: *Schematic sketch of steel corrosion sequence in concrete[22]*

13

The service life of a concrete structure with regard to reinforcement corrosion can be divided into an initiation stage and a propagation stage. It should be noted that this model provides only an approximate overall picture of the service life. It does, however, give the probability of approximating the effects of various parameter values and of predicting an approximate service life and the remaining service of concrete structures[22]. The process is subdivided into the initiation and propagation stages because the controlling parameters and the rate determining factors differ in the two stages[23]. This chapter reviews the many factors affecting the time until corrosion initiates and the rate at which corrosion propagates.

2.2 Initiation Stage

The initiation period of the corrosion process consists of the time from the erection of the structure until the steel depassivates due to the external aggressive agents reaching the reinforcement surface[24]. The pore solution, which surrounds the embedded steel, is highly alkaline with a pH value between 13 and 14. An environment of this type causes the steel to be passivated, thereby allowing the formation and maintenance of a stable thin passive film on the steel surface[22]. The corrosion rate is depressed to an insignificantly low level by the formation of the iron oxides on the steel surface. This state of passivation is maintained until the concrete in contact with the reinforcement becomes carbonated, or until a sufficient concentration of aggressive ions (normally chloride ions) reaches the steel surface, which implies lowering of the concrete pH to values near 8 or 9. The ions either move through the concrete pores or through the cracks.

Corrosion of steel initiates if the concrete is not of adequate quality, that is the structure was not properly designed for the service environment, or the environment was not anticipated or it changed during the service life of the concrete structure[25]. The factors influencing the initiation period, namely the environmental conditions, the material properties and the design of the structure will be discussed, but first the transport mechanisms by which aggressive substances enter the concrete are reviewed.

2.2.1 Transport Mechanisms in Concrete

For the ingress of external agents, the continuous pore network, cracks and other defects provide the paths along which transport occurs into the cover concrete (covercrete)[26]. The process of fluid flux is generally described in terms of absorption, diffusion and permeability[27]. These will now be defined while in the following chapter the processes will be explained more in detail.

2.2.1.1 Absorption

Absorption is the process whereby the concrete takes in a liquid by capillary suction to fill the pore space available within the material[27].

2.2.1.2 Diffusion

Diffusion is the process by which a liquid, gas or ion migrates through the concrete under the action of a concentration gradient. It is generally defined by a diffusion coefficient or a diffusivity value[27].

2.2.1.3 Permeability

Permeability is a flow property and is defined as that property of a porous medium which characterizes the ease with which a fluid will pass through it, under the action of a pressure differential. It is strictly related to the flow that occurs under an applied pressure differential[27]. The terms permeability and porosity are often misinterpreted. Porosity is a measure of the proportion of the total volume occupied by pores. It is possible for a material to be porous, but impermeable, if it contains a series of disconnected air voids separated by impermeable material[27, 28].

2.2.2 Influence of Environmental Conditions

The deterioration of the nation's infrastructure is proceeding at an alarming rate. A major element of the problem involves chloride-induced corrosion of reinforcing steel in concrete bridge

15

components and parking garages[29]. Concrete in aggressive environment is strong, durable and long lasting building material. However, concrete structures such as bridge decks are exposed to many severe environments, which promote the penetration of corrosion-inducing elements. The bridge deck environment constitutes a very severe exposure condition for the concrete where it is subjected to wetting and drying, freezing and thawing, and application of deicing salts[30].

2.2.2.1 Ingress of Chlorides

Chloride ion contamination has been identified as a major culprit in the breakdown of the protection afforded by the passive film[31]. Hence, the major cause for the initiation of corrosion in reinforced concrete bridge decks is the pore solution, which surrounds the steel and contains excessively high chloride concentrations. As a result of this, numerous researchers have studied the ingress of chloride into the concrete[22, 29, 31].

Sources of Chlorides

Chlorides may be present in the concrete during its manufacture, or they may have penetrated from some source during service[32]. Internal chlorides are contained in the mix constituents and could originate from[32, 33]:

- Admixtures such as calcium chloride (strength gain accelerators widely used until the mid-1970s);

- Use of chloride-contaminated water (sea or brackish water); and

- Chloride bearing aggregates.

It should be noted that adding materials containing chlorides when manufacturing concrete always increases the risk of corrosion and for this reason none of these materials should be permitted in reinforced concrete, and standards generally give guidance on the maximum total chloride ion content[32]. For reinforced concrete exposed to chlorides in service, the maximum permissible water soluble chloride ion in concrete is 0.15% by mass of cement according to both the ACI 318 Committee[34] and the CSA Standard A23.1[35].

The most common source of chlorides in concrete is from the environment. External sources of chlorides during the post-construction period include marine environment and road de-icing salts, although industrial environments may also provide a source. By far the most common source of

destructive chloride levels for concrete structures on land (such as bridges and parking garages) is the de-icing salts. More than 9.1×10^9 kg of road salt is used in the United States each winter. A typical bridge in the snow belt will receive about 1.2 kg/m^2 during each winter season; some receive as much as 4.9 kg/m$^{2[29]}$.

Chloride Transport Through Concrete

The time to the initiation of chloride-induced corrosion depends mainly on the rate at which chloride ions enter the concrete. The continuous pore network, cracks and other defects provide the path along which the transport of external chlorides occurs[26]. As mentioned earlier, the most common transport mechanisms are diffusion, absorption and permeation[36]. The mechanisms of chloride ingress depend on the exposure conditions and the moisture condition of the concrete. Diffusion is a result of chloride gradients in the water in the pore system and can only occur through a saturated or partly saturated concrete[37]. With capillary suction, the chloride-contaminating solution is absorbed through the pore system into the dry concrete. Water containing chloride ions could permeate through the concrete under a pressure head. Several mechanisms may act simultaneously, or one mechanism may exclusively control the chloride transport[36].

Chloride Attack Mechanism

Concrete provides resistance to these processes by means of its physical pore structure, and the ability of the hydrated cement paste to bind chloride ions[22, 31, 32]. Chlorides can occur in the concrete in three forms. Some of the chlorides are chemically bound to the cement hydrates, other chlorides are physically bound being adsorbed on the surface of the gel pores[22]. The remaining chlorides are the free chloride ions dissolved in the pore solution (Figure 2-2).
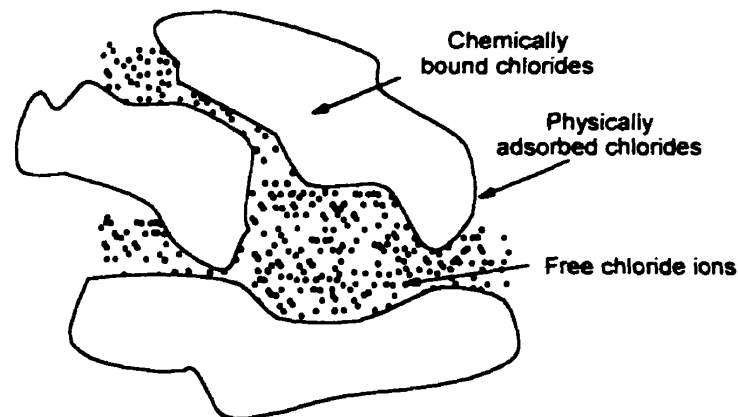
Figure 2-2: *Three different forms of chloride in concrete[22]*

Chloride binding reduces the concentration of the free chloride ions in the pore solution. Consequently, this binding benefits the service life of a concrete structure as follows:

- The rate of chloride ingress into the concrete decreases[38, 39]; and

- Only the mobile chloride ions present in the pore solution (free chloride ions) are considered to be capable of initiating steel reinforcement corrosion[3, 22, 23, 32, 33].

It should be noted that the distribution of the chloride ions among the three forms is not permanent, as there is an equilibrium situation such that some free chlorides are always present in the pore water. It follows that only the chloride ions in excess of those needed for this equilibrium can become bound[32].

For corrosion to be initiated, there has to a certain minimum concentration of chloride ions at the surface of the steel, which is termed as the threshold value[22,31]. The threshold can be presented as a total chloride content, a free chloride content or as the ratio of the free chloride ions to hydroxyl ions (Cl^- : OH^-). Haussman[40] determined that a Cl^-/OH^- ratio above 0.6 in the concrete pore solution can initiate corrosion. Lambert et al[41] found that the threshold of Cl^-/OH^- ratio in concrete subjected to external chloride contamination was greater than 3, although lower for specimens where the contamination was from within the concrete mix. There is considerable difficulty in determining the ratio of Cl^-/OH^- ratio in the pore solution, hence it is more practical to specify the critical total (acid-soluble) chloride content with respect to the cement mass or the critical water soluble chloride content with respect to the cement mass. As the name implies the water-soluble chlorides is that which can readily dissolve in water[38]. In a review of literature, Glass and Buenfeld[31] suggested that the threshold levels are best expressed as the total chloride content. Because of the uncertainties connected with the threshold level, any recommendations tend to be conservative and no widely accepted chloride threshold concentration has been established and further research is required in this area[22, 31]. The recommended maximum chloride contents specified by the various codes are presented in Table 2-1. These values are limits and not the true threshold values for the onset of corrosion.

Table 2-1: *Threshold chloride content values reported by various codes*

	Threshold chloride (percent by weight of cement)	
Source	Free (water-soluble)	Total (acid-soluble)
ACI 201[42]	0.10 to 0.15*	-
ACI 222[25]	-	0.20
BS 8110[43]	-	0.40

* 0.10% for moist environment exposed to chlorides; 0.15% for moist environments not exposed to chloride environment

2.2.2.2 Carbonation

Carbonation of concrete results in reduction of its alkalinity, thereby permitting corrosion of embedded steel. Carbonation, however, is a slow process in concrete and carbonation-induced corrosion is not as common as the corrosion induced by chloride ions[22, 44, 45]. In bridges, it is common to see negligible carbonation after 20 years or more[33].

Carbonation Reactions

Carbonation of concrete normally involves a chemical reaction between atmospheric carbon dioxide and the products of cement hydration. There are a variety of hydrates in the hydrated cement paste matrix of the concrete, and it is agreed that virtually all of them can react with carbon dioxide at the normal atmospheric concentration of about 0.03% by volume[44].

Carbon dioxide from the air penetrates air-filled pores of the concrete and it reacts with the calcium hydroxide [$Ca(OH)_2$] to form $CaCO_3$. The net effect is to reduce the alkalinity as follows[3, 10]:

$$Ca(OH)_2 \quad + \quad CO_2 \quad \rightarrow \quad CaCO_3 \quad + \quad H_2O \qquad (2.1)$$

The process is schematically represented in Figure 2-3. The reaction gives rise to neutralization of the pore solution to pH values under 9[22]. The maintenance of passivation is conditional on an adequately high pH of the pore water in contact with the passivating layer. Thus, when the low pH front reaches the vicinity of the surface of the reinforcing steel, the protective oxide film is eliminated and corrosion is initiated[32].

CO₂
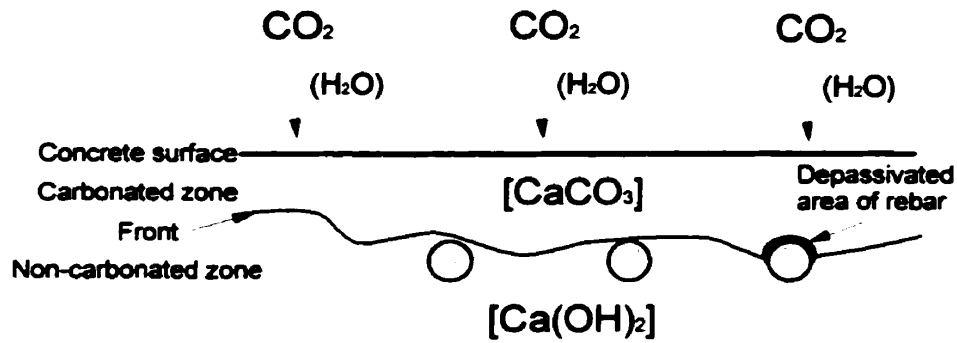
Figure 2-3: *Schematic representation of the carbonation process*[45]

The outer zone of concrete is affected first, but with the passage of time, carbonation proceeds deeper into the mass as carbon dioxide diffuses inwards from the surface. It is common to think of a carbonation 'front' progressing inwards from the surface, the front being the dividing line between the carbonated and the uncarbonated concrete (Figure 2-3)[25, 44, 45].

For the reinforcing steel in the alkaline environment of the concrete, the corrosion condition depends on both the pH and the potential. The Pourbaix diagram, a simplified form of which is shown in Figure 2-4, demonstrates how carbonation is a threat as it lowers pH and therefore it may bring the steel from the passivation state to corrosion[45].
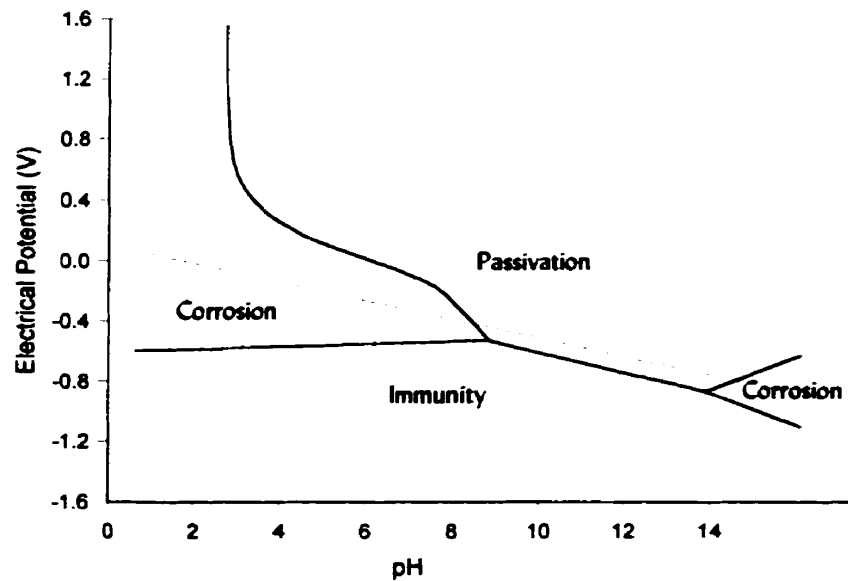
Figure 2-4: *Simplified Pourbaix diagram for iron*[25]

It can also be seen from the figure that reinforcement is in passive condition at the high pH likely to be found in freshly cast concrete, but could start to corrode if the pH were lowered. As noted earlier, carbon dioxide gradually penetrates through the pores and cracks in concrete causing a reduction in the alkalinity. The reduction in alkalinity destroys the passive environment and leaves the reinforcement in a condition where it is susceptible to corrosion[25, 45].

Rate of Carbonation

Carbonation usually proceeds relatively slowly by diffusion or permeation of carbon dioxide from the atmosphere into the concrete. The rate of carbonation has been widely studied and a parabolic model is generally accepted to describe the depth of carbonation expected over a period of time[10, 22]. The rate of carbonation can be predicted[3, 10, 22]:

$$X = k\sqrt{t}$$
(2.2)

where
$X =$ Carbonation depth;

$t =$ Exposure time; and

$k =$ A constant which is a function of the material properties and the environmental conditions.

Carbonation and Corrosion

The rate of carbonation is decisively influenced by the permeability of the concrete which depends substantially on the moisture content of the concrete[22]. It must be emphasized that conditions under which carbonation or corrosion may occur are not always coincident[45]. The highest rate of carbonation occurs at a relative humidity between 50 and 70 percent[10, 21, 46]. On the other hand, the rate of corrosion will be significant only where the relative humidity values in the pores adjacent to the steel are higher than about 75%. The fact that corrosion increases with an increase in the relative humidity (at least up to 95%) suggests that at high relative humidity values, the carbonation front does not penetrate to any significant depth[22, 44, 45].

2.2.2.3 Freeze-Thaw Action

One of the most important aspects of concrete durability in Canada and much of the northern United States is the resistance to various forms of deterioration associated with cycles of freezing and thawing[47]. The cyclic freezing and thawing process is commonly encountered in cold

climates. Typical problem structures in the frost belt are parking garages and bridge decks. There are two possible sources of dilating pressure[32, 48]:

- Freezing of water results in an increase of volume of approximately 9 percent; and

- Diffusion of water leading to a growth of a relatively small number of bodies of ice.

Concrete in exterior, damp situations is frequently in a condition where the pores in the outer zone are saturated with water. When exposed to freezing, ice crystals develop in the pores. As the crystals grow, they exert pressure on the surrounding concrete, which may eventually exceed its tensile strength causing cracks. Alternating freezing and thawing cycles cause progressive damage[32]. Each cycle of freezing causes a migration of water to locations where it can freeze. These locations include thin cracks, which become enlarged by the pressure of the ice and remain enlarged during thawing when they become filled with water. Subsequent freezing repeats the development of pressure and the associated consequences.

Application of Deicing Salts

It is a tedious fact that most of the highly industrialized nations lie in the winter snow and ice regions of the northern hemisphere. These nations are very dependent on sophisticated highway networks which must be kept clear during winter, when the common remedy of spreading road salt for de-icing is applied. There is no difficulty in understanding why salt spreading has become the universal panacea. Salt is readily available, easily applied, highly efficient in ice and snow removal, and relatively cheap[47].

The combined action of freeze-thaw cycles and the use of deicing salts has a more severe effect than the former alone[32]. The deicing salts lower the freezing point and hence prevent the formation of ice. However, when the salts are used for deicing road or bridge surfaces, some of these salts become absorbed by the upper part of the concrete. This produces a high osmotic pressure, with a consequent movement of water toward the coldest zone where freezing takes place and hydraulic pressure is developed[32]. The ice removal agents contribute to the deterioration of concrete causing cracking of the surface layer, but most importantly it is an important source of chlorides, increasing largely the possibility of a faster rate of corrosion of the reinforcement.

22

2.2.3　Influence of Material Properties

The corrosion protection of the reinforcing steel is influenced by the properties of the concrete. The factors affecting the concrete quality/characteristics necessary to provide sufficient corrosion protection for the reinforcement and to ensure the predicted life under the actual environmental conditions, are the water/cement ratio, cement content, aggregates, cements, supplementary cementing materials, and admixtures. The success of the correct choice of the concrete composition adapting to all environmental conditions can only be guaranteed by an adequate placement, compaction and curing[23].

The importance of the above factors affecting concrete quality may be directly or indirectly linked to the corrosion mechanism. While dealing with the corrosion mechanism, one of the fundamental properties that influence the initiation of corrosion and the extent of damage of concrete is its permeation characteristics[12, 14, 48, 49]. Such a model relating permeability to corrosion is shown in Figure 2-5. The constituent materials, mix proportioning, method of preparation and subsequent treatment decide the permeation characteristics at the inception of a structure. They also form the formation of microcracks near the surface and the integrity of the cover zone[10, 25, 32]. In essence, the permeability of the concrete influences the primary mode of transport of moisture and aggressive ions into the concrete, and the subsequent increases in the permeation properties are responsible for an increased rate of corrosion. This model shows that corrosion is related to the permeability of the concrete, and hence their interaction for assessing durability must be considered. It is obvious that permeability of hardened concrete is the key to control the various processes involved in the corrosion phenomena[48]. The following subsections will investigate the material properties affecting both corrosion and permeability.

Attempts should be made to ensure that the composition of concrete guarantees a passive state of steel reinforcement commencing from the moment of fabrication of the structure and maintains it throughout the design service life. For this purpose, the permeability of concrete to the environment should be low and its thickness and reactivity adequate.
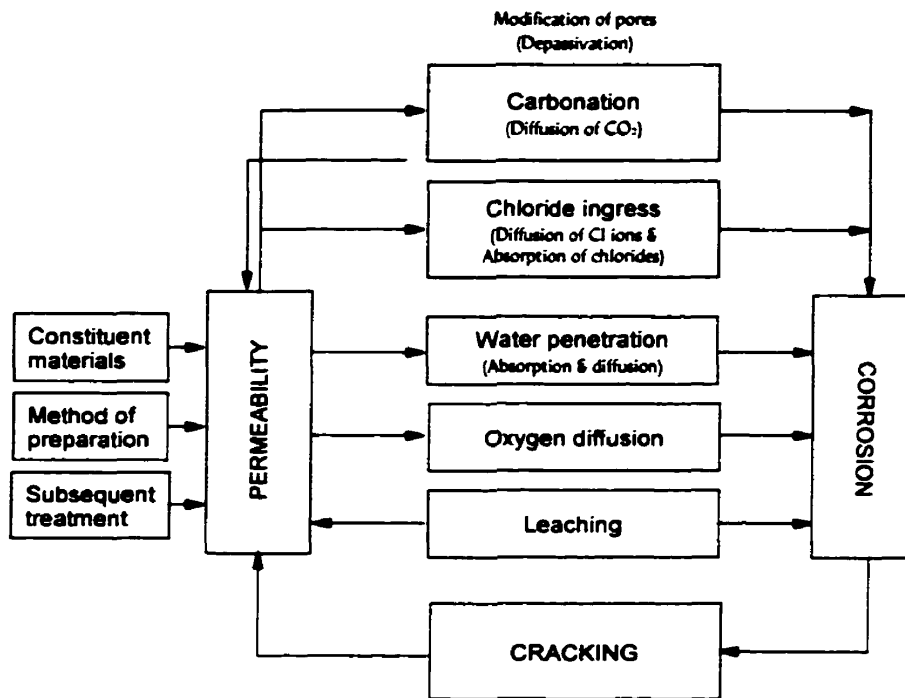
Figure 2-5: *Corrosion-permeability interaction model* [12, 14, 49]

2.2.3.1 Effect of Water/Cement Ratio (w/c)

The water/cement ratio influences the permeability and strength of the concrete [48]. The water/cement ratio has a dominant influence on the capillary pores and consequently on the permeability [23, 32, 48]. An increase in permeability results ultimately in an increase in chloride diffusivity, easier ingress of oxygen and lower resistance to corrosion. Consequently, with an increase in the chloride diffusivity, depassivation of the reinforcement will occur initiating corrosion more rapidly, and with an increase of oxygen and a decrease in the resistance to corrosion, the corrosion rate will increase. For high quality concrete of low permeability, it is suggested to use a low water/cement ratio [48]. The ACI Building Code 318 [34] specifies a maximum 0.4 w/c ratio for reinforced normal weight concrete exposed to deicing chemicals.

2.2.3.2 The Effect of Cement Content

The most important constituents of the cement with regard to steel corrosion are the tricalcium aluminate [C_3A] and calcium allumino ferrite [C_4AF] compound[21]. The main form of binding of the chloride ions is by reaction with C_3A to form an insoluble calcium chloroaluminate hydrate, sometimes referred to as Friedel's salt. Chlorides also react with C_4AF to form calcium chloroferrite[23, 32].

Corrosion initiation time and threshold values were found to increase systematically whereas the initial loss from the reinforcement decreased as the C_3A content of the cement increased. It should be noted that for a given C_3A and chloride content, more chloride are bound, if they are present initially in the mix at the time of mixing concrete compared to chlorides that penetrate into concrete from external sources during the service life of the structure. Also, as the presence of chlorides increases, the benefits of the C_3A characteristics become less perceptible[50]. Research has shown that increasing the cement factor with no reductions in the water-cement ratio causes no noticeable reduction in the reinforcement corrosion[32].

2.2.3.3 Aggregates

The aggregates constitute approximately 70 percent of the total volume of the concrete, hence they play a major role in determining the permeability of concrete and their effect on the resistivity of the concrete against environmental aggressors. Control of aggregate size and grading is needed to ensure low permeability. The permeability of the concrete can be decreased by selecting a more rounded and well-graded aggregates[23, 48].

Any aggregates supplying a source of chloride ions may have a serious effect on reinforcement corrosion. These include sea-dredged aggregates or porous aggregates. If the aggregates are too absorbent, during the wetting and drying cycle, the aggregate can retain a large quantity of water that helps the corrosion process. Some quantities of minerals might be present which contaminate the aggregates by becoming reactive. The most common example is the alkali-silica reactivity which generates disruptive expansive forces initiating the formation of cracks which provide an easier access for water and any environmental aggressors to reach the steel reinforcement[23, 48].

2.2.3.4   The Effect of Curing

The curing process is the final and one of the most important elements in concrete construction, and it effectively promotes increasing hydration of the cement. Inadequate curing can result in a weak, porous and permeable material near the surface of the concrete that is vulnerable to the ingress of various harmful substances from the environment. A short curing period is not sufficient to allow a fully protective passive film to be formed before the ingress of chloride ions. The time to the initiation of corrosion is substantially increased by prolonged curing. However, only fresh water must be used for curing because blackish water greatly increases the ingress of chlorides[32].

2.2.3.5   Admixtures and Supplementary Cementing Materials

Numerous chemical admixtures have been suggested as specific inhibitors of steel corrosion[25]. These include water reducers, plasticizers and air-entraining agents that reduce the water/cement ratio and are beneficial in retarding corrosion. Air-entrainment greatly enhances the resistance to reinforcement corrosion when subjected to numerous freeze-thaw cycles. Most commonly used supplementary cementing materials are pozzolans, including fly ash, silica fume, and ground-granulated blast-furnace slag have all been found to be beneficial in retarding reinforcement corrosion. This can be attributed to significant improvements in the pore structure and the increase in binding capacity which retards the diffusion of chloride ions to the steel-concrete interface, thereby delaying the onset of corrosion[32, 48, 50].

2.2.4   Design Details

Long term problems can be avoided if design details and adequate drainage are addressed during the design phase of a structure. Concrete cover and bar size have a significant effect on corrosion initiation and corrosion cracking. The structure provides higher resistance against environmental aggressors by providing an adequate cover and drainage, and by maintaining simplicity of the layout of the steel reinforcement. The effects of these parameters in providing corrosion protection to reinforcing steel are discussed in the following subsections.

2.2.4.1 Concrete Cover

Where the performance of structural reinforced concrete is in question, it is primarily that portion of concrete within 50 mm of the outside surface that is of interest, since the outer steel bars will almost invariably be located within this region. Schiessl[23] has identified the controlling parameters for the durability of reinforced concrete as the quality of the concrete and the thickness of the cover to reinforcement. If the concrete cover over the embedded steel is sufficiently thick and dense, it will provide the steel with the permanent protection against corrosion and will contribute to the production of good bond between the concrete and steel. The protecting effect of the concrete cover against corrosion can be summarized as follows[32, 51]:

- Chemical protection due to the high alkalinity of the concrete in which steel is passivated by the formation of an oxide film on its surface; and

- A relatively impermeable physical barrier that hinders penetration of aggressive agents through the pore network.

The quality of the concrete cover and the thickness of the cover are both important to achieve the above-mentioned protection. A thick, good quality cover helps to delay the carbonation and the ingress of chloride ions, thereby, preserving the passivity of the reinforcement and consequently delaying the initiation of corrosion. The less permeable and thicker the cover, the longer it will take to initiate corrosion, with an associated longer service life of the concrete structure[22, 32, 51].

2.2.4.2 Steel Reinforcement

Steel and concrete are complementary in their properties. Steel is strong in tension, but in the form of reinforcing bars, it is not able to resist large compressive loads because of the risk of buckling instability. Concrete is weak in tension but strong in compression; its mass provides stability against buckling failure of embedded reinforcement[32]. Since the main objective of the steel reinforcing bars is to counteract tension in the concrete, sufficient steel is necessary to ensure an adequate level of safety.

The crack width is reduced with a decrease of the bar diameter and an increase in the number of bars. By decreasing the crack width, the transport of environmental aggressors will be controlled and the initiation of corrosion will be delayed. In addition, the steel reinforcement layout should be kept as simple as possible, to permit placement and consolidation of the concrete. As a matter

of fact, it has been found that the cover to bar diameter ratio is a more definitive protection parameter against corrosion initiation and corrosion cracking than either cover or bar diameter separately. Clear cover specifications without consideration of the bar size leads to inadequate and misleading design for corrosion protection[52].

2.2.4.3 Drainage

Poor drainage often increases the degree of saturation of the concrete and aggravates the consequences of frost action. Provision of falls and drainage systems on slabs and on horizontal members will reduce the time during which the surface of the concrete is in contact with water and the dissolved aggressive substances, and results in a delay in the initiation of corrosion. However, often the drainage systems are installed at the wrong location or are not well maintained, hence, they cannot serve their purpose and play their role in influencing the service life of the structure.

2.3   Propagation Stage

The propagation period commences from the moment of depassivation at the face of the reinforcing steel and it includes the development of corrosion at a perceptible rate until the limiting stage is attained when the structure loses its bearing capacity, operational properties or external form[22, 24, 53].

This stage can be divided in three parts and is schematically represented in Figure 2-6[54]. A higher emphasis is assigned to chloride-induced corrosion, as it is the most common cause of deterioration in bridge components. During this stage, the expansive corrosion products around the steel bar usually propagate to the concrete surface causing cracks. At this point, the supply of deleterious substances increases due to the presence of longitudinal cracks and thereby accelerates the rate of corrosion. Rust stains and spalling follows resulting in the loss of serviceability of the concrete structure. After the end of functional service, the deterioration process continues with a decrease in the load bearing capacity of the member, which is related to the corrosion rate via a reduction in cross section of the reinforcing steel and the deterioration of bond at the steel-concrete interface, causing failure as shown in Figure 2-6[54].

The propagation period is clearly a function of the rate at which the steel corrodes[24]. Once corrosion is initiated, the progress of corrosion is influenced by the corrosion rate-determining parameters, namely water penetration, oxygen diffusion and electrical resistivity of the concrete[22, 23, 25].
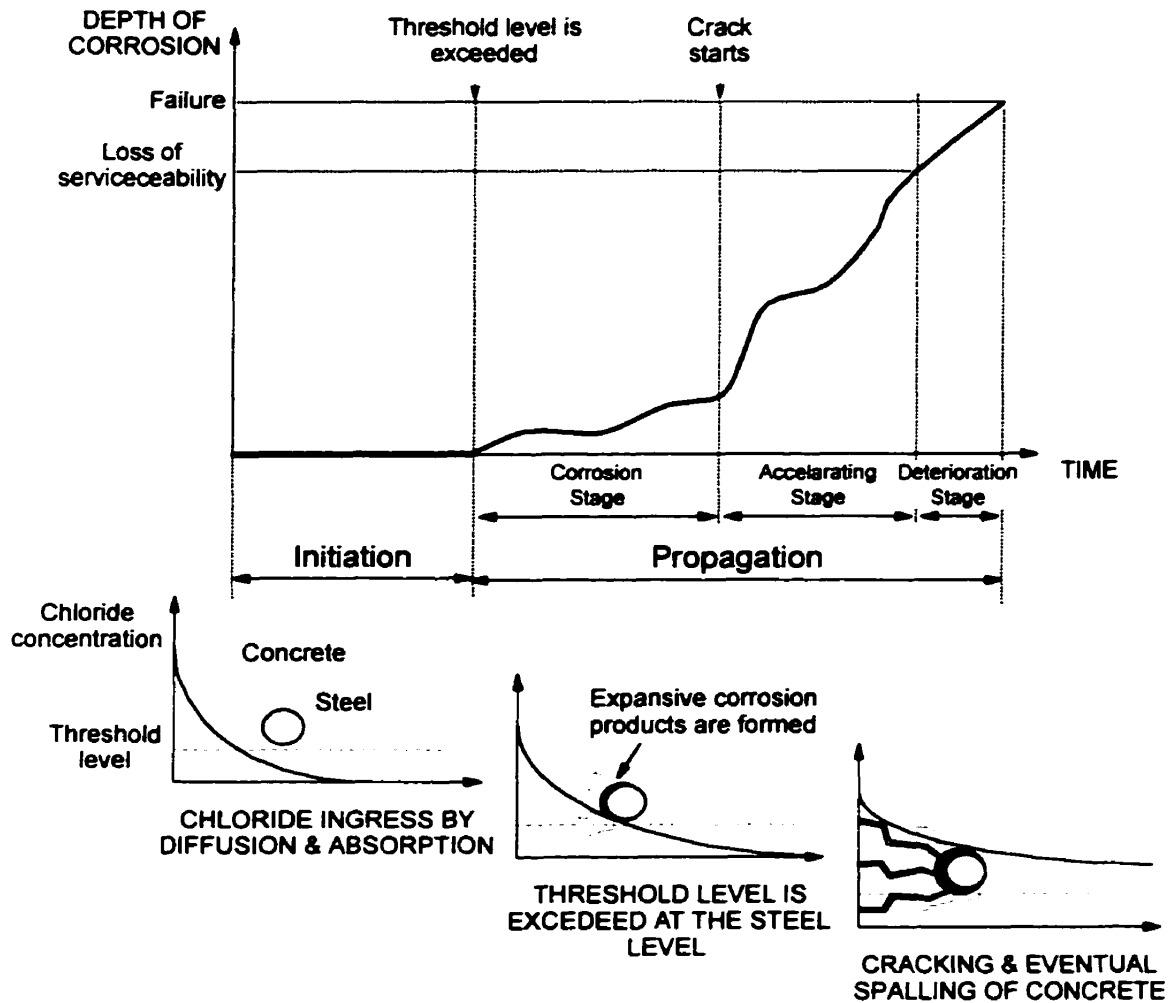
Figure 2-6: *Corrosion stages*[54]

2.3.1   Corrosion Process

Corrosion of steel in concrete is an electrochemical process, that is, both chemical process and flow of electricity are involved[55, 56]. The basic principles of electrochemical corrosion can be traced to the components of the electric cell (galvanic cell) which must be established for

corrosion to occur[57]. Generally, there are four components: an anodic site, a cathodic site, electrical conductivity between the cathodic and anodic sites, and a path (electrolyte) that provides ionic continuity between the anodic and the cathodic sites[3, 57]. The corrosion process is similar to the reaction of a battery cell where an anode, a cathode, a connection between the poles, and an electrolyte are needed[25].

2.3.1.1 Mechanism of Electrochemical Corrosion in Concrete

The mechanism of the corrosion process of reinforcing steel bars in concrete is electrochemical in nature and it involves the loss of electrons from the environment (usually water and oxygen) and the formation of the corrosion products such as oxides. The electrochemical reaction involves oxidation and reduction[55, 56]. At the anodic section, the metal ionizes to yield ions in the form of hydrated anions and free electrons. The free electrons move towards the cathodic section along the steel (conductor) where they combine with oxygen and water to produce hydroxyl ions. Once the hydroxyl ions are produced, they migrate to the anode through the concrete and react with the hydrated anions (Fe^{2-}) to yield ferrous hydroxide. In the presence of oxygen, the ferrous hydroxide oxidizes and is converted to a more stable form to produce hydrated oxide of iron. This is the familiar red rust. The flow of electrons in the metal and in the electrolyte is shown in Figure 2-7[48].
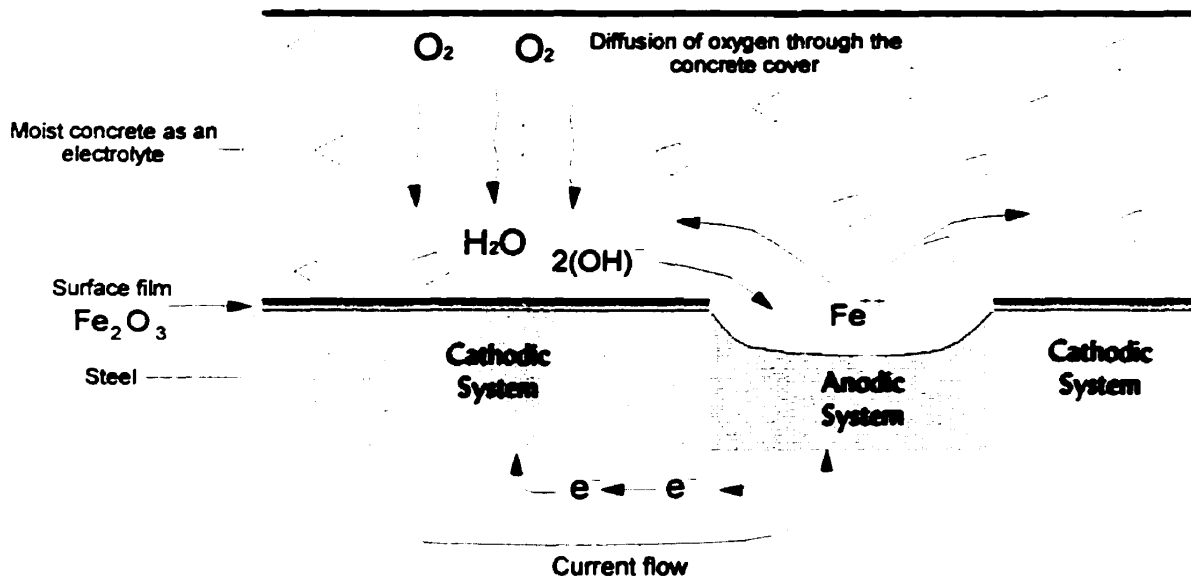
Figure 2-7: *Corrosion process[48]*

The above steps can be summarized as follows[53-58]:

OXIDATION (anodic reaction)

$$Fe \rightarrow Fe^{2-} + 2e^- \qquad (2.3)$$

REDUCTION (cathodic reaction)

$$O_2 + 2H_2O + 4e^- \rightarrow 4OH^- \qquad (2.4)$$
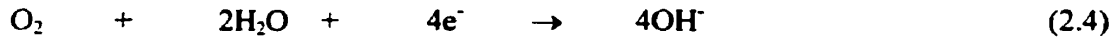
The intermediate reaction can be obtained by adding the partial anodic and cathodic reactions:

$$2Fe + 2H_2O + O_2 \rightarrow 2Fe^{2-} + 4OH^- \rightarrow 2Fe(OH)_2 \qquad (2.5)$$

Ferrous hydroxide [$Fe(OH)_2$] precipitates from the solution, however, this compound is unstable in an oxygenated solution and oxidizes to the ferric form as:

$$2Fe(OH)_2 + H_2O + \frac{1}{2}O_2 \rightarrow 2Fe(OH)_3 \qquad (2.6)$$
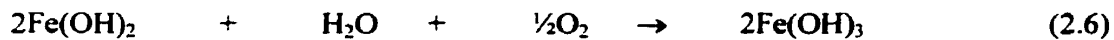
This final product, [$2Fe(OH)_3$], is known as rust[53].

2.3.2 Corrosion Rate-Determining Parameters

Once steel corrosion is initiated, the corrosion rate will depend on the ambient humidity, that is the concrete resistivity, and the availability of oxygen and water[22-24].

2.3.2.1 Electrical Resistivity of Concrete

The current which drives the anodic and cathodic reactions flows through a medium called the electrolyte. In order for the electrochemical reaction to occur, a potential difference must exist along the bar to drive the corrosion current through the concrete from the anodic site to the cathodic site. The magnitude of the corrosion current is controlled by the resistivity of the concrete[57].

The electrolyte conducts current primarily through ionic diffusion, and therefore it must have a specific minimum ion content and a minimum water content to allow the flow of ions[57]. The factors which influence the resistivity of the concrete are the pore structure and mineralogy of the

31

cement matrix, concentration of chlorides, and the moisture content[54]. If a material is dried, the conductivity decreases by several orders of magnitude for a change in its relative humidity (RH) from 100% to 50%, indicating that the degree of water saturation is a main controlling factor for the electrical resistivity of the concrete[22, 32]. This also indicates that the factors controlling the permeability of the concrete affect the electrical resistivity as well. When the RH increases, the resistivity is high, thus the corrosion current is quite small which inhibits corrosion[3, 57].

2.3.2.2 Water Penetration

The more permeable the concrete, the greater the availability of water at the cathode for the electrochemical reaction. Gonzalez et al[59] have shown that higher concentrations of water in the vicinity of the cathode will increase the rate of corrosion. This is supported by the Nernst equation (Equation (3.3)) which demonstrates that the corrosion rate increases as the concentration of the reactants increases. Also, the resistivity is dependent upon the degree of saturation.

2.3.2.3 Oxygen Diffusion

The presence of oxygen at the cathodic site is dependent on the permeability of the concrete. The corrosion process cannot occur without the availability of oxygen at the cathodic site[3]. The anodic corrosion reaction (Equation (2.3)) tends to decrease the steel potential and the cathodic reaction (Equation (2.4)) tends to increase it. This implies that the steel potential decreases with the availability of free oxygen in the concrete. The rate of corrosion increases as the concentration of oxygen increases at the cathodic site and it is also indicated by the Nernst equation (Equation (3.3))[59].

The impermeability of the concrete against oxygen increases with an increase in the relative humidity[22]. The cathodic process, which consumes oxygen can be the limiting factor in certain cases. With a high degree of water saturation, the electrical resistivity will be low, hence the rate of oxygen will be controlled primarily by the diffusion of dissolved oxygen through the wet concrete cover[22, 32]. This is true because both water and oxygen are needed for the corrosion of reinforcing steel to occur. The need for oxygen and water in the reaction leads to the common misconception that these two substances produce rust. Rust products are water containing compounds. Only oxygen is consumed to form rust. The oxygen diffuses through the concrete

cover towards the reinforcement and reacts with it, while water is needed only for the electrolytic process to occur within the concrete[55, 56]. When concrete surface layers are subjected to wetting and drying conditions, the corrosion rate is the highest. It should be noted that the electrolytic process cannot take place in a dry environment and oxygen cannot penetrate in a water saturated concrete, therefore, these two extreme conditions do not favour corrosion.

2.3.3 Forms of Corrosion

Corrosion of reinforcement can take different forms, ranging from widespread general (uniform) corrosion to very localized attack[32, 33, 53]. The type of corrosion is determined by the prevailing environment and the rate of corrosion, by the degree of polarization of anodic or cathodic processes and their potential differences, or the electrical resistance of the cement matrix[53].

For corrosion to occur, a difference in the electrochemical potential at the steel-concrete interface is needed[60]. Non-uniformity within the electrolyte, or between the anode and cathode can produce a cell with a different potential. Dissimilar metals, oxygen concentrations and temperature differentials are examples of such non-uniformities[57]. The differences in electrochemical potential can also arise from the differences in the environment of the concrete, for example, when part of a structure is saturated and a part is exposed to periodic wetting and drying. Substantial difference in the thickness of the concrete cover to a steel system which is electrically connected is a situation where this can occur. Variation in salt concentration in the pore water, or due to a non-uniform access to oxygen, can produce cells with different potentials[32].

2.3.3.1 Pitting Corrosion

The mechanisms by which chloride ions act as a catalyst for the loss of the protection afforded by the passive film are not well understood, however, two theories have been addressed by Foley[60] and appear most often in literature. According to the adsorption theory, the chloride ions become incorporated in the passive film, replacing some of the oxygen held within the passive film, which causes the film to become unstable[3, 21, 60]. On the other hand, the oxide film theory states that the passive film contains inherent defects and pores. Chloride ions penetrate the film at these sites more readily than other anions present in the pore solution[3, 60]. However, both mechanisms

suggest that the breakdown of the passive film occurs locally, which results in the creation of macro-galvanic cells[60].

For pitting corrosion to occur four conditions must be fulfilled[33]:

• A local breakdown of the passive film;

• A low concrete resistivity;

• Migration of chloride ions to the anodic sites and a reduction in pH; and

• Sufficient overall oxygen transport to the steel to support a high localized corrosion rate.

The anodic and cathodic reactions are separated with larger cathodic areas supporting small concentrated anodic areas. Such a macrocell is usually associated with high levels of moisture giving low electrical resistance in the concrete and easy transport of ions so the anodes and cathodes can be separated. Chloride induced corrosion is particularly prone to macrocell formation as a high level of water is usually present to carry the chlorides into the concrete. The presence of high level of water in the pores results in a higher conductivity allowing the separation of anode and cathode as the ions can move through the water filled pores[33]. Localized corrosion is also favoured by the presence of chloride ions, because as a local drop in pH occurs at the anode, a soluble complex of iron chloride forms progressively lowering the pH value at the pit (Figure 2-8). The cathodic area retains a high alkalinity, thus further localizing corrosion[21, 23].
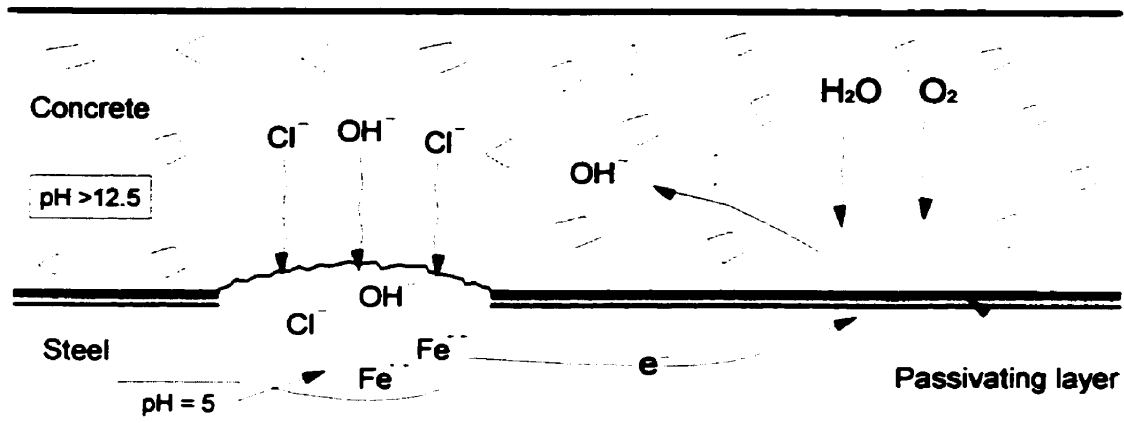
Figure 2-8: *Schematic representation of pitting corrosion (in the presence of chlorides)*[23]

The reactions involved are as follows[32]:

$$Fe^{2-} \quad + \quad 2Cl^- \quad \rightarrow \quad FeCl_2 \qquad\qquad (2.7)$$

$$2FeCl_2 \quad + \quad 2H_2O \rightarrow \quad Fe(OH)_2 \quad + \quad 2HCl \qquad (2.8)$$

Thus, Cl⁻ is regenerated so that the rust contains no chloride, although ferrous chloride is formed as the intermediate stage.

Pitting starts on horizontal surfaces and instead of spreading laterally along the reinforcing bar, the corrosion continues at the local anodic area causing the development of deep pits[21]. The volume of corrosion products generated may be insufficient to cause surface cracking, and it is possible that there could be eventual severance of the bar with very little prior warning from visible signs on the surface.

2.3.3.2 General Corrosion

General corrosion is normally characterized by (a continuos corrosion observed) a reaction which proceeds uniformly over the entire surface of the metal. All points of the surface corrode at a similar rate because corrosion occurs on a microcell level. This occurs when the concrete is generally drier not allowing the separation of the anode and cathode as ions cannot move a large distance as shown in Figure 2-9[33].
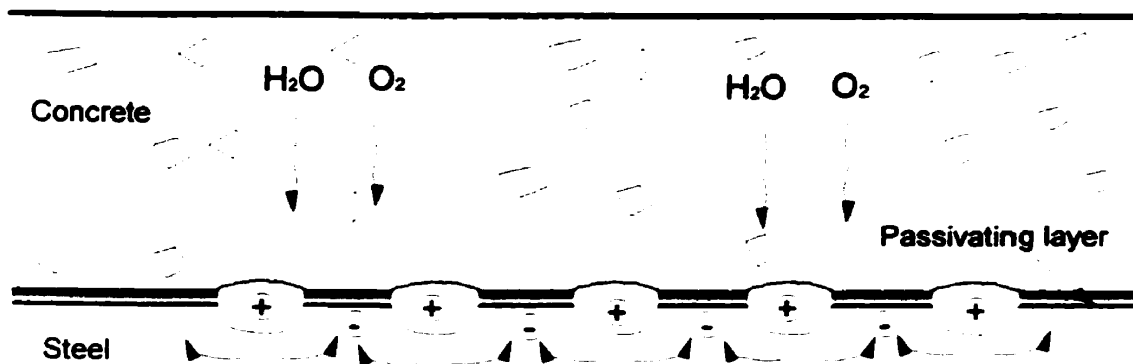
Figure 2-9: General corrosion[33]

External signs such as cracking, rust staining and spalling of the concrete occur as a result of the general corrosion[32, 33]. There is usually sufficient warning, hence this form of corrosion is not as dangerous as the pitting corrosion.

3 Measurement of Corrosion and Influencing Factors

3.1 Introduction

In the previous chapter, the various stages in the corrosion process were identified and the effects of the various influencing factors were discussed. The different ways of quantifying these parameters will be discussed in this chapter, to provide a critical evaluation of the existing methods for assessing the condition of concrete bridge components. It will focus on methods that are able to detect damage resulting from the corrosion of steel in concrete, and the poor quality of deteriorated concrete. The discussion of the techniques is limited to those being used presently for field evaluation purposes.

3.2 Monitoring Corrosion Activity

An introduction to the electrochemical principles that describe the corrosion process of steel was presented in the previous chapter. This will be expanded as a necessary requirement for interpreting the results of the various corrosion measurements.

3.2.1 Metals in Equilibrium

While considerations of equilibria are irrelevant to the study of corrosion, the equilibrium state of the system must be known for an appreciation of the various factors entering the non-equilibrium states and recognition of calculation of corrosion rates[56]. A metal in its processed state is thermodynamically unstable and if no external forces act on the system, it has a tendency to return to its natural state to reestablish equilibrium. Therefore, there is a natural spontaneous tendency of the system to transform to its lowest energy state[56].

3.2.1.1 Thermodynamic Aspects of Corrosion / Nernst Equation

The free energy difference, ΔG, is the energy necessary to transform the metal oxide into a processed metal. However, it may also be defined as the net free energy change for spontaneous corrosion to transform the metal into a hydrated iron n oxide as shown in Figure 3-1[58]. There is an energy barrier between the metal and the corrosion product, that is the activation free energy, ΔG^*. The magnitude ΔG^* determines the rate of the corrosion reaction as this energy represents the maximum energy to be exceeded by the metal atoms for the corrosion reaction to occur, and the environmental conditions have to provide this extra energy. At equilibrium, the free energy is zero and it is negative when it proceeds in the spontaneous direction[56, 58].
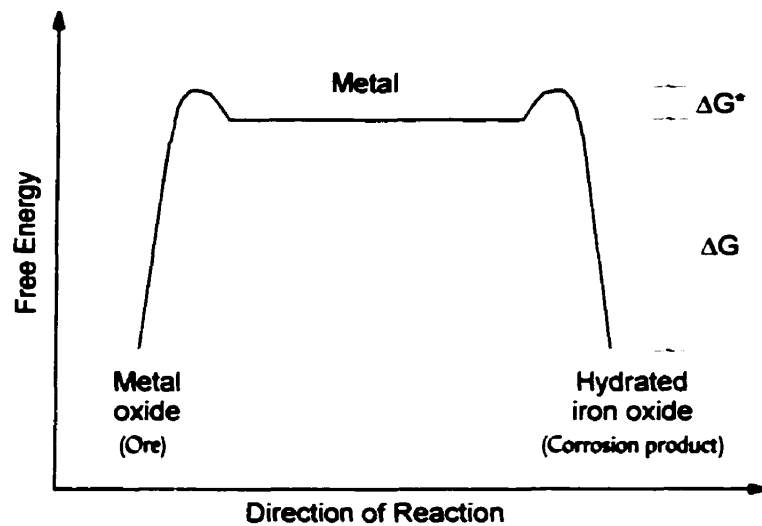
Figure 3-1: *Amount of free energy needed during corrosion reaction*[58]

The free energy change accompanying an electrochemical reaction can be calculated by the following equation[56, 58]:

$$Reactants^X + ne \Rightarrow Products^Y$$

$$\Delta G = \Delta G^o + RT \log \frac{(Reactants)^X}{(Products)^Y} \qquad (3.1)$$

where
n = Number of electrons (e^-) transferred during corrosion reaction;

R = Gas constant (8.314 $J.K^{-1}.mol^{-1}$);

T = Absolute temperature (K);

| *(Reactants)* = | Concentration of oxidized species; and |
| *(Products)* = | Concentration of reduced species. |

When the reaction is at equilibrium there is no change in free energy ($\Delta G = 0$). On the other hand, when all activities (concentration) of reactants and products are equal to unity, the logarithmic term becomes zero (log 1 = 0) and $\Delta G = \Delta G^o$. The free energy change is known as the Faraday's Law and can be expressed as follows[53, 55, 56, 58]:

$$\Delta G = -nF\phi_N \qquad (3.2)$$

where
| $\phi_N =$ | Measured potential; and |
| $F =$ | Faraday's constant (96500 C/eq). |

It follows that $\Delta G^o = -nF\phi_N{}^o$, where $\phi_N{}^o$ is the Standard Nernst potential (when all reactants and products are in their standard states and activities equal to unity). Equation (3.1) then becomes:

$$\phi_N = \phi_N^o + \frac{RT}{nF} \log \frac{(Reactants)^X}{(Products)^Y} \qquad (3.3)$$

The Nernst Equation is of great importance and practical significance because it facilitates the calculation of the electropotential of a corrosion reaction for any concentration of reactants and products at any temperature[53, 55, 56, 58].

The electrochemical reaction is accompanied by a potential, $\phi_N{}^o$, for the reaction to proceed spontaneously. These potentials are measured with respect to a standard which is the reduction of hydrogen ions where $\phi_{NH}{}^o = 0.000V$. The electrochemical series, which is an ordered list of each element accompanied by its reduction, is used to determine the anodic reaction in the overall electrochemical reaction. In any electrochemical reaction, the most negative reaction tends to be oxidation and the most positive one tends to be reduction[56].

3.2.1.2 The Exchange Current Density and Electrical Double Layer

A metal surface starts to dissolve to form ions as it comes in contact with a solution until equilibrium is reached. This situation constitutes an electrical double layer in a state of dynamic equilibrium, which will allow no further reaction to proceed until the equilibrium is disturbed[58].

This means that the dissolution continues until the equilibrium state is reached where the number of ions dissolving is equal to the number of ions depositing. Thus, the rate of dissolution and deposition reactions are in equilibrium. In terms of current density, this equilibrium is represented by the exchange current density, i_o, which is a ratio of the anodic to the cathodic area, and not an overall current[56]. The double layer theory is important because when the reinforcing steel comes into contact with the electrolyte solution within the concrete, a potential difference is established between the anode and the solution, that is $i_{dissolution}$ is equal to $i_{deposition}$, and for such a state of equilibrium, corrosion is not present[58].

3.2.2 Departure from Equilibrium

When a metal electrode is in equilibrium, the anodic dissolution current (i_a) and the cathodic deposition current (i_c) are precisely equal. No net reaction occurs; the extent of the ionic flux across the double layer is the exchange current density (i_o) and the equilibrium drop across the layer corresponds to $\phi_{N(cathode)}$ for the cathodic reaction and $\phi_{N(anodic)}$ for the anodic reaction[55, 56]. These are the so-called open-circuit potentials (no current through the cell).

When an electrode is no longer at equilibrium, there is a net balance of dissolution or deposition of the metal surface. The electropotential is altered, and the electrode is then said to be polarized. The extent of this polarization is measured by the change in electropotential across the double layer; this quantity defines the overpotential (η)[55, 56, 58].

3.2.2.1 Causes of Polarization

Polarization, η, is the potential change from the equilibrium electrode potential. The causes of electrode polarization fall two categories: activation polarization and concentration polarization[55]. At $\eta = 0$, there is no significant net reaction.

Activation Polarization

Activation polarization makes up 90% of the cases. It occurs when the rate of a reaction is controlled by the slowest of the steps in the reaction sequence, i.e., the electrochemistry of the system governs the rate[55]. The anodic and cathodic overpotential can be calculated as follows (Figure 3-2)[56]:

$$\eta_a = \phi_2 - \phi_{N(anode)} \qquad\qquad (3.4)$$

$$\eta_c = \phi_1 - \phi_{N(cathode)} \qquad\qquad (3.5)$$

For cathodic polarization, η_c, electrons are supplied to the surface, and a build up in the metal due to the slow reaction rate causes the surface potential, ϕ_1, to become negative to $\phi_{N(cathode)}$ (Figure 3-2). Hence, η_c is negative by definition (Figure 3-3)[53]. For anodic polarization, η_a, electrons are removed from the metal, a deficiency results in a positive potential change (Figure 3-2) due to the slow liberation of electrons by the surface reaction, and η_a must be positive (Figure 3-3). The potential difference of the polarized electrodes (position 1 to 2 in Figure 3-2) is equal to the current corresponding to current density, i_l, multiplied by the total resistance of both the external metallic resistance (R_m) and the internal electrolytic resistance (R_e). On short-circuiting, the current density becomes maximum (i_{max}). Then R_m can be neglected and the potential difference of both electrodes decreases to a minimum of $I_{max}R_e$ which is termed as an IR_{drop} (Figure 3-2).
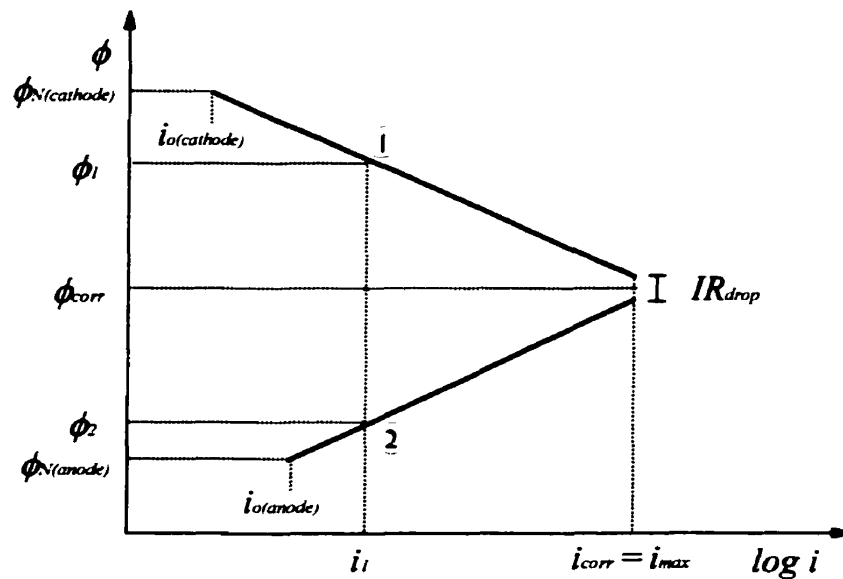
Figure 3-2: Electropotential vs. Current density[56]
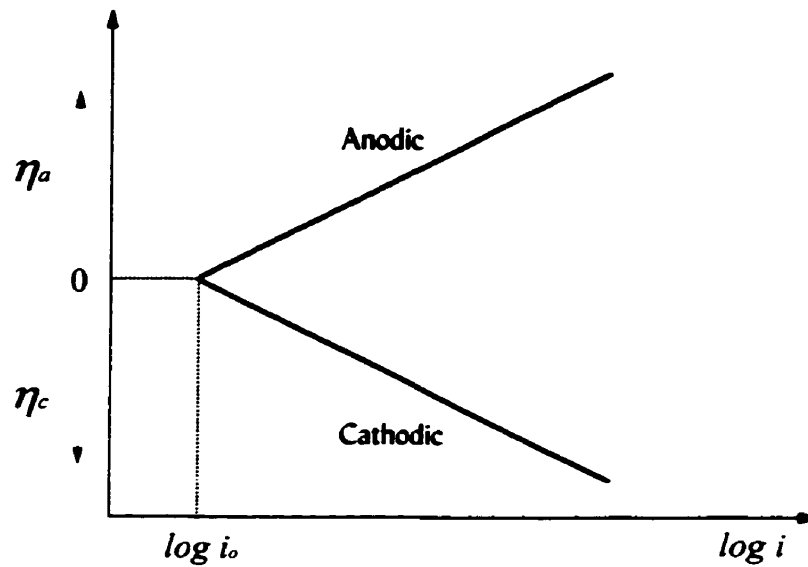
Figure 3-3: *Polarization curves*[53]

Polarization is an extremely important parameter that helps to determine the rate of corrosion. In activation polarization, both reduction and anodic reactions display Tafel behaviors, that is they both behave linearly (Figure 3-3). The relationship between activation polarization or overpotential, η, and the rate of the reaction presented by corrosion current density, i_{corr} is given by Tafel's Equation[53]:

$$\eta_a = \beta_a \, log \frac{i_{corr}}{i_{o(anode)}}$$

$$(3.6)$$

for anodic polarization, and,

$$\eta_c = \beta_c \, log \frac{i_{corr}}{i_{o(cathode)}}$$

$$(3.7)$$

for cathodic polarization, where β_a and β_c are Tafel constants[56].

Concentration Polarization

In concentration polarization, the concentration of the reduced species changes between the electrolyte adjacent to the metal surface and the bulk electrolyte. At high rates, the cathodic reduction depletes the adjacent solution of the dissolved ions[55]. Only the cathodic reaction is

41

affected, while the anodic reaction exhibits Tafel behavior. A typical concentration polarization diagram is shown in Figure 3-4.
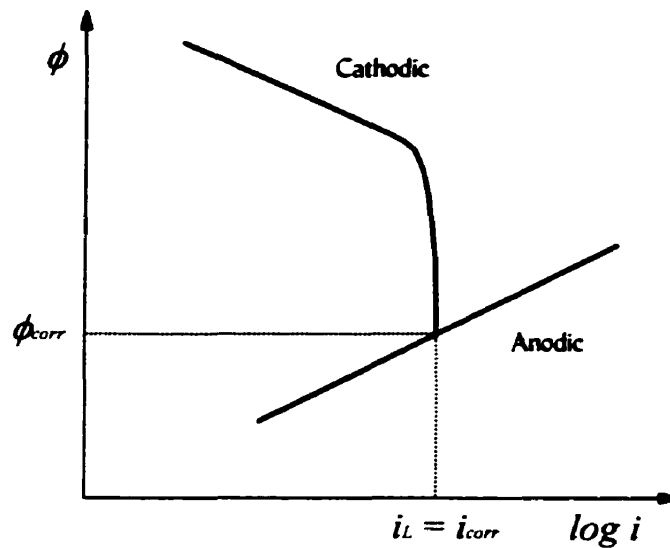
Figure 3-4: *Concentration potential curve*[56]

The rate of mass transfer of the ions controls the rate of reaction. The maximum expected current in concentration polarization is called the limiting current, i_L[55, 56]. When concentration polarization governs, i_{corr} is smaller that it would be if activation polarization governs as shown in Figure 3-4. The limiting current is calculated as follows[55]:

$$i_L = knF[C]_b \tag{3.8}$$

where $k =$ Mass transfer coefficient (cm/sec);

$n =$ Number of electrons transferred in the reduction;

$F =$ Faraday's constant (96,500 C/eq); and

$[C]_b =$ Concentration of reduced species (in the bulk electrolyte).

Concentration polarization usually governs in cases where the solution is stagnant. The rate of the reaction depends on how quickly certain species are capable of diffusing through the stagnant solution towards the metal surface where corrosion occurs[55]. When the solution is stagnant, the initial condition is represented by Figure 3-5(a). However, with a depletion of ions, a boundary layer forms which is only a few millimeters thick (Figure 3-5(b)). The concentration of the reacting ions in the boundary layer varies from the concentration in the bulk electrode $[C]_b$ to zero.
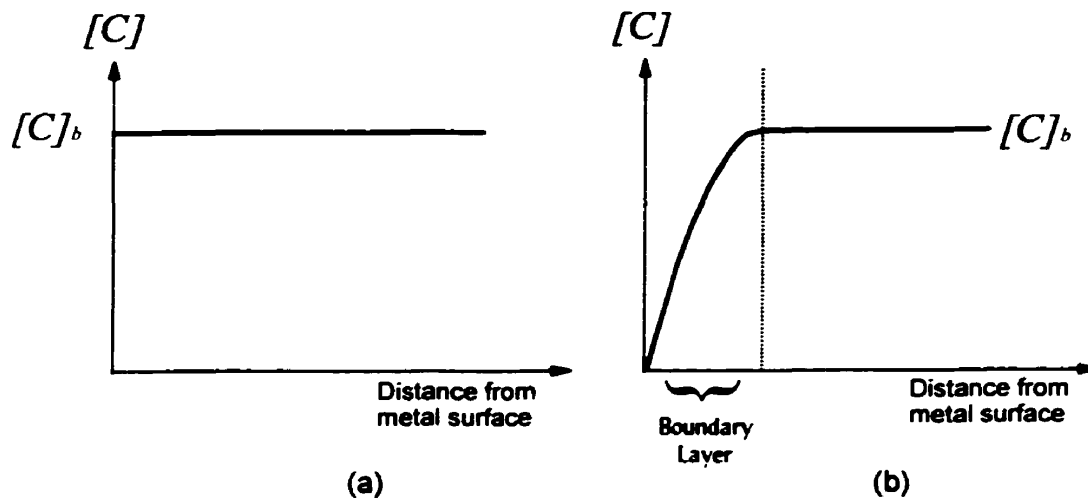
Figure 3-5: *Distribution of [C] with time*

3.2.2.2 Determining the Rate of Corrosion

Corrosion rates are determined by studying the polarization of the two reaction halves (Equations (2.3) and (2.4)). The polarization diagrams of corroding metals, called Evans diagrams, are graphs of potential versus log currents or log current density ($I_{corr} = i_{corr}A$, where A is the surface area of the anode). The values of I_{corr} and ϕ_{corr} are obtained from the intersection point between the anodic and the cathodic lines of polarization diagrams. The shape of the polarization lines are determined by either the concentration or activation polarization, as discussed previously.

The density corrosion rate (i_{corr}) is one way of expressing the rate of corrosion. Other ways of expressing the corrosion rate are summarized in Table 3-1. It is useful to have an expression with familiar units, which can be converted easily to service life in years, or depth of penetration[56].

Table 3-1: *Rates of corrosion*[56]

Phenomena or Ratios	Units
Weight change	$mdd = mg / (dm^2 \cdot day)$
	in / yr
	mm / yr
	μm / yr
	mpy = 0.0254 mm / yr
Corrosion current density	mA / cm^2

3.2.2.3 Influence of Polarization on Corrosion Rate

Both the resistance of the electrolyte and polarization of the electrodes limits the magnitude of current produced by a galvanic cell[55]. When polarization occurs mostly at the cathode, the corrosion rate is said to be cathodically controlled (Figure 3-6(a)). The corrosion potential is near the open circuit anode potential. When polarization occurs mostly at the anodes, the reaction is considered to be anodically controlled (Figure 3-6(b)). The corrosion potential is close to the open-circuit potential of the cathode. Resistance control occurs when the electrical resistance is so high that the resultant current is not sufficient to polarize anodes or cathodes (Figure 3-6(c)). The corrosion current is then controlled by the IR_{drop} through the electrolyte. It is common for polarization to occur in some degree at both anodes and cathodes. This situation is described as mixed control (Figure 3-6(d))[55].

3.2.3 Predicting Corrosion Behavior Using Polarization Diagrams

Different environmental variables are considered from an electrochemical point of view to visually understand and predict the corrosion behavior. The effects are considered for both activation and concentration polarization[55].
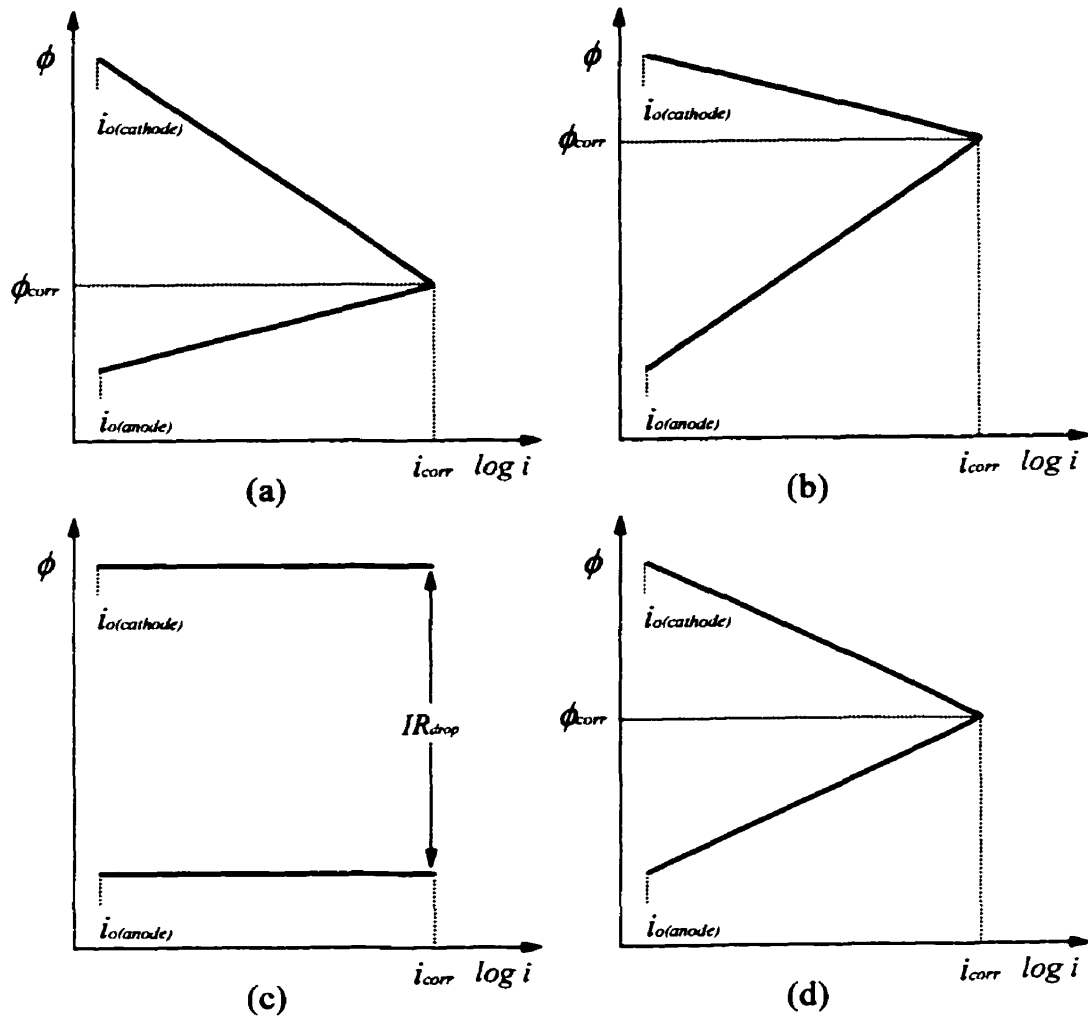
Figure 3-6: Types of corrosion control[55]

3.2.3.1 Oxygen Pressure

As the value of the partial pressure of oxygen (P_{O2}) changes, it affects the value of the Nernst potential, ϕ_{NO2}[56].

$$\phi_{N_{O_2}} = \phi_{N_{O_2}}^o + \frac{2.303RT}{4F} log \frac{P_{O_2}}{[OH]^4} \qquad (3.9)$$

where the terms R, T, F are defined in Equation (3.3) and [OH] is the concentration of the reduced species in Equation (2.4). As the value P_{O2} increases, the value of ϕ_{NO2} increases. As a result, the

45

cathodic line shifts upwards as shown in Figure 3-7(a). In the case of concentration polarization, as P_{O2} increases, so does the value of concentration of oxygen $[O_2]$ and this leads to an increase in i_L (Equation (3.10). Therefore, the vertical portion of the cathodic reaction is shifted to the right (Figure 3.7(b))[55, 56].

$$i_L = knF[O_2]_b \qquad (3.10)$$

For both activation and concentration polarization, the results of increasing P_{O2} are as follows:

- Increase in i_{corr} and ϕ_{corr}; and

- No change in i_o and in the anodic line.
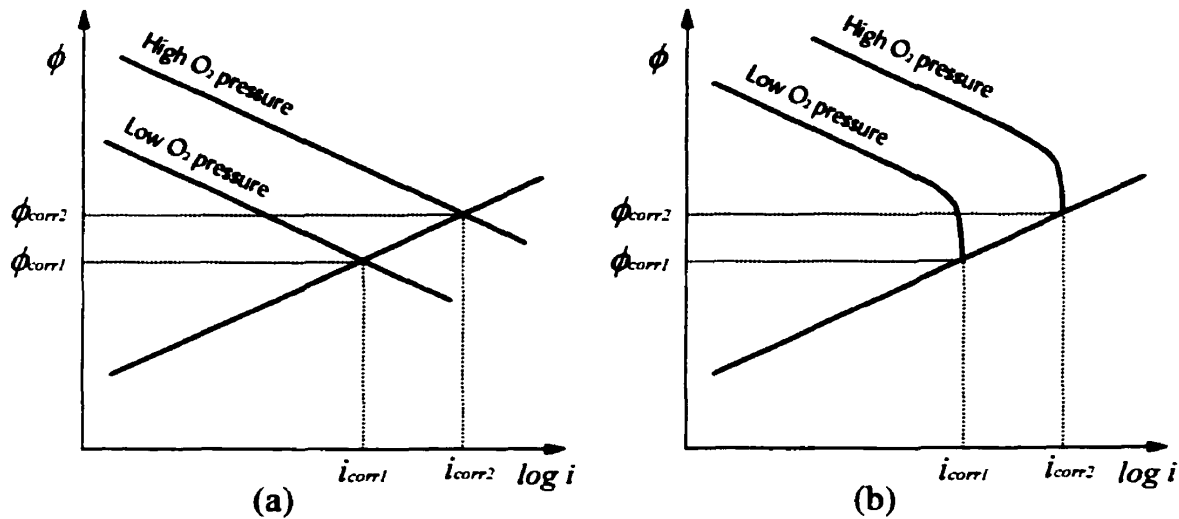
Figure 3-7: *Influence of oxygen pressure in activation and concentration polarization*[55, 56]

3.2.3.2 Oxygen Solubility

As the P_{O2} is kept constant, the solubility varies depending on the presence of impurities such as chloride ions in the aqueous medium as shown in Figure 3-8. The solubility of O_2 does not affect the corrosion reaction for the case of activation polarization; there is no change in the electropotential (Equation (3.9)). Where concentration polarization governs, an increase in the concentration of dissolved O_2 causes an increase in i_L (Equation (3.10)). Consequently, there is an increase in i_{corr} and ϕ_{corr}.
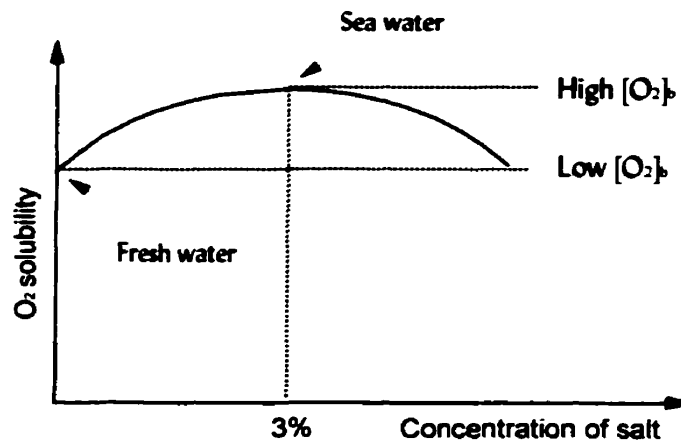
Figure 3-8: *Variation of O_2 solubility with salt concentration* [55, 56]

3.2.3.3 Anode / Cathode Surface Area Ratio

The overall anodic current (I_{anode}) is always equal to the overall cathodic current ($I_{cathode}$) in any corrosion process. A corrosion reaction, depending on the anode/cathode surface area ratio, can manifest itself as a uniform attack or a non-uniform attack (Figure 3-9).
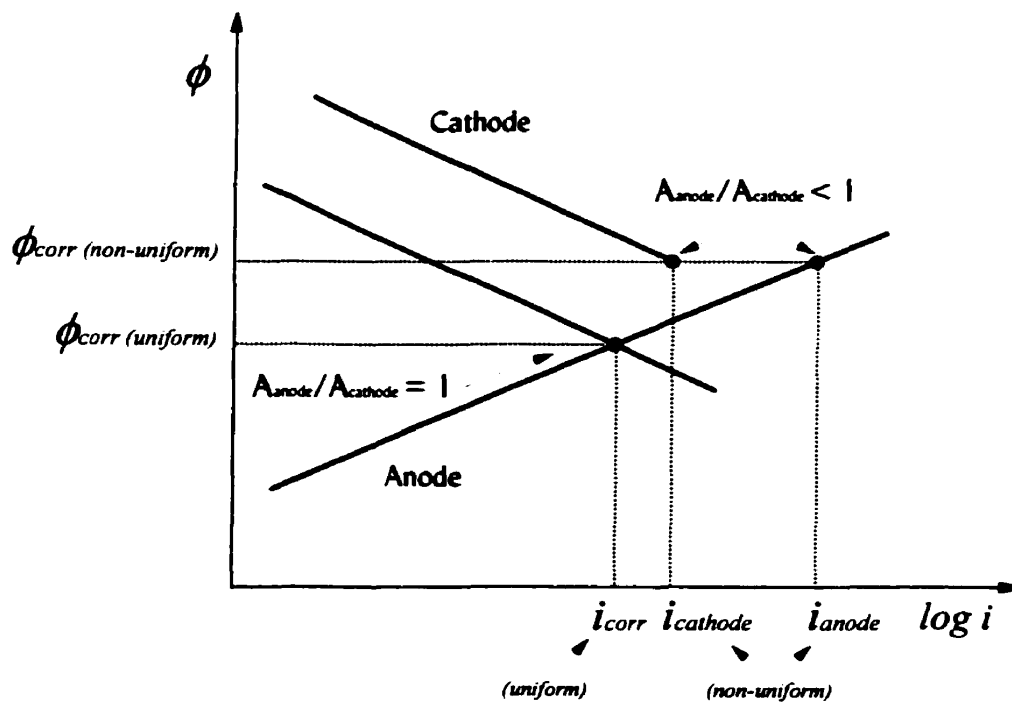
Figure 3-9: *Effects of anode/cathode surface area ratio on corrosion reaction* [55, 56]

47

Uniform Attack

This form of corrosion has been previously described in Section 2.3.3.2. In this type of corrosion, the area of cathode is approximately the same as the area of the anode $(A_{anode}/A_{cathode} = 1)^{[55]}$.

Non-uniform Attack

There is a dominance of the cathodic surface area over the anodic surface area in a non-uniform attack. This was previously mentioned as pitting corrosion section (Section 2.3.3.1). In order to respect the basic rule, that is $I_{anode} = I_{cathode}$, the anodic current density should be much larger then the cathodic current density. As a result, the corrosion rate at the anode is larger and more significant than that at the cathode (Figure 3-9)$^{[55]}$.

3.2.3.4 Passivity

Passivity is the property underlying the useful natural corrosion resistance of structural metals, including stainless steel. Steel on its own is not naturally passive. However, it can be made passive by exposure to passivating environments$^{[25]}$. The high alkalinity of the cement paste offers protection against corrosion of the steel reinforcement embedded in concrete. This protection is largely electrochemical in nature and its due to the existence of a self-generating protective layer at the steel/concrete interface. The protective layer has normally been considered to be a tightly adhering film of γFe_2O_3 $^{[60]}$. The passivity state has the advantage that the corrosion rate is much less than that the predicted by Tafel behavior$^{[55, 56]}$. Figure 3-10 illustrates a typical polarization line for a metal which exhibits passivity.

Three distinct regions can be discerned: the active region, the passive region and the transpassive region. In the active region, the metal exhibits Tafel behavior and it is the region limited by the Nernst potential ϕ_{NM} and the passive potential, ϕ_{pp}. The magnitude of i_{corr} in this region may vary from the exchange current density, i_o, and the critical current density, i_C. In the passive region, the dissolution rate decreases and it is only achieved within the potential, ϕ_{pp}, and the transpassive potential, ϕ_{tp}. As it can be seen in Figure 3-10, the lower is the values of i_p, the lower is the value of i_{corr} obtained when the intersection of the two polarization lines occurs within the passive region. The transpassive zone occurs when an increase in the electropotential occurs and the dissolution rate increases. The breakdown of passivity begins at ϕ_{tp}, where the passive layer is no longer stable and begins to disintegrate$^{[55, 56]}$.
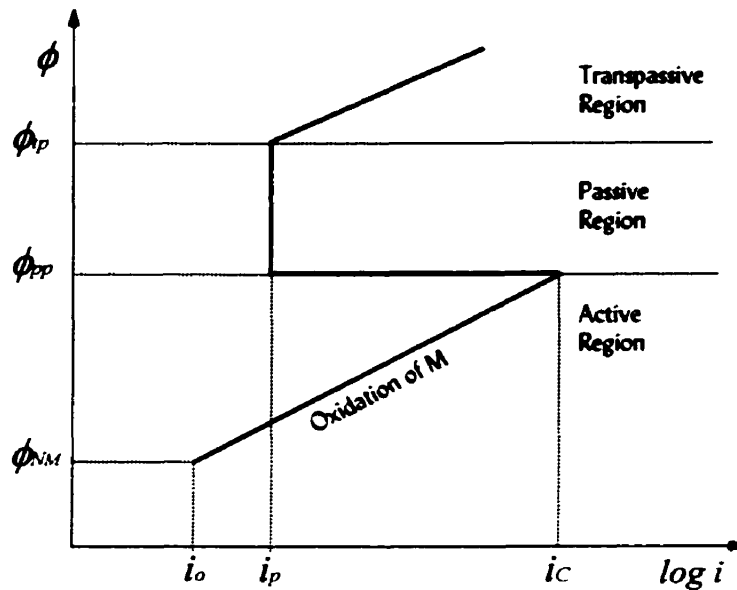
Figure 3-10: *Polarization diagram of a metal exhibiting passivity*[55, 56]

3.2.4 Measuring Corrosion and Corrosion Rate

Since corrosion is an electrochemical process, it is rational to monitor it using electrochemical techniques[33, 60]. These techniques are based on the basic principles explained above. The methods available to assess and monitor corrosion of steel in concrete which are appropriate for site work will be outlined. Emphasis is given to the use of in-situ electrochemical techniques since these offer advantages for both the inspection of existing structures and as an aid in engineering material research. Less reliance on destructive testing will encourage inspection of existing structures[62].

3.2.4.1 Potential Measurements

The corrosion of reinforcement is an electrochemical process dependent upon the establishment of a current flow between the anodic and the cathodic half-cells set up in the reinforcement, hence, the potential difference between the half-cells could provide an indication of the corrosion activity[63]. It is possible to measure the potential difference across the steel-concrete interface relative to a suitable reference electrode using a technique shown in Figure 3-11. A reference electrode provides a source of constant potential when used under defined conditions. In this way,

any change in the potential difference between a reference electrode and a steel-concrete interface can be ascribed to the steel-concrete double layer (double layer concept is explained in Section 3.2.1.2). The magnitude of the potential across the double layer at the steel-concrete interface depends, amongst other things, on the electrochemical reaction taking place, hence the presence of corrosion can be inferred from the half-cell potential[63].
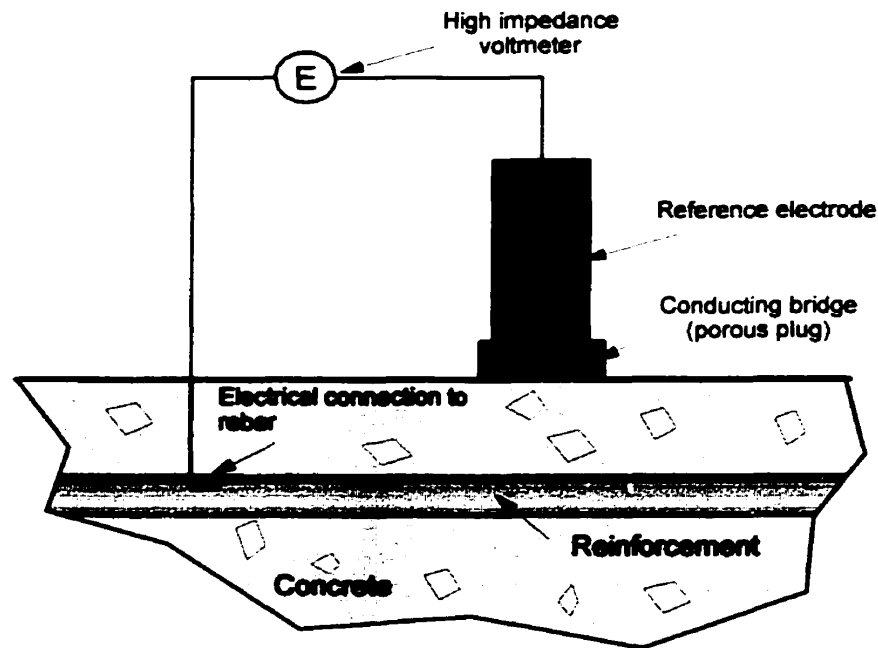
Figure 3-11: *Electrical circuit for measuring half-cell potentials*[62, 63]

Many types of reference half-cells can be used, such as copper/copper sulphate (CSE), silver/silver chloride, or a similar combination. In practice, for site work the CSE is the most durable and is sufficiently accurate[63]. The concrete functions as an electrolyte and it is anodic. The corroding regions of the steel reinforcement in the immediate vicinity of the test point may be related empirically to the potential difference measured by a high-impedance voltmeter (Figure 3-11)[62, 63]. The method is described in detail in ASTM Standard C876-80[64], the basis of which is that the corrosion potential of the rebar will shift in the negative direction if the surface changes from a passive to an active state. It establishes qualitatively the thermodynamics of the corrosion process, but not the corrosion rate. The half-cell potential measurement gives an indication of the corrosion risk of the steel and can be categorized as seen in Table 3-2. Care should be taken in applying these guidelines to different environmental conditions[62-64].

Table 3-2: *Criteria for interpretation of half-cell measurements[64]*

CSE Potential (mV)	Risk of Corrosion
> -200	< 10%
-200 to -350	50% (uncertain)
-350 to -500	50% to 90%
< -500	< 90%

In practice, this potential measurement can be influenced by the electrical characteristics (resistivity) of the concrete cover, due to its moisture content and salt content and the uniformity of these within the concrete[63]. These may show very negative potentials. The corrosion rate measurements may be required to determine whether the potential is an artefact or due to high corrosion rates. There has been a tendency to correlate half-cell potentials with corrosion rates. The half-cell is a mixed potential representing anodic and cathodic areas on the rebar. It is not a driving potential in the corrosion cell[33].

3.2.4.2 Measurement of Corrosion Rate

There are several methods of measuring the 'true', instantaneous rate of corrosion. Within the past 15 years there have been important advances in non-destructive electromechanical techniques for measurement of corrosion rates of steel embedded in concrete, each with certain advantages and limitations[33, 41, 61, 62]. They can be broadly divided into two categories, the first of these being measurements on the actual structural rebar and the second involving measurements on smaller, strategically positioned, embedded rebar probes. The former category is mostly of interest to engineers and will be discussed in this section. Successful applications have been reported on a number of methods including DC linear polarization and AC impedance[41]. These can monitor the corrosion rate of steel in concrete, whereas, mass loss or visual observation require destruction of the concrete to observe the bar.

DC Linear Polarization

The best known technique of evaluation of the instantaneous corrosion rate in the laboratory and in the field is called Polarization Resistance (or the Linear Polarization Resistance, LPR) test[33, 61, 62]. This test procedure is based on Stern-Geary characterization of the typical polarization curve

for the corroding metal. That is, a linear relationship is described mathematically for a region on the polarization curve in which slight changes in current applied to the corroding metal in the concrete cause corresponding changes in the potential of the metal. Simply stated, if a large current is required to change the potential by a given amount, the corrosion rate is high; on the other hand, if only a small current is required, the corrosion rate is low[65].

The technique involves imposing a small potential change, $\Delta\phi$ ($\phi_{corr} \pm$ 20mV), on a metal sample (Figure 3-12). The slope of the resulting *log* i vs. ϕ curve around ϕ_{corr} (i.e., the zero-current portion of the curve) is linear and is termed the polarization resistance (R_p)[66].

$$R_p = \frac{\Delta\phi}{\Delta i}$$

(3.11)
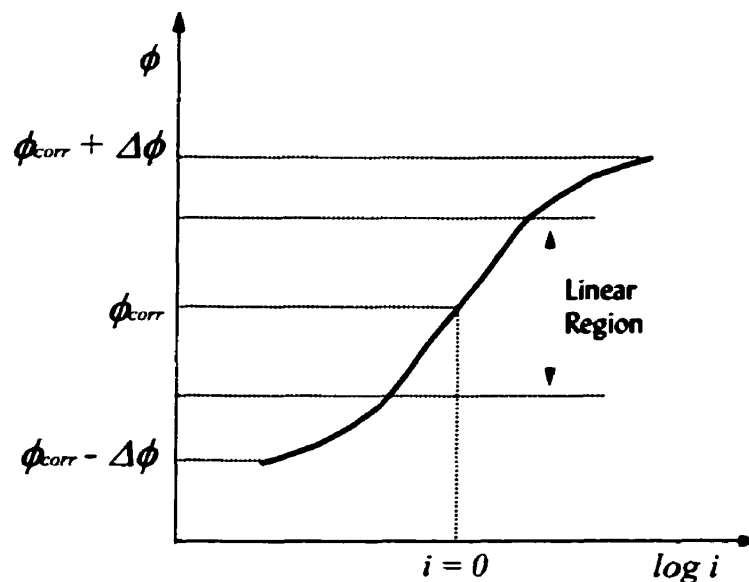
Figure 3-12: *Linear polarization curve*[66]

The corrosion current (i_{corr}) can be calculated from the relationship developed by Stern-Geary[67]:

$$i_{corr} = \frac{\beta_a \beta_c}{2.3(\beta_a + \beta_c)} \frac{\Delta i}{\Delta\phi} = \frac{B}{R_p}$$

(3.12)

where β_a and β_c are the anodic and cathodic Tafel slopes, respectively. It is noted that the Tafel constants are determined by the method of Tafel Extrapolation. The Tafel constants are the slopes

52

of the *log i* vs. ϕ from the polarization curves in the Tafel regions, i.e., the region where the curve is linear (Figure 3-13)[66].

Polarization scans using a greater $\Delta\phi$ ($\phi_{corr} \pm$ 250mV), need to be run independently to determine the Tafel constants, but acceptable Tafel regions are difficult to obtain on site. The experimental anodic polarization does not correspond to the idealization (Figure 3-13). In practice, the anodic data generally is curved on the semi-log plot, and no sensible linearity or value of β_a can be found. This is possibly due to the oxygen reduction or the passive film breakdown, which distorts the Tafel behavior in this region[66]. Consequently, the Tafel constants are estimated or assumed. As the value of the Stern-Geary constant (B value in Equation (3.12)) for concrete can range from 26 to 52 mV, this can result in an error by a factor of up to two[62]. However, the scale is logarithmic, therefore, such errors are less critical[33].
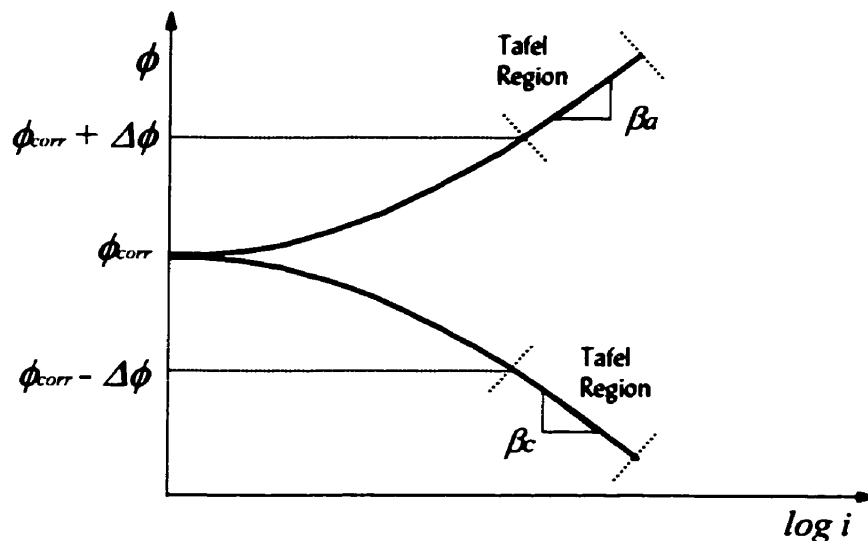
Figure 3-13: *Tafel regions[66]*

Knowing the i_{corr}, the rate of corrosion in mm/year can be calculated using Faraday's Law[66]:

$$m = \frac{Ita}{nF}$$ (3.13)

and, dividing Equation (3.13) through by t and by the surface area, A, yields the corrosion rate, CR (mdd):

$$CR = \frac{m}{tA} = \frac{ia}{nF} \qquad \qquad (3.14)$$

where $m =$ Mass in the reaction;

$F =$ Faraday's constant;

$a =$ Atomic weight; and

$n =$ Number of equivalents exchanged.

I_{corr} is found by $I_{corr} = A \; i_{corr}$, where A is the surface area of the steel bar that is perturbed by the test. Evaluating the area of measurement A is not simple. Some studies have been undertaken by Clear[65] (3LP device using a three-electrode linear polarization technique) who recommends using a large auxiliary electrode and assumes that the surface area of measurement is the shadow area of the steel reinforcement lying directly beneath the auxiliary electrode (Figure 3-14).

An alternative approach to calculate the R_p value, first developed by Feliu et al[68], is to accept that the perturbation current will spread laterally outside the shadow area and confine this lateral spread to a particular area by means of a probe known as the guard ring. The use of a second electrode located concentrically around the central counter confines the electrical signal to a defined region of the reinforced concrete structure. Both counter electrodes (central and ring) are maintained at the same electrical potential with regard to the working electrode (the rebar) and the current, which flows from the central electrode, is measured. Therefore, while the central counter polarizes the bar locally, another auxiliary electrode, concentric with the former, provides polarization to the rest of the bar around the area affected by the central electrode (Figure 3-15)[33, 61, 69].

Although the guard ring appears to be a simple solution, in reality, the practical problems posed by its application have not been completely resolved. The actual area polarized during measurement of R_p is smaller that the entire circumference of the rebar. When the concrete resistance, R_c, between the surface of the concrete and the steel reinforcing bar is high (IR_{drop}), this can result in significant errors in measuring R_p unless the internal electrolytic (concrete) resistance, R_c, is either electronically compensated, or explicitly measured and deducted from R_p[61, 62]. Another fundamental source of error, is the assumption of uniform rebar corrosion. It is known that actual reinforced concrete structures experience localized attack rather than a uniform attack. Confinement is obtained only when the measurements are carried out over the active part
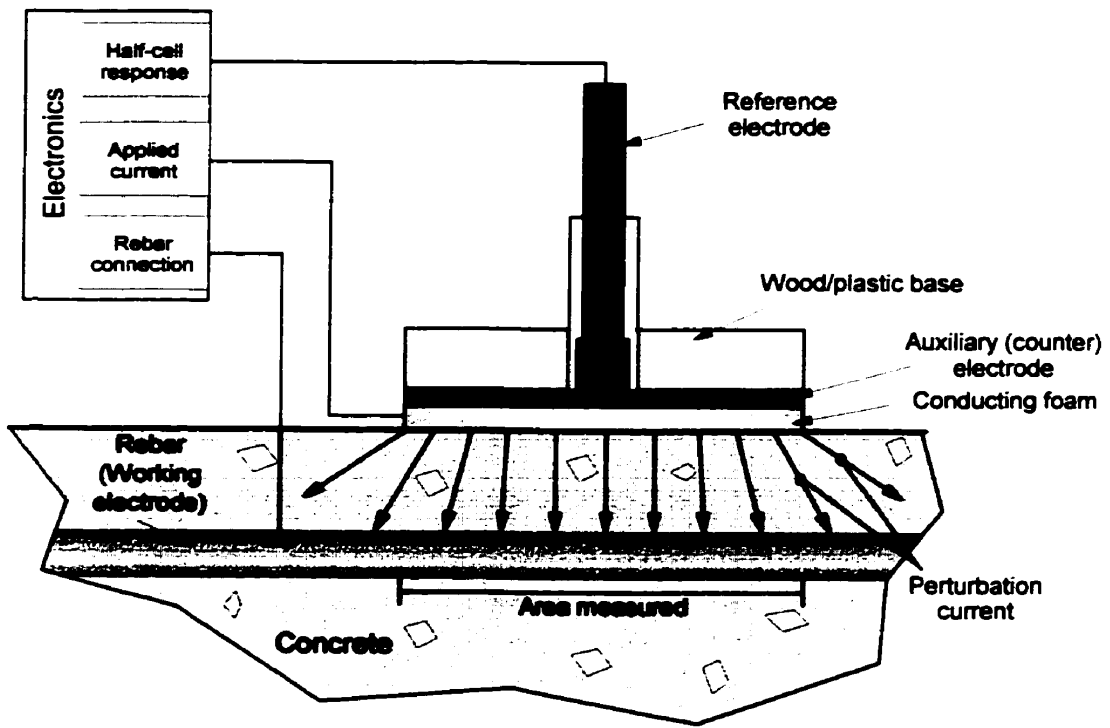
Figure 3-14: *Schematic of the setup for linear polarization*[33, 65]
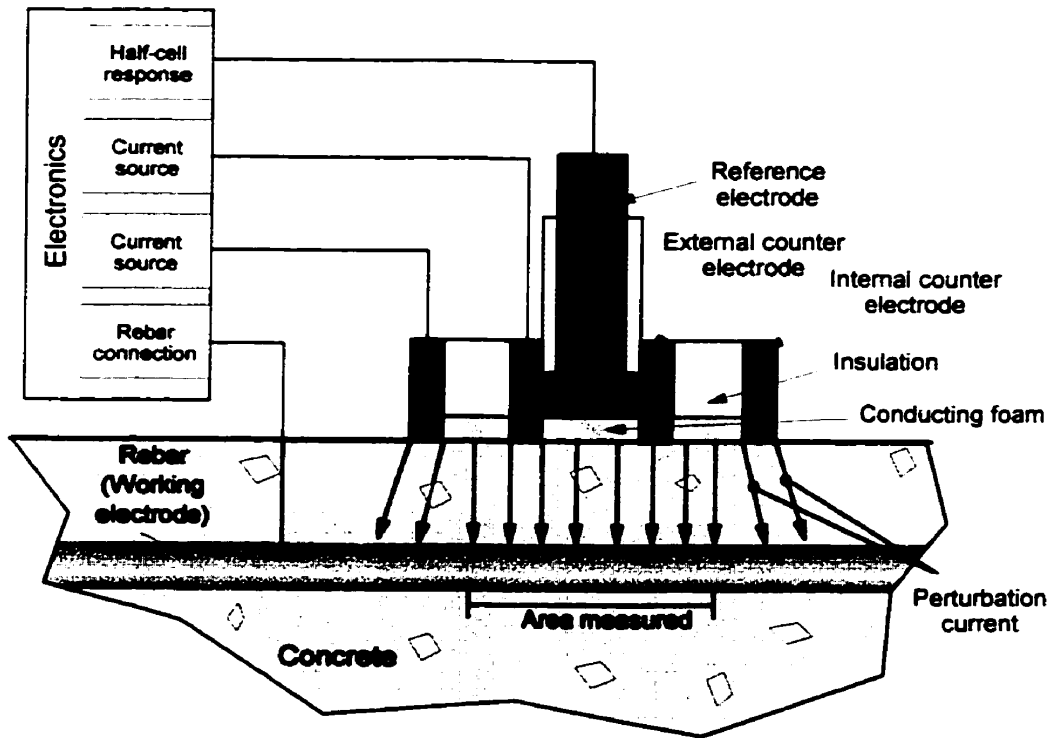
Figure 3-15: *Schematic of linear polarization device with controlled guard ring*[33, 68]

(which is surrounded by the passive part) of the macrocell. When measurements are made over the passive part (which is surrounded by the active areas), the confinement is poor[61].

This non-destructive technique represents a fast and simple measurement method. Although the LRP technique can be in error by a factor of two as suggested by Stern, its usefulness remains undisputed and the studies on its limitations have, on the contrary, enhanced its reliability. Through the measurement of hundreds of values in laboratory experiments and on real structures, it was possible to map the expected values of the corrosion current density and of the corrosion rate as a function of the risk level as listed in Table 3-3[62, 70].

Table 3-3: *Typical corrosion rates for steel in concrete*

Rate of corrosion	Corrosion current density, i_{corr} ($\mu A/cm^2$)	Corrosion rate, CR ($\mu m/year$)
High	10 to 100	100 to 1000
Medium	1 to 10	10 to 100
Low	0.1 to 1	1 to 10
Passive	< 0.1	< 1

AC Impedance

The AC techniques, commonly referred to as Electrochemical Impedance Spectroscopy (EIS) are equally well suited for use in rather low-conductivity environments. Hence, in principle, they should be capable of measuring the corrosion rate of steel in concrete[71]. It is possible to obtain information on the electrical resistivity and the dielectrical properties of the concrete cover, and on the corrosion rate. It involves measuring electrical impedance while scanning frequencies[61]. Based on the equivalent circuit for a rebar in concrete, at high frequencies, the impedance is due to the ohmic or uncompensated resistance, R_c, and at low frequencies it is due to the sum of this and the polarization resistance (R_p). The experimental data are commonly displayed using Nyquist or Bode plots[71]. Once R_p is known, the corrosion current is determined as before using Equation (3.12). A more accurate corrosion rate value should theoretically be obtained, compared with the more simplistic DC Linear Polarization analysis. However, EIS data generation and analysis generally requires specialist electrochemical knowledge and can be rather lengthy, making it unsuitable for rapid evaluation of the corrosion rates. To derive the corrosion rates, the Tafel constants also still have to be estimated or assumed.

Another evolving technique closely related to EIS measurements is harmonic analysis, which is performed in a narrow frequency range and the mathematical data treatment facilitates the computation of the Tafel constants and the corrosion rate. However, from the practical viewpoint of field application, a complete frequency scan is simply too time-consuming. Since only very low- and very high-frequency response data are needed in order to define the corrosion rate, any method developed for field use should scan only those regions[61]. A new AC Impedance method has been investigated in Japan to evaluate the on-site corrosion rate of steel rebars. Impedance values are measured at two frequencies: a high frequency of 100Hz and a low frequency 10 or 20mHz[72]. A severe restriction in AC Impedance analysis, as in the LPR technique, is that the fundamental assumption of uniform rebar corrosion has to be made in the calculation of penetration rates. This technique is a powerful tool and is quite promising, although it requires more expensive instrumentation and larger measurement times than DC measurements, particularly with small rates, which call for very low frequencies[69].

3.3   Measurement of Resistivity of Concrete

The rate of corrosion of steel in chloride contaminated concrete depends on both the permeation properties and the electrical conductivity of the near surface concrete. Therefore, measurement of these properties on site is important to predict the service life of reinforced concrete structures exposed to chloride environments. Suitable testing techniques have been developed or refined so that the electrical resistivity of the near surface concrete can be determined on site.

Corrosion is an electrochemical phenomenon, hence, the electrical resistivity of the concrete will have a bearing on the corrosion rate of the steel embedded in concrete, as an ionic current must pass from the anode to the cathode for corrosion to occur. The electrical resistivity is an indication of the amount of moisture in the pores, and the size and tortuosity of the pore system. Resistivity of a material is defined as the resistance of a cube of one unit in size. Hence the resistivity (ρ) of a prismatic section of length L and section A is given by $\rho = R_cA/L$ where R_c is the concrete resistance. However, cutting cores from a concrete structure in order to determine the resistivity is not a practical proposition[73].

3.3.1 Wenner Probe

Electrical resistivity tests have been used for soil testing for many years using the Wenner four-probe technique. Specialized modifications of the Wenner probe are frequently used for measurement of concrete resistivity on site[33, 62, 73]. A schematic is shown in Figure 3-16.

It is used by pushing the electrodes directly onto the concrete with conductive gel to enhance the electrical contact. A low frequency alternating current, I, is passed between the outer electrodes and the voltage drop, ΔV, is measured between the inner electrodes. For an electrode spacing of s, the apparent resistivity, ρ, of a homogenous, semi-infinite material is given by[73]:

$$\rho = 2\pi s \left(\frac{\Delta V}{I} \right) = 2\pi s R_e \qquad (3.15)$$

By Ohm's Law, the ratio $\Delta V/I$ represents the measured resistance, R_e, of the concrete.
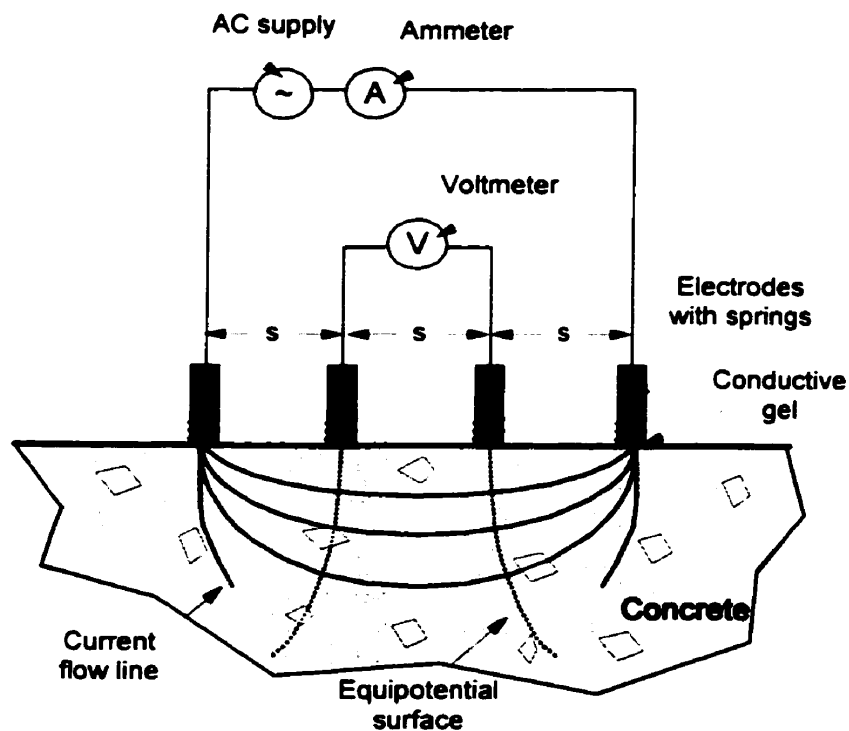
Figure 3-16: *Wenner probe set-up*[73]

58

3.3.1.1 Practicability and Reliability of Test

The four-point resistivity method promises to be a very effective technique in assessing the severity of corrosion problems in a quick and non-destructive manner. The measurement of the electrical resistivity is usually carried out to assist the half-cell potential measurements. Although many researchers have used the electrical resistivity measurements in in-situ investigations, the influence of moisture and temperature on the data obtained limits its application in corrosion investigations[33, 62]. Laboratory studies have shown a clear link between the resistivity of the concrete and the rate of corrosion of steel reinforcement. However, the errors that occur in in-situ measurements can make a correlation between these measurements and the rate of active corrosion meaningless, if these errors are not eliminated or compensated. In the absence of further research, a general guideline summarized in Table 3-4 has been offered by Millard[62, 73].

Table 3-4: *Typical empirical resistivity threshold[73]*

Probable corrosion rate	Resistivity, ρ (kΩ.cm)
Very high	< 5
High	5 to 10
Moderate/Low	10 to 20
Low	> 20

Apparent electrical resistivity is affected by many factors including electrode characteristics, element geometry, surface layers and reinforcing bars within the test zone as well as environmental factors such as moisture conditions and temperature. The results are again most usefully presented in the form of contour plots, to be interpreted alongside the half-cell potential test results[73].

An alternative to this technique is to use Electrochemical Impedance Spectroscopy, by applying an alternating current over a range of frequencies, the measured impedance can be related to various elements of the circuit depending on the frequency. The concrete resistance is one variable that can be determined, but, as mentioned earlier, the technique is slow and the equipment is expensive.

3.4 Measurement of Chloride Penetration into Concrete

Over recent years, an increasing amount of premature steel corrosion in concrete structures has created a significant problem. Most of this corrosion is due to an uncontrolled penetration of chlorides from the surrounding environment. This is partly due to the increasing use of deicing salts and partly due to an increasing amount of concrete construction in the marine environment. Therefore, there is a great need for better quality parameters and test methods, which can characterize the resistance of concrete against chloride penetration. This is important for both job specification and control of in-situ quality as well as for estimation of service life.

Depending on the environmental conditions, chloride ions penetrate concrete through various mechanisms such as diffusion, permeation and capillary suction. In general, capillary suction may dominate the penetration through a surface layer of the concrete, which is very porous and only partly water saturated. However, for a very dense concrete in a moist environment or for concrete which is more or less continuously wet, a diffusion mechanism may dominate[36, 37]. Hence, the resistance of concrete to the transport of chloride ions is defined by the coefficient of diffusion. Different procedures and methods for testing chloride diffusivity of concrete are reviewed briefly and discussed in the following sections.

3.4.1 Standard Diffusion Cell Test

The procedure to find the coefficient of diffusion from a standard diffusion test is well established[39]. The technique employs a diffusion cell and calculation of an effective diffusion coefficient based on the diffusion of the selected ion through a thin slice of concrete, which is placed between a chloride source solution (solution A) and a neutral solution (solution B) as shown in Figure 3-17(a)[74]. A concentration gradient across the test sample is applied, until a steady state diffusion is reached (Figure 3-17(b)). The ionic flux is determined by measuring the increase in chloride ions in the downstream solution[75]. It is important that the chloride source solution is maintained constant to achieve and maintain steady state conditions.

(b) Diffusion test arrangement

(b) Steady state diffusion
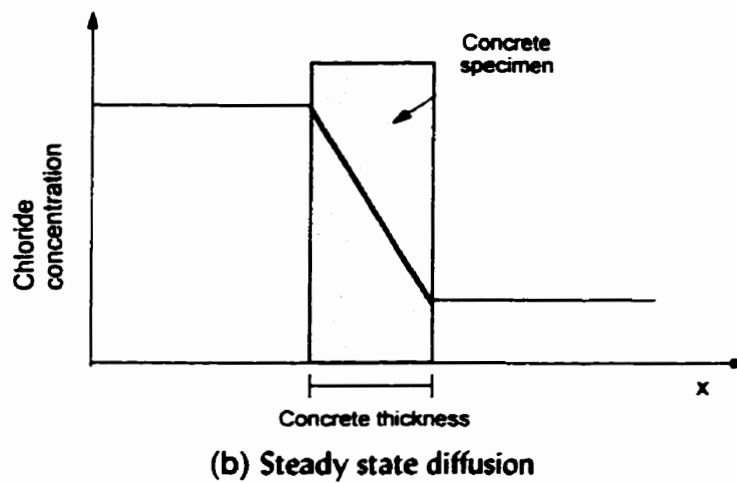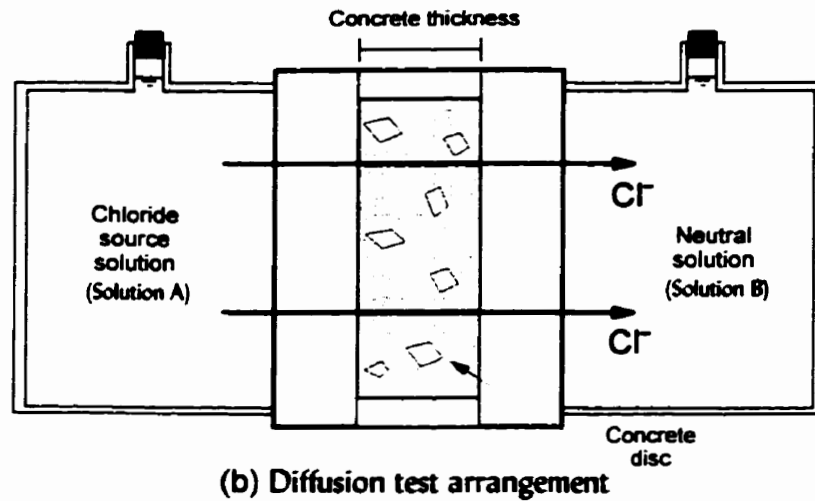
Figure 3-17: *Schematic diagram of standard diffusion cell*[74]

3.4.1.1 Mathematical Modeling

Fick relates the mass of ions diffusing through a unit area per unit time during the steady state of flow to the concentration gradient with the coefficient of diffusion, as follows[76, 77]:

$$J = -D\frac{dc}{dx} \tag{3.16}$$

where
$J =$ Ion flux entering solution B (moles.cm^{-2}s^{-1});

$D =$ Effective diffusion coefficient (cm^{-2}s^{-1}); and

$dc/dx =$ Concentration gradient through the specimen (moles.cm^{-3}s^{-1}).

3.4.1.2   Practicability of Test

This method has become a standard for determining the chloride diffusion coefficient and typical values of chloride diffusion coefficients are supplied by the Concrete Society[27]. However, the technique does have several drawbacks when used to monitor changes in diffusion rates on site:

* The test duration may take relatively long period (typically 12-15 months) to achieve a steady state of diffusion;

* In order to use this method for in-situ concrete, cores must be extracted and sliced to suitable thickness, hence it is destructive and expensive; and

* As the cores are extracted, the values obtained in lab might not be representative of the real conditions on site.

3.4.2   Chloride Concentration Profile Test

The ingress of the chloride ions into the concrete from its environment will increase the chloride concentration of the concrete in its surface layers. The graphical presentation of the chloride concentrations versus the distance perpendicular to the concrete surface is called the chloride profile[37]. The chloride ion diffusion can be monitored directly by analyzing the concrete under consideration at various depths after exposure to a chloride solution, thereby producing a concentration profile[74]. This method can be applied to in-situ concrete structures. Drilled dust samples are taken at predetermined depths perpendicular to the exposed concrete surface. By collecting the dust from the various depths separately, it is possible to determine how the chloride content changes with the depth from the surface.

3.4.2.1   Determination of Chloride Content

There are many commonly used techniques for the chloride analysis of concrete. The Volhard (BS 1881: Part 124) and the potentiometric titration (AASHTO T260-84) methods are both extremely accurate and give results close to the actual chloride contents[78]. However, they are both arduous, time-consuming, and expensive. Alternative methods for measuring acid-soluble chloride contents have been developed such as the specific ion probe, spectrophotometer, digital titrator and Quantab titrator strips. All these methods have been investigated and the selective ion

probe has been proven to give accurate results. Results based on the samples from the field indicated that it has strong correlations with AASHTO T260 for the lower concentrations and increased accuracy for the higher ranges[78]. The method digests a 3 g, powdered sample in a chloride extraction solution. A combination specific chloride ion electrode connected to a voltmeter is inserted into the sample mixture, and the voltage is recorded in millivolts. The chloride content at each depth is determined by using a calibration equation, which is determined every time the instrument is operated. The results are plotted with respect to the depth.

3.4.2.2 Mathematical Modelling

The most widely used formula for predicting chloride levels in concrete is derived using Fick's 2nd law for non-steady diffusion. The change in concentration $(\partial c/\partial t)$ will be affected by the chloride binding and not just by the diffusion, hence, the equation yields an apparent diffusivity, D_a. For unidirectional diffusion, Fick's 2nd law states[37, 76, 79]:

$$\frac{\partial c}{\partial t} = D_a \frac{\partial^2 c}{\partial x^2}$$

(3.17)

The solution to Equation (3.17) obtained by establishing certain boundary conditions, is commonly used for calculation for chloride diffusivity. Chloride ingress into concrete is generally modeled using a solution equation derived using Fick's 2nd Law for non-steady state diffusion. This is called the error function and takes the form[37]:

$$C(x,t) = C_i + (C_s + C_i)erfc \frac{x}{\sqrt{4tD_a}}$$

(3.18)

where $C(x,t) =$ Denotes the chloride profile, i.e. the chloride concentration of the concrete versus the distance x from the exposed surface at time t, since the chloride exposure started;

           $C_i =$ Initial chloride concentration of the concrete;

           $C_s =$ Chloride concentration of the concrete surface; and

           $D_a =$ Apparent chloride diffusion coefficient.

The function $y = erfc(z)$ is referred to as the error function complement defined by the following expression[37]:

$$ercf(z) = 1 - erf(z)$$ (3.19)

where, the error function $erf(z)$ is defined by:

$$erf(z) = \frac{2}{\sqrt{\pi}} \int_{o}^{z} \exp(-\zeta^2)d\zeta$$ (3.20)

The table of the error function complement can be found in mathematical handbooks. Poulsen[37] considered the solution of Equation (3.18) to be straightforward provided that the parameters C_s, D_a, and C_i are known. To determine these parameters a non-linear regression analysis must be applied. This is inconvenient as it requires a computer program to run the process, and it is necessary to estimate a set of initial values for C_s, D_a, and C_i before starting the iteration procedure. Poulsen[37] found that an estimation of their values can be equally satisfactory and it is described in detail in Reference [37]. It is possible to write Equation (3.18) as follows:

$$y = \alpha x + q$$ (3.21)

where, $$y = \sqrt{C(x,t) - C_i}$$ (3.22)

$$q = \sqrt{C_s - C_i}$$ (3.23)

$$\alpha = -\sqrt{\frac{C_s - C_i}{12tD_a}} = -\frac{q}{\sqrt{12tD_a}}$$ (3.24)

The procedure for the determination of C_s, D_a, and C_i outlined by Poulsen[37] is as follows:

• The value of C_i is determined as the mean value of the test results from the heartcrete, or taken as zero;

• The measured concentration values, $C(x,t)$, are included in Equation (3.22);

• A regression analysis of the y values obtained against depth, x, is then carried out. This enables α and q to be calculated from Equations (3.21) and (3.23);

• The surface concentration, C_s, is read off from the profile graphs; and

• The diffusion coefficient is obtained from Equation (3.24), that is:

$$D_a = \frac{\left(q/_a\right)^2}{12t}$$

(3.25)

3.4.2.3 Practicability of Test

The main limitation of this type of method is that it is sensitive to the accuracy of determining the chloride concentration in the concrete sample. Sample collection technique and exposure might change the chloride concentration profiles. Also, all chloride analysis methods, including the two titration methods, require the acquisition of drilled powder samples, hence they are classified as destructive techniques.

3.4.3 Electrical Field Migration Tests

The above two test methods involve lengthy procedures, therefore various accelerated test methods where an external electric field is applied for accelerating the chloride penetration have been developed. The types of tests used are either non-steady, or steady state tests. There are many tests that have been developed but only two of these are applicable on site.

3.4.3.1 Rapid Chloride Permeability Test

Perhaps the only non-steady state in-situ test available at present to determine some measure of the chloride diffusivity in the near surface concrete is the test developed by Whiting[80]. The apparatus details are shown in Figure 3-18. The test method consists of monitoring of electrical current passing through a test area on a concrete specimen when a potential difference of 80 V DC is applied between a surface mounted copper mesh electrode placed in a sodium chloride solution and the reinforcement for a period of six hours[81].
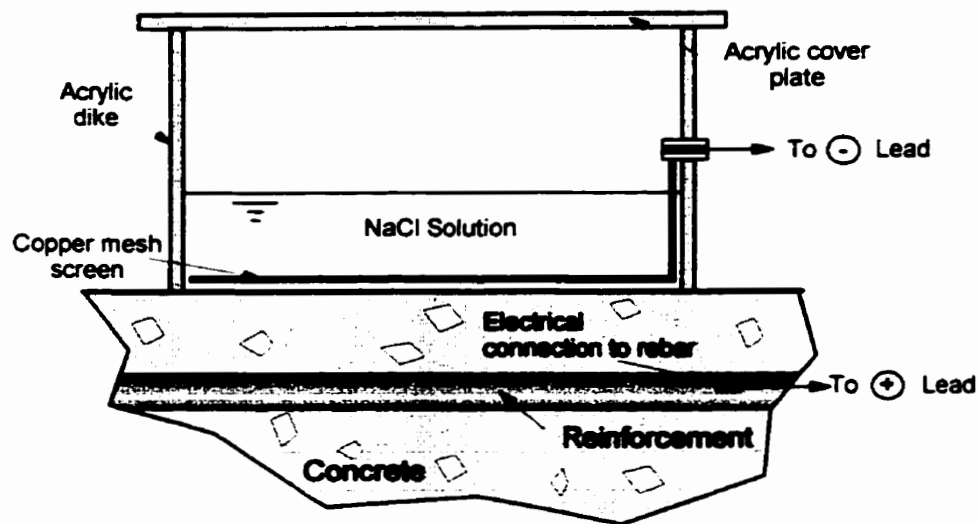
Figure 3-18: *Applied voltage apparatus used on slab specimens*[80, 81]

The field test procedure can be conveniently broken into four separate stages: location of reinforcing steel and bonding of test dike, vacuum saturation and heating of test area, applied voltage test, and chloride sampling which is optional[81]. By making the reinforcing bar anodic and keeping chloride solution (NaCl) with a negative charge on the surface of the concrete, the negatively charged chloride ions will migrate into the concrete. As the electrical resistivity of the concrete decreases with increasing chloride ion concentration, a measure of the increase in current, with time, is correlated with the amount of chlorides entering the concrete. Therefore, a measure of the total quantity of the electric current in coulombs passed over a period of six hours has been used as an indication of the chloride diffusivity of the concrete. A complete description of the test procedure is presented by Whiting[80, 81]. Although this test was well received initially, reducing the time needed to test concrete for resistance to ionic diffusion, it has the following drawbacks, as indicated by Andrade[82]:

•• It measures the total charge passed through the specimen and not that corresponding to chloride flux;

•• The test requires a connection directly to the reinforcement; and

•• The rise in temperature during testing may give a false value of the chloride permeability.

In view of the current limitations on the field device, a laboratory version of the apparatus was developed by Whiting to test accurately a variety of materials[81]. The method has been adopted by ASSHTO as Test Method T277[83] and by ASTM as C1202[84] and partial details are shown in

66

Figure 3-19. The equipment and procedures of the ASSHTO T277 method are similar to that used in the field test, except that the voltage is set at 60V DC, rather than 80V DC, to prevent excessive heating of the cell. The technique determines the total charge in coulombs that passes through a 50 mm thick disk that is 100 mm diameter subjected to the 60 V DC with NaCl solution at one face and NaOH solution at the other.
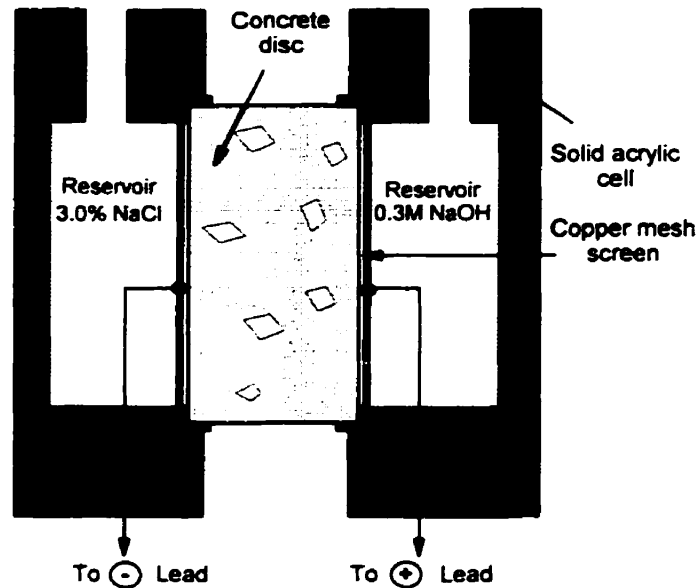
Figure 3-19: *Applied voltage cell for core specimens*[80, 81]

The laboratory cell test offers the most reliable alternative to field testing. However, this requires extraction of cores from the structure. Moreover, this method is based only on the measurement of the total electrical charge passed through the concrete for a given period of time, and this charge depends on both the type and amount of all ions present in the system. Therefore, this test method gives no specific information about either the chloride flux or the chloride mobility through the concrete. Typical values have been reported by the Concrete Society[27], however, they have expressed reservations about the suitability of this method because of the pore surface interaction during the passage of ions.

3.4.3.2 In-Situ Chloride Migration Test

A new test for determining the chloride migration coefficient of the near surface concrete on site is being developed at The Queen's University of Belfast[77, 85, 86] following the earlier studies by

Whiting[81]. The development is based on the evidence showing that a reliable value of chloride diffusivity can be obtained from steady state migration tests[77, 86]. That is, the tests that place a thin disc of concrete between two cells, one containing a salt solution and the other cell containing distilled water. A voltage is applied to the system by means of electrodes placed in the cells to force the negatively charged chloride ions to migrate through the concrete into the cell containing distilled water. The steady state flow of chloride ions is used to calculate a migration coefficient[77, 86]. Details of the in-situ chloride migration test are shown in Figure 3-20.
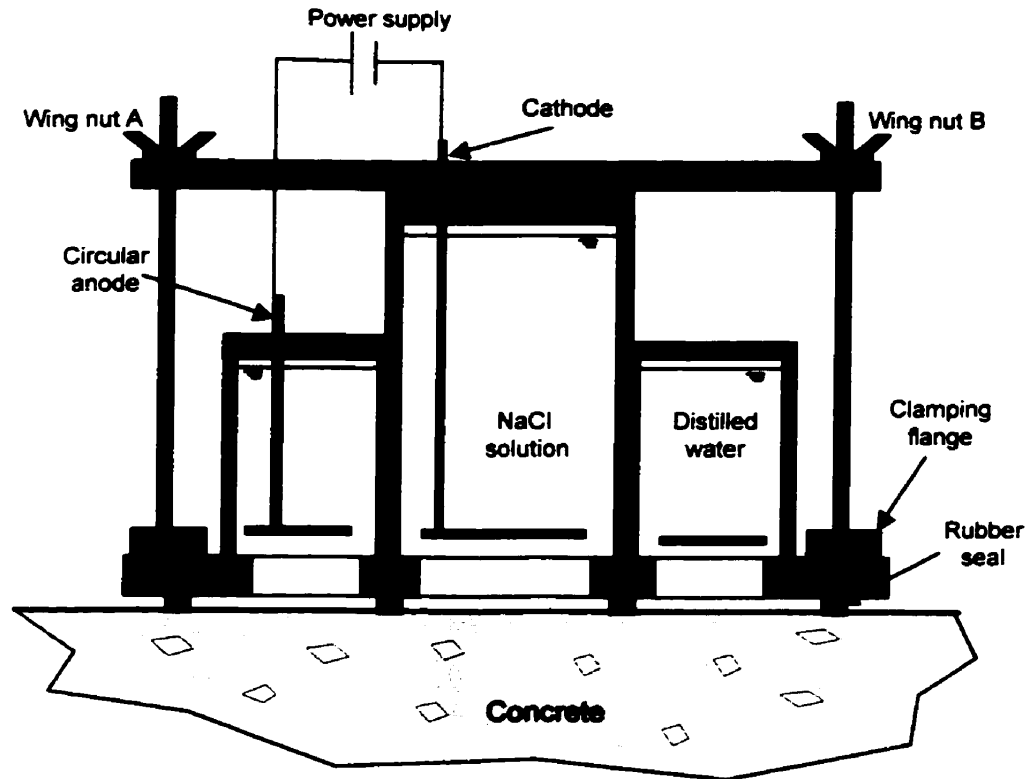
Figure 3-20: *In-situ chloride migration test*[86]

There are two plexiglas cylindrical cells, one inside the other. The inner cell contains a sodium chloride solution and a cathode, while the outer cell contains distilled water and the anode. The clamping flange is made of metal, based on its properties of strength and rigidity. On application of a potential difference, the chlorides migrate from the inner cell to the outer cell through the concrete. The design of the lid allows for the insertion of an ion selective electrode and a reference electrode to monitor the chloride content of the solutions[77, 86].

Mathematical modeling

All ions present in the pore solution that have been generated at the electrode by the application of a voltage, move towards the counter pole. This movement follows the mass transport law for electrolytes (Nernst-Plank)[77, 82], which states that the total net flow is the addition of:

$$Total\ flow\ = diffusion + migration + convection \qquad (3.26)$$

In the case of concrete, the contribution of both diffusion and convection can be neglected in applied voltage tests[82]. Therefore, the unique term to be taken into consideration in Nernst-Plank equation is that corresponding to migration. Thus the total flow (in steady state conditions) is:

$$J = D\frac{ZFC}{RT}\frac{dE}{dx} \qquad (3.27)$$

Considering uni-axial flow and rearranging Equation (3.27), it is possible to calculate the diffusion coefficient in steady state conditions as[77, 86]:

$$D = \frac{JRTL}{ZFC\Delta E} \qquad (3.28)$$

and

$$J = \frac{dc}{dt}\frac{V}{A} \qquad (3.29)$$

where

$D =$ Chloride diffusion coefficient of concrete ($cm^2.s^{-1}$);

$J =$ Unidirectional flux of chloride ions ($mol.cm^2.s^{-1}$);

$dc/dt =$ Steady state migration rate of chloride ions ($mol.cm^3.s^{-1}$);

$V =$ Volume of collecting cell (cm^3);

$A =$ Transmission area (cm^2);

$R =$ Gas constant ($8.31\ J.K^{-1}.mol^{-1}$);

$T =$ Absolute temperature (K);

$L =$ Distance between electrodes (cm);

$Z =$ Valency of chloride ions (-1);

$F =$ Faraday's constant ($9.65 \times 10^4\ J.V^{-1}.mol^{-1}$);

$C =$ Source chloride concentration ($mol.cm^{-3}$); and

$\Delta E =$ Potential differnce between the electrodes (V).

The flow of chlorides in an in-situ chloride migration test can be approximated by a uni-axial flow in a tapered region. By considering the continuity for a typical section, and by using a finite element model and verifying experimentally, the value of the effective flow length (L) of the chlorides in the in-situ test obtained by Andrews[86] is 12.25 cm. After substituting the value of L into Equations (3.28) and (3.29), the effective area through which chloride ions travel was found to be 117 cm^{2}[86]. By knowing both these parameters, Equation (3.27) can be used to obtain the chloride migration coefficients (D_{mig}) from the in-situ chloride migration test.

Test Practicability and Reliability

At this stage, no attempt has been made to apply correction factors for ionic interaction, or to consider the potential drop due to an interaction between the electrodes and the solution. This phenomenon is being investigated presently at The Queen's University of Belfast[86]. There is no standard classification available for use for this particular coefficient as it is presently under a detailed investigation and further development at The Queen's University of Belfast. A validation of the test was carried out by comparing the coefficients calculated from the in-situ chloride migration test with the data obtained from the following tests[86]:

- Chloride migration test (providing the chloride migration coefficient for one dimensional flow conditions);

- Standard diffusion test (providing the effective diffusion coefficient); and

- Chloride exposure test (providing the chloride profile to calculate an apparent diffusion coefficient).

The proposed test for calculating the chloride migration coefficient of concrete correlates very well with the other established tests for measuring chloride diffusivity of the concrete. This validation study shows that the in-situ chloride migration test can be a practical alternative in quantifying the diffusivity of concrete on site. However, further tests are required to confirm the findings. The validation of the test in the laboratory is now completed and the assessment of the usefulness of the test to determine the relative importance of those parameters related to corrosion (time to initiation of corrosion and average resistivity of the concrete in the near surface zone) in reinforced concrete structures is in progress at present. Table 3-5 lists the results from in-situ chloride migration tests at The Queen's University of Belfast using 6 mm maximum size aggregates[86].

Table 3-5: *Results from in-situ chloride migration test[86]*

Water/cement ratios	D_{mig} (cm^2.sec)
0.45	1.0×10^{-8}
0.55	2.0×10^{-8}
0.65	3.0×10^{-8}

The in-situ chloride migration test is quite promising and has many advantages such as[77, 86]:

♦ It can be conducted at any stage of the service life and a skilled operator is not needed;

♦ It is a non-destructive in-situ test which avoids taking cores and testing in the laboratory. Hence, diffusivity can be determined on site with the new test instead of taking cores and testing in the laboratory;

♦ Migration coefficients can be obtained based on the steady state achieved on site in one working day, hence, it is much quicker; and

♦ It does not affect the condition of concrete as the chlorides put into the concrete can be removed by reversal of polarity. Hence, there is no need for any concern with regard of the state of steel in the concrete tested.

3.4.4 Summary

It is important to distinguish between the various chloride diffusion coefficients that have been defined, and to realize that all these coefficients are not fundamental material properties as they are influenced by a number of factors such as binding, and they change with time. A chloride profile can be characterized by a surface chloride content (C_s) and an apparent chloride diffusion coefficient (D_a)[37]. The coefficient D_a is so named since it is influenced by both the physical resistance of the concrete to chloride ingress (steady state diffusivity (D_s)), and the chemical resistance of the concrete to chloride ingress (chloride binding capacity). Depending on the binding capacity, D_s can be 3 times higher than D_a[79]. Note that D_s can be affected by the chemical effects, should the physical pore structure be altered by the presence of chloride ions. Laboratory steady state diffusion tests, as well as steady state rapid chloride tests generally determine or estimate D_s and in the case of the in-situ chloride migration test, the chloride migration coefficient is determined. Rapid chloride tests determine mainly the physical resistance

of the concrete to chloride ingress, while on site, both the physical and chemical (binding) properties influence the resistance of concrete to chloride ingress. D_s and D_{nig} do not include the effect that chloride binding has on the non-steady state diffusion. Correlations would, therefore, differ for cements which differ in their chloride binding capacity.

3.5 Measurement of Permeability of Concrete

While much of the interest in concrete permeability dates back to the initial construction of hydroelectric structures in the 1930s, there is a renewed awareness of the role that permeability plays in the ultimate durability of concrete structures[48]. The long-term performance of concrete is presently a topic of great interest. Concrete structures are designed to ensure acceptable limits of deformation and ultimate strength values, and for a long time the compressive strength has been considered to be the only indicator for durability. Currently, control of durability is being realized by means of requirements of minimum values of strength, cover thickness, time of curing and restrictions of constituents and mix proportions[32, 48]. However, these parameters are not completely valid for ensuring the long-term performance of the concrete because they neither take into account the chemical and physical changes in the concrete due to the penetration of aggressive external agents nor do they consider the influence of intrusion of these agents on the rate of deterioration.

During the service life of the structure, the surface layer is usually subjected to more severe environmental attacks than the core concrete. The surface layer is especially important with regard to the corrosion of reinforcing steel. The customary quality control for concrete using compressive strength tests on standard cubes or cylinders, or cores cut from the structure, do not measure the properties of the surface layer, instead they evaluate the properties of the entire thickness covered by the core. Hence, tests are required to evaluate the quality of the surface concrete, especially on site. When concrete is subjected to external aggression, the most effective way to decrease the intensity of this aggression is to reduce its porosity and permeability. Mehta[48] stated, 'Impermeability of concrete should be the first line of defense against any of the physio-chemical processes'. Correlations between permeability and durability have been established by many researchers and it is now widely accepted that permeability is a key indicator of concrete durability[62]. It has been deduced that a direct correlation between porosity and permeability in concrete remains uncertain and, therefore, the direct measurement of permeability is presently the most reliable method for assessing this property[28]. Hence, the permeability of the

concrete cover is critical for problems related to the corrosion of reinforcing steel in structural concrete.

While various methods are available for determination of the concrete permeability in the laboratory, these are mostly time-consuming and require the removal of cores from the structure. Since coring is a destructive process, this limits the amount of information that can be obtained from a given structure. A number of more rapid, in-situ techniques have been developed for assessing water absorption as well as air and water permeability. Considerable attention has been paid to this area recently and the topic is covered comprehensively in the Concrete Society Technical Report 31[27] and by Basheer[87]. Both review a wide range of testing techniques and the fundamental theory. Only a selection of these test methods is included in this chapter emphasizing the most widely established in-situ testing.

3.5.1 Depth of Carbonation

Carbonation is the process of reaction of carbon dioxide from the atmosphere with hydrated cement paste compounds[27]. The permeability of concrete to carbon dioxide can be assessed by measuring the position of the carbonation front. This depends on the movement of carbon dioxide into the concrete as it proceeds inwards from the surface. The usual method of monitoring the depth of carbonation involves spraying a solution with phenolphthalein in alcohol and water onto a freshly exposed concrete surface[27, 44, 45]. Where the alkalinity of the concrete is unaffected, the phenolphthalein indicator gradually changes from colourless to purple, whereas the carbonated surface layers remain colourless.

A standard test procedure has been proposed by RILEM[88]. It is convenient to use and it can give reproducible results[44, 45]. However, cores need to be extracted and the indicator indicates the depth at which the pH is about 9.0 and this does not necessarily correspond to either the boundary between uncarbonated and partially carbonated concrete, or the boundary between partially carbonated and fully carbonated concrete[27]. A number of alternative methods are available for monitoring carbonation such as x-ray diffraction, infrared absorption, etc., although none are as convenient, as the rapid and inexpensive phenolphthalein indictor method.

As the carbonation of concrete is caused by diffusion of carbon dioxide into the concrete, the depth of carbonation has been related to rapid air permeability of structural concrete tested at site[87]. These tests are discussed in the following sections.

73

3.5.2   Absorption Test

The water absorption, determined by shallow immersion of a dried specimen, is referred to as the water absorption capacity. This consists generally of drying a specimen to a constant weight, immersing it in water for a specific time and measuring its increase in weight as a percentage of the dry weight. The Concrete Society[27] reported inconsistencies in the water absorption capacity due to the variations in both drying and saturation of the specimens. An absorption test on several small portions of concrete, as prescribed by ASTM C642-90, consisting of drying at 100°C to 110°C and immersing in water at 21°C for at least 48 hours, are used[32]. The requirements of BS 1881: Part 122: 1983[89] are similar, except that the test is performed on whole core specimens, drying at 105°C for 72 hours, cooling for 24 hours in an airtight vessel and immersing in water for only 30 minutes. While the British code does not stipulate a complete saturation of the specimen, the American code specifies it. It is unlikely that all of the capillary cavities in concrete are filled after only 30 minutes.

Typical values for water absorption of concretes, as established by the BS 1881, 30 minute immersion procedure, and reported by the Concrete Society[27] are:

Table 3-6: *Typical values water absorption of concretes*[27]

Level of absorption	Absorption (%)
Low	< 3
Average	3 to 4
High	> 4

Although a number of in-situ tests described below can also be carried out in the laboratory, this test measures the absorption capacity of concrete on samples in the laboratory. In most instances, a sample of concrete taken from the structure lends itself to a true measurement of permeability better than the in-situ test, as the sample can be cut or cored to the precise size required for the particular laboratory test, and the moisture can be brought to a standard condition[27]. Laboratory testing can be carried out under more controlled conditions, however, it is not practical to remove several samples from structures.

3.5.3 Initial Surface Absorption Test (ISAT)

Among the absorptivity tests, the longest established method is the Initial Surface Absorption Test (ISAT) prescribed in BS 1881: Part 5[90]. The test was initially proposed to test roof tiles and has been developed extensively since.

3.5.3.1 Interpretation of Test

In this method, a cap with a minimum surface area of 5000 mm^2 is sealed to the concrete surface and filled with water (Figure 3-21). The glass capillary tube is mounted at a height of 200 mm from the surface of the test specimen so that the head of water remains at this value throughout the test. This head is only slightly greater than that which would be caused by driving rain[32]. The rate at which water is absorbed at intervals of 10 minutes, 30 minutes, 1 hour and 2 hours from the start of the test are measured on the capillary tube[90]. The rate of initial surface absorption is expressed in milliliters per square metre per second[32]. This test and the units for the results do not represent concrete permeability. Hence, interpretation and practical use of the results can be made only by comparison with the other concretes of known performance when this test is used on site. The British standard gives guideline results to be expected for well-cured concrete and oven dried concrete[27]. Whereas oven dried specimens give reasonably consistent results, concretes on site give less accurate results.
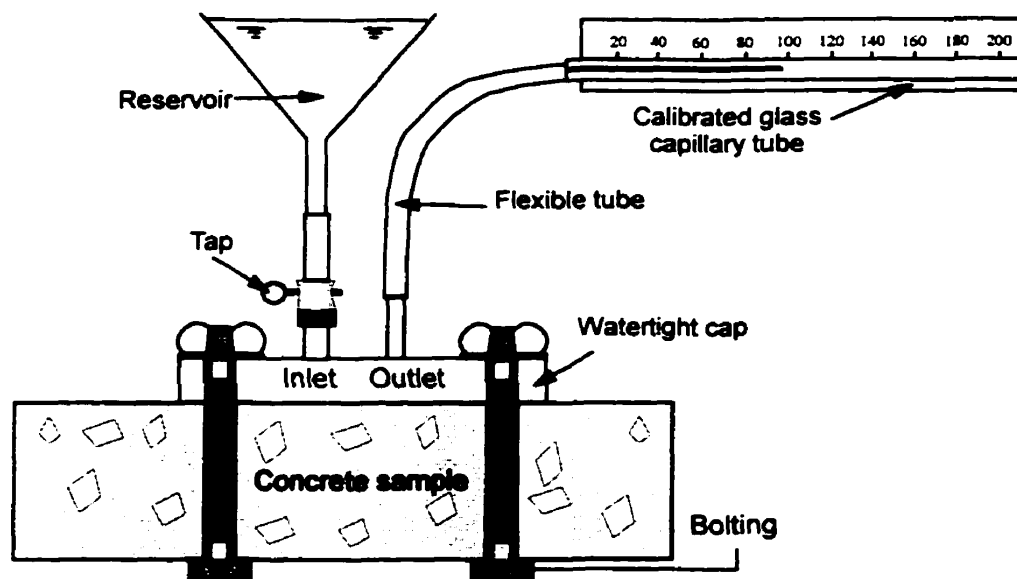
Figure 3-21: *Initial Surface Absorption Test (ISAT)*[27]

3.5.3.2 Practicability and Reliability of Test

The mass of water which is absorbed by the concrete during the test depends on the pre-existing moisture content, hence, the concrete needs to be conditioned prior to the tests. This requirement cannot be satisfied in in-situ concrete. For in-situ testing, a minimum drying period of 48 hours is specified, however, these requirements are very unlikely to produce comparable moisture conditions within the concrete. In consequence, a low value of the initial surface absorption may be due either to the inherent low absorption characteristics of the concrete tested, or else due to the fact that the pores in poor-quality concrete are already full of water[27].

The main practical problem in the use of the ISAT on site is the difficulty in achieving a satisfactory watertight seal between the cap and the surface of the concrete, especially in securing the cap in place without the use of clamps when used on site[62, 87]. This can be problematic and even the slightest leak can give spurious results. Another shortcoming of the initial surface absorption test is that the flow of water through the concrete is not uni-directional. To remedy this, several modified tests have been proposed but none have gained general acceptance[32]. Lastly, the test equipment is quite fragile and susceptible to damage on a construction site.

3.5.4 Figg Air and Water Permeability Tests

Figg described the development of a test for air and water permeability, which involves drilling of a hole into the concrete surface[27]. A number of versions of this approach have subsequently been developed in the various countries, but the most widely accepted procedure is the modified Figg method[27, 62, 87]. Although Figg proposed both water and air permeability tests, it is the air permeability test which has been used on many occasions for testing on site, hence, only the air permeability test will be discussed.

The modified Figg method uses a 10 mm diameter by 40 mm deep hole with a silicone rubber plug 20 mm from the surface and a battery-operated manometer as shown in Figure 3-22. Air permeability measurements are implemented by means of a hand-operated vacuum pump and digital manometer connected by a three way tap and plastic tubing to the hypodermic needle as illustrated by Figure 3-22. The pressure is reduced to -55 kPa by means of the hand pump and then isolated, with the manometer and the concrete connected together. The air permeability of the concrete is measured as the time taken for a pressure change from -55 kPa to -50 kPa[27, 87].
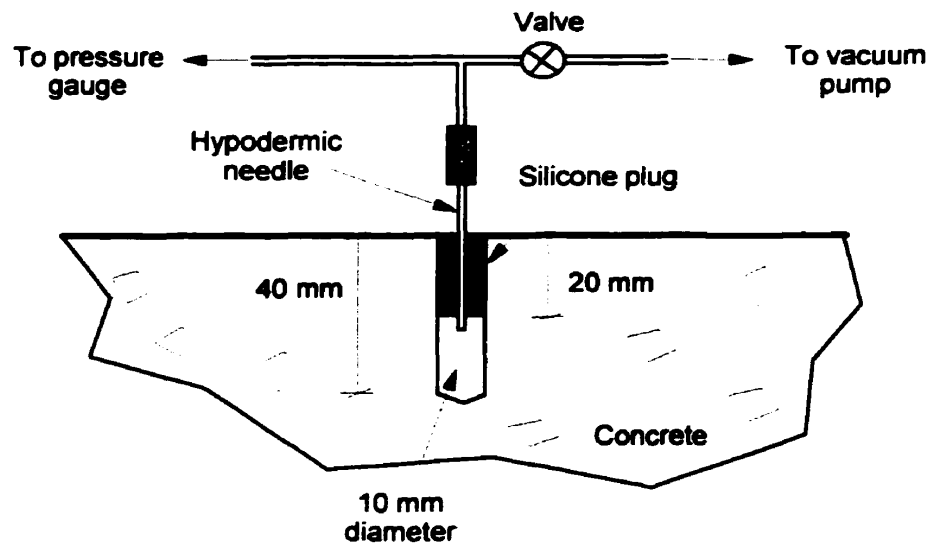
Figure 3-22: *Modified Figg air permeability test* [27]

3.5.4.1 Practicability and Reliability of Test

As with the initial absorption method, the moisture content will have considerable influence the results, although it has been proposed that the straight line relationship between the Figg air permeability values and the moisture content can be used to compensate for this effect[87]. This seriously restricts in-situ usage of this test, but a general classification for dry concrete is presented in the Concrete Society Report[27, 62]. It should be pointed out that the term permeability is not really valid because the output of the Figg tests is not directly related to the coefficient of permeability. Nevertheless, the results are useful for comparative purposes.

Another drawback of this method is that drilling is required. Methods which involve drilling holes have the disadvantage that the drilling may disturb the cement matrix by introducing microcracks, which may alter the permeability values[87].

3.5.5 Autoclam Permeability System

Early development of this method has been reported by Montgomery and Adams[91]. In concept, the test is very similar to the ISAT, but uses a hydrostatic pressure of 0.5 bar to measure in-situ water permeability and the equipment is portable and can be used on site[27]. Further development

undertaken by Basheer on the Autoclam can alternatively be used to measure a low-pressure, 0.02 bar water sorptivity, and in addition, a measure of air permeability, through decay of air pressure applied to the concrete surface, can also be measured[14, 62, 87].

The Autoclam consists of a measurement head and a control unit. The measurement head has a chamber with a pressure transducer at the base and a moveable piston. There are two valves which give access to the chamber and these can be used for either priming or bleeding. The unit is clamped to the 50 mm base ring which is in turn is bonded to the surface of the concrete (Figure 3-23).
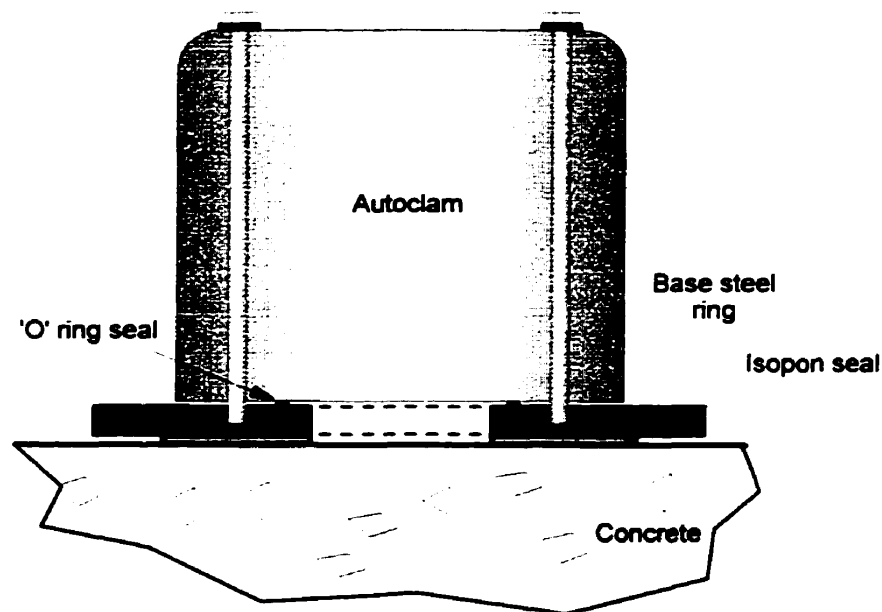
Figure 3-23: *Clamping the base plate of the Autoclam to the concrete surface*

3.5.5.1 Air Permeability Test

With the bleed valve closed and the priming valve open, the piston is reset to the base of the cylinder as shown in Figure 3-24. The air pressure in the chamber is increased using a syringe connected to the lower valve to a pressure in excess of 0.5 bar. The priming valve is then closed and the test starts by pressing the appropriate button on the control unit (Air Permeability in this case). The test commences and the decay of pressure with time is monitored over a 15 minute period as the pressure is recorded every minute for the duration of the test[14, 92].

Test pressure
Sorptivity test : 0.02 bar

Test duration
15 or 60 minutes

Measurement
Piston is pushed down to keep the pressure
constant and the travel of the piston is monitored
to determine the flow into the concrete

Bleed valve

Piston

Hydraulic
Cylinder

Water

Priming

Priming
Valve

**Display of
pressure & piston travel**

20 mB   2 mins
0.156 mm

Mounting
screw

Pressure
transducer

Base ring

(a)   Method of operation for sorptivity test

Test pressure
Air Permeability
test : 0.5 bar

Test duration
15 minutes

Measurement
Air pressure in the test area is increased to 0.5 bar
and the pressure decay is monitored at every
minute for a total duration of 15 minutes

Bleed valve

Piston

Cylinder

Priming

Priming
Valve

**Display of
Pressure**

356 mB   2 mins
0.000 mm

Mounting
screw

Pressure
transducer

Base ring
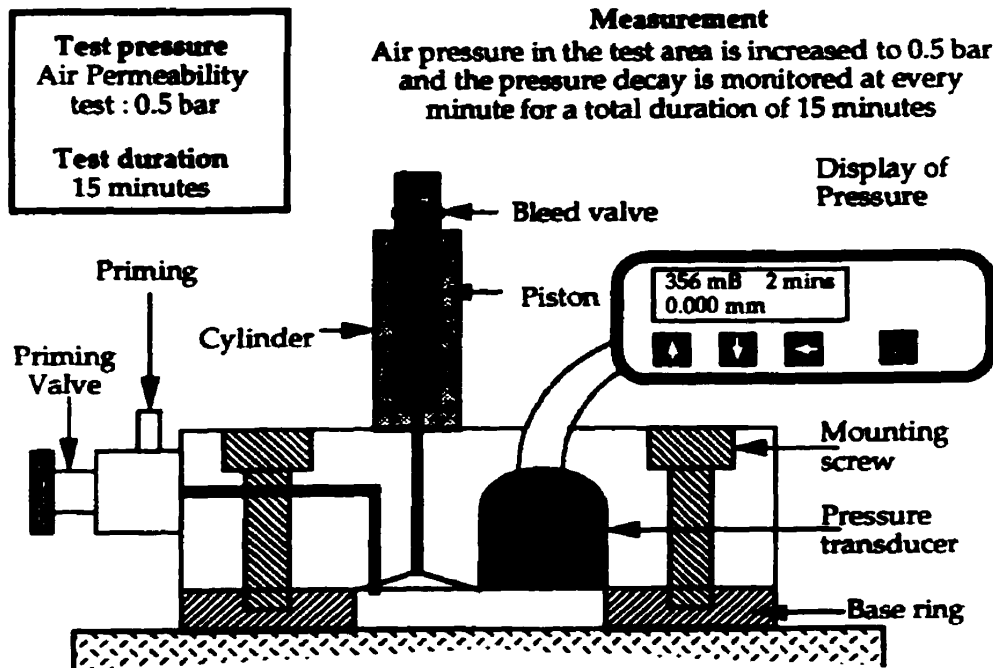
(b)   Method of operation for air permeability test

Figure 3-24: *The Autoclam method of operation*[14]

Calculation of the Air Permeability Index

A plot of the natural logarithm of pressure versus time is linear and the slope is taken as the Air Permeability Index (API) in ln(bar)/min. In tests where there is a measurable pressure in the test area after 15 minutes, the results from 5 minute readings are used. However, where the pressure decays to zero before 15 minutes, all results are used in the formation of the plot[14, 92].

3.5.5.2 Sorptivity Tests

This test is similar in concept to the ISAT. The procedure is different from the air permeability test as follows. With both the priming valve and bleed valve open, the piston in the clam is brought to the top of the cylinder in order to accommodate the maximum volume of water in the system as shown in Figure 3-24. The chamber is filled with water through the lower valve using a syringe. Air is allowed to escape through the bleed valve at the top of the piston. The upper valve is then closed and the pressure inside the chamber is brought to just below the operating pressure of 0.02 bar. The priming valve is closed and the test is started. As water is absorbed by capillarity, the piston lowers to maintain a pressure of 0.02 bar throughout the test (Figure 3-24). The travel of the piston is displayed and stored at one minute interval until the end of the test. The test may finish before 15 minutes if the piston reaches the end of its travel. At the end of the test, the data may be retrieved from the control unit by either manually scrolling through the data or downloading to a computer[14, 92].

Calculation of Sorptivity Index

The volume of water absorbed over the test area can be estimated precisely by multiplying the movement of the piston by the cross-sectional area of the cylinder. The measurements between 5 and 15 minutes are normally used for determination of the Sorptivity Index as the initial readings are prone to be influenced by the 'skin' effects. The plot of volume of water against the square root of time is linear and the slope is taken as the Sorptivity Index in $m^3/\sqrt{min}$[14, 92].

3.5.5.3 Water Permeability Test

There are two alternatives for the water permeability test. In order to calculate the Water Permeability Index (WPI), the procedure for the water permeability test is identical to that of the sorptivity test but with a test pressure of 0.5 bar[87]. However, on site the ambient relative

humidity may be quite high and the concrete cannot be dried to a constant moisture content, hence affecting the indices[92]. Early development of the Autoclam permeability method, assumed a steady state of flow, and accordingly, the coefficient of permeability is calculated[91]. This equipment was developed to facilitate the measurement of the coefficient of permeability of concrete on site, i.e., without removing cores from the structure. A steady state of flow during the permeability test may be achieved by ponding water in the 50 mm internal diameter ring (after being glued onto the surface) for 48 hours prior to testing. After 48 hours, the body of the apparatus is bolted onto the ring, and the same procedure as for the sorptivity test applies. Montgomery and Adams[91] undertook some work using ponded specimens, however, they used a pressure of 1.76 bars (25 psi) which is much larger than the value that is now used (0.5 bar). It is noted that if a steady state of flow is not established, the concrete should not be saturated and the permeability is expressed as a Water Permeability Index as in the case of the sorptivity test[87].

Calculation of Coefficient of Permeability

The volume is calculated in the same manner as in the case of the sorptivity test. It has been shown that a bilinear relationship exists between the volume of water flowing into the concrete and the time elapsed, in which the second portion of the graph represents a steady state of flow[91]. As the pore system is saturated, water will flow as a fluid if a sufficiently high pressure head exists and the flow is governed by Darcy's[27]. Therefore, the coefficient of permeability may be calculated with the use of Darcy's formula, with the incorporation of calibration factors in the equation for a radial flow net. That is, the coefficient of permeability (in m/s) is given by the equation[91]:

$$k_w = qc \qquad (3.30)$$

where $\quad q =$ Rate of flow for the steady state (m³/sec); and

$\qquad c =$ Calibration factor.

The latter depends on the geometry of the specimen and the applied pressure. For a pressure of 1.76 bars, the calibration factor was found to be 0.714×10^{-3}[91]. Any other chosen pressure requires a proportionate calibration factor. Although Montgomery and Adams[91] reported that a steady state of flow could be achieved by ponding water, the validity was questioned as the flow takes place though bigger pores in which the surface tension force is less than the applied pressure, and the flow does not take place through the fine pores. The value obtained from equation needs to be adjusted for the area through which the flow took place[14] .

81

Practicability and Reliability of Test

In general, the Autoclam test has been found to yield useful results, however, variations in the moisture content of the surface concrete can make the interpretation of these results problematic. In such cases, the Air Permeability and Sorptivity Indices are most significantly affected. However, by using the Water Permeability test, it is possible, after some experience, to obtain valuable information. The relationship between the moisture of the concrete and the indices needs to be investigated further so that the results from the site investigations can be corrected[12].

Basheer[14, 87] has established a classification, but it is limited as this was done using dry concrete in a laboratory, thus preconditioning the specimen. It is necessary to establish appropriate criteria for the classification of concrete when based on the Autoclam indices, by which different mechanisms of deterioration may be predicted. Some initial progress has been made as the establishment of the useful correlation between the carbonation depth and the Air Permeability Index, and between the Autoclam permeability indices and the freezing and thawing resistance of the concrete[12].

Regardless of the difficulties mentioned above, the Autoclam Permeability system is a promising tool as it is robust and can be easily used on site for non-destructive testing. In addition, tests on both vertical and horizontal surfaces can be carried out for all three permeation tests. The air permeability test can also be performed underneath a slab, such as the soffit of a bridge deck. Also, the theoretical support for the Autoclam permeation tests has indicated that it is possible to obtain the intrinsic permeability and sorptivity from Autoclam measurements. This may be a useful alternative to the development of empirical relationships. Further research is needed and is presently underway to overcome the challenges identified above[12].

3.6   Concluding Remarks

This chapter reviewed some of the various tests that are able to assess the damage resulting from the corrosion of steel and the poor quality of concrete. Information was also included on methods that have been developed and introduced recently. While actual field experiences with these methods/procedures are limited, they are included as it is anticipated that they may have a significant impact on condition surveys of deteriorated concrete structures in the near future.

4 Experimental Program and Calculation of Parameters

4.1 Introduction

The previous chapter dealt with the different ways of quantifying the various parameters relating to the corrosion phenomenon. This chapter will describe the experimental program undertaken on the Dickson Bridge for the assessment of the corrosion damage and the determination of the quality of concrete. The calculation of each parameter involved with each test will be detailed and the accompanying assumptions will be stated.

4.1.1 Test Program

The scheme of the testing program is shown in Figure 4-1. Since it was required to test the concrete deck for corrosion induced deterioration, the test methods are related to either the mechanisms causing the corrosion, or properties indicative of the probability of corrosion. Most of the factors that initiate and propagate the corrosion process of reinforcing steel are directly related to the properties of the concrete. Thus susceptibility of reinforced concrete structures to corrosion and their rate of deterioration can be approximated, provided that the physical properties of the concrete and the exposure parameters can be defined rationally. Hence, the in-situ tests that are able to measure permeability, resistivity, chloride diffusivity and strength of the concrete were used to assess the existing structure and explain the accelerated deterioration of the concrete. The damage was measured using all other available techniques.

4.1.1.1 Investigation Methodology

The first part of the investigation emphasized methods for assessing the probable corrosion damage to the concrete structure. A thorough visual inspection included detection of delamination by tapping the surface with a hammer, the location of the reinforcement and the depth of the

Establish aims of
investigation

Decide on information
required

Interpretation criteria
for results

Visual inspection

Select most
appropriate test
methods

Preliminary work

Half-cell potential
survey of entire deck

Selection of sites for
detailed investigation

Detailed testing
✓ In-situ tests
x   Laboratory tests

Corrosion damage
assessment

Physical properties of
concrete

✓ Open circuit potential
✓ Corrosion rate
✓ Concrete cover to steel level
✓ Delamination
x Chloride content
x Carbonation depth

✓ Resistivity
✓ Chloride diffusivity
✓ Permeability
x Compresive strength

Overall analysis

Figure 4-1: *Scheme of test program*

concrete cover using a covermeter. The extent and the rate of corrosion of the reinforcing steel
were measured using the half-cell potential and linear polarization tests, respectively. The
chloride content at the level of the reinforcement was determined using the acid-soluble chloride
technique, while the depth of carbonation was measured using the phenolphthalein test. The
second part of the investigation evaluated the properties of the concrete, such as its compressive
strength (from drilled cores) and durability characteristics, namely the permeability, diffusivity

and resistivity of the concrete. The permeability was measured using the Autoclam Permeability System[87, 92], while the diffusivity was determined both from the chloride profiles and by using a recently developed In-Situ Chloride Migration test[77, 86]. The electrical resistivity was evaluated using the Wenner four probe apparatus. Description of the various methods is presented in this chapter.

4.1.1.2 Selection of Test Techniques

The selection of the test techniques and procedures in this investigation were based on several criteria. Obviously, the most important criterion was that the test should be nondestructive in nature and have the ability to carry out the required function at an acceptable performance level. Simplicity of operation was another criterion. Further, it had to be field-ready and possess a high degree of reliability.

4.2   Half-Cell Potential Survey

The purpose of conducting a half-cell potential survey on the entire deck was to select sites where a more detailed investigation would be carried out. In other words, the survey was utilized as an initial guideline. In carrying out the half-cell potential survey, a grid of one metre by metre was marked on the North side of the bridge (Figure 4-2) in order to sample the surface potentials.
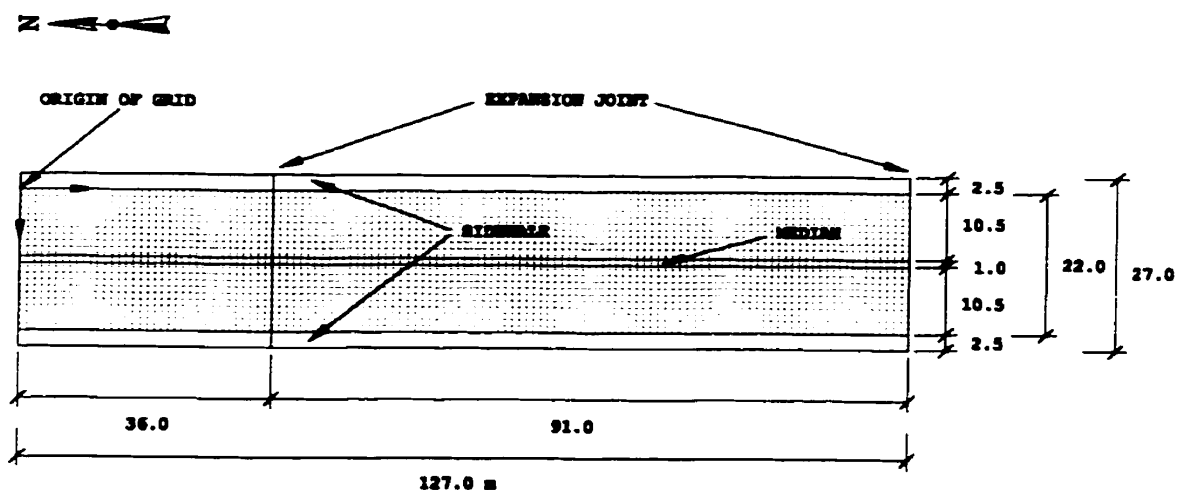
Figure 4-2: North section of bridge deck (detail from Figure 1-3)

The covermeter was used to locate the steel and determine rebar spacing. Two layers of reinforcing steel were detailed on the original plans. The top layer was at 25 mm from the top surface of the deck and the second layer was at 25 mm from the bottom surface or the soffit. The bar spacing on the original plans was 210 mm transversely and 610 mm longitudinally, however, it varied throughout the deck. Usually the grid coincides with the rebar spacing on small surveys, but not on larger scans[33]. Hence, a grid of one meter by one meter was chosen to survey the whole surface of the concrete deck of the North portion of the bridge.

4.2.1 Apparatus and Procedure

The equipment was assembled to form a continuos electrical circuit from the reinforcement via the concrete, the copper sulphate solution, the copper rod, the voltmeter and back to the reinforcement as shown in Figure 3-11. The MICAPS CDL 200 (developed at Corexco, Montreal), a computerized datalogger with integral A/D converter specifically designed for undertaking potential surveys of large areas quickly and economically was utilized in this investigation (Figure 4-3).

Figure 4-3: *Half-cell potential apparatus*

A more detailed procedure is found in the ASTM C876 Standard[64]. The following highlights the sequence of operations carried out on site:

- A strong electrical connection to the steel was ensured by drilling a hole in the reinforcing bar and inserting a self tapping screw with an attached lead into the hole in the steel.

- Six widely spaced connections to the reinforcement were checked for electrical continuity using a DC resistivity meter between the two points. The resistance was less than 1Ω, which confirmed continuity. The potential difference was also measured. On the average, it was 3mV which indicates good steel connectivity across the test area[63, 64]. Two connections were situated below the first expansion joint (Grid Location 36 m (Figure 4-4)) and the remaining four above with two on each side of the bridge.

- The deck was covered with an asphalt overlay, hence at every grid point, holes were drilled through the asphalt until it reached the concrete. Water was poured in the hole and a wetted sponge was used over the cell to ensure that the concrete was damp enough for the charged ions to flow from the steel to the half-cell; and

- The automated logging equipment stored the readings at every grid point.

The half-cell potential survey was conducted on the external lanes where a concrete overlay was laid over the original concrete deck (Figure 4-4). This was achieved by making a connection to the steel from the deck underneath the concrete overlay. It is noted that the reinforcing steel within the overlay was not connected to the underlying steel in the original deck, hence making it possible to survey the external lanes.

4.2.1.1 Preliminary Work

Ideally, the asphalt overlay should be removed before testing for half-cell potentials, but in order to make the test as non-destructive as possible, some preliminary tests were undertaken in a five meter square area in order to ensure that the procedure was acceptable. Holes were drilled at every grid point, water was poured in the hole, the cell with the wetted sponge was placed over the hole and the readings were recorded. Later, the asphalt in the immediate area near the grid point was totally removed and the readings were recorded again. The difference between the two half-cell readings taken at the same location with the same cell did not exceed 20mV which is acceptable according to ASTM C876[64].

4.2.2 Reliability and Classification of Results

It is essential to recognize that the half-cell method cannot indicate the actual corrosion rate, or whether corrosion has even commenced. The test only indicates zones requiring further investigation, and the likelihood of corrosion occurring in these regions. Hence, the half-cell potential readings were used to select thirty-five sites, measuring approximately 1 m by 2 m, for further detailed analysis (Figure 4-4). For all its limitations, the half-cell is a very powerful diagnostic tool for corrosion investigation[63]. Its main problem is that some people rely on very simplistic interpretations, such as the ASTM C876[64] guidelines presented in Table 3-2. However, in this investigation, corrosion was located from iso-potential contour maps by considering the magnitude of the potentials and qualitatively assessing the potential gradients. The contour map showed high corrosion and low corrosion risk areas (Figure 4-5). A rapid change in the potential represented a steeper gradient indicating a greater risk of corrosion. The selected sites corresponded to the positions of the highest and the lowest potentials and the steepest potential gradients. These were chosen throughout the bridge deck where the risk of corrosion for each site varied from low to high as shown in Figure 4-5. It is noted that the external lanes were omitted for any detailed investigation (except one meter away from the curb where the overlay was asphalt), as the deck was covered with a concrete overlay, making it difficult to remove the above overlay and expose the deck lying underneath (Figure 4-4).

4.2.3 Scheme of Detailed Investigation

The detailed testing, which followed the half-cell potential testing, was conducted only on the 35 selected sites. The work was conducted in a systematic manner. The flowchart shown in Figure 4-6 summarizes the sequence of the tests planned for the detailed investigation of each of the 35 sites.

Once the sites were selected, the asphalt overlay was removed using a jackhammer. This was carefully done to keep the concrete deck under the overlay as intact as possible. It was not possible to do the same for the lanes with a concrete overlay on top of the concrete deck (Figure 4-4). When trying to remove the concrete overlay, the concrete deck top got damaged as well. Hence, it was decided not to include the lanes with the concrete overlay in the detailed investigation.
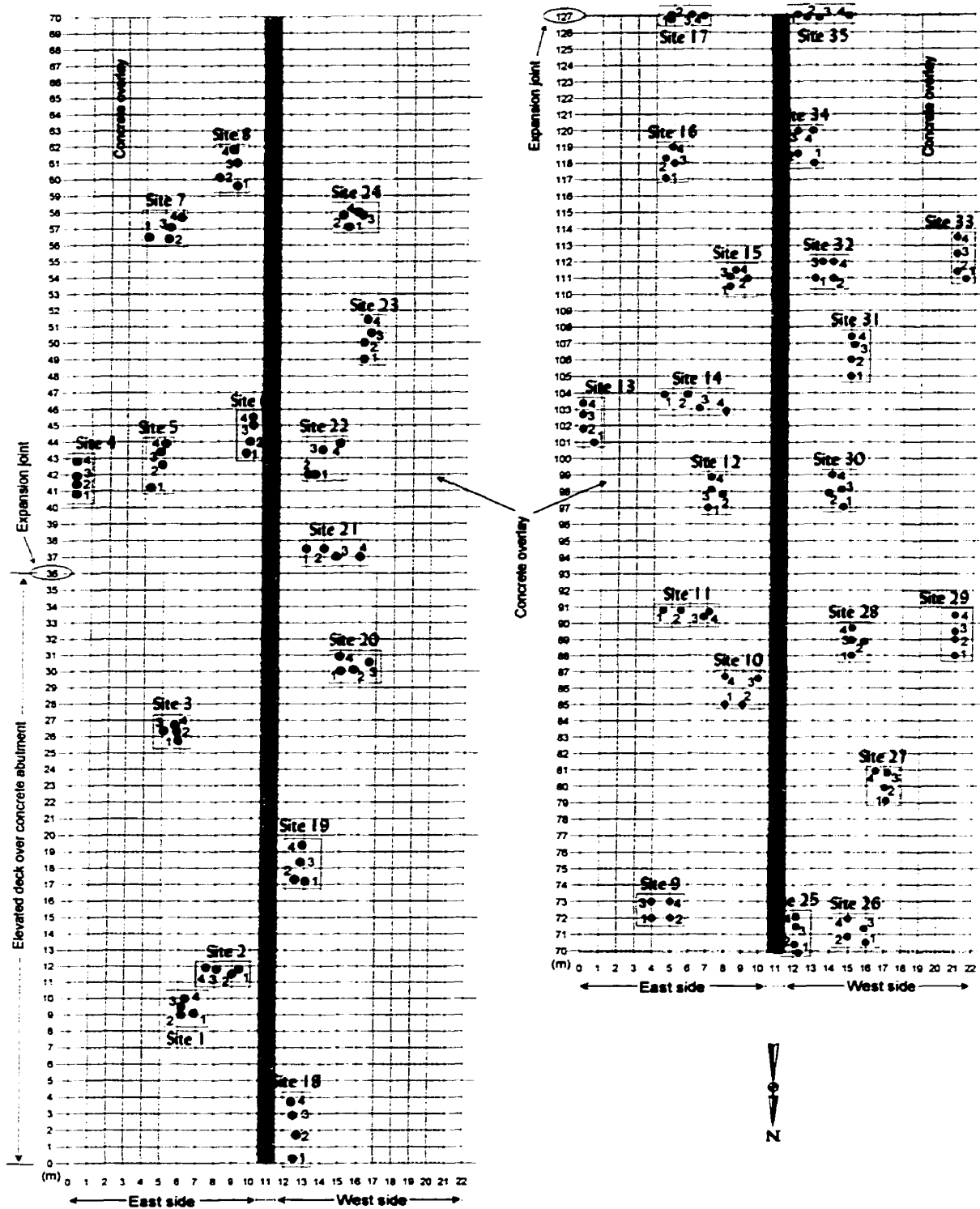
Figure 4-4: *Location of 35 sites selected for detailed investigation*

89
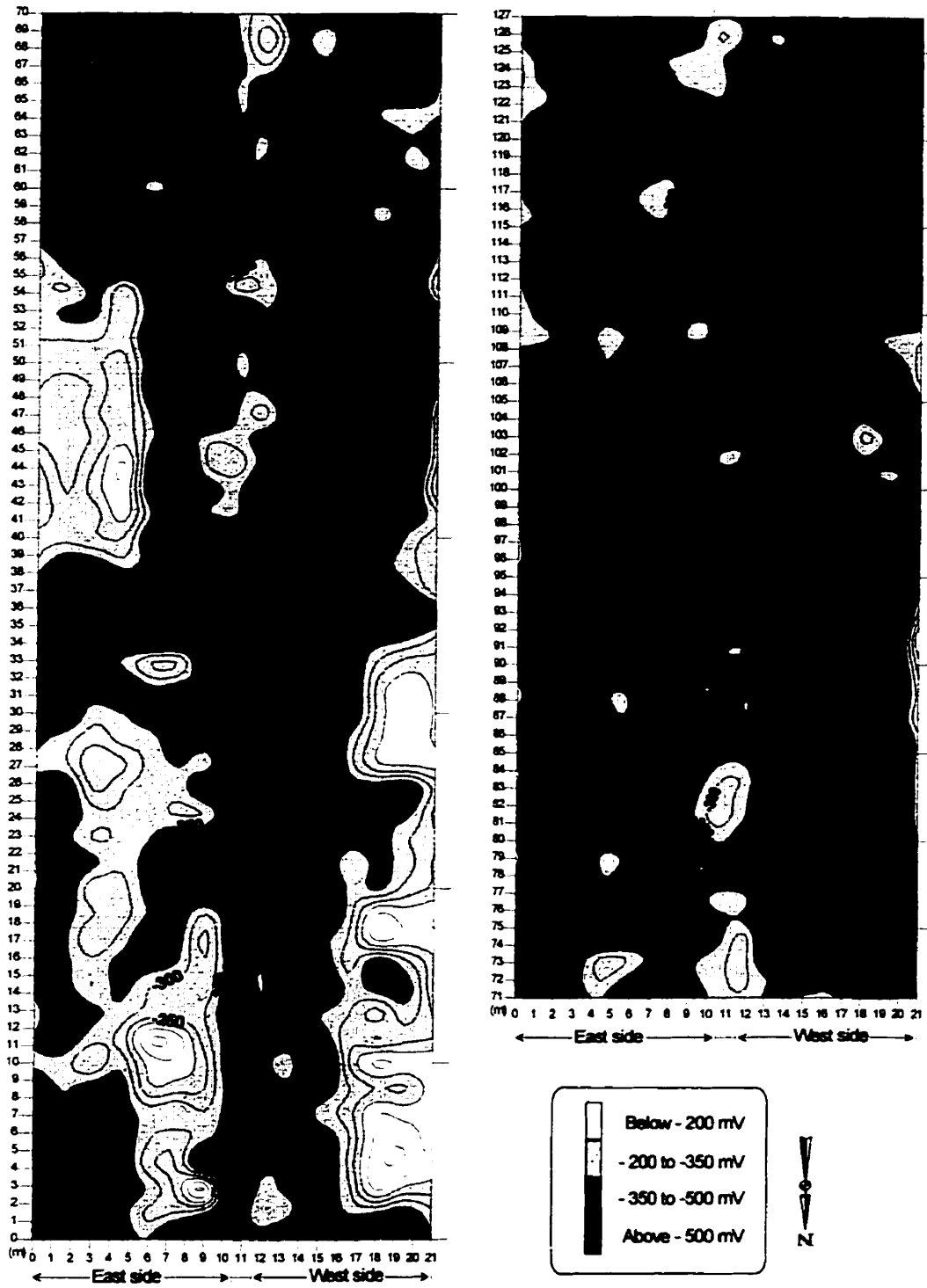
Figure 4-5: *Half-cell potential survey of the northern portion of the bridge deck*

Selection of 35 sites

Removal of asphalt overlay

Selection of 4 locations where corrosion rate measurement at each site be undertaken

Detection of steel bar at the 4 locations.

Determination of concrete cover at the 4 locations

Delamination survey at the 4 locations

Resistivity measurements of the concrete at the 4 locations avoiding the rebar

Linear polarization survey measuring open circuit potential & corrosion rate at the 4 locations

RH measurements

Permeability measurements on 3 of the 4 locations per site

In-situ migration test on 1 of the 4 locations per site

Concrete dust sampling on the same location where in-situ migration test was conducted

Chemical analysis

Coring for:
-Compressive strength (1 of the 4 locations per site)
-Absorption (1 location on 10 selected sites)
-Carbonation depth (1 location on 10 selected sites)

Testing for:
-Compressive strength
-Absorption
-Carbonation

Figure 4-6: *Detailed investigation plan*

When only one reading was planned per site, this would be considered representative for the entire site. The same location was chosen for these tests for later correlation and comparison of the results. When more than one reading was planned, these would be conducted on predetermined locations on each site where all the different tests would be conducted at the same spot. Figure 4-4 illustrates the position of all of the sites with reference to the grid; the four locations selected at each site are also identified. Figure 4-7 illustrates a photograph of the layout of a typical site (Site number 20) showing the locations where the readings were obtained.
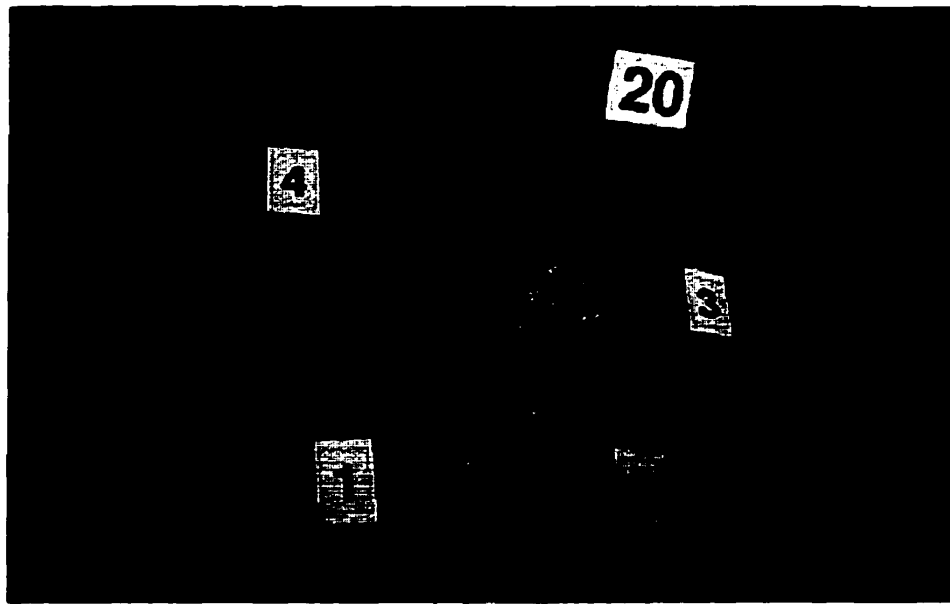
Figure 4-7: *Typical site (Site 20, locations 1 to 4)*

4.3 Covermeter Survey

A low cover increases the corrosion rate both by allowing the agents of corrosion a more rapid access to the reinforcing steel, and also allowing more rapid access of moisture and oxygen. Hence, a cover survey was undertaken to explain why the reinforcing steel in the structure was corroding and show which areas were more susceptible to corrosion due to a low concrete cover.

4.3.1 Equipment and Procedure

An electromagnetic device, called the covermeter was used. Although the main purpose of a covermeter survey is to measure the concrete cover thickness over the reinforcing steel in a specified area within a grid marked on the structure, this was not done in this investigation as the area was too large. Instead, only the concrete cover thickness was determined at all 4 locations in each site, where the corrosion rate would be measured. Once the steel bar was detected with the aid of the covermeter, the location was marked on the concrete surface and the concrete cover thickness was measured. Figure A-1 (Appendix A) illustrates the cover obtained at each location.

The covermeter model that was used in this investigation was CM4 CoverMaster by Protovale (Oxford) Ltd. The procedure in the user manual was followed in detail together with the BS Standard 1881:Part 2204 and a report by Alldred[93] to properly locate the position of the reinforcing steel in the concrete and to accurately measure the depth of concrete cover to the bar[33]. The basic principle of the covermeter is that the presence of steel affects the electromagnetic field. The disturbance caused by the presence of the metal in turn produces a local change in the magnetic field strength as detected by the search head and indicated by the meter. Therefore, it was possible to locate the reinforcing bars and determine their orientation. A calibration was performed to determine the cover for the particular size of bar in the concrete. At particular sections of the bridge, the accuracy of the device was checked by actually exposing the area. It confirmed with the initial reading of the covermeter. The BS 1881: Part 204 suggests that an average site accuracy of about 15% at cover thicknesses less than 100mm can be expected[62].

4.4 Delamination Survey

The corrosion products take up a larger volume than the volume of the steel consumed, which causes a build up of tensile stresses around the rebars causing the concrete to crack along the weakest plane in the concrete cover, followed by spalling of the concrete. The fracture plane, or the delamination, due to corrosion of the reinforcement may be confined to a local area or may extend over a substantial portion of the structure if the concrete cover is uniformly low[13, 33, 62]. It is not uncommon for more than one delamination to occur on different horizontal planes above the reinforcing steel.

4.4.1 Equipment and Procedure

Delamination can be detected at the surface by various means from hitting the surface with a hammer to sophisticated techniques using radar, infrared, sonic and ultrasonic equipment. The hammer survey is usually quicker, cheaper and more accurate than the other alternatives. However, the more sophisticated techniques do have their uses for instance in large-scale surveys[33].

In this investigation, delamination was detected systematically over the four marked locations on each site. The planar fracture was detected by a hollow sound when the surface was hit with the

hammer. These hollow sounding areas were considered to be delaminated. Figure A-2 (Appendix A) illustrates the results obtained for each location. One major drawback is that this method is subjective and does not indicate the depth where the delamination is present[33, 62].

4.5   Resistivity of Concrete

During the corrosion rate measurements, a current must flow through the concrete in order to polarize the steel bar under study. High electrical resistance of the concrete will interfere with an accurate evaluation of the corrosion rate test results. Hence, the resistivity measurements were conducted prior to the corrosion rate survey to assess the conductivity of the concrete in terms of the electrolytic resistivity of the material.

4.5.1   Equipment and Procedure

A Wenner four probe apparatus was used as shown in Figure 4-8. The probes were held against the surface of the concrete as shown in the schematic diagram in Figure 3-16. The meter measured the resistance, R_c, of the concrete in ohms. The electrode spacing, s, of this particular probe was of 4.38 cm and together with the measured R_c value, it was possible to calculate the resistivity of the concrete using Equation (3.15).

4.5.1.1   Resistivity Sampling

The resistivity measurements were taken at all four locations on each site. The four-point technique measures the resistivity of a region of concrete in the general vicinity of the electrodes rather then providing a localized spot measurement. It is unlikely that the resistivity of in-situ concrete will change very quickly from one location to another unless there are physical differences in the conditions between the locations that would induce such a change[62, 73]. Figure A-3 (Appendix A) illustrates the resistivity results obtained at each location.
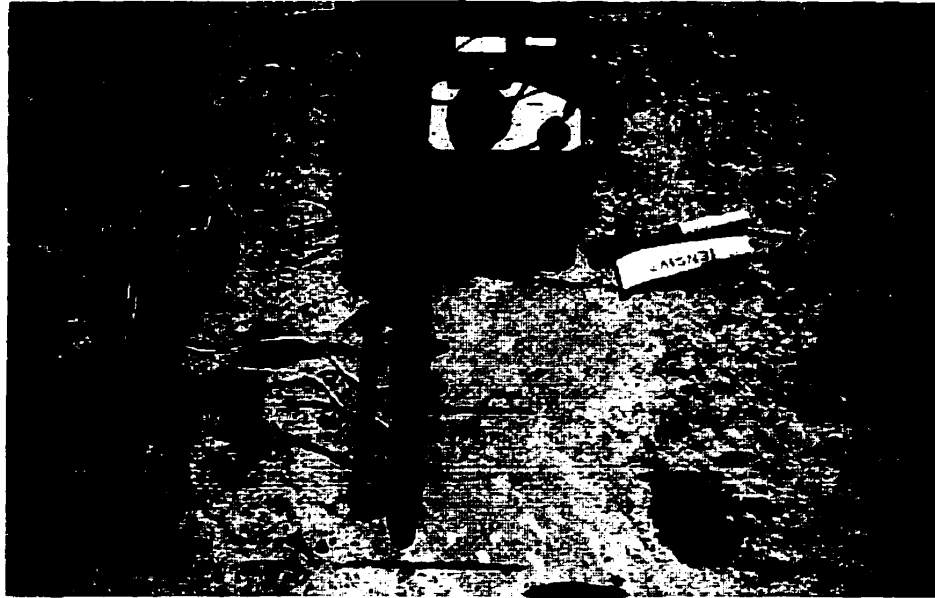
Figure 4-8: *Wenner probe*

4.5.1.2 Minimizing Errors in Resistivity Readings

Survey points were selected so as to avoid being close to the steel reinforcement as far as possible. Hence, to minimize the error caused by the reinforcing bars, the locations of the rebars were detected using a covermeter and subsequently the resistivity measurements were taken midway between the bars. The readings were taken at right angles to the steel in order to avoid a short circuit 'path' for the current during the measurement. Moreover, the use of spring-loaded electrodes and a high conductivity contact gel on the concrete surface ensured that a good electrical contact was made. It also avoided drilling holes in the concrete.

The resistivity calculation in Equation (3.15) assumes the concrete to be homogenous which is not the case for the concrete in the bridge deck. The error was minimized by selecting a spacing (4.38 cm) large enough to avoid measuring the resistivity of a piece of aggregate rather than the paste and the aggregate.

In order to minimize the errors in the readings, the above procedure was used. However, in addition to the factors discussed, the resistivity of concrete can fluctuate with changes in the ambient conditions. Although many researchers[62, 73] have used the electrical resistivity measurements in in-situ investigations, the influence of moisture and temperature of the data

obtained limits its application to similar investigations. The moisture was very high in the concrete on the Dickson Bridge deck (an average *RH* of 86% and 90% at depths of 10mm and 25mm from the concrete surface, respectively (Figure A-9 in Appendix A)). Another practical difficulty of measuring the resistivity of concrete on site was that in addition to the local resistive non-homogeneities caused by the aggregate particles, the global resistivity may change with depth beneath the surface of the concrete. These surface layer effects are difficult or maybe impossible to account on site[73].

4.6   Linear Polarization Resistance Test

Corrosion rate measurement is slow compared with the half-cell potential measurement, hence, it is important to take measurements at the most significant locations on the structure, i.e., by following up a potential survey with strategic corrosion rate measurements. Hence, the corrosion rate measurements were taken at 35 sites (four points per site with a total of 140 readings).

In this investigation, the linear polarization resistance (LPR) technique was used as it is the most suitable to be applied on-site, requiring a minimum of equipment. It is also relatively inexpensive and easy to learn and use[33, 62]. The technique has been shown to produce results in good agreement with gravimetrically determined corrosion rates, provided the measurements are made at appropriate potentiodynamic rates of scan and with suitable provision for *IR* compensation[33, 41, 62].

4.6.1   Corrosion Rate Devices

Two types of LPR probes were used. The first one was based on the three-electrode linear polarization (3LP)[65] technique as shown in Figure 3-14. This method is less accurate as it assumes that the area of measurement is directly below the counter electrode. Thus, the length (*L*) of the polarizing electrode was 150 mm. The probe consists of a working electrode (the steel bar being tested for its corrosion condition), the reference electrode (pencil CSE) used to sense the potential changes induced in the steel bar (working electrode) by a current, which is introduced into the ionically conductive system through an auxiliary electrode (copper mesh counter electrode, CE).

The second probe consisted of a guard ring shown in Figure 3-15. The device is unique in its ability to accurately confine the area of measurement by using a guard ring[68, 69]. This means that the corrosion rate measurements were not carried over an undefined area, but show the true corrosion rate at the measurement location. The device uses an internal counter electrode and an external counter electrode (guard ring), which confines the current to an area of 111mm in diameter. A photograph of both probes is shown in Figure 4-9. The 3LP device is on the left side of the picture while the guard ring device is on the right side.

Figure 4-9: *Types of probes used on site*

4.6.2 Test Procedure

The polarization resistances (R_p) of the bars were determined by means of a microprocessor-controlled corrosion measurement system. A potentiostat (CMS100 Electrochemical Measurement System by Gamry, Inc.) which controls the potential of the system, and which acts as an electrical conductor between the anode and the cathode was used with both probes. The CMS105 DC Corrosion Measurement System was also used. This is an add-on application package to the CMS100, which runs the DC corrosion tests such as polarization resistance.

97

Since the corrosion rates vary with the weather conditions, readings were taken under comparable weather conditions, that is all the readings were taken within a time lapse of two days. The corrosion rate measurements were normally proceeded by a period of five days of no rain. Strong connections and electrical continuity was ensured in the same manner as in the half-cell potential survey. Before each test, water was sprayed on the immediate area of measurement. The sponge within the probe was kept moist throughout the test. The probe was centered over the rebar as indicated by the covermeter. The probes were weighted with a load of about 1kg for the three-electrode probe and 15kg for the guard ring.

4.6.2.1 Setup Parameters

The variables listed in Table 4-1 were introduced into the program (CSM105 DC Corrosion Measurement System) prior to polarization. The scan rate parameter defines the speed of the potential sweep during the data acquisition. This was set to a low rate as higher rates may yield unreliable data due to a deviation from the steady state. The surface area of the steel bar under the probe was determined from the relation: $A = \pi D_{rb} L$, where D_{rb} is the diameter of the rebar (5/8" or 15.87 mm) and L is the length of the polarized electrode (150 mm for the 3LP and 110 mm for the guard ring).

Table 4-1: *Polarization resistance setup parameters*

Parameters	Values
Scan Rate	0.125 mV/sec
Scan Range	± 20 mV from Open Circuit Potential ϕ_{oc}
Anodic area A, i.e., metal surface area	55.36 cm^2 (74.81 cm^2 for 3LP probe)
Density of metal	7.87 g/cm^3
Equivalent weight of metal	27.92 g
Delay provided to attain ϕ_{oc}	500 s
Beta A (βa) and Beta C (βc)	120mV/decade
IR_{drop} compensation	ON

The density of the metal being studied is required for the evaluation of the speed of corrosion in terms of mass lost per unit of time. The equivalent weight of an element is the theoretical mass of metal that oxidizes with the passage of one Faraday as defined in the ASTM Standard G102-

$89^{[94]}$. This is equivalent to the ratio a/n in Equation (3.14) where a is equal to the atomic mass of Fe and n is equal to 2 (the number of electrons freed during oxidation (Equation (2.3)). Tafel constants were assumed to be 120mV/decade (see Equation (3.12)) as B was kept constant at 26mV for all of the tests. This can result in an error of up to a factor of two$^{[62]}$. The CMS100 uses current interrupt IR compensation to dynamically correct uncompensated resistance errors. Hence, the IR checkbox in the program was switched on for the IR_{drop} to be compensated and for the actual value of R_p to be measured (Table 4-1).

4.6.2.2 Open Circuit Potential

Before applying current to the system, the potential was measured with a CSE reference electrode placed at the center of the probe. In the CMS100, the equilibrium potential assumed by the metal in the absence of electrical connections to the metal is called the open circuit potential (ϕ_{oc}), while the corrosion potential (ϕ_{corr}) is reserved for the potential at which no current flows as determined by a numerical fit of the current versus potential data. It is noted that the values of ϕ_{oc} and ϕ_{corr} will be almost identical if no changes occur in the electrode surface during the scan, which was the case for all the tests undertaken in this investigation. Hence, prior to polarization, the potential was allowed to attain equilibrium, as the anodic and cathodic reactions were allowed to proceed in an undisturbed manner. At this particular moment, there is no net flow of electrons, i.e., $i_a=i_c=i_{corr}$ and $\phi=\phi_{corr}=\phi_{oc}$. An initial delay of 500 seconds was used to allow the open circuit potential to stabilize and reach steady state prior to the potential scan (Table 4-1). Dry concrete (high resistivity) takes longer for the ϕ_{oc} value to stabilize than moist concrete (low resistivity), hence the concrete surface was kept moist to maintain the electric contact. A plot of potential versus time was always displayed on the screen as shown in Figure 4-10 and the last measured potential was recorded as ϕ_{oc}.

4.6.2.3 Linear Polarization Scan

Once the value of ϕ_{oc} was recorded, the potential was lowered (ϕ_{corr} - 20mV). It was then raised incrementally up to the potential of (ϕ_{corr} + 20mV) and the current was recorded at each step. It is noted that all potentials recorded were with respect to the open circuit potential. When the LPR

test was completed, a curve such as that illustrated in Figure 4-11 was obtained. It is noted that Appendix B includes supplementary polarization resistance plots.
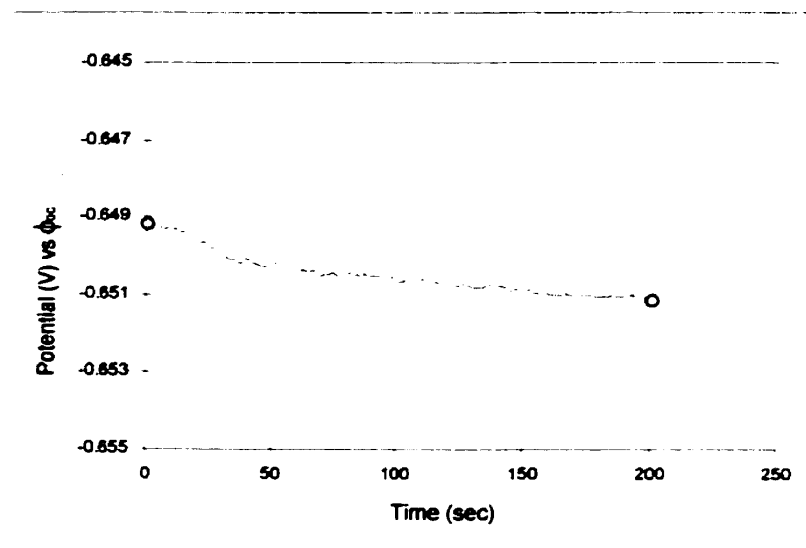
Figure 4-10: *Stabilizing of open circuit potential (Site 10, location 1)*
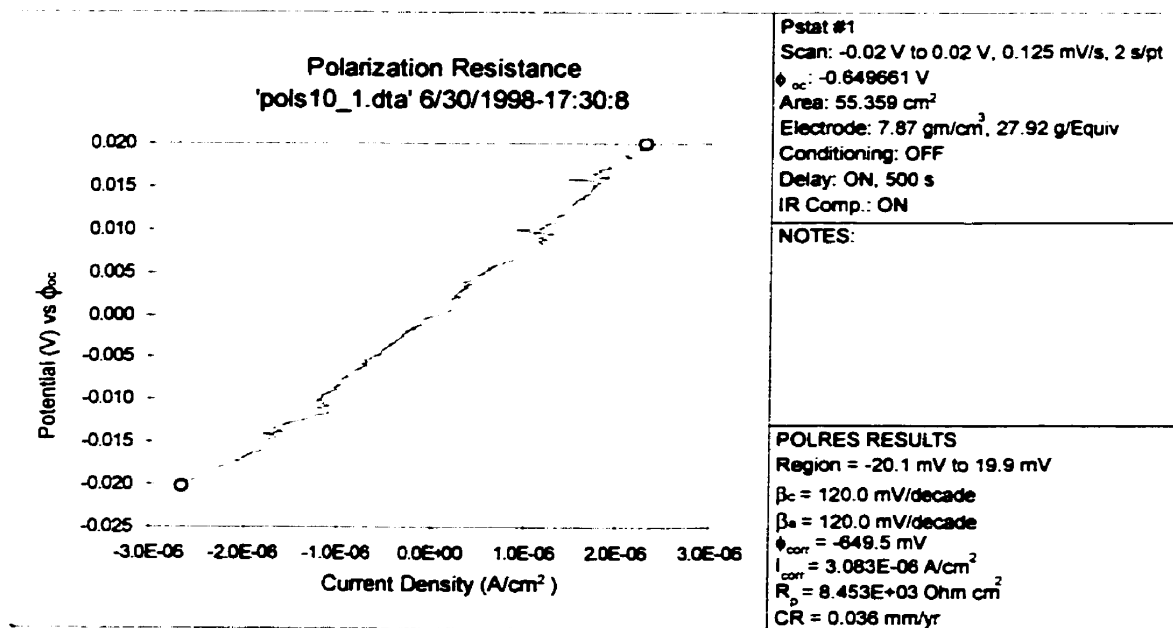
Figure 4-11: *Typical polarization resistance plot (Site 10, location 1)*

4.6.3 Calculation of Corrosion Rate

Using the input information shown in the top right box in Figure 4-11, the software program was able to compute the appropriate parameters of interest based on Stern-Geary and Faraday's Laws[94]. These are shown in the lower right box in Figure 4-11. The corrosion potential was recorded (ϕ_{corr}) which is almost identical to the ϕ_{oc} originally measured, and the polarization resistance (R_p) was calculated using Equation (3.11), that is by taking the slope of the resulting i vs. ϕ curve. The corrosion current density was calculated using Equation (3.12), the Stern-Geary's relationship, and lastly the corrosion rate (mm/year) was calculated using Faraday's Law (Equation (3.14)). Figures A-4 and A-5 (Appendix A) illustrate the corrosion potential and corrosion rate values obtained at each site.

4.6.4 Comparison of Corrosion Rate Measuring Methods

The same procedure was applied to the two types of probes. The guard ring was used at all 140 locations instead the three-electrode probe only at 10 locations. It is noted that at three locations (Site 9, locations 1 and 3; Site 11, location 4) the test could not be undertaken as no steel was detected. A correlation coefficient of 0.842 was obtained between the corrosion rate readings taken at the same location with the two the different probes as shown in Figure 4-12.
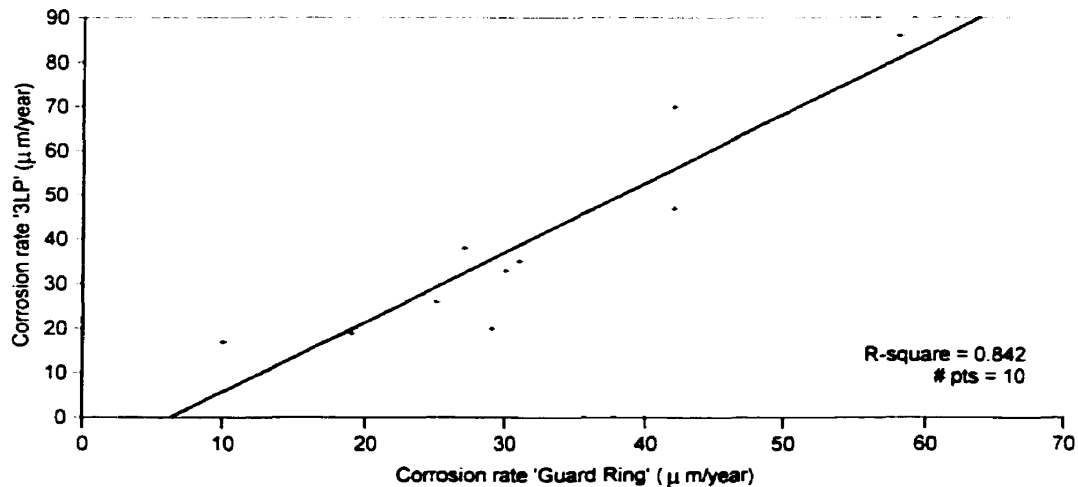
Figure 4-12: *Comparison of corrosion rate values obtained with different probes*

Also, the i_{corr} values obtained with the three-electrode device were higher compared to the values obtained with guard ring. Evidently, this is related to the differences in the current confinement. The higher i_{corr} (3LP) is attributable to the lack of confinement, whereas the lower i_{corr} (guard ring) apparently results from the enhanced confinement. The readings using the guard ring will be used for further analysis in Chapters 5 and 6 while the remaining readings using the 3LP were only conducted to compare the two types of devices.

4.7   In-situ Chloride Migration Test

The newly developed portable in-situ chloride migration kit was used in this investigation to measure the chloride diffusivity of the concrete directly on site without subsequent laboratory analyses. This was conducted on one location of each of the 35 sites.

4.7.1   Preliminary Work

During the month of September 1997 (prior to the main experimental program), a preliminary investigation was undertaken to verify the suitability of both the In-situ Chloride Migration test and the Autoclam Permeability System for on-site work. This was undertaken with the collaboration of R.J. Andrews[86], a research assistant at The Queen's University of Belfast designing and developing the in-situ chloride migration test (Ph.D. Thesis). The work during the main experimental program was conducted in collaboration with both E. McCafferty[95] and R.J. Andrews[86].

The preliminary work for the Autoclam will be discussed later in the chapter. However, the preparation of sites and grid locations that apply to both tests will be discussed in this section. Grid locations were chosen on the deck for permeability and chloride migration tests. In this preliminary work, the deck surface was divided into two sections, the new concrete (the concrete overlay) and the old concrete (the original concrete deck covered by asphalt) which corresponded to the outer lanes reinforced for the truck traffic, and the four central lanes, respectively (Figure 4-4). The sites were chosen near the joints, away from the joints, and at the top and bottom of the bridge.

A total of 12 in-situ chloride migration tests were undertaken to obtain an appropriate testing technique. The procedure best suited will be discussed in detail in the following section where the main in-situ chloride migration work was investigated further. The preliminary work was beneficial in gaining confidence in the test setup as it was the first time the test was used on site and to properly plan the inclusion of the test in the main experimental program. The findings of the preliminary work of the in-situ chloride migration test are presented by Fazio and Andrews[96]:

- The equipment was robust for this type of work, hence it was included in the plan of the main experimental program for further investigation;

- Steady state was achieved in one working day; and

- The in-situ migration coefficients were able to identify poor concrete in the central lanes (original deck) and concrete with much less permeability in the outside lanes (concrete overlay). Also, they indicated that the concrete at the joints was in a worse condition compared with that away from the joints.

4.7.2   Field Test Procedure

The apparatus consists of 2 plexiglas cells, as shown by the schematic diagram in Figure 3-20. The variables used for on-site testing were: a voltage of 60 V, 0.5 M sodium chloride solution. a stainless steel cathode and a mild steel anode.

4.7.2.1   Preconditioning of Concrete Surface

In order to achieve the steady state during testing, the area to be tested was saturated for 48 hours prior to testing. This was achieved by means of polythene rings, which were attached to the concrete using silicone and then filled with water. Ionic migration by diffusion through the free water within the concrete pore structure occurs if the concrete is saturated, but it stops once the concrete is dried out. The pre-saturation of the capillary pores provides a medium that facilitates the passage of chloride ions through the concrete, hence making it possible to reach the steady state. After the saturation period, the rings were debonded, the area patted dry with a sponge to remove surface water and allowed to dry sufficiently to secure the rubber seal without any leak.

4.7.2.2 Test Setup

The plexiglas base plate was secured to the concrete surface by mechanical clamping. Three holes were drilled and fitted with wedge-anchors, which held down the vice-clamps, which are used to seal the unit to the concrete surface. The plexiglas cell, the anode and cathode were assembled and placed in position. The clamping flange was placed over the plexiglas cell and using the vice-clamps pressure was applied to the metal clamping flange to seal the outer ring to the concrete surface (Figure 4-13).

The inner ring was sealed by tightening the wing-nuts on the cross-bar. Distilled water was placed in outer cell and it was ensured that no leaks occurred. The inner cell was filled with the sodium chloride solution with a syringe avoiding any cross-contamination of the two solutions. The DC power supply was connected to the apparatus, with the positive lead connected to the mild steel anode and the negative lead to the stainless steel cathode (Figure 4-14). The potential difference was set to 60 V. This arrangement proved to be satisfactory during the preliminary work and was used during the main experimental program.

Figure 4-13: *Chloride migration test setup on site*

Figure 4-14: *Chloride migration testing apparatus being used on site*

4.7.2.3 Test Measurements

On application of a potential difference, the chlorides migrate from the inner cell to the outer cell through the concrete. After the power was switched on, the time and the initial condition readings were recorded; temperature in the cell was measured using a thermometer and the current flowing in the system was monitored using a multimeter. The apparatus was covered with a specially built housing to minimize temperature fluctuations in the solutions caused by any intermittent sunny spells. This also protected the apparatus from any blown dust, which prevented the contamination of the solutions.

During the progress of each test, the concentration of chloride ions arriving in the distilled water may be monitored by inserting an ion selective electrode and a reference electrode through two openings (specifically designed) in the lid. Hence, it is possible to measure the chloride content of the solution directly in the cell. However, in this investigation, it was decided that the electrodes might break and it would be better to collect samples of 20 ml in plastic bottles for later measure the chloride content in the samples. The samples were taken from the outer cell after 2 hours and then hourly thereafter, until a total of 6-8 samples were collected. The temperature and current were also recorded in the accelerated tests. The first reading was taken after a steady state

105

condition was reached, that is after 2 hours. The interval is usually maintained in the laboratory at two hours throughout the test duration. However, on site, one-hour interval was used after the first reading in order to curtail the test duration to one working day. In addition, on site number 15 tests were run using two-hour intervals and one hour intervals and compared to ensure that the slope of the concentration was consistent.

The concentration of chlorides in the collected samples were measured using an Orion Ion Specific Electrode (ISE) together with a double junction reference electrode and an Orion multimeter. More details follow in Section 4.8 as the same electrodes and meter were used for the chemical analysis. In an ion selective electrode (ISE), the potential difference developed between the sensing and the reference electrodes is a measure of the activity (concentration) of the reactive species. As the activity of the species reacting at the sensing electrode varies, so does the potential measured between the two electrodes. The sample chloride concentrations were measured after performing a calibration of the electrodes using two calibration solutions (100ppm and 1000ppm of sodium chloride solutions). By measuring the electrode potential using both the calibration solutions, and in a sample solution, it was possible to calculate the unknown concentration of the solution by using the following equation which is a different form of Nernst equation:

$$C_{cl} = C_c 10^{\Delta\phi/s} \qquad (4.1)$$

where
C_{cl} = Concentration of the unknown solution;

C_c = Concentration of the standardizing (calibration) solution;

$\Delta\phi$ = Difference between the observed potentials in the standardizing and the sample solutions; and

S = The change in electrode potential per ten-fold change in concentration (electrode slope).

4.7.3 Calculation of Chloride Migration Coefficient

A typical concentration versus time graph is shown in Figure 4-15. The test duration for the test on site number 15 was 6 hours. Regression analysis of the straight line portion of the graph gives the amount of chlorides passing through the concrete per unit time in ppm/hour (dc/dt). The steady state conditions was obtained after two hours during the test as indicated by the straight line with a coefficient of regression of 0.998 which is very close to unity, thus linearity.

It is noted that on this particular site (Site 15), the test was rerun adjacent to the 6-hour test for 12 hours with a two hour interval throughout the test to ensure that the steady state condition was maintained, and the slope of the concentration plot was consistent. Figure 4-16 illustrates the concentration versus time plot for the 12-hour test conducted on site 15. Steady state condition was maintained and the value of the steady state migration rate of chloride ions (dc/dt) for the two tests compared well, being 157 and 153ppm/hr, respectively, hence, the decrease in the time interval did not affect the final results as the slope values are very close.
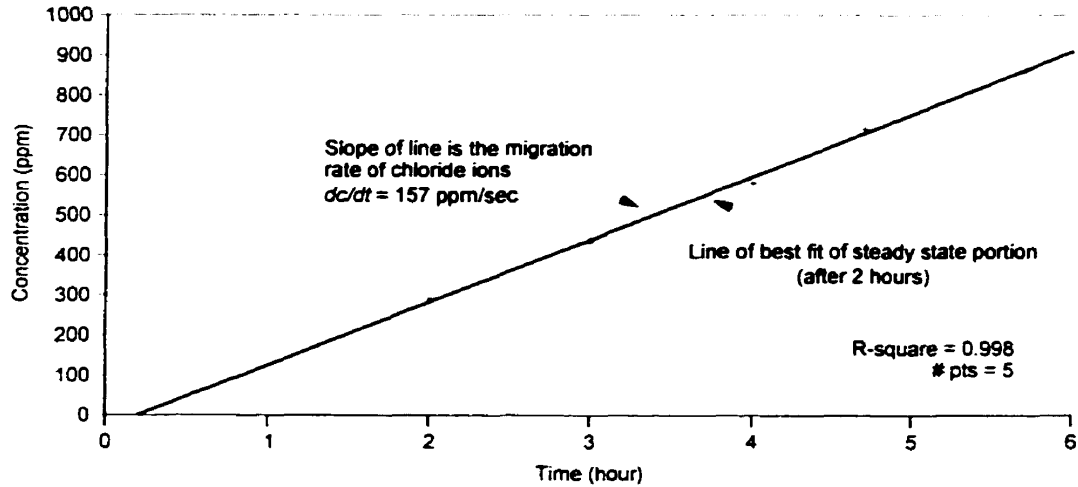
Figure 4-15: *Typical concentration vs. time graph for Site 15 (6-hour test duration)*
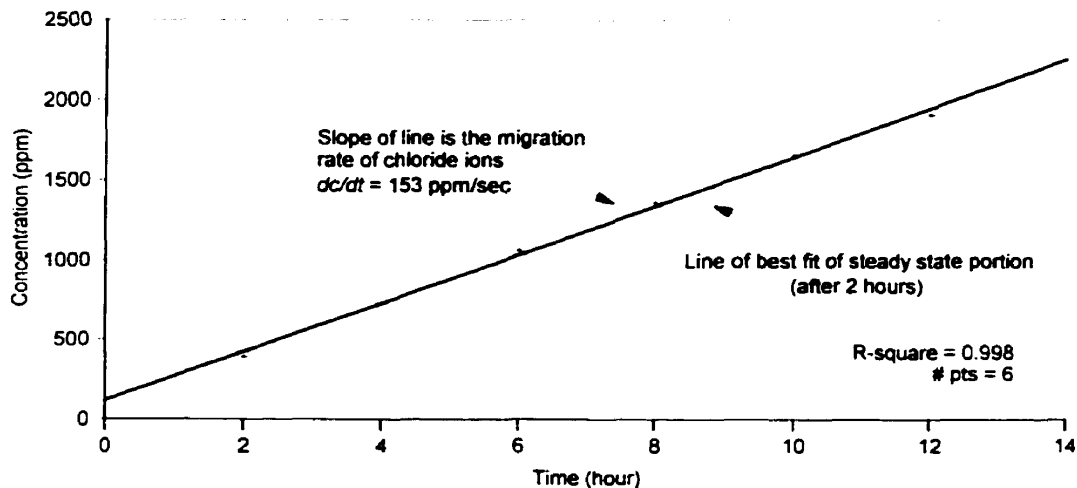
Figure 4-16: *Concentration vs. time plot for Site 15 (12-hour test duration)*

Figure 4-17 shows the current versus time graph for the test conducted on site 15 (12-hour duration). There was an increase in the current corresponding to the start of the steady state condition. The current reached a peak value during the steady state and the measurements can be used as an indication of when steady state occurs during a test[86]. The start of steady state indicated by the current versus time plot (Figure 4-17) was consistent with the result of the concentration plot indicating steady state conditions after 2 hours (Figure 4-16) in this particular case and all other cases in this investigation (Figures C-1 to C-3 in Appendix C).
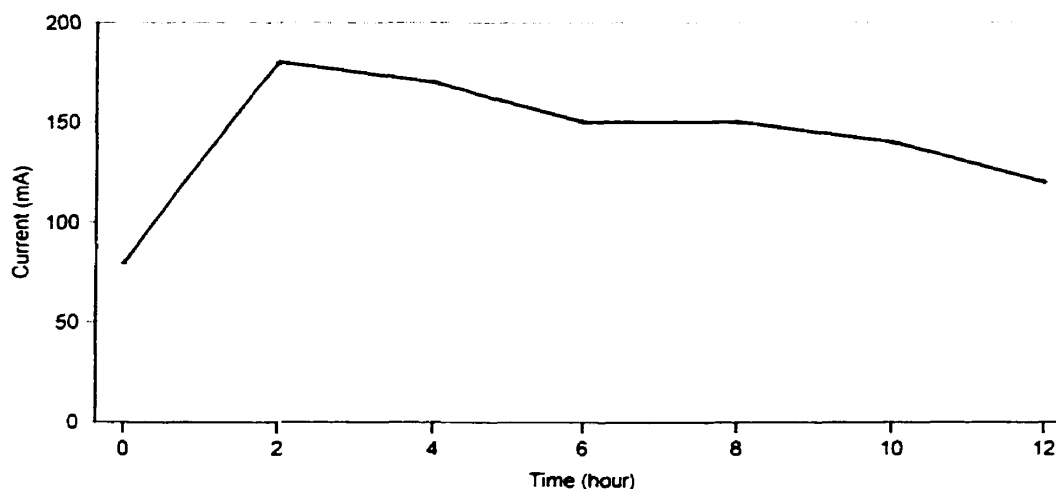
Figure 4-17: *Current versus time plot for Site 15 (12-hour test duration)*

Figure 4-18 shows the temperature versus time graph for the concentration versus time graph for the test conducted on site 15 (12-hour duration). There was no significant temperature increase, with an average temperature of 31.5°C for the steady state portion. This is important as a rise in temperature during testing may give a false value of the chloride diffusivity.

Andrews[86] presented the theoretical basis for the calculation of a migration coefficient and described how the theory was used to obtain a coefficient for the in-situ chloride migration test. A brief description is included in Chapter 3 (Section 3.4.3.2). With the value of dc/dt obtained from Figure 4-16, the flux of chloride ions (J) is calculated using Equation (3-29). Consequently, with the flux value and the average temperature obtained from Figure 4-18, the chloride diffusion coefficient of concrete ($cm^2.s^{-1}$) is calculated using Equation (3.28). The values of C, ΔE, L, V, and A needed in Equations (3.28) and (3.29) were 0.55 M, 60V, 12.25 cm, 725 cm^3 and 117 cm^2, respectively (see Section 3.4.3.2 and Appendix C). The same procedure and calculations were

conducted for all 35 tests (Appendix C). The in-situ chloride migration coefficients (D_{mig}) obtained for each site are shown in Figure A-5 (Appendix A).
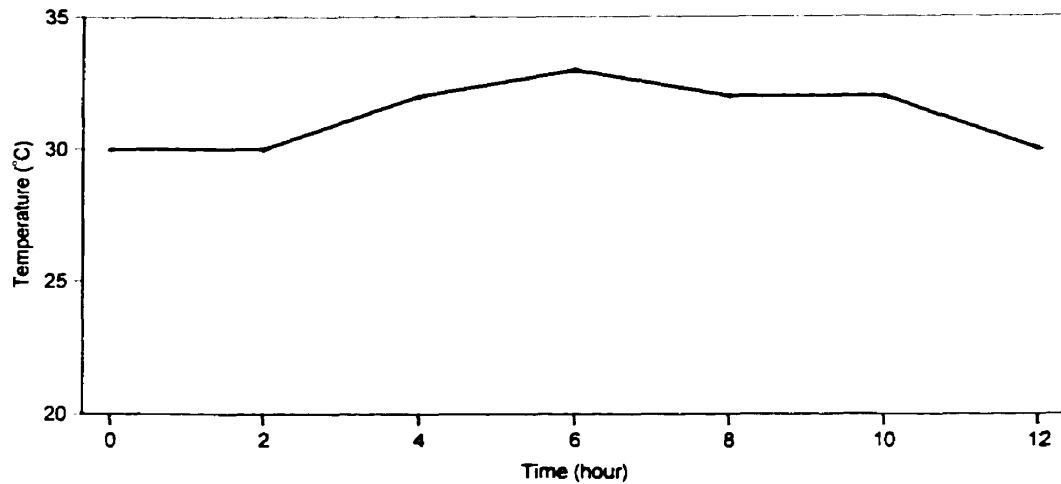
Figure 4-18: *Temperature versus time plot for Site 15 (12-hour test duration)*

4.8 Chloride Profiles

The determination of chloride content is part of any investigation into the corrosion of reinforced concrete structures. This method of sample analysis was used to obtain the chloride concentration profiles at various depths from the face of the chloride environment.

4.8.1 Concrete Dust Sampling

Obtaining a representative sample of the concrete dust to be analyzed was considered as important as the accuracy of the method for analyzing the concrete samples for chloride[78].

4.8.1.1 Sample Collection Equipment and Procedure

The sampling procedure selected for the field use was in accordance to the method endorsed by the Strategic Highway Research Program (SHRP), unit of the National Research Council in the United States[78]. The sampling procedure consisted of drilling holes using a rotary impact drill

and a 29 mm (1 1/8") diameter Hilti bit. This diameter was considered sufficiently large to negate or minimize the influence of the maximum aggregate size on the test results. A standard Hilti carbide vacuum bit with a hole through the center of the shaft was used. The Hilti carbide vacuum bit and its collection adaptor allowed the drill cuttings to be removed from the cutting surface by means of a vacuum system. A drill-stop depth indicator controlled the drilling depth. The sample collection system consisted of a 2.25 hp wet and dry vacuum cleaner chamber, with a plexiglas sample collection chamber, filters, and plastic tubing connected to the Hilti bit assembly. The system significantly reduced the concrete sample collection time and the accuracy was improved as well.

4.8.1.2 Test Procedure

Concrete powder samples were obtained for total chloride ion concentration analysis using the carbide-tipped bit, at 5 mm depths increments. Three holes were drilled in the selected location to ensure that a representative sample was obtained. The concrete dust was collected in the sample collection unit retained by the filter. At every increment, the dust sample was placed in a sealed polythene bag and the filter was replaced with a new one until a total of 10 samples were collected (total depth of 50 mm).

4.8.2 Chemical Analysis for Concentration Profiles

The powder samples were analyzed for their acid-soluble chloride content (i.e. approximate total chloride content percent by weight of concrete) using a chloride ion specific ion electrode. The specific ion electrode technique was chosen as it has been considered to be the best method by SHRP for field measurements based on accuracy, cost, time to perform the test, and technical expertise needed to conduct the test[78].

4.8.2.1 Apparatus and Materials Used

The apparatus and materials needed to conduct the chemical analysis is as follows:

- Orion Ion-Specific-Electrode (ISE) together with a Double Junction Reference Electrode;

- Orion 420A benchtop meter;

- Five calibration solutions 0.01-, 0.03-, 0.3-, 0.6-, and 1.25-percent chloride concentration, based on a 3.0 g powdered concrete specimen;

- 20 ml of digestion solution for each measurement (940 g distilled water, 60 g glacial acetic acid and 50 g of isopropyl alcohol);

- 80 ml of stabilizing solution for each measurement (standard 3.75 ppm chloride solution made from 0.1545 g of sodium chloride and 1 liter of distilled water).

- An electronic scale sensitive to 0.1 g needed to weigh the specimen and sensitive to 0.0001 g needed to weigh sodium chloride for the calibration and stabilizing solutions;

- Magnetic stirring plate; and

- Beakers, spatulas and weighing papers.

4.8.2.2 Instrument Calibration

The chloride ion concentration was calculated indirectly from the potential that is measured using an ion-specific probe. It is based on the principle that the measured potential of a solution depends on the concentration of the reactants and the products involved in a cell reaction. The potential resulting from the presence of Cl⁻ is not converted automatically, but must be obtained through a series of steps, which are discussed in the following.

Preparation of Calibration Solutions

To calibrate the electrode, the potentials of 5 known Cl⁻ concentrations are recorded. These solutions were prepared by adding sodium chloride to distilled water in the correct quantities such that solutions with the desired concentrations of Cl⁻ ions were obtained. Solutions with 1.25, 0.6, 0.3, 0.03 and 0.01% by weight Cl⁻ based on a 3 g concrete sample. Table 4-2 shows the weight of sodium chloride added to one liter of distilled water in order to obtain the desired concentrations, as well as the equivalent concentration in ppm.

Calibration of the Specific Ion Probe

The specific ion probe was calibrated against the set of five solutions each time it was used. The reference electrode was rinsed thoroughly with distilled water. Twenty millilitres of each solution was dispensed in 50 ml Nalgene bottles and labeled appropriately. The probe was placed in each

liquid until the reading did not change by more than 0.2 mV during a 60 second period starting with the lowest concentration standard and progressing to the highest. The entire series of readings was repeated another nine times. The average of the ten readings was calculated for each solution as well as the deviation between the readings. If no deviations exceeded the maximum limits (the allowable deviations of the specific ion electrode were: 4.5 mV for 0.01%, and 1.5 mV for the remaining solutions), then the average of the ten readings for each concentration was used to plot a calibration curve for the specific probe meter combination. If this condition was not satisfied, the electrodes were checked closely for any problem.

Table 4-2: *Preparation of calibrating solutions*

Calibrating Solution (%Cl⁻)	NaCl (g) added to distilled water	Concentration (ppm of Cl-)
1.25	0.6169	374
0.60	0.2961	180
0.30	0.1481	90
0.03	0.0148	9
0.01	0.0049	3

Calibration Curve and Equation

The calibration equation was determined by performing a linear regression of the millivolt responses (X) versus the $\log_{10}$ of the chloride concentrations of the respective calibration solutions (Y) which produced an equation in the following format[78]:

$$log_{10}(ppmCl^-) = A + Bx \qquad (4.2)$$

where A and B are constants, that is the intercept and the slope respectively derived from the calibration graph. The slope inverse was found to be between 54 and 60 mV/decade at 25°C. If not, the electrode were checked for any possible problem. Figure 4-19 illustrates a calibration graph of one of the calibration exercises undertaken during the experimental program. The potentials obtained to plot the calibration curve shown in Figure 4-19 are included in Appendix D where an example of the details of the calibration series are included (Figure D-1).

R-square = 0.998
y = log (ppmCl⁻) = 4.61 + -0.0186x
Inverse slope = 56.9mV/decade
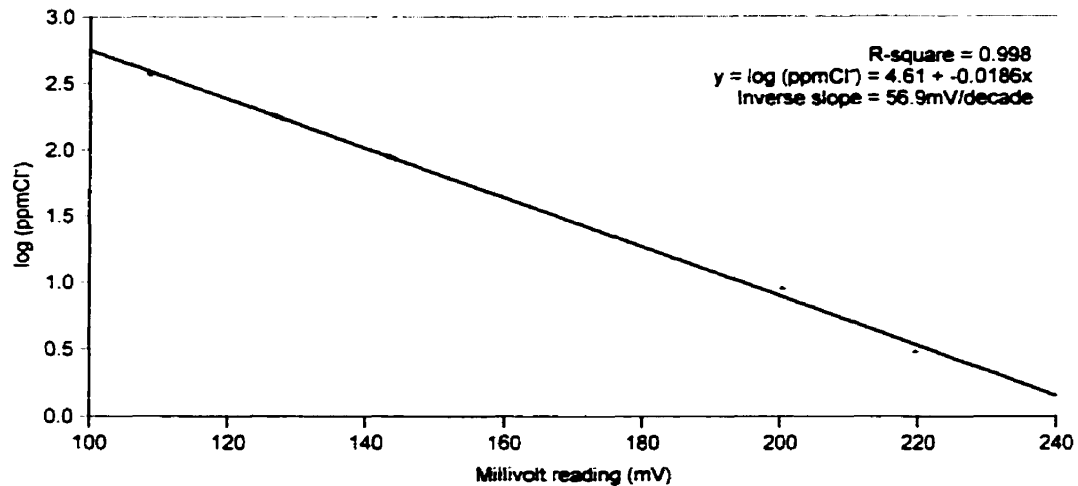
Figure 4-19: *Typical calibration curve*

4.8.2.3 Test Procedure

There is a strong relationship between the specific ion electrode test results conducted by SHRP of the companion crushed (number 50 sieve) and uncrushed (as-collected) chloride samples[78]. Hence, in this investigation the concrete powder for concentration profiles of acid-soluble chlorides was tested as collected.

After calibrating the probe, the acid-soluble chloride content of every powdered sample was measured using the following method endorsed by SHRP[78].

• 20ml of digestion solution was placed in 150 ml glass beaker;

• 3.0 ± 0.1 g of well stirred powdered concrete sample was weighed;

• Sample was placed in the beaker with the digestion solution and mixed vigorously using magnetic stirring plate to suspend the powder in the solution and the powder was allowed to digest for 3 minutes;

• 80ml of the stabilizing solution was added to the mixture and the total solution was well mixed for an additional minute;

• Specific ion probe was placed in the solution and the reading was recorded after the millivolt reading had stabilized; and

- After each reading, the electrodes were rinsed with distilled water.

The above procedure was conducted for every 10 samples of the concrete powder collected at each of the 35 sites.

4.8.2.4 Calculation of Chloride Percentage

The acid-soluble chloride content percent by weight of the concrete was determined from the logarithmic inverse of the regression equation (Equation (4.2)) minus the chloride added by the stabilizing solution, and converted to percentage of chlorides by weight of concrete (%Chl), as follows[78]:

$$\%Chl = \left(10^{(A+Bx)} - 3\right)(0.0033) \tag{4.3}$$

where 0.0033 adjusts the resulting concentration of chlorides in ppm for the use of a 3 g powdered concrete sample of concrete in a 100 ml solution, that is the total solution made up of 20 ml and 80 ml of digestion and stabilizing solution, respectively. This test method was found by SHRP to have no bias in comparing the experimental results with the reference values determined in accordance with the standard laboratory titration procedures (AASHTO T 260-84)[78].

In addition, approximate conversion of the chloride by the weight of concrete to chloride by weight of cement was performed by direct proportioning of the cement to the concrete in the mix design. A sample density of 2400 kg/m^3 and cement content of 375 kg/m^3 were assumed. Hence, to convert chloride percent by weight of the cement, the values obtained from Equation (4.3) were multiplied by 0.15625 (i.e. by the ratio 375/2400).

From the chemical analysis results obtained, the distribution of chloride concentration at the different depths of cover were plotted to obtain the chloride concentration profiles. Figures 4-20 and 4-21 illustrate how the chloride content changed with depth from the surface (12 sites out of the 35). The remaining concentration profiles are illustrated in Figures D-2 to D-5 (Appendix D).
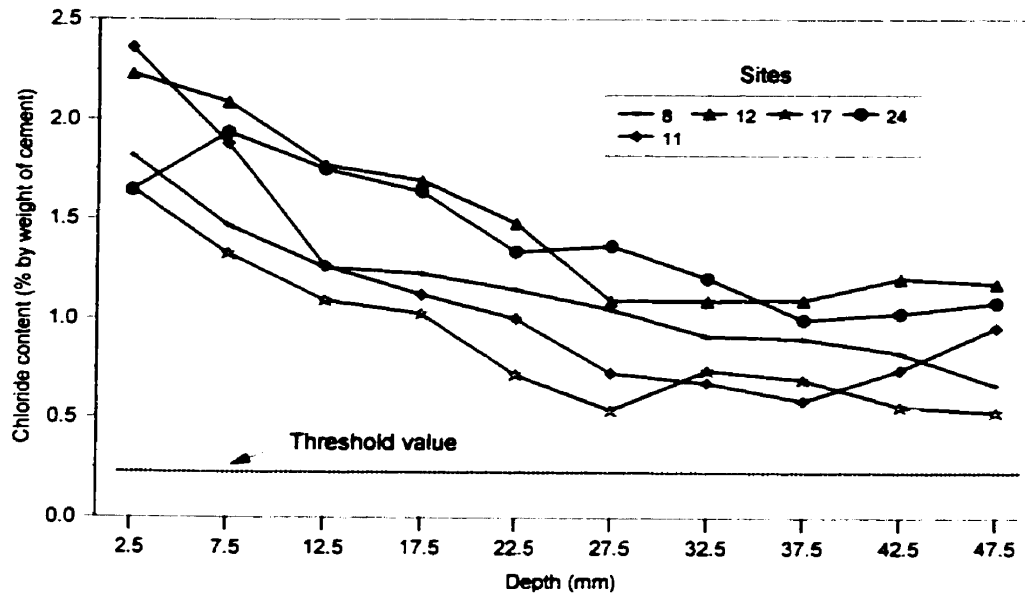
Figure 4-20: *Concentration chloride profiles through concrete (Sites 8, 11, 12, 17 and 24)*
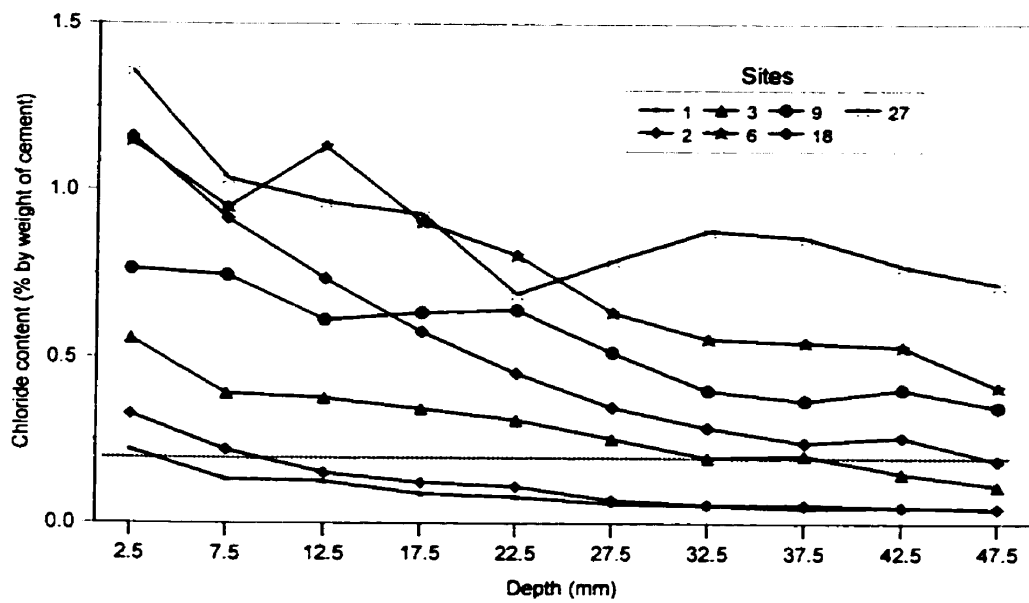
Figure 4-21: *Concentration chloride profiles through concrete (Sites 1-3, 6, 9, 18 and 27)*

4.8.3 Chloride Profile Evaluation

By inspecting the curves shown in Figures 4-20 and 4-21 and in Appendix D, it can be noted that for most cases, the chloride content decreases with increasing depth into the concrete, indicating that the chloride has penetrated the hardened concrete from the surrounding environment and was not present in the concrete when it was cast. In addition, the curves lie well above the threshold acid-soluble chloride content value (percent by weight of cement) reported by the ACI Committee 222[25], which is 0.2% as reported in Table 2-1, with the exception of sites 1, 2, 4, 14 and 29.

4.8.3.1 Chloride Content at Steel Level

The chloride content at the reinforcement level was determined to confirm the electrochemical test results. This is a measure to predict if corrosion is present according to the threshold values. As the concrete cover was determined previously at all four locations on each site, the concrete cover of the corresponding location where the powdered concrete was collected was used to determine the chloride content at the steel level (%Cl) from the plotted chloride profiles. Figure A-7 (Appendix A) illustrates the chloride content at steel level values obtained at each site.

4.8.3.2 Calculation of Apparent Chloride Diffusion Coefficient

Determining the apparent chloride diffusion coefficient (D_a) of the concrete surface involved first determining the total chloride content of the concrete over a range of depths as previously demonstrated. The data obtained from the chloride content as a function of depth for all 35 sites was evaluated by conducting a curve-fitting of the chloride profiles by means of a linear regression analysis. The chloride diffusion characteristics were determined using the method outlined in Section 3.4.2.2 based on Fick's 2nd Law. Following the procedure outlined by Poulsen[37], the measured concentration values, $C(x,t)$, for each profile were included in Equation (3.22) assuming an initial chloride concentration (C_i) value of zero. A regression analysis of the y values obtained from Equation (3.22) against depth, x, was then carried out for each site. Figure 4-22 illustrates a typical example of a linear regression analysis of the transformed variables for site number 3. This enabled q and α values (the y-intercept and the slope of the straight line) to be calculated using Equation (3.21) as shown in the top right in Figure 4-22. The straight line shown in the plot indicated that the data followed Fick's diffusion law. Finally, the apparent diffusion

coefficient was obtained from Equation (3.25) assuming a chloride exposure period of 35 years, that is since the structure was built until 1994, when the bridge was decommissioned.
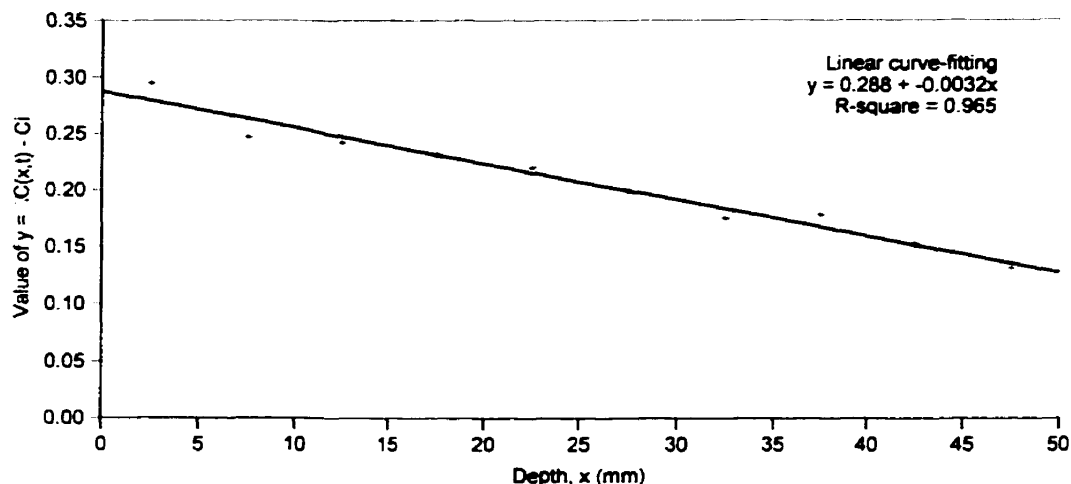
Figure 4-22: *Linear regression analysis of the transformed variables (Site 3)*

The above procedure was conducted for chloride profiles at all 35 sites as shown in Figure A-8 (Appendix A) and Table D-1 (Appendix D). An apparent chloride diffusion coefficient was not calculated for sites 16, 20 and 21 as the plotted data did not show a linear relationship between y and x, hence it did not follow Fick's Law. This is an approximate method; the profiles are not the most accurate, as it depends considerably on the sampling techniques and also on exposure conditions which are variable. Therefore, it's difficult to calculate an apparent diffusion coefficient.

4.9 Autoclam Permeability System

The Autoclam Permeability System was used in this investigation to measure the permeation properties of the concrete directly on site without any subsequent laboratory analyses. This was conducted on three of the four locations at each of the 35 sites. The preliminary work was undertaken prior to the main experimental program to investigate which of the three test techniques (sorptivity, air permeability or water permeability) was most suited for site work and if the equipment was robust enough for this type of work[96]. The preliminary work was undertaken with the collaboration of R.J. Andrews[86], while the work during the main experimental program

was conducted in collaboration with both E. McCafferty[95] and R.J. Andrews[86] from The Queen's University of Belfast.

4.9.1 Preliminary Work

The sites were chosen as discussed in Section 4.7.1. A total of fifty tests were undertaken to develop an appropriate testing technique. The procedure used is detailed in Section 3.5.5 with slight differences, which will be pointed out. The air permeability tests depends strongly on the moisture content of the concrete, and therefore, the concrete was preconditioned by surface drying for 20 minutes using a propane heater prior to the air permeability test. The relative humidity was measured at 10 locations and at depths of 10 mm and 25 mm from the concrete top surface; these were found to be on the average 85% and 89%, respectively. The Autoclam findings showed the limitations of using the air permeability and the sorptivity tests due to the high moisture content of the surface concrete. However, by using the water permeability test, it was possible to assess the water permeability of the concrete on the bridge deck on a relative basis. The procedure best suited for the water permeability work will be described in detail in the following section where the main water permeability work was further investigated. The findings of the preliminary work on the water permeability test were[96]:

*   The applied pressure for the water permeability was only 0.5 bar. The Autoclam was being modified by Queen's University to withstand a higher pressure (1.5 bars) as the test pressure was lower than the surface tension forces in capillary pores filled with water;

*   The equipment was robust for this type of work and the procedure was quick (20 minutes per test);

*   The readings were obtained at the rate of one per 15 minutes, allowing a large amount of information to be developed at close intervals across a given concrete member; and

*   The coefficients of permeability values were used to identify the poor concrete in the central lanes (original deck) and the concrete with much less permeability in the outside lanes (concrete overlay).

4.9.2 Water Permeability Test Procedure

Based on the preliminary work undertaken, the water permeability test was chosen to be the most suited for site work. The water permeability test was conducted at every one of the 35 sites. Three tests were undertaken at each site where an average of the three tests was conducted.

4.9.2.1 Relative Humidity Measurements

The properties of concrete are a function of time and ambient humidity, and this is why the permeability tests were performed under specified or known conditions. The relative humidity was measured next to the permeability tests for sites 1 to 8 and 18 to 25 (Figure A-9 in Appendix A). The readings at depth of 10 mm and 25 mm were from the concrete top surface were found to be on the average 86% and 90% with a standard deviation of 7% and 2%, respectively. This was consistent with the preliminary work. A hand-held relative humidity meter (Novasina Model MS1) was used to measure the *RH* and the temperature as shown in Figure 4-23. This meter enables an accurate evaluation of the relative humidity as it is able to measure over the entire range from 5 to 95% and at temperatures of $-10°C$ to $50°C$ with an accuracy of $\pm 1\%$ and $\pm 0.3°C$, respectively. The sensor, which is mounted on the meter, is developed for use in the concrete utilizing an expandable gland to enable a seal within the hole drilled. The diameter of the hole in the investigation was 16 mm.
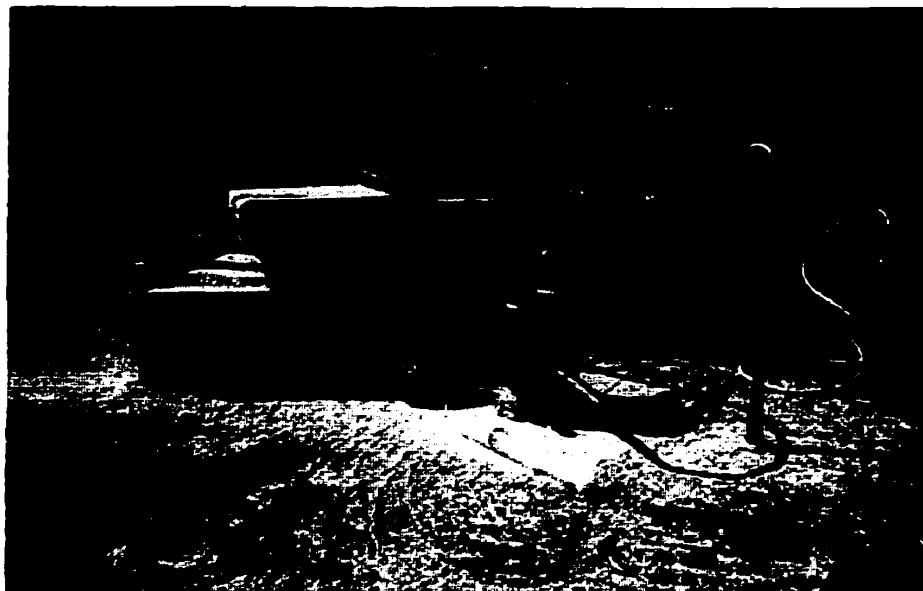
Figure 4-23: *Measurement of RH next to permeability test*

4.9.2.2 Preconditioning of Concrete

It has been suggested that if a measurement of the moisture content at the time of test is possible, the Autoclam indices could be reported for a standard moisture content after applying appropriate corrections[92]. However, with the available information it is difficult to apply on site and needs further investigation. These tests were undertaken in the laboratory with known water/cement ratios and concrete mix designs. Samples removed from site for laboratory testing can be conditioned to a controlled moisture condition. For in-situ tests, this cannot be achieved and pragmatic steps may have to be adopted such as not performing water permeability tests within 48 hours of a rainfall. However, for the present study, this was not enough as the ambient relative humidity was quite high (Section 4.9.2.1) even on a hot summer day (temperature = 35°C) after two weeks without any rain. The concrete could not be dried to a constant moisture content as the RH would rise up to 90% after simply three to four minutes after drying, thereby not permitting enough time to run the test which took about 15 minutes in total. It is noted that if steady state of flow is established, the concrete should be saturated and the permeability is expressed as a coefficient of permeability and not as a water permeability index[87]. The difference of the two is explained in Section 3.5.5.3. Hence, it was decided to pond water for 48 hours by means of polythene rings which were attached to the concrete using silicone, and then filled with water prior to testing in order to achieve a steady state of flow during the permeability test. This was considered the most appropriate choice considering the high moisture content in the concrete even though it has been reported that a steady state is not achieved through the entire pore system under the test area[14]. Montgomery and Adams[91] undertook some work using ponded specimens using a pressure of 1.76 bars which is much larger than the value used in this investigation (0.5 bar), however, the pressure was not changed from 0.5 bar for the present study.

4.9.2.3 Checks and Calibration

Before a series of tests, the Autoclam unit was checked for air tightness. The Autoclam was fixed onto a solid metal plate and the air pressure increased to approximately 0.5 bar. The priming valve was then closed and the pressure monitored for 15 minutes. If the pressure was observed to fall, this implied that the Autoclam needed to be checked for any possible problem as the steel plate is impermeable to air flow, hence the pressure should remain at the initial reading (0.5 bar).

4.9.2.4 Water Permeability Test Setup

After ponding for 48 hours, the polythene rings and water were removed. The test area was patted dry with a sponge to remove the surface water and allowed to dry sufficiently to bond the base ring of the Autoclam to the concrete surface using isopon (car body filler). After the unit was clamped to the 50 mm base ring, the procedure described in Section 3.5.5.3 was followed. Figure 4-24 illustrates the Autoclam being used on site.

Figure 4-24: *Water Permeability measurement on site*

4.9.3 Calculation of Coefficient of Permeability

The data was downloaded from the data-logger and the volume of water absorbed over the test area was calculated by multiplying the movement of the piston (from the readings downloaded from the unit) by the cross-sectional area of the cylinder. The volume of water flowing into the concrete and the time elapsed was plotted for each test and the slope of the line for the last 10 minutes (5 to 15 minutes) of the test duration was extracted as shown in Figure 4-25 for site 6 (location one). As shown in this case, the graph illustrates that a steady state has been reached as the line is quite straight. This is the case for all the tests undertaken in this investigation, and which are included in Appendix E.
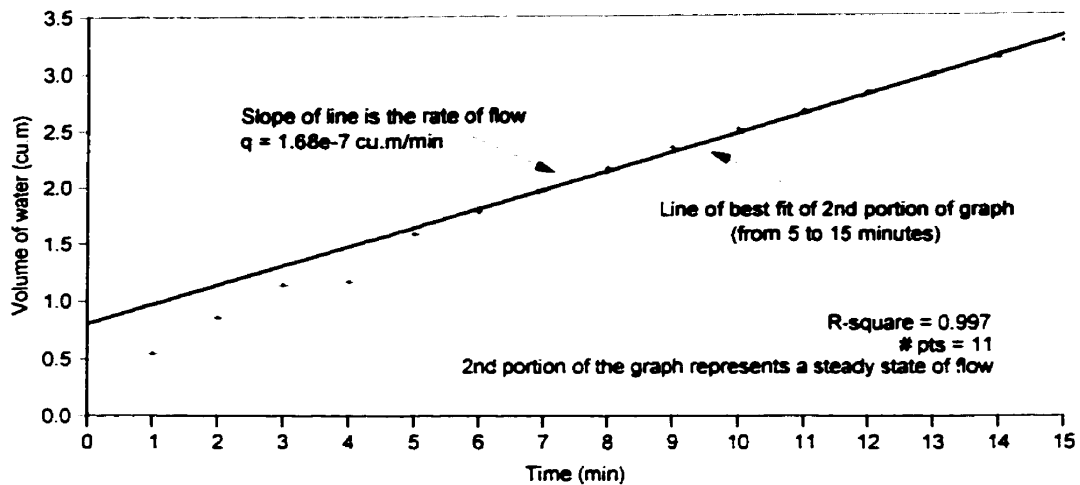
Figure 4-25: *Calculation of rate of flow for the steady state (Site 6, location 1)*

The slope of the second portion of the graph represents the rate of flow for the steady state (q). The flow values of the three readings are shown in Figure E-3 (Appendix E) with the corresponding average values of each site. These values were used to obtain an average coefficient of permeability for the site. Knowing the rate of flow, q, Equation (3.30) was applied to calculate the coefficient of permeability. In Equation (3.30) the calibration factor, c, needs to be known as explained in Section 3.5.5.3. This was possible by calculating a proportionate calibration factor for the steady pressure of 0.5 bar that was applied during the test compared to the 1.76 bar (25 psi) pressure used by Montgomery and Adams[91]. The calibration factor is equal to 0.714×10^{-3} for the 1.76 bar as indicated in Section 3.5.5.3 and for 0.5 bar pressure, the coefficient was found to be 0.207×10^{-3}.

It is noted that the values of the coefficient of permeability values were expected to be low as the applied pressure during the test (0.5 bar) is smaller than the surface tension forces. In addition, the coefficient values need to be adjusted for the area which took part in the flow. That is, flow takes place through bigger pores and not through the fine pores as the surface tension force is small for the larger pores[14]. This was not calculated in this investigation as it requires detailed calculations using Washburn's equation[27] where the capillary radius, depth of penetration, surface tension, fluid viscosity, and contact angle need to be known. Figure A-10 (Appendix A) illustrates the coefficient of permeability values obtained for each site.

4.10 Water Absorption Test

In addition to the nondestructive permeability testing, 12 cores were obtained from 10 sites and subsequently tested in the laboratory for water absorption capacity. The in-situ testing was not sufficiently quantitative to allow for prediction of actual permeabilities from the results of the field tests as the RH was so high and the applied pressure was so low. The in-situ test must therefore be regarded as an indicator of the relative permeability, hence it was decided to use a standardized laboratory technique to obtain a quantitative value. However, it is noted that the absorption test measures the total volume of water absorbed and not the permeability of the concrete. The standard followed for this test was the British Standard 1881:Part 122:1983[89] which is performed on core specimens.

4.10.1 Test Procedure

Twelve cores, each measuring 75mm in diameter were obtained from the various sites, thereby ensuring a result that would be representative of the entire area being tested. The specimens were then cleaned and cut or planed. The cores were dried at 105°C for 72 ± 2 hours, cooled for 24 ± 0.5 hours in an airtight vessel and then weighed. They were then immersed in water for 30 minutes, then they were removed from the water, dried with a cloth and weighed again.

4.10.2 Analysis of Results

The absorption of each specimen was calculated as the increase in mass resulting from immersion expressed as a percentage of the mass of the dry specimen. A correction factor according to the length of the specimen was obtained from the British Standard 1881:Part 122:1983[89]. The product of this correction factor and the measured absorption was considered to be the corrected absorption, this being the equivalent absorption of a core with a standard length of 75 mm. Figure A-11 (Appendix A) illustrates the water absorption values obtained for all 12 cores.

123

4.11　Concrete Compressive Strength

The concrete compressive strength was measured using cores extracted from the structure. The fundamental purpose of measuring the strength of concrete test specimens was to estimate the strength of concrete in the actual structure. The concrete on site is of much lower quality than the results of indirect tests would indicate[32]. In-situ strength testing overcomes some of these problems provided the test methods give reliable results. The values obtained is only an estimation as the strength of a test specimen depends on its shape, height-diameter ratio and size, so that a test result does not give the value of the intrinsic strength of concrete. There exist some methods of determining the in-situ strength of concrete, but the limitations on the interpretation of the test results must be taken into account. Non-destructive testing methods should not be used on their own but in combination with coring or partially destructive tests such as the pull-off test[32, 62]. In this investigation, it was decided to test drilled cores as the bridge was being demolished, but in normal circumstances such as inspections of bridges, non-destructive measures should preferably be exercised.

4.11.1　Test Procedure

The standard adhered to during this test was the ASTM C39-93a (Standard Test Method for Compressive Strength of Cylindrical Concrete Specimens)[97] and involved applying an axial compressive load to the core at a rate which is within a prescribed range until failure occurs.

4.11.1.1 Core Drilling

One core per site was obtained by means of a core drill. The specimen was carefully removed by drilling with a diamond bit perpendicular to the horizontal surface. Both the British and the ASTM Standards specify a minimum core diameter of 100 mm (4") with the proviso that the core diameter be at least 3 times the maximum size aggregate; however, ASTM C42-90 allows, as an absolute minimum, this ratio to be 2[32]. In this investigation, 100 mm diameter cores were impossible to obtain because of the congestion of the reinforcement. The spacing between the steel bar was 152 mm (6") center to center (approximately 136 mm clear cover spacing), hence, making it very difficult to obtain a core without the reinforcing steel. In addition, the thickness of the slab was only 152 mm (6") in total, hence the cores would not have been long enough as the

124

minimum allowable height-diameter ratio specified in the ASTM C39-93a Standard[97] is 1.00. Only one core of 95 mm in diameter was obtained and then it was decided to use 75 mm diameter cores as it was easier not to drill through a steel bar and would be long enough to satisfy the ratio stated in ASTM C42-90.

4.11.1.2 End Preparation and Moisture Conditioning

The cylindrical specimens were obtained usually with end surfaces which were far from being plane and square. The ends of the cores to be tested in compression need to be essentially smooth, perpendicular to the longitudinal axis, hence the ends of the cores were sawed and grinded to meet the requirements stated in ASTM C42[97]. The specimen were submerged in water at 23.0 ± 1.7°C for 48 hours immediately prior to performing the compression test.

4.11.1.3 Specimen Testing

Prior to testing, the length of the specimen was measured in accordance with the provisions of test method ASTM C174[97]. Just before testing, the cores were removed from water and patted dry. The specimen was placed on the platen of the testing machine directly under the spherically upper bearing block. The testing machine used was MTS Rock Frame. Each core was placed in turn in the machine with its axis aligned with the centre of thrust of the spherically seated block. A load was applied by the testing machine at a rate of 0.0056 mm/sec. The load was then applied until the specimen failed, and the type of failure was recorded. The data including the dimensions of the cores, the rate of the applied load, the load and the displacement at each step of each test were recorded by a data acquisition system connected to the testing machine.

4.11.2 Calculation of Compressive Strength

The load and the corresponding displacement obtained for each test was plotted. An example is shown in Figure 4-26. The maximum load was determined from the load versus displacement plots. The compressive strength of each specimen was calculated by dividing the maximum load carried by the specimen during the test by its cross-sectional area. In instances, where the specimen length to diameter ratio was less than 2, the result was corrected by multiplying with the

125

appropriate correction factor in the ASTM C39[97]. The above procedure was conducted for all 35 cores. Figure A-11 (Appendix A) illustrates the compressive strength values obtained for each site. It is noted that on site 1, two cores were extracted next to each other, one with 75 mm diameter as the rest of the cores, and the other with a 95 mm diameter. The compressive strength after applying the strength correction factor of the former was of 22 MPa while for the latter was of 19 MPa.
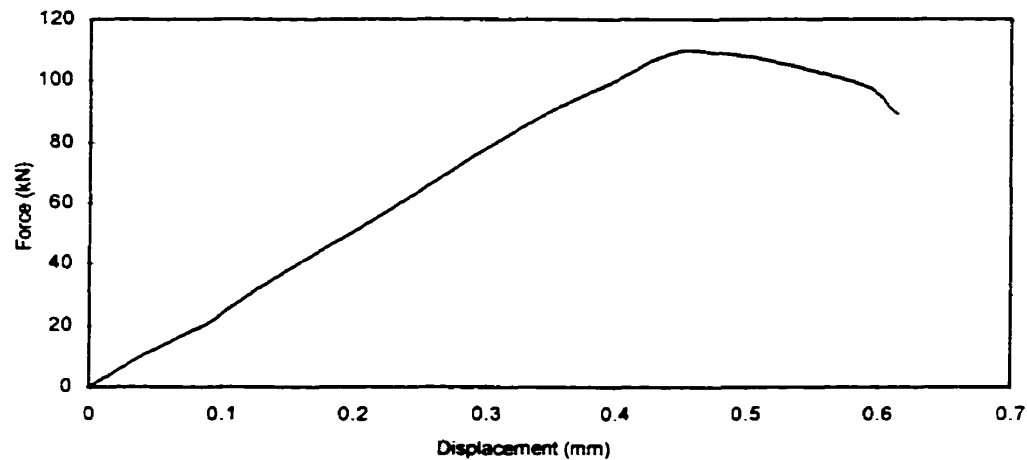
Figure 4-26: *Force versus displacement plot (Site 24)*

4.12 Carbonation Depth

The determination of the depth of carbonation was carried out using drilled cores (75 mm in diameter) in accordance with the RILEM Recommendation CPC-18[88]. A total of 6 cores which were unsuitable for compression testing due to the delamination, thus being too short, or due to the presence of reinforcing steel were tested immediately on site for the carbonation depth. The objective of the test was to obtain information as to whether the carbonation front had reached the reinforcing steel. The core was broken by a chisel and the test carried out directly on site. A solution of 1% phenolphthalein in 70% ethyl alcohol was sprayed immediately after the core was slit and the depth of carbonation was measured after 24 hours as recommended by RILEM[88]. The depth of carbonation was found to be zero, that is there was hardly any carbonation of the concrete. This can be due to the high *RH* of the concrete, which inhibits ingress of carbon dioxide.

5   Presentation of Experimental Results

5.1   Introduction

The details of the experimental program and the evaluation of appropriate parameters were included in the previous chapter. The results of the experimental program are presented in this chapter. The quantitative parameters in question are the half-cell potential (both the half-cell potential survey and the corrosion potential (ϕ_{corr}), the corrosion rate (CR), the delamination ($Delam$), the concrete cover thickness ($Cover$), the percentage chloride at steel the level ($\%Cl$), the apparent chloride diffusion coefficient (D_a), the in-situ migration coefficient (D_{mig}), the electrical resistivity (ρ), the coefficient of permeability (k_w), and the concrete compressive strength (Str).

5.2   Field Test Results: Condition of the Bridge

The existing state-of-health vis-a-vis corrosion damage and concrete quality is determined by having a close examination of the data obtained from the experimental program. Sufficient data was collected to determine the cause of the problem, and to determine the extent of the damage. This will be presented visually to detect any trends in the distribution of the data which will be discussed for all of the parameters influencing the behavior of the bridge deck with reference to the visual plots and the basic descriptive statistics. The east and west sides of the bridge are investigated individually and the different trends are reviewed.

5.2.1   Descriptive Statistics of Experimental Data

The basic descriptive statistics of all of the experimental data (as-collected/original data) are summarized in Table 5-1. The findings show a large variance in some of the parameters such as the apparent chloride diffusivity coefficient and the coefficient of permeability. This large

variance (*COV* in Table 5-1), requires that before undertaking any regression analysis of the various parameters involved, the distribution of the data of each variable must be examined for signs of normality, outliers and skewness. Also, appropriate transformations can be applied to the parameters when the *COV* is large to improve agreement with normality. This will be discussed in detail in the following section. Meanwhile, in this section the original data is presented, which represents the 'as-collected' data.

5.2.2   Assessment of Corrosion Risk Levels

Assessing the corrosion risk represents a tremendous challenge especially to establish the various levels of corrosion activity. Although there have been a few attempts in the past to define durability of concrete bridges based on certain observed parameters, the scales proposed were based only on visual evaluations[62]. In the present study, the quantitative criteria for assessing deterioration risks and for predicting durability was obtained from the data for the parameters under investigation, partly from the codes and partly from the published data. Tables 2-1 and 3-2 to 3-6 in the previous chapters give the criteria, which were used for classifying the condition of the bridge deck. These are recommendations from the various codes indicating the risk levels. The other parameters were classified on a relative basis (by comparison within the measured values). Table 5-2 lists the number of readings in each range and the percentage distribution of the readings for each parameter. The visual plots (Figures 5-8 to 5-13) are based on these ranges which are discussed in the corresponding subsection. References will be made to the descriptive statistics as well.

5.2.3   Visual Inspection

The bridge deck was inspected for the varying levels of concrete deterioration related to the different degrees of corrosion of the steel reinforcement. Based on the visual inspection of the bridge deck, it was found that most of the deck was in bad condition as shown by the photographic records presented in Figures 5-1 to 5-7. Presence of rust, spalling of the concrete cover, exposure of the reinforcing steel, and loss of the steel cross-sectional area were noted at several locations (Figure 5-1 to 5-4). This was noticed mostly towards the crest of the bridge. The west side of the bridge deck showed more damage, especially on the underside of the bridge deck (Figures 5-5 to 5-7). The expansion joints situated at grid locations 36 m and 127 m were found to

128

Table 5-1: *Descriptive Statistics (Analysis 1: as-collected/original data)*

Quantity measured	(a) Entire deck					(b) East side of deck					(c) West side of deck				
	No. of Readings	Max Value	Min Value	Mean Value	COV	No. of Readings	Max Value	Min Value	Mean Value	COV	No. of Readings	Max Value	Min Value	Mean Value	COV
Half-cell potential survey (mV)	2484	-44	-750	-423	0.25	1408	-44	-750	-406	0.26	1076	-102	-710	-445	0.22
Corrosion potential (mV)	137	-123	-700	-444	0.33	65	-123	-657	-403	0.38	72	-175	-700	-481	0.27
Corrosion rate (µm/year)	137	130	4	52	0.55	65	129	4	48	0.63	72	130	13	55	0.49
Delamination	140	-	-	-	-	68	-	-	-	-	72	-	-	-	-
Concrete cover (mm)	137	90	1	35	0.48	65	90	1	33	0.56	72	81	1	36	0.40
Percentage chloride at steel level	35	2.20%	0.07%	0.73%	0.72	17	1.68%	0.07%	0.57%	0.79	18	2.22%	0.11%	0.88%	0.63
Apparent Cl diffusion coefficient (cm²/sec)	32	51.6×10^{-9}	1.4×10^{-9}	9.3×10^{-9}	1.02	16	16.7×10^{-9}	1.4×10^{-9}	7.1×10^{-9}	0.69	16	51.6×10^{-9}	2.0×10^{-9}	11.6×10^{-9}	1.07
In-situ Cl migration coefficient (cm²/sec)	35	13.5×10^{-8}	1.6×10^{-8}	6.3×10^{-8}	0.48	17	13.5×10^{-8}	1.6×10^{-8}	5.6×10^{-8}	0.57	18	12.1×10^{-8}	2.3×10^{-8}	6.8×10^{-8}	0.40
Electrical resistivity (kΩ.cm)	137	27	1	6	0.72	67	27	1	7	0.81	70	18	2	6	0.57
Coefficient of permeability (m/sec)	34	84.2×10^{-14}	1.8×10^{-14}	16.3×10^{-14}	1.18	16	40.4×10^{-14}	1.8×10^{-14}	13.1×10^{-14}	0.86	18	84.2×10^{-14}	3.0×10^{-14}	19.1×10^{-14}	1.27
Concrete compressive strength (MPa)	34	48	10	27	0.36	16	48	10	26	0.38	18	45	12	28	0.34

Table 5-2: *Criteria for classification of test results*

Quantity measured	Range of values	Number of values in each range		
		Entire deck (%)	East side of deck (%)	West side of deck (%)
Half-cell potential survey	Above –500 mV	25	19	34
	–350 to –500 mV	51	52	50
	–200 to –350 mV	22	27	14
	Below –200 mV	2	2	2
Corrosion (open-circuit) potential	Above –500 mV	42	35	47
	–350 to –500 mV	31	31	32
	–200 to –350 mV	21	23	19
	Below –200 mV	6	11	1
Corrosion rate	Below 1 μm/year	-	-	-
	1 to 10 μm/year	1	3	-
	10 to 45 μm/year	47	52	43
	45 to 100 μm/year	44	37	50
	100 to 1000 μm/year	7	8	7
Delamination	Delaminated	53	34	71
	Non-delaminated	47	46	29
Concrete cover thickness	Below 25 mm	29	37	22
	25 to 40 mm	30	26	33
	40 to 50 mm	26	18	32
	Above 50 mm	15	18	13
Chloride content at steel level	Below 0.2%	17	29	6
	0.2 to 0.4%	11	18	6
	0.4 to 0.6%	17	12	22
	Above 0.6%	54	41	67
Apparent chloride diffusion coefficient	Below 3.0×10^{-9} cm^2/sec	19	25	13
	3.0 to 13.0×10^{-9} cm^2/sec	59	56	63
	13.0 to 23.0×10^{-9} cm^2/sec	16	19	13
	Above 23.0×10^{-9} cm^2/sec	2	0	13
In-situ chloride migration coefficient	Below 3.0×10^{-8} cm^2/sec	11	12	11
	3.0 to 6.0×10^{-8} cm^2/sec	37	53	22
	6.0 to 9.0×10^{-8} cm^2/sec	29	18	39
	Above 9.0×10^{-8} cm^2/sec	23	18	28
Electrical resistivity of concrete	Below 5 kΩ.cm	52	52	51
	5 to 10 kΩ.cm	31	25	36
	10 to 20 kΩ.cm	15	18	13
	Above 20 kΩ.cm	2	4	0
Coefficient of permeability of concrete	Below 10.0×10^{-14} m/sec	56	50	61
	10.0 to 20.0×10^{-14} m/sec	21	25	17
	20.0 to 30.0×10^{-14} m/sec	9	13	6
	Above 30.0×10^{-14} m/sec	15	13	17
Water absorption of concrete	Below 3%	83	100	75
	3 to 4%	17	0	25
	Above 4%	0	0	0
Concrete compressive strength	Below 20 MPa	29	31	28
	20 to 30 MPa	29	31	28
	30 to 40 MPa	29	31	28
	Above 40 MPa	12	6	17

be leaking and there were signs of run down from the bridge deck to the underside of the deck. It is noted that there was no specific drainage system on the bridge.

Upon removal of the asphalt, it became clear that some parts of the concrete deck had been repaired in the past. This was evidenced by certain areas having different colour and texture as well as different sizes of aggregate sizes (mostly in the vicinity of the two expansion joints, that is grid locations 36 and 127 (Figure 4-4)) from the rest of the deck. Unfortunately, no records of the exact locations of repair or the material used were available, but the city engineer (Mr. Robert Cardin) confirmed that some repairs were undertaken throughout the past years. In addition, the placement of reinforcing steel was not properly done as illustrated in Figure 5-1. The concrete cover to the reinforcing steel was deficient in several places and thus the reinforcing steel did not get the desired protection from the alkaline environment. Some of the rebars were within the asphalt surface, where it is exposed directly to the aggressive agents from the environment. It is evident that quality control during construction was not adequate.

Figure 5-1: *Exposure of reinforcing steel and concrete deterioration (Site 7)*

Figure 5-2: *Corrosion of reinforcing steel and spalling of concrete cover (Site 11)*
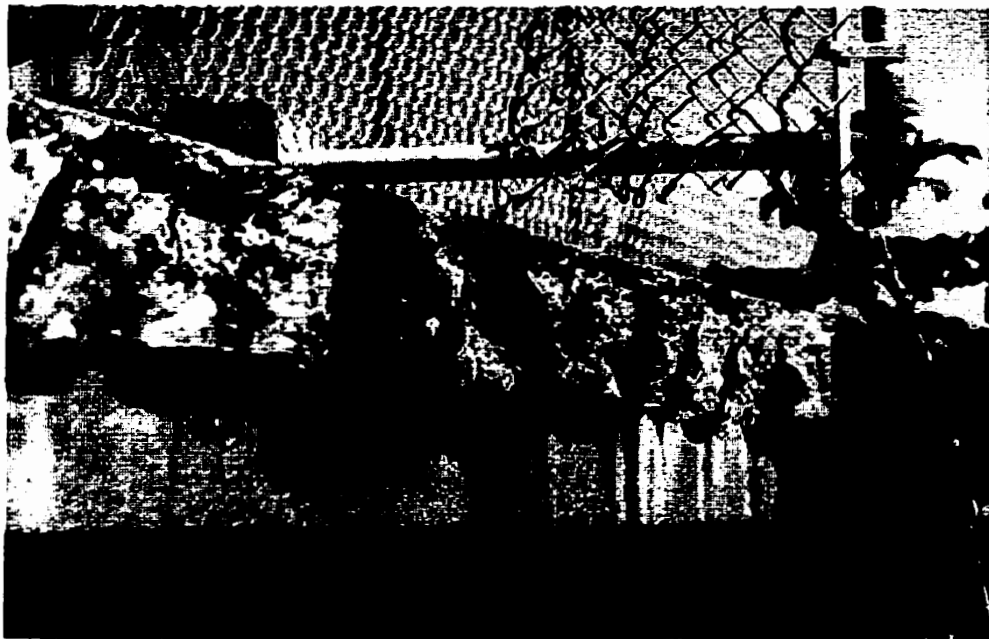
Figure 5-3: *Spalling of the concrete cover (west side of bridge deck)*

Figure 5-4: *Loss of the steel cross-sectional area (Site 22)*

Figure 5-5: *Underside of bridge deck (Site 28)*

Figure 5-6: *Underside of bridge deck (Site 30)*
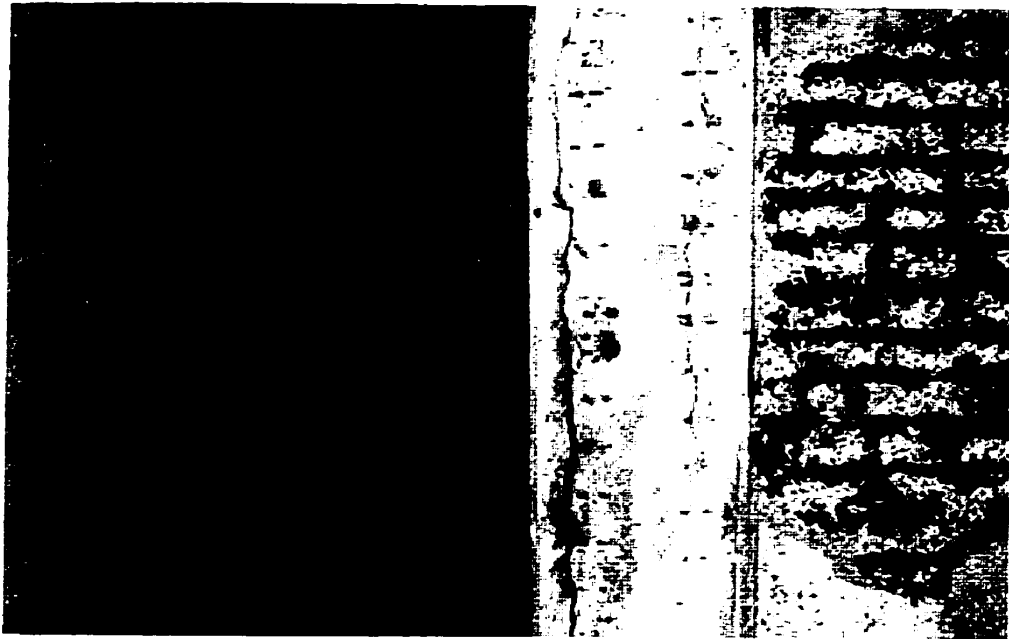
Figure 5-7: *Underside of bridge deck (Site 31)*

134

5.2.4   Potentials and Corrosion Rate

A half-cell potential survey of the entire bridge was undertaken over a grid of one meter by one meter as indicated in Section 4.2. The corrosion (open-circuit) potential (ϕ_{corr}) and the corrosion rate (CR) of the reinforcing steel (using linear polarization test) were obtained only at the locations where the detailed investigation was undertaken (Sections 4.6.2.2 and 4.6.2.3).

5.2.4.1   Half-Cell Potential Survey

Half-cell potentials are sensitive to the variations in the environment; the most sensitive variable is the moisture content. However, it is important to realize that the moisture of the concrete does not influence the potential contours. The potential become more negative as the moisture content of the concrete varies[63]. The relative humidity (RH) was observed to be quite consistent throughout the bridge, but on the average it was quite high. The RH at depths of 10 mm and 25 mm from the concrete top surface were found to be on the average 86% and 90%, respectively (Figure A-9 in Appendix A). This may have enhanced the high negativity of the potential readings, but the fact that the moisture was consistent throughout the bridge means that the actual contours are not affected. The probability of occurrence of corrosion was studied using both the ASTM C876[64] guidelines and the iso-potential contour maps, that is the magnitudes of the potential were considered and the potential gradients were qualitatively assessed.

The half-cell potentials varied from –750 mV to –44 mV with a mean value of –423 mV and a coefficient of variation (COV) of 0.25. Table 5-2 lists the number of readings in each potential range, and the percentage distribution of these readings. A contour map of the entire bridge is shown in Figure 4-5 in which the potential ranges are indicated for a contour interval of 50 mV. The plot was used to choose the 35 sites as explained in Section 4.2.3. Figure 5-8(a) is the reproduction of the same data with a contour interval of 25 mV. The potential measurements indicate active corrosion of embedded reinforcement in most of the deck (Figure 5-8(a)). Fifty-one percent of the readings suggest that there is a 50% to 90% risk of corrosion, while 25% of the readings suggest that the risk of corrosion is more than 90% (Table 5-2). The low values of potential are concentrated in the first 33 rows of the grid (Figure 5-8(a)). The half-cell potential gradients are quite pronounced throughout the entire deck. The very steep half-cell potential gradients indicate extensive pitting corrosion at local anodes. This is common for structures contaminated by deicing salts. The west side of the bridge has a larger number of readings in the

135
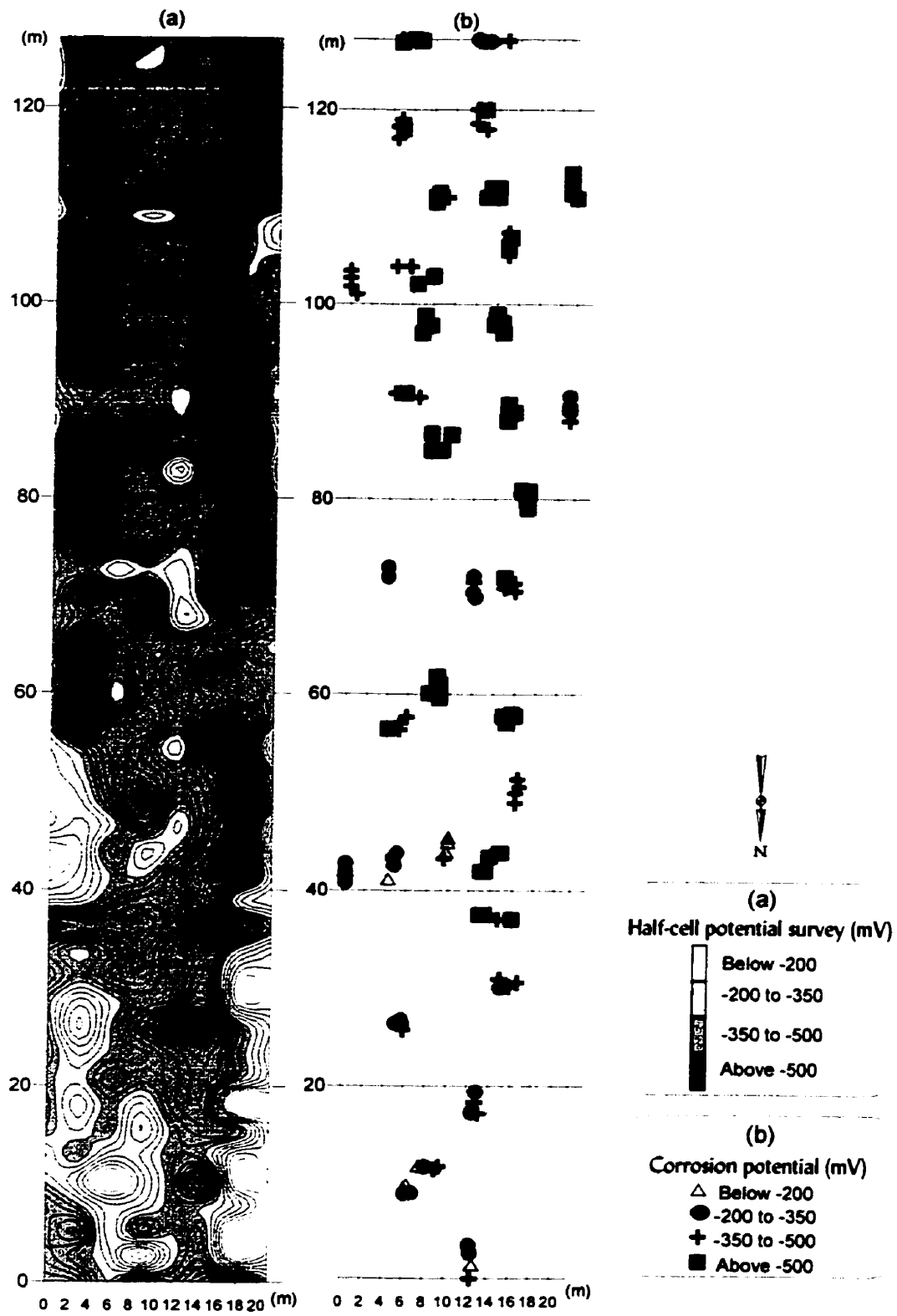
Figure 5-8: *Half-cell potential and corrosion potential results*

range of -500 mV and algebraically smaller potential values (Table 5-2) with a mean value of -445 mV which is more negative compared to the mean value of the east side (Table 5-1). The results show that the west side is deteriorating more rapidly than the east side (Table 5-2). Therefore, more corrosion deterioration can be expected on the west side, which was the case, confirmed by visual examination (Figures 5-4 to 5-7).

5.2.4.2 Corrosion Potentials

The corrosion (or open-circuit) potentials, ϕ_{corr}, varied from -700 mV to -123 mV with a mean value of -444 mV and a COV of 0.33. Figure 5-8(b) shows a visual presentation of the results using the same interpretation as for the half-cell potential measurements. A contour map was not plotted as the readings were taken at 137 discrete locations (4 per site) and not at equal intervals. Forty-two percent of the readings are smaller than -500 mV and they predominate the top portion of the grid from grid locations 70 m to 127 m (Figure 5-8(b)). Again, the west side of the bridge deck displayed a greater percentage of readings in this range compared to the east side (Table 5-2) with a more negative mean value as shown in Table 5-1 (-481 mV compared to -403 mV), which is in agreement with the results of the half-cell potential (Figure 5-8(a)) and visual surveys.

5.2.4.3 Corrosion Rate

The RH values are very high values as indicated in Section 5.2.4.1 suggesting that the rate of corrosion is significant, with the corrosion activity increasing with an increase in the relative humidity. In fact, the corrosion rate (CR) values obtained from the linear polarization test varied from 4 to 130 µm/year with a mean of 52 µm/year and a COV of 0.55 (Table 5-1). The corrosion rates are plotted in Figure 5.9(a), which shows that 91% of the readings (Table 5-2) represent a high risk of corrosion (based on the criteria presented in Table 3-3). Similar results are depicted on the east and west sides of the bridge. However, by dividing the range in two, i.e., by adding a range in the middle of 10 to 100 µm/year, it was also observed that 52% of the readings lie between 10 and 45 µm/year, and 37% between 45 and 100 µm/year for the east side, and only 43% and 50%, respectively, in the west side (Table 5-2). As a whole, the rebar corrosion rates for the west side are higher and the readings from the bottom half of the grid are lower than the values for the top half as shown in Figure 5-9(b). The trends are consistent with the potential values and the visual survey. Higher corrosion rates are present at the top part of the grid,

137
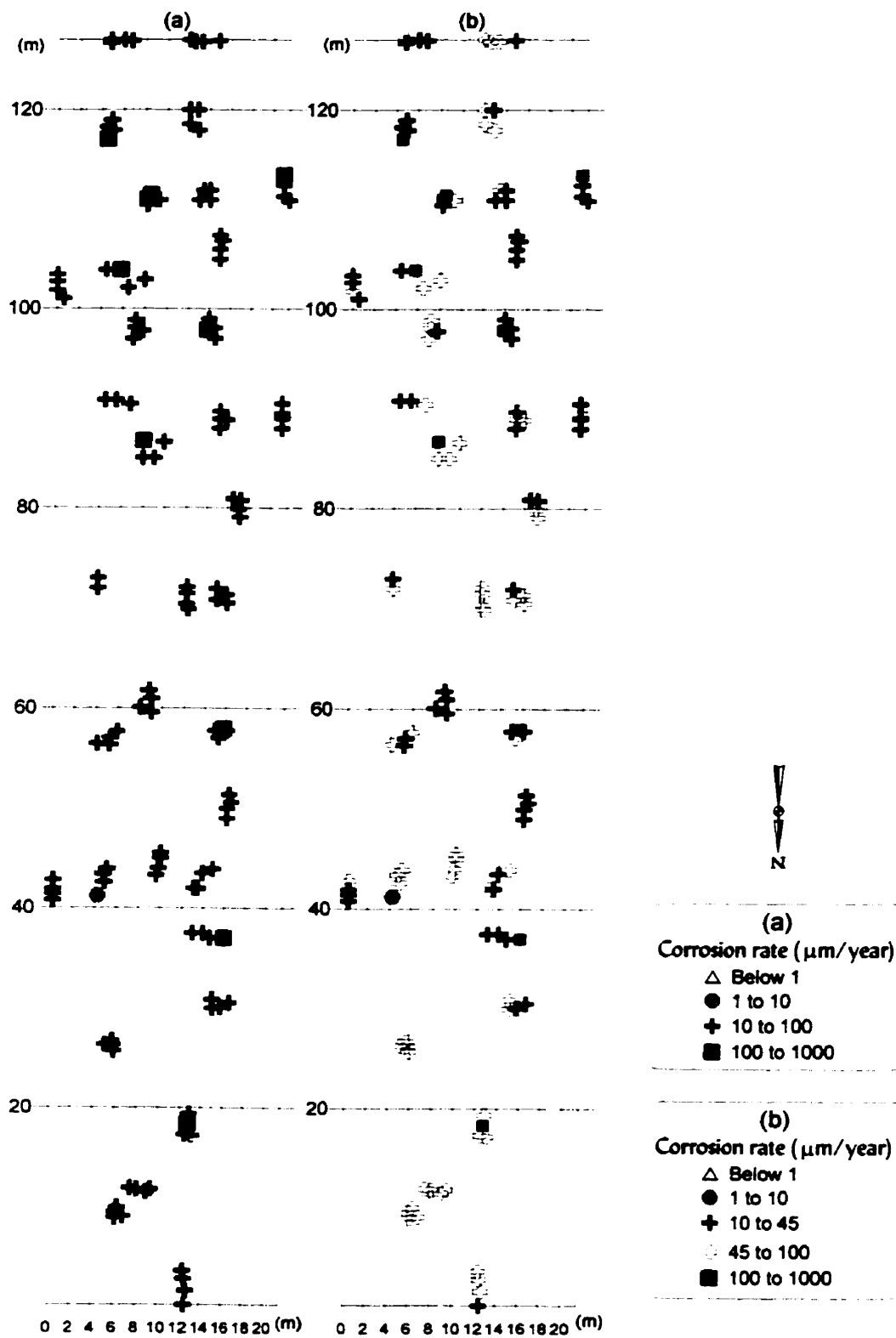
Figure 5-9: *Corrosion rate results*

particularly to west side of the deck (Sites 27 to 35).

5.2.5 Delamination

Figure 5-10(a) shows the delamination (*Delam*) results of the 140 selected areas (4 readings per site) throughout the northern part of the bridge. The fracture plane, or delamination, may be confined to a local area, or it may extend over a substantial portion of the deck if the concrete cover is uniformly low. The delamination was very extensive, with half of these areas being delaminated. The exposure of reinforcement for the measurement of half-cell potentials indicated delamination to occur at the level of steel. In addition, compressive tests performed on cores at the top of the deck indicated concrete deterioration. The cores were visually examined; some cores contained delamination and cracks, and the reinforcement in the cores had corroded to the extent that the bond between concrete and steel was severely affected.

Although no specific data for exposure conditions exists for the Dickson Bridge, it can be assumed that the conditions are similar to those experienced in the Province of Quebec. In Montreal, minimum temperatures reach $-40°C$ in the winter period and in the summer temperatures are as high as $35°C$. In addition, on a given 3-day period, in certain cases the temperature varies only between $+1°C$ and $-1°C$, but in other cases it drops from $+4°C$ to $-13°C$ in 10 hours. Of course, the temperature of any portion of a concrete element exposed to natural cycles does not necessarily follow directly the variation of the ambient temperature. In addition, due to alternate sunny and cloudy periods on cold winter days, the surface layer can be subjected to several freezing and thawing cycles per day. Freezing rates of more than $12°C$/hour are noted in certain cases[98]. Hence, the freeze-thaw cycles and the impact of traffic may have also added to the delamination growth. These areas are located mostly from grid locations 70 m to 127 m. The non-delaminated areas are concentrated in the first 40 meters of the grid. Seventy-one percent of the west side areas are delaminated while only 34% of the selected areas in the east side sites are delaminated (Table 5-2). The delamination results are consistent with the corrosion potential and the corrosion rate survey. The damage is much greater in the top portion, especially in the west side of the deck.
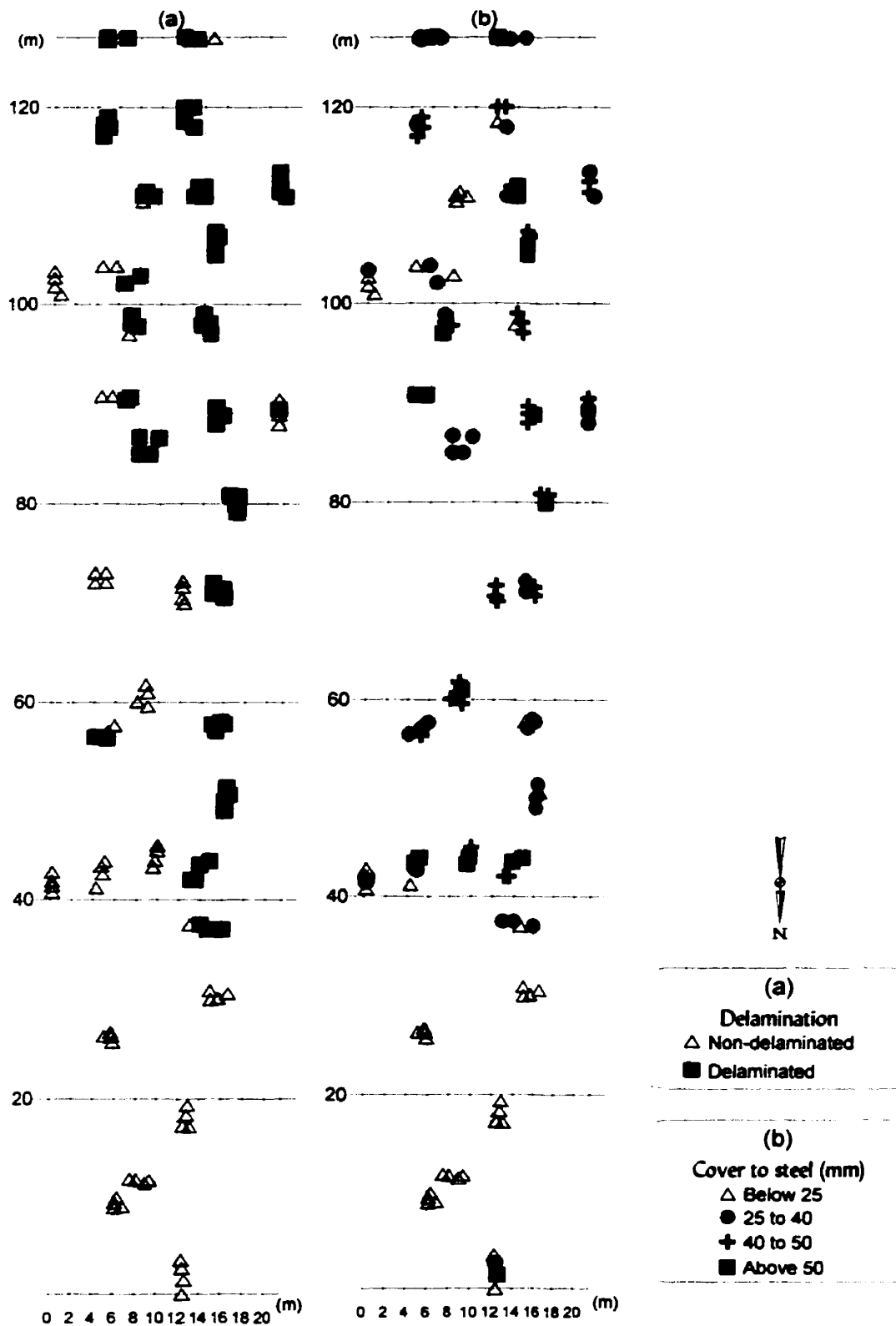
Figure 5-10: *Results of delamination and concrete cover surveys*

140

5.2.6   Concrete Cover Thickness

The concrete cover thickness (*Cover*) obtained using the covermeter varied from 1 to 90 mm with a mean of 35 mm and a *COV* of 0.48 (Table 5-1). Table 5-2 indicates that 29% of the readings are smaller than 25 mm, which was the cover thickness specified in the original design. At many locations, the cover was found to be inadequate. Extreme values as low as only 1 mm in thickness were observed near the bottom portion of the grid (Figure 5-10(b)), thus making the system very susceptible to corrosion allowing the aggressive agents (such as chlorides) more rapid ingress to the steel, and also allowing more rapid access of moisture and oxygen. Lower values of the concrete cover were common near the bottom portion of the grid (Figure 5-10(b)), however, there was not much difference between east and west sides. The higher values of concrete cover near the top portion of the grid, that is where the corrosion damage is much greater as indicated in the previous sections, illustrate that the thickness of cover to reinforcement is not the only important factor, but also the quality of the concrete cover is equally important in terms of its low diffusivity and permeability. That is, thick cover is of no avail if the concrete is highly penetrable. The quality of the concrete is discussed in the following sections.

5.2.7   Chloride Content at Steel Level

The percentage of chloride content *(%Cl)* by weight of the cement at the level of steel reinforcement varied from 0.07% to 2.20% with a mean of 0.73% and a *COV* of 0.72. The threshold acid-soluble chloride content value (percent by weight of cement) as agreed by the ACI Committee 222[25] is 0.2% (Table 2-1). The chlorides have penetrated from an external source during service as indicated by the chloride profiles in Section 4.8.3. Hence, it can be concluded that the high values found in the bridge deck are due to the ingress of chlorides from the use of deicing salts during the winter period. The high relative humidity (Figure A-9 in Appendix A) indicates that the concrete on the bridge contains a high degree of moisture, which usually represents favourable conditions for chloride ingress. From the profiles, it can be shown that 83% of the *%Cl* data lies above the permissible 0.2% threshold value. The higher chloride percentages are concentrated more on the west side of the bridge (Figure 5-11(a) and Table 5-2). Figure 5-11(a) shows that the low chloride values are mostly in the bottom portion of the grid, particularly in the east side of the bridge. On the other hand, the trend is not as strong in the west side as the *%Cl* values are high throughout the whole span (Figure 5-11(a)), that is 67% of the *%Cl* values are above 0.6% (Table 5-2). The high chloride content indicates a high vulnerability to corrosion

in the embedded reinforcement, which is consistent with the corrosion results obtained in the previous sections of this chapter. It is noted that the measured chloride is the total chloride content (percent by weight of cement) and if some inconsistencies are present it might be because only the free chloride ions are considered to be responsible to initiate corrosion. Chlorides can be bound chemically (by aluminates in the concrete) and physically (by adsorption on the pore walls). This removes them (temporarily or permanently) from the corrosion reaction and an increase in moisture content will dilute the chloride in the pore solution giving rise to lower concentrations, but at the same time, it may also increase the corrosion risk[31].

5.2.8 Electrical Resistivity of Concrete

The resistivity, ρ, of concrete varied from 1 to 27 kΩ.cm with a mean value of 6 kΩ.cm and a COV of 0.72. Figure 5-11(b) illustrates the electrical measurements using the ranges described by Millard[73]. Fifty-two percent of these values lie in the very high probable rates of corrosion activity (Table 5-2). It is evenly distributed among the east and west sides of the bridge, with a larger concentration of values in the high corrosion risk level being observed near the top portion of the grid. The results are consistent with the previous results in the earlier sections of this chapter.

5.2.9 Diffusivity of Concrete

The resistance of concrete to the transport of chloride ions is defined by the coefficient of diffusion, hence chloride diffusivity is one of the important properties of concrete affecting the durability of a structure. The diffusion of concrete was determined directly on site and from the measured profiles.

5.2.9.1 Apparent Chloride Diffusion Coefficient

The apparent chloride diffusion coefficient (D_a) values calculated from the measured chloride profiles varied from 1.4×10^{-9} to 51.6×10^{-9} cm^2/sec with a mean value of 9.3×10^{-9} cm^2/sec and a COV of 1.20, indicating great variance in the results. The west side exhibits a greater variance than the east side, that is the COV is 0.39 greater (Table 5-1). The presence of large delaminations
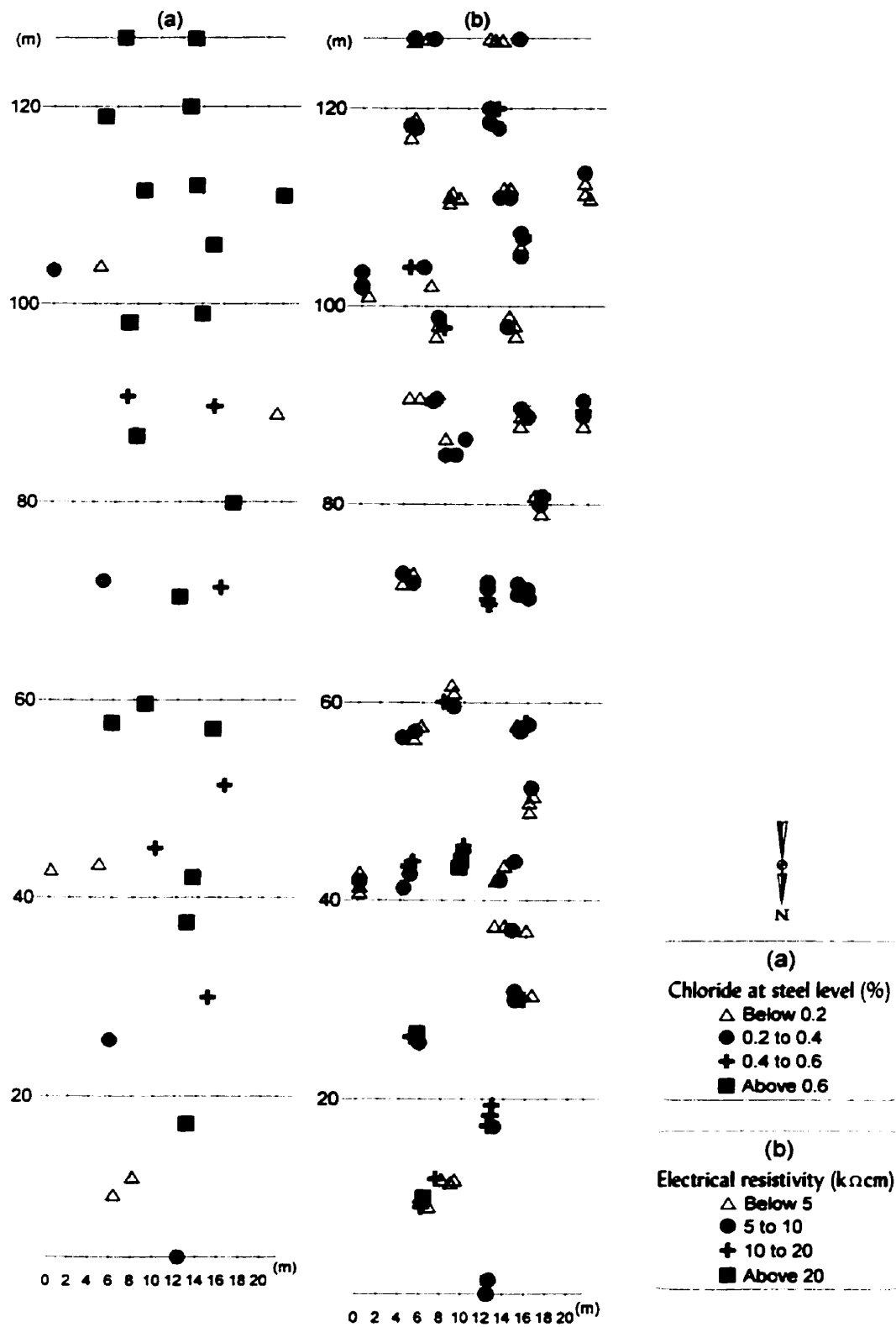
Figure 5-11: *Chloride percentage at steel level and resistivity results*

in the west side (Figure 5-10(a)) might have had an effect in the accuracy in the sampling of the concrete dust. The error function solution to Fick's second law of diffusion is commonly used to determine D_a from chloride profiles. Many researchers[9, 27, 37, 74] have investigated diffusivity and obtained widely varying results, as the D_a value is influenced by several factors such as chloride concentration, exposure duration, ambient temperature and degree of saturation of the concrete as well as the material properties, making it difficult to compare the different published works. Regardless of the present state-of-the-art, the data can be compared on a relative basis within itself. The D_a values are plotted (Figure 5-12(a)) using the ranges listed in Table 5-2. It is observed that the values of D_a lie mostly in the range 3.0 to 13.0×10^{-9} cm^2/sec and they are distributed evenly between the west and the east side.

5.2.9.2   In-Situ Chloride Migration Coefficient

The in-situ chloride migration coefficient (D_{mig}) varied from 1.62×10^{-8} to 13.48×10^{-8} cm^2/sec with a mean value of 6.26×10^{-8} cm^2/sec and a COV of 0.48. This variance in the in-situ chloride migration coefficient, D_{mig}, is lower than that for D_a, indicating that on site, the former is a more appropriate parameter to measure the diffusivity of the concrete. This phenomenon is being investigated presently at The Queen's University of Belfast[86]. However, compared to Andrews'[86] results from tests at Queen's University (Table 3-5), the values obtained for the bridge were much higher because of the exposure conditions, however, they can be analyzed on a relative basis (by comparison within the measured values). The D_{mig} values are plotted in Figure 5-12(b) using the ranges used in Table 5-2. It is noted that a very high percentage of the results smaller than 6.0×10^{-8} cm^2/sec exist on the east side (Table 5-2), showing that the in-situ chloride migration coefficient values are higher in the west side of the bridge, being consistent with the above-mentioned results. In addition, the D_{mig} values in the east side of the bridge are low at the bottom of the grid and increase in value towards the top. On the other hand, the D_{mig} values in the west side do not show the same trend. Higher values are found at the bottom of the grid compared to the top of the grid (Figure 5-12(b)). This is interesting as most probably the high presence of delamination in the west side (especially at the top of the grid (Figure 5-10(a))) might have an effect on the reliability of the in-situ chloride migration test. The delamination and cracking might effect the preconditioning of the concrete prior to the test, that is the concrete might not have been fully saturated. However, a steady state condition was achieved while conducting the test (Figures C-1 to C-3 in Appendix C), hence the concrete was saturated enough not to stop the ion migration through the free water within the concrete.

144
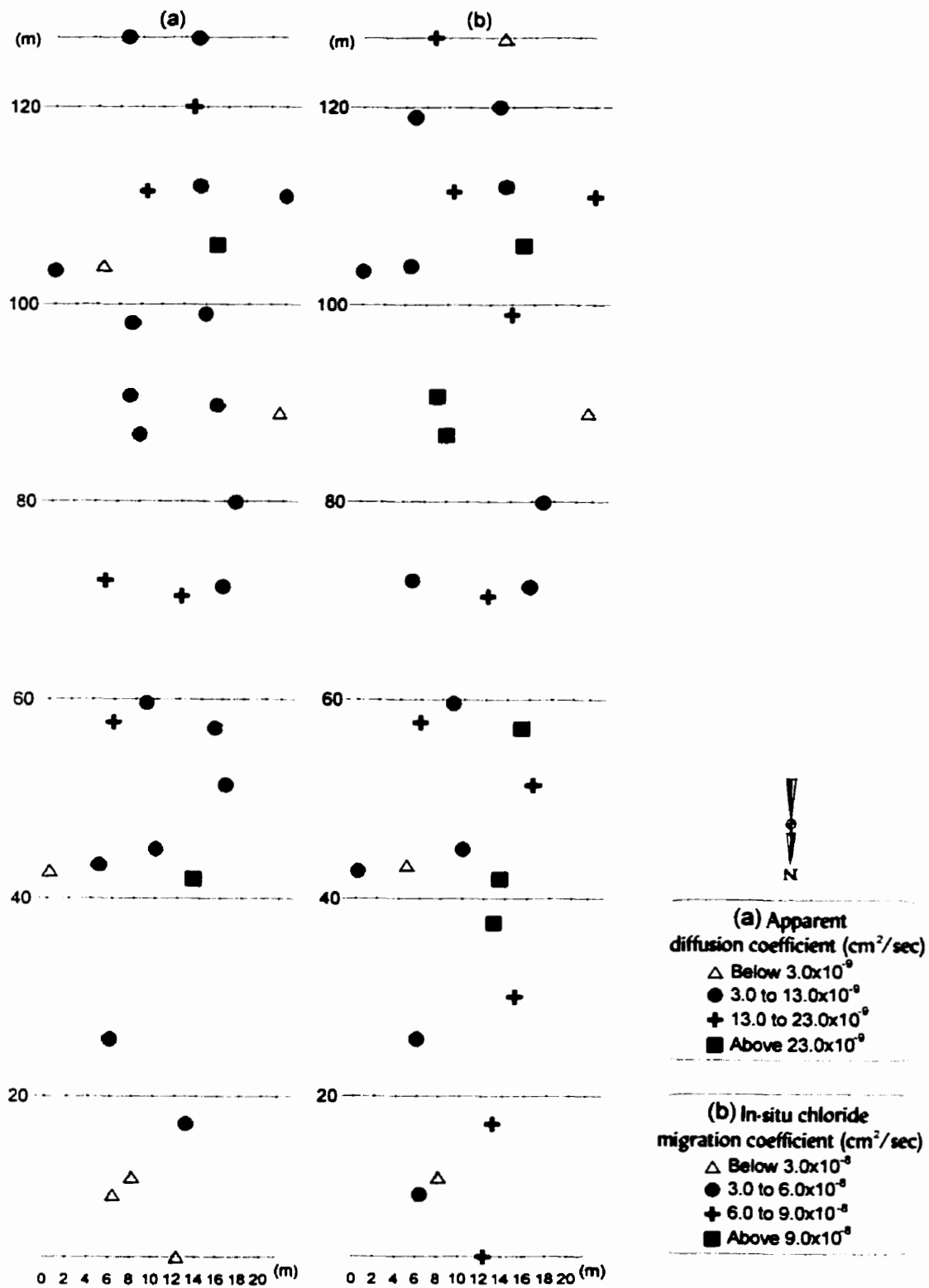
Figure 5-12: *Chloride diffusivity results*

The figure contains the following legend text:

(a) Apparent diffusion coefficient (cm²/sec)
△ Below 3.0x10⁻⁹
● 3.0 to 13.0x10⁻⁹
✛ 13.0 to 23.0x10⁻⁹
■ Above 23.0x10⁻⁹

(b) In-situ chloride migration coefficient (cm²/sec)
△ Below 3.0x10⁻⁸
● 3.0 to 6.0x10⁻⁸
✛ 6.0 to 9.0x10⁻⁸
■ Above 9.0x10⁻⁸

145

5.2.10 Permeability of Concrete

Cores were tested for water absorption simply to get an idea of the absorption capacity of the concrete without any moisture and environmental effects from the site conditions. Hence, both the coefficient of permeability obtained from the Autoclam apparatus and the water absorption results are discussed in this section.

5.2.10.1 Water Absorption Capacity

The water absorption capacity (from 12 cores as shown in Figure A-11 in Appendix A) varied from 1.8 to 3.6% with a mean of 2.5% and a COV of 0.20 compared to the values listed in Table 3-6. The majority (83%) of the readings indicate a low level of absorption. However, while the British code does not stipulate a complete saturation of the specimen, the American code specifies it. It is unlikely that the capillary cavities in concrete are filled after only 30 minutes of immersion in water. This might be the cause of the low water absorption. The cores seemed porous when visually inspected, but the results from the water absorption test resulted in low values.

5.2.10.2 Coefficient of Permeability of Concrete

The coefficient of permeability (k_w) varied from 1.76×10^{-14} to 84.20×10^{-14} m/sec with a mean value of 16.31×10^{-14} m/sec and a COV of 1.18. There is considerable variability in the coefficient of permeability results, with a COV figure slightly lower for the east side of the deck (Figure 5-1). A direct comparison with the data developed at The Queen's University of Belfast was not possible as the tests by Basheer[14, 87] and others used dry concrete. As the ambient relative humidity was quite high (at depths of 10 mm and 25 mm from the concrete top surface, the relative humidity values were found to be on the average 86% and 90%, respectively) and the concrete could not be dried to a constant moisture content, a steady state of flow during the permeability test was achieved by ponding water in the ring for 48 hours prior to testing. Montgomery and Adams[91] undertook some work using ponded specimens, however, they used a pressure of 1.76 bars which is much larger than the value of 0.5 bar used in this investigation. The k_w values obtained in this investigation were very small, which indicated that the concrete is not permeable, however, it must be noted that the water pressure applied during test was only 0.5 bar. This pressure is lower than the surface tension forces in the capillary pores filled water, hence, no

significant amount of water is able to penetrate through the saturated concrete as explained in Section 4.9.2. Therefore, the permeability results should be considered with caution as the applied pressure was small and because the environmental conditions (*RH*) at the time of testing can significantly influence the results. The permeability values are plotted in Figure 5-13(a) using the ranges listed in Table 5-2. It is noted that 56% of the values are under 10.0×10^{-14} m/sec where most of them are concentrated at the top of the grid, but no particular trend is observed between the west and the east sides of the deck. Lower permeability is noticed at the top of the grid where the corrosion damage is very advanced. This is the opposite to what was expected, that is the lower the permeability, the lower the corrosion damage. Once again, the permeability results should be considered with caution as explained above.

5.2.11 Concrete Compressive Strength

The concrete compressive strength determined using 75 mm diameter cores varied from 10 to 48MPa with a mean value of 27MPa and a *COV* of 0.36 (Table 5-1). At the time of construction (in 1959), the specified concrete strength was 28MPa. As the strength of concrete depends on both age and temperature, that is strength is a function of the maturity of the concrete[32]. Therefore, considering the maturity of the concrete over 39 years, this strength should have been much higher. This value was not calculated for this research program, however, it is noted that 58% of the strength values lie below 30MPa (Table 5-2). The strength was found to be sufficiently low, except at four places where the values were between 40 and 60MPa near the bottom of the grid. The low values of strength are concentrated more at the top portion of the grid and they are evenly distributed between the east and west sides of the deck (Figure 5.13(b)).

5.3 Summary of Existing State-of-Health of the Bridge Deck

Overall, the methods that assess the damage, such as half-cell potential, corrosion rate, delamination, and chloride content indicate that the top portion of the grid is at high risk of corrosion. The areas of high chloride content generally coincide with the locations of significant reinforcement corrosion. Most probably more de-icing salt was applied to the top of the grid as it is near the crest of the bridge and this part of the bridge has a steeper slope compared to the bottom part, hence it is possible that to ensure safety of the motorists, more de-icing salt was used
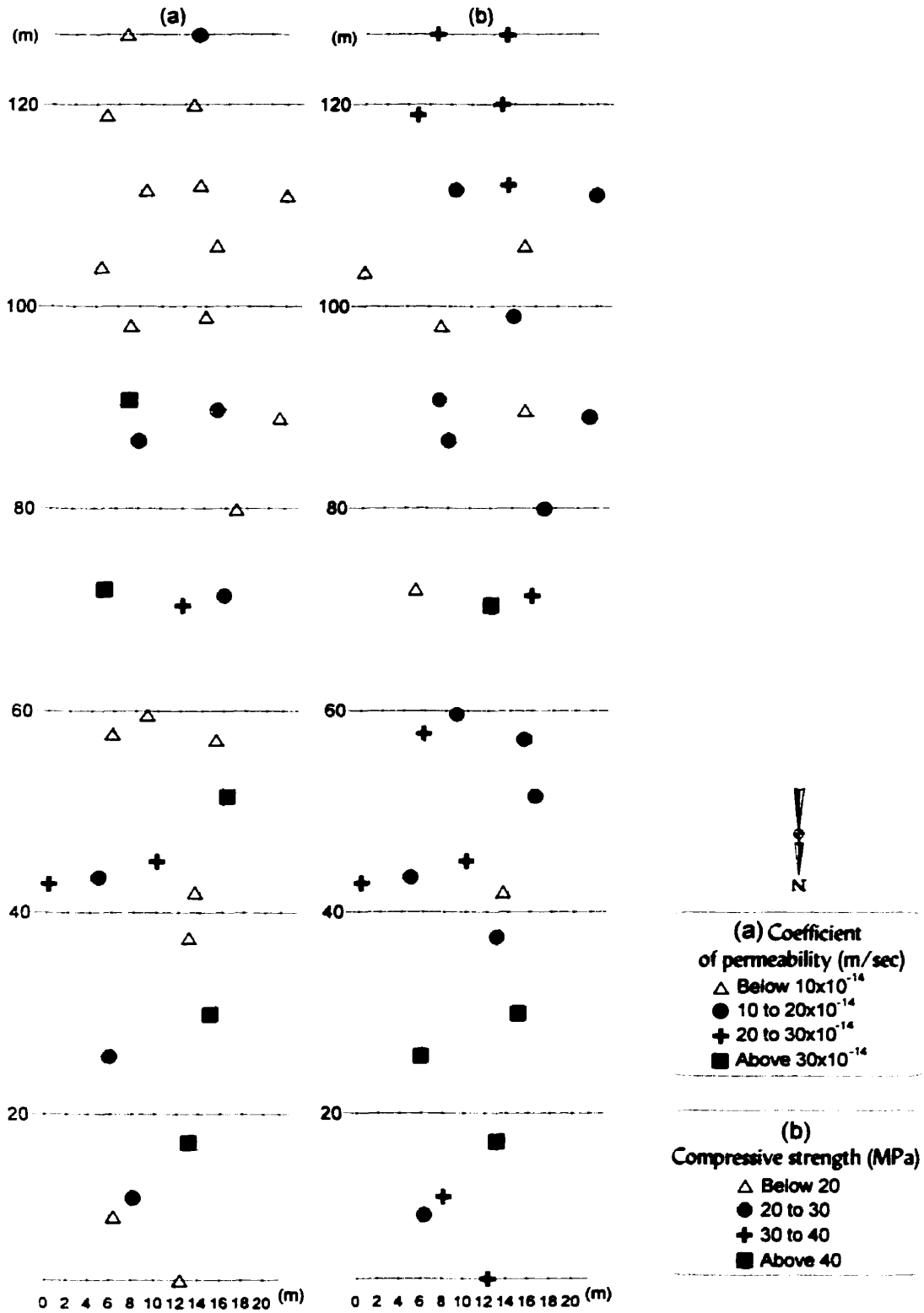
Figure 5-13: *Coefficient of permeability and compressive strength results*

on the steeper slopes to avoid accidents. Below the expansion joint (grid location 36 m), the damage is less. The reason for this may be attributed to the fact that the deck from grid location 0 m to 36 m is supported by an enclosed concrete abutment (Figures 1-3 and 4-2). The abutment might have acted as a protective system from the environmental agents from the underside reducing its susceptibility to corrosion. It was noted (Figures 5-5 to 5-7) that the underside of the deck at the top of the grid displayed extensive damage. This might have been caused by the easier ingress of water and oxygen to the embedded steel reinforcing.

Moreover, the lack of a drainage system suggests that the water would drain down the slope of the deck keeping the bottom of the grid reasonably wet while the top portion would undergo wet and dry cycles. This might constitute a very severe exposure condition for the concrete where it was subjected to alternate wetting and drying cycles and this along with the application of deicing salts promoted corrosion. Even though the bottom portion was exposed more to moisture creating a nearly saturated condition, the corrosion process might have been controlled by the availability of oxygen, which becomes the limiting factor. Also, the extracted cores (used for the compression strength test) showed that the concrete deck was thinner towards the top portion. Since the bridge was built in 1959, it was unlikely that proper quality control was instituted during construction. The clear cover from the underside might have been inadequate, thereby increasing the risk of corrosion. In addition, the damage was more pronounced in the west side of the deck. There is no clear explanation for this phenomenon, but that is clearly the case as indicated earlier.

Although the various assessment methods were indicative of the magnitude of corrosion damage, they cannot detect the susceptibility to corrosion. In addition, the results of the cover survey seem to contradict all other results. Lower covers are found at the bottom of the grid and thicker cover at the top. Lower concrete covers would suggest that these particular sites would be more susceptible to deterioration. However, it was seen that at the bottom of the grid the damage was less compared to the top. This enforces the limitation in simply providing a large cover. The quality of the concrete in terms of its permeation properties (diffusivity and permeability) and electrical resistance is of great importance. The areas of high diffusivity, and low resistivity and strength were found to coincide with the locations of significant reinforcement corrosion. The permeability results gave the impression that the bridge is in good condition. This anomaly may be due to the inadequacy of the criteria used for the test and due to the low applied pressure as explained earlier. Thus, the early evaluation of the material properties of the surface of concrete on site, along with the knowledge of exposure to salt may provide useful indications of the likely future deterioration of concrete.

It is noted that the performance of the cover-zone is a major factor governing the rate of degradation of reinforced concrete structures and provides the principal barrier to water and aggressive agents. The ability of concrete to imbibe water and other aggressive agents is a starting point for indexing durability of concrete and terms such as diffusivity and permeability have been used in the present study in this respect. It is clear that there exists a need to determine quantitatively those near-surface characteristics of the concrete which promote the ingress of water or liquids containing dissolved contaminants. In addition, in-situ monitoring of the microclimatic conditions (temperature and RH) helps in explaining the variability in such properties and assists in evaluating the in-service performance of the structure, deterioration rates for the particular exposure condition, or compliance with the specified design life. Many concrete structures built in the 1960s and 1970s are now showing significant signs of deterioration. The Dickson bridge is a typical example. Measurement of strength and workability is not sufficient to prevent the occurrence of these problems. It is evident, therefore, that some other property of concrete, which is more closely related to corrosion, needs to be monitored to effectively overcome this problem. Diffusivity, resistivity and permeability are such properties which have been found by many researchers and confirmed in this investigation to give much more useful information on the likely durability of the concrete. Therefore, methods to predict durability should be included in inspections of the bridge stock. The reliability of the test results obtained from the methods used in predicting corrosion is discussed in the next chapter.

6 Analysis and Reliability of Results to Assess / Predict Corrosion of the Dickson Bridge Deck

6.1 Introduction

Before undertaking a statistical analysis for correlating the observations to the measured properties, trends will be identified visually on the northern sector of the bridge deck, and between the west and east sections of this sector. Useful relationships between the rate of corrosion and different variables in the concrete quality, workmanship and environment will be investigated along with their role in the assessment of the residual service life of the structure. No single test method can detect or predict the damage, however, when a combination of test methods is used, it is unlikely that any center of deterioration will get missed. A multivariable statistical analysis is the most appropriate way of quantifying and correlating the results of the various tests. Both methods (measuring damage, and measuring material properties and exposure parameters) have been used to predict the corrosion rate of this particular structure. A multivariate statistical analysis will follow to quantify the condition of the bridge.

6.2 Variation of Test Results

Prior to performing a detailed statistical analysis correlating the parameters, the variations of the various pairs of the relevant corrosion related parameters will be investigated. The data of the various tests are affected by the environmental conditions. Hence, when applying statistical analysis no significant relationship may be evident. However, this might be misleading. This type of data analysis is usually appropriate for laboratory investigation where the testing conditions are monitored and a linear relationship can usually be obtained. On site, there are many other factors which may have to be considered before interpreting relationships between the various parameters. It is important that the statistical analysis is part of a broader-analytical approach to problem solving. That is, the numerical outcome from the analysis may not be the primary

objective of the study. It is more important to provide insight the system generating the data, that is to understand the data both qualitatively and quantitatively[99].

Significant findings are detected between various pairs of the relevant corrosion related parameters. These will be illustrated to establish confidence in the behavior of the experimental results. The results will be presented in graphical form (double y-axis graphs where the two y-ordinates have different scales) in order to illustrate trends. Given the large number of potential, corrosion rate and resistivity readings (that is, 35 sites with four readings per site), the readings undertaken at the same site where the chloride survey (profiles and in-situ migration tests) are only investigated in this section. That is, the information in this section is selective and consists only of the material deemed to be essential.

6.2.1 Relationship of Corrosion Rate with Potential

Figures 6-1 and 6-2 illustrate the variation of the corrosion rate (CR) with the corrosion potential (ϕ_{corr}) at the location on each of the 35 sites where the chloride survey was undertaken. A close relationship is observed in the east side (Figure 6-1), and it is slightly on the lower side in the west side (Figure 6-2). The purpose of this analysis was to determine whether the variation of the corrosion potential data could be used to predict the variation of the corrosion rate values.
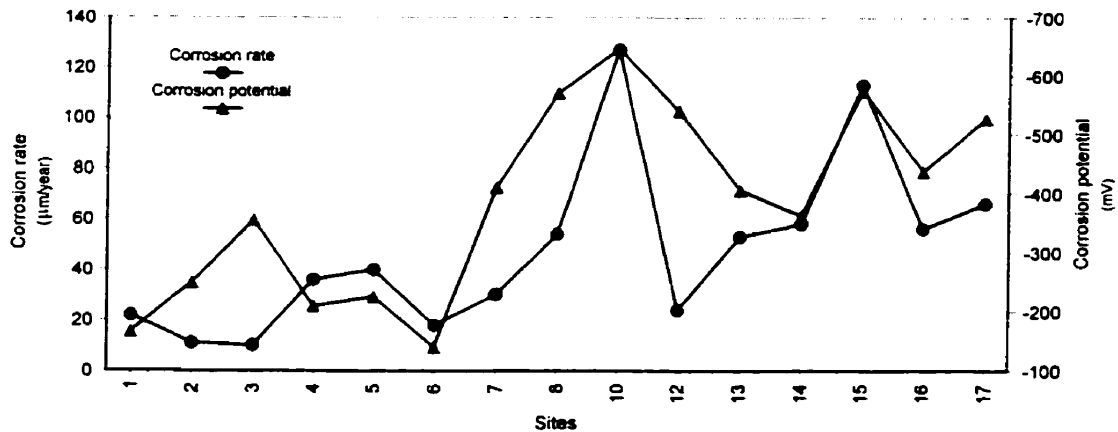
Figure 6-1: Dependence of potential on corrosion rate (east side of deck)
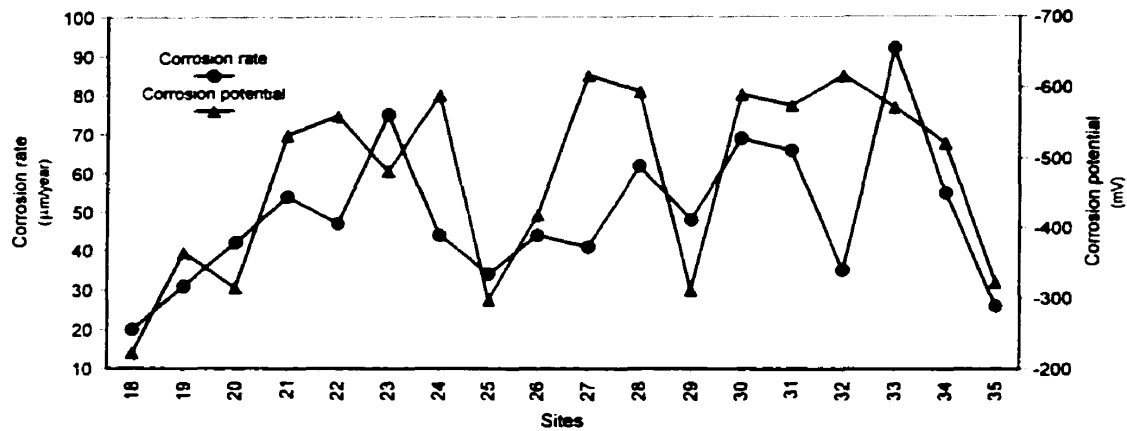
Figure 6-2: *Dependence of potential on corrosion rate (west side of deck)*

Changes in the corrosion rate were generally mirrored by the potential values recorded. The half-cell potential survey was used to scan the entire bridge deck and detect areas of low, medium and high corrosion risk. Hence, to a certain extent, the corrosion potential could validate and supplement the corrosion rate data in determining the overall significance of corrosion activity in the Dickson Bridge deck, excepting at some points, such as site 12 and 32, where the variations in the two data sets are not consistent.

6.2.2 Relationship of Chloride Migration with Corrosion Rate and Potential

The variations of the in-situ chloride migration coefficients, D_{mig}, and the corrosion rate (CR) values, and D_{mig} and corrosion potential (ϕ_{corr}) are presented in Figures 6-3 to 6-6. A dependence of D_{mig} values on both CR and ϕ_{corr} is evident. Interestingly enough, the results presented in Figures 6-3 to 6-6 would indicate that both corrosion rate and the potential vary with the in-situ chloride migration coefficient. However, this is not the case for all situations. Presence of moisture and chloride affect the diffusivity measurements and these two vary throughout the bridge deck. Moisture has also a great influence on both potential and corrosion rate readings. The variations are more consistent in the east side of the bridge (Figures 6-3 and 6-5) and follow a good trend, that is, an increase in D_{mig} results in an increase in both CR and ϕ_{corr}, and vice versa. It is not surprising that as it was stated in Section 5.2.9.2, the D_{mig} values in the west side were found to be higher at the bottom of the grid and lower at the top, not correlating to the CR values

153

as well as the values in the east side. The D_{mig} values are an indication of the concrete resistance to chloride ion migration through the pores in the concrete cover, hence, it is not surprising that there is a close relationship between the D_{mig} values and the corrosion data, as the chloride ingress is one of the determining factors with respect to the initiation of corrosion (Section 2.2.2.1). The inconsistencies might be due to the fact that the accelerated migration test determines mainly the physical resistance of the chloride ingress, however, on site both the physical and the chemical (binding) properties influence the resistance of the concrete to chloride ingress (Section 3.4.4). As the chloride migration apparatus is predictive of chloride ingress and the resulting reinforcement corrosion, the results in the west side indicate that as the corrosion damage has reached a high level, the D_{mig} values are somewhat less clear in predicting the corrosion rate (Figure 6-6).
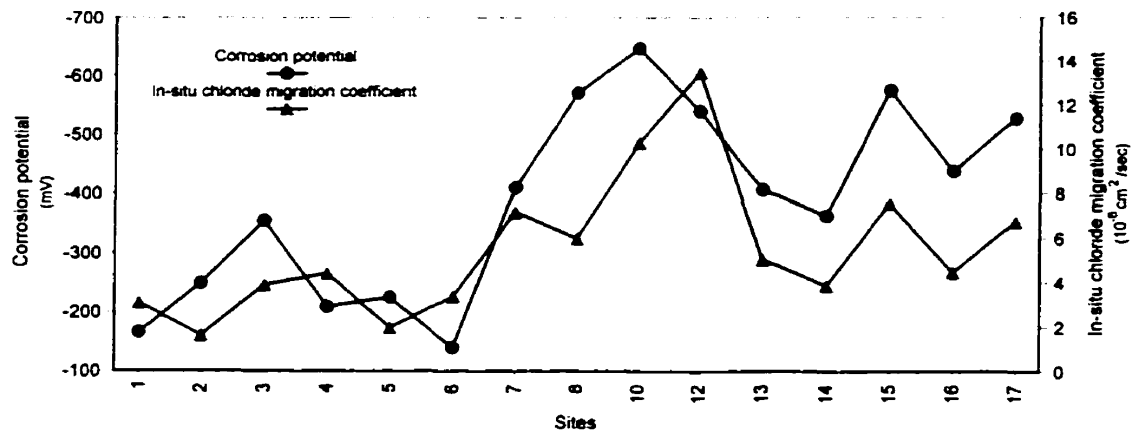
Figure 6-3: *Dependence of in-situ chloride migration coefficient on corrosion potential (east side of deck)*
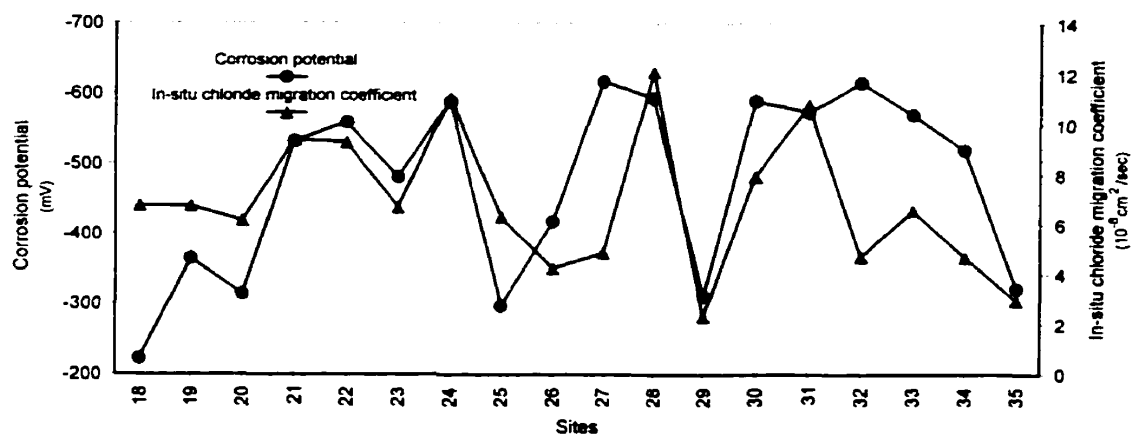
Figure 6-4: *Dependence of in-situ chloride migration coefficient on corrosion potential (west side of deck)*
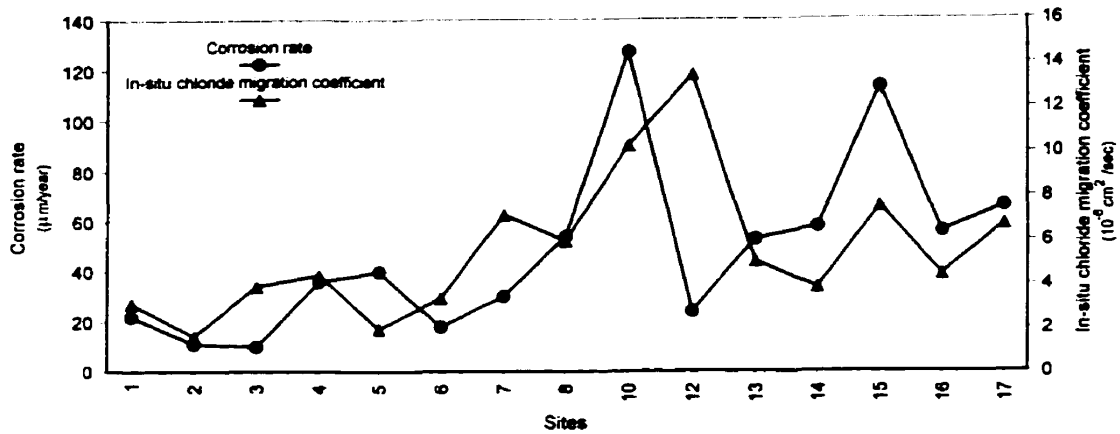
Figure 6-5: *Dependence of in-situ chloride migration coefficient on corrosion rate (east side of deck)*
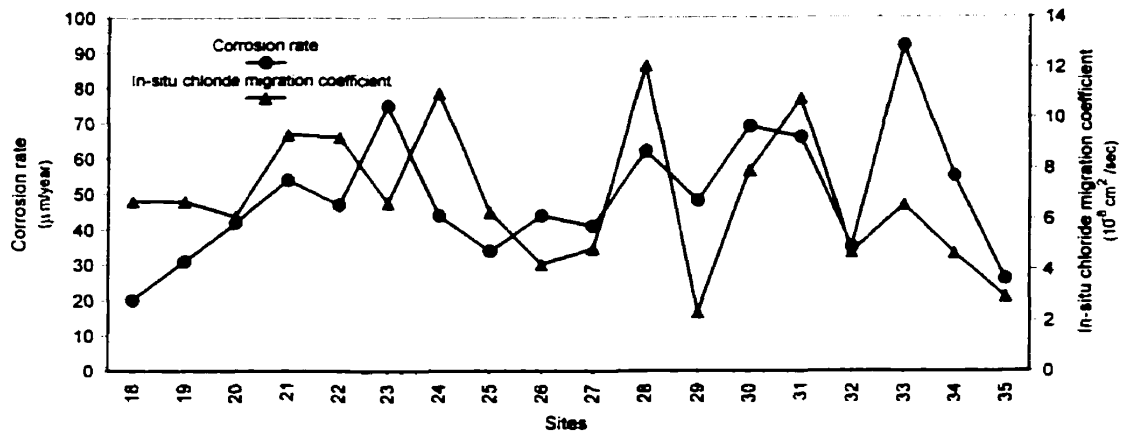
Figure 6-6: *Dependence of in-situ chloride migration coefficient on corrosion rate (west side of deck)*

6.2.3 Relationship of Chloride Content at Steel Level with Corrosion Potential and Corrosion Rate

As noted in Section 2.2.2.1, the free chloride ions are responsible for the breakdown of the protection afforded by the passive film. Previous research[29, 39, 78] showed an increase in the corrosion rate with increasing chloride ion contents. In order to achieve confidence in the measurements, the behavior of the variations of the readings are studied in Figures 6-7 to 6-10. The chloride content at the steel level varies significantly and there is a rather close relationship with the variation in the corrosion potential and the corrosion rate values, especially in the east

side (Figures 6-7 and 6-9). As the chloride content increases, the risk of corrosion is higher and vise versa, hence, the variation in chloride content has an effect on the corrosion activity. From Figures 6-8 and 6-10, except for some points, it is noted that there is no strong relationship.
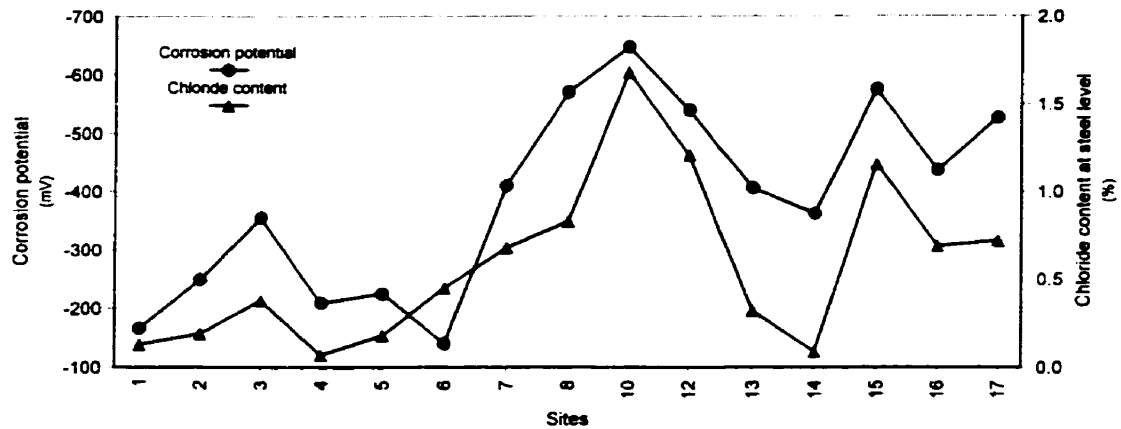
Figure 6-7: *Dependence of chloride content at steel level on corrosion potential (east side of deck)*
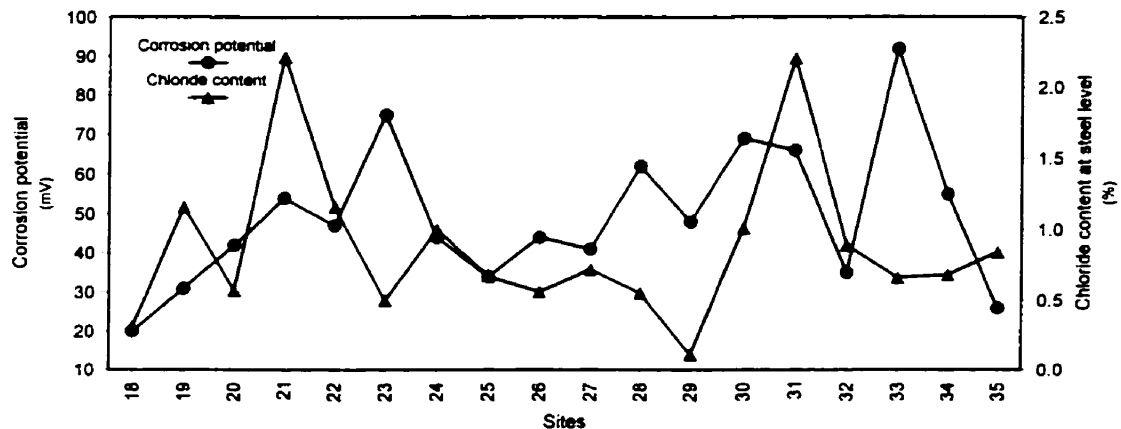
Figure 6-8: *Dependence of chloride content at steel level on corrosion potential (west side of deck)*

The results are consistent with what was noted in Sections 5.2.4 and 5.2.7, that is the corrosion potential and the corrosion rate values for the west side are higher and the readings from the bottom half of the grid are lower, while the chloride content values were high throughout the entire west side. The explanation might be that the free chloride ions are responsible to initiate the corrosion process, but once corrosion is at an advanced stage (such as in the west section), the corrosion is influenced only by the corrosion rate-determining parameters (water penetration,

oxygen diffusion and electrical resistivity) with the exception of pitting corrosion. In addition, the chloride content plotted in the graphs is the total content and might contribute to the lack of relationship of certain points. The above results may have been influenced by the ambient conditions at the bridge site. The accuracy of the collection of the dust samples might have been affected by the delamination present in the deck.
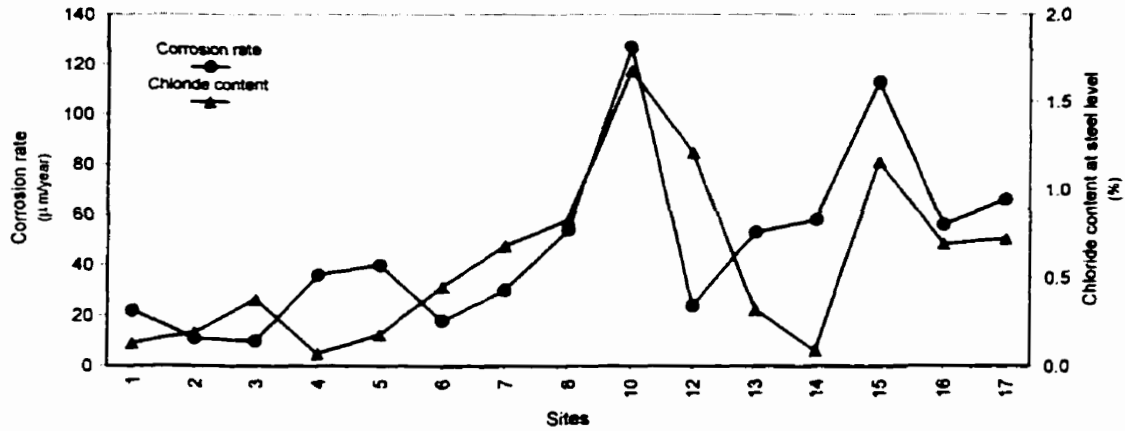
Figure 6-9: *Dependence of chloride content at steel level on corrosion rate (east side of deck)*
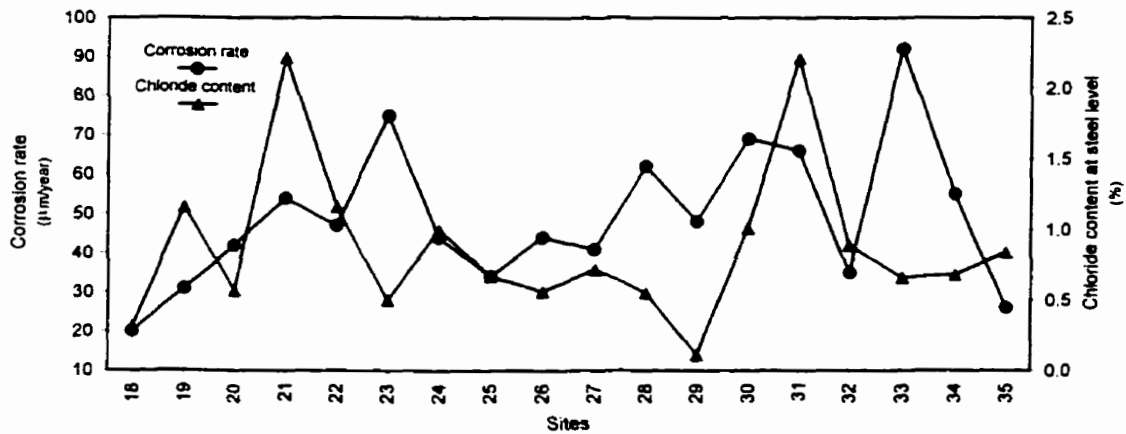
Figure 6-10: *Dependence of chloride content at steel level on corrosion rate (west side of deck)*

157

6.2.4 Relationship of Resistivity of Concrete with Corrosion Potential and Corrosion Rate

When the passivation of the reinforcing steel is overcome, the strength of the corrosion attack depends on the degree of saturation of the concrete pore network, and the corrosion rate is determined over a very broad range by the concrete resistivity. The electrical resistivity measurements are usually carried out to assist the half-cell potential measurements. As it can be seen in Figures 6-11 to 6-12, the variations of the two parameters are quite consistent with the exception of some points such as sites 34 and 35. On the other hand, it is obvious from Figures 6-13 and 6-14 that the resistivity values are not sufficient to predict the corrosion rate of the bridge deck, as the variations in the corrosion rate values were not obtained using the resistivity values. Covercrete resistivity measurements have also been developed to assess the corrosion risk, however, in such cases, resistivity is taken on the whole cover region, hence, any measurements simply provide a weighted mean value for the cover zone and are highly influenced by the variations in the ambient humidity at the time of the test.
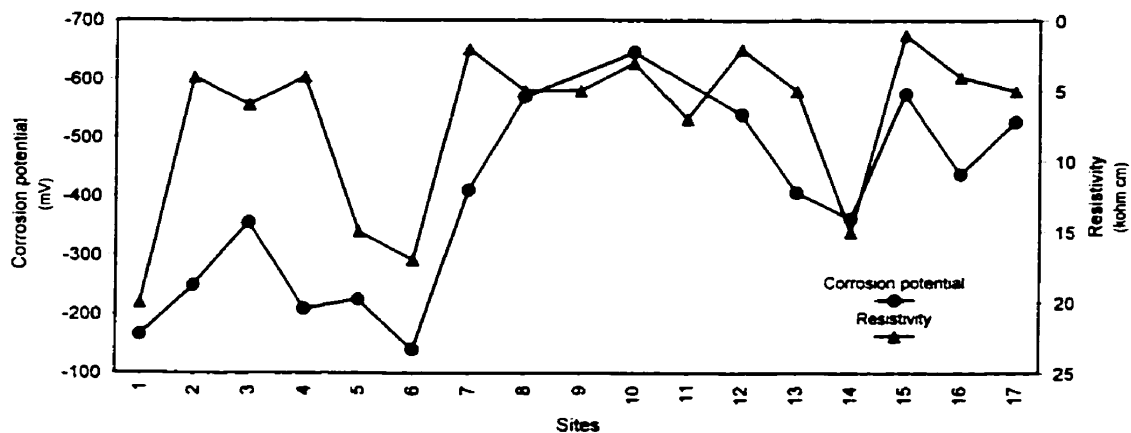
Figure 6-11: *Dependence of resistivity of concrete on corrosion potential (east side of deck)*
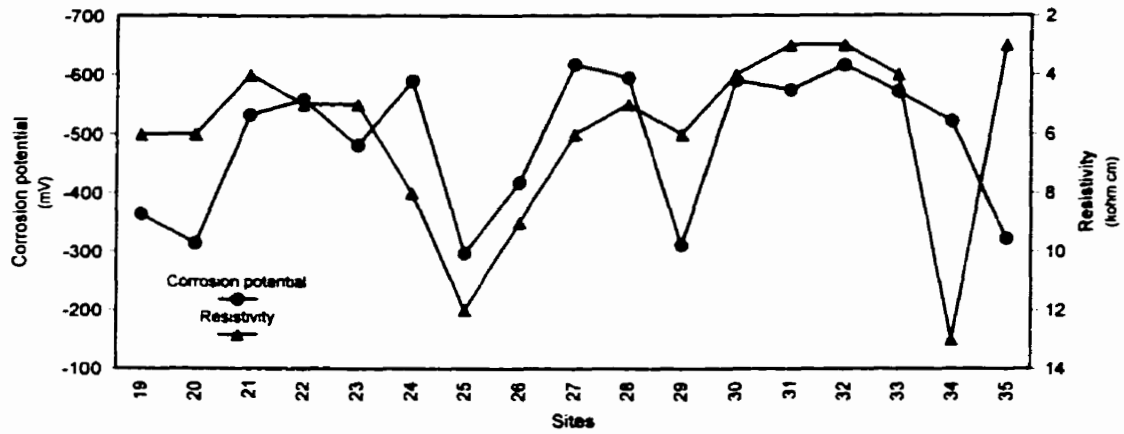
Figure 6-12: *Dependence of resistivity of concrete on corrosion potential (west side of deck)*
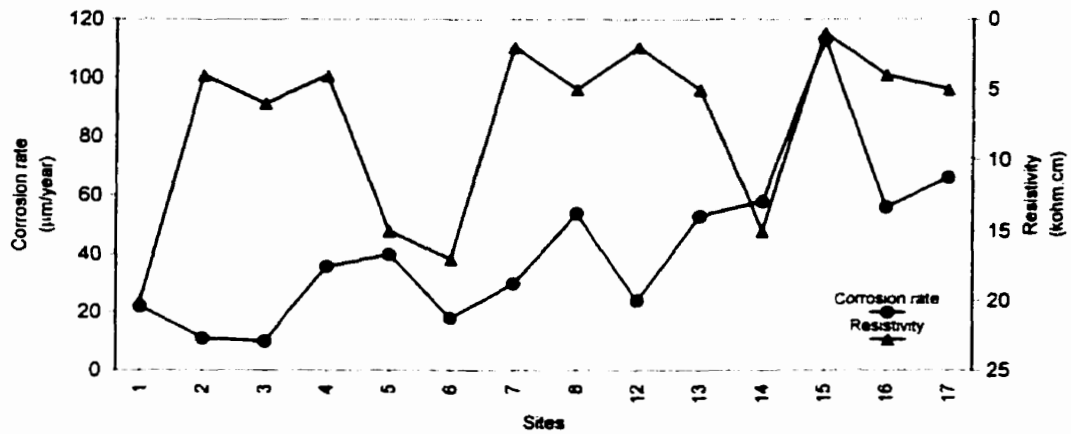
Figure 6-13: *Dependence of resistivity of concrete on corrosion rate (east side of deck)*
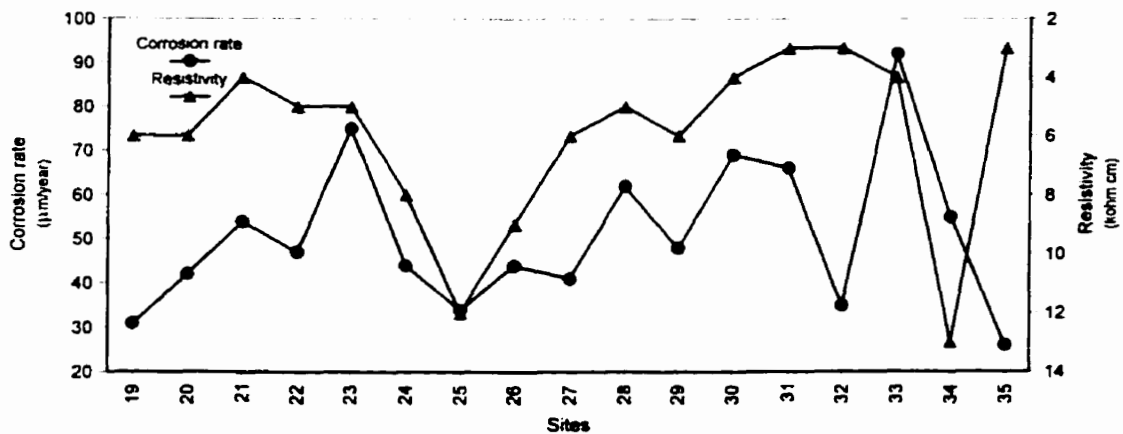
Figure 6-14: *Dependence of resistivity of concrete on corrosion rate (west side of deck)*

159

6.2.5   Relationship of Concrete Compressive Strength with Corrosion Rate

Concrete is inherently weak in tension and for this reason its fracture strength is one of the most important factors in relation to the rate of deterioration. For example, expansion associated with the by-products of reinforcement corrosion tends to initiate tensile cracking which ultimately results in spalling. In this investigation, the concrete compressive strength was measured, but it is known that the two types of strength are closely related, that is as the compressive strength increases, the tensile strength also increases but at a decreasing rate[32]. The relevance of the concrete compressive strength to the corrosion rate of the reinforcing steel within the concrete is illustrated in Figures 6-15 and 6-16. There is a strong relationship between the two variables (with the exception of some points), that is the corrosion rate increases, if the compressive strength is lower, and vice versa. The strength depends to a large extent on the amount of capillary pores in the concrete, which in turn depends on the water/cement ratio used during construction[32]. Corrosion also depends on the capillary pore for the transport of the prerequisites of the corrosion reaction as well as the increase in conductivity associated with large volumes of pores. This does not imply that high strength concrete is durable, but that the compressive strength of the concrete reduces as corrosion increases, resulting in an increasing compromise of the structural integrity of the concrete structure.
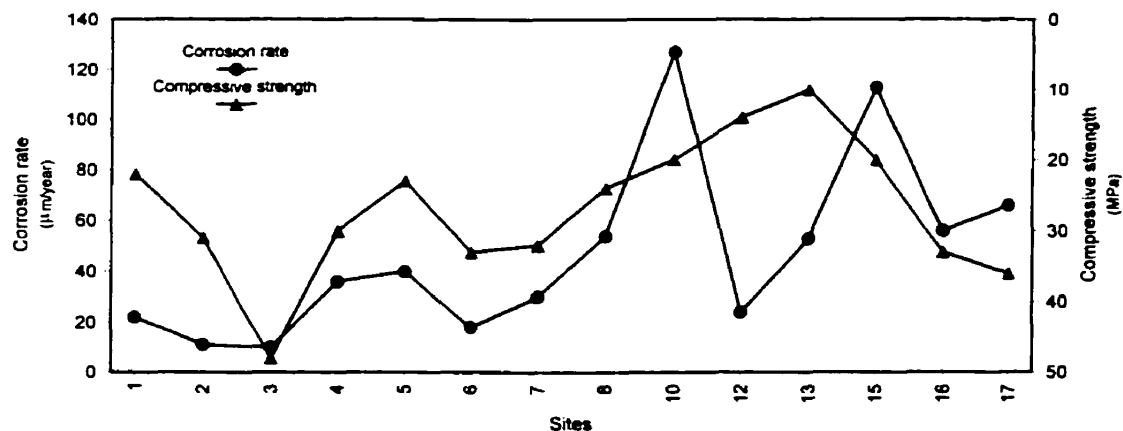
Figure 6-15: Dependence of concrete compressive strength on corrosion rate (east side of deck)
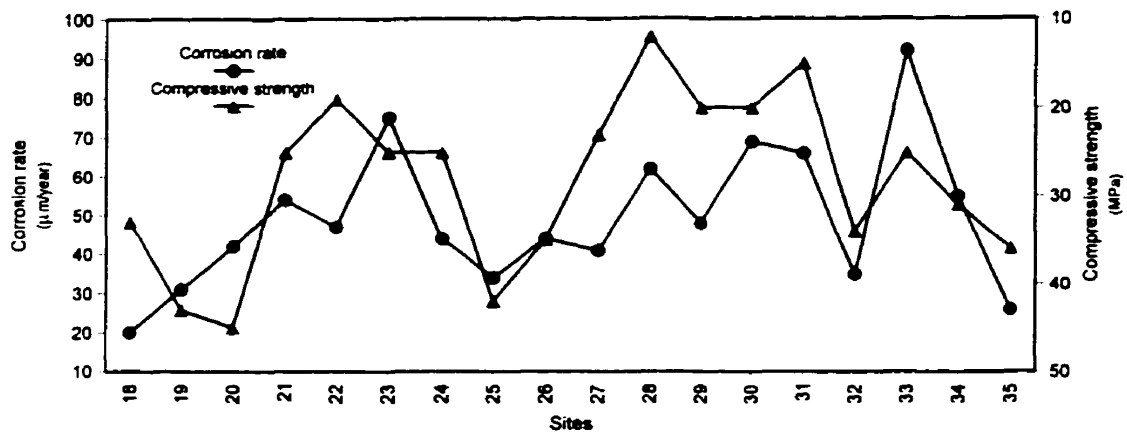
Figure 6-16: *Dependence of concrete compressive strength on corrosion rate (west side of deck)*

6.2.6 Relationship of Chloride Content with Chloride Diffusivity

The concrete cover quality is of utmost importance. The time before the chlorides get to the steel can vary from less than a year to more than a hundred years depending on the concrete cover quality. The time to initiation of chloride induced corrosion depends mainly on the rate at which chloride ions enter the concrete. The three techniques dealing with chloride ingress, that is the chloride content at steel level (%Cl), the in-situ chloride migration coefficient (D_{mig}), and the apparent diffusion coefficient (D_a) are compared in this section. Figures 6-17 to 6-18 illustrate the relationship of the D_a values for all 35 sites with corrosion potential and corrosion rate. The parameter D_a showed no significance in its variation against both the corrosion rate and potentials values, unlike the behavior of D_{mig} indicated earlier in Section 6.2.2. The D_a values are influenced by several factors such as the chloride concentration, exposure duration, ambient temperature and the degree of saturation of the concrete, the material properties and the accuracy of the profiles as well. As a result, the values are not as predictive as the D_{mig} values. As indicated in Section 3.4.4, it is important to distinguish between the various chloride diffusion coefficients, and to realize that all these coefficients are not fundamental material properties as they are influenced by a number of factors such as chloride binding, and they change with time. Hence, when plotting D_{mig} and D_a values for each of the 35 sites, as shown in Figure 6-19, except the first eight points, no important trend is detected.

161
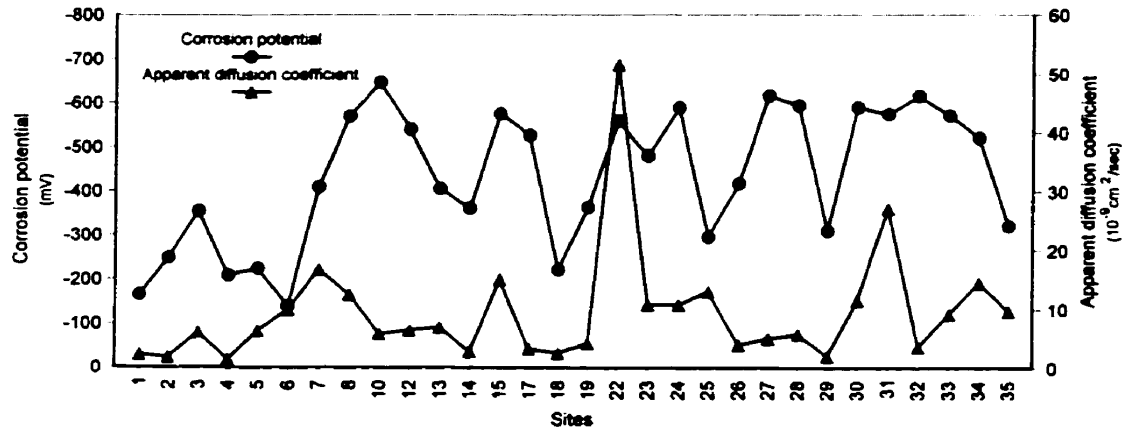
Figure 6-17: *Dependence of apparent diffusion coefficient on corrosion potential (entire deck)*
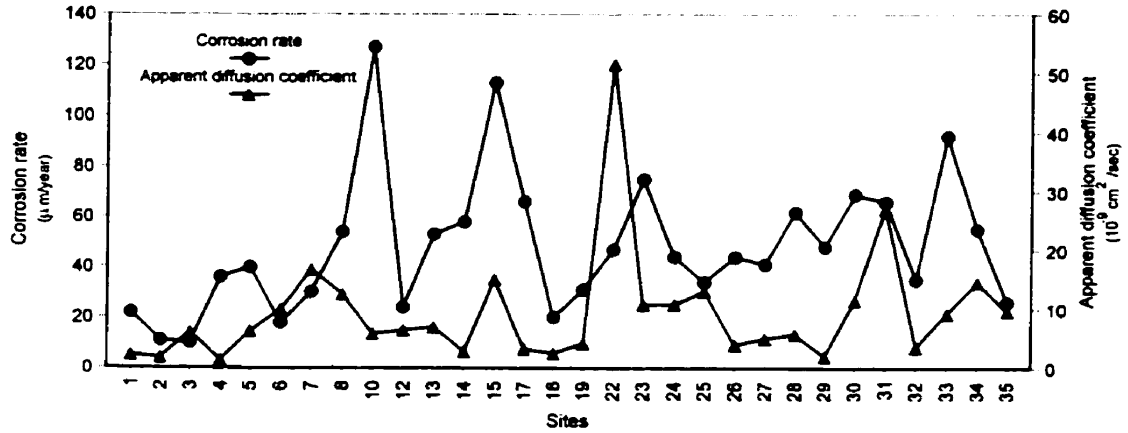
Figure 6-18: *Dependence of apparent diffusion coefficient on corrosion rate (entire deck)*
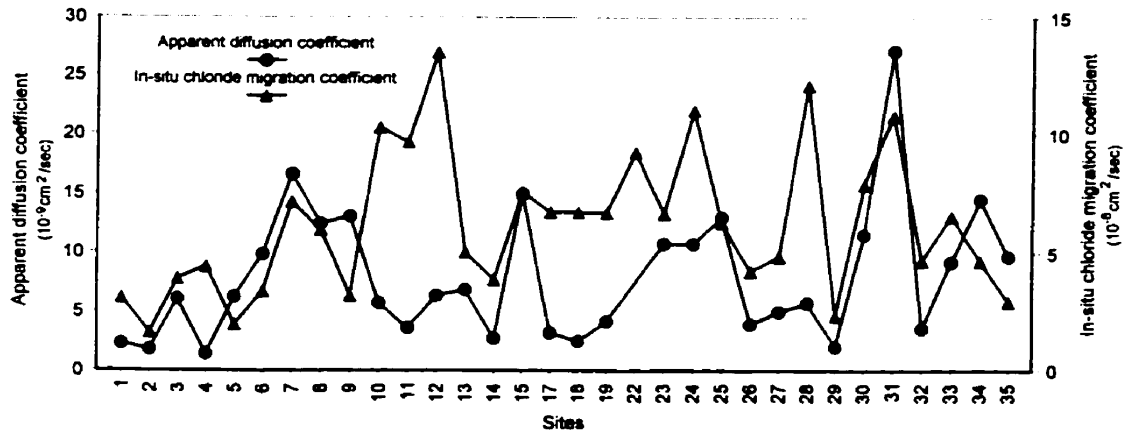
Figure 6-19: *Dependence of in-situ migration coefficient on apparent diffusion coefficient (entire deck)*

Moreover, when plotting D_a and $\%Cl$ values for each of the 35 sites as shown in Figure 6-20, except for the first seven points, no important trend is detected. However, with reference to Figure 6-21, it can be stated that the in-situ migration coefficient varies more with the chloride percentage content at the depth of steel. Diffusivity is a parameter that can be used to assess the present condition of a concrete structure and also to predict the future risk. Both tests measure diffusivity. However, the D_{mig} is more consistent with the corrosion readings and the chloride content found at the steel level. Obviously, the in-situ test does not measure the present chloride content already in the concrete, but it gives an idea of the quality of the concrete, which is very important in long-term monitoring and preventive maintenance.
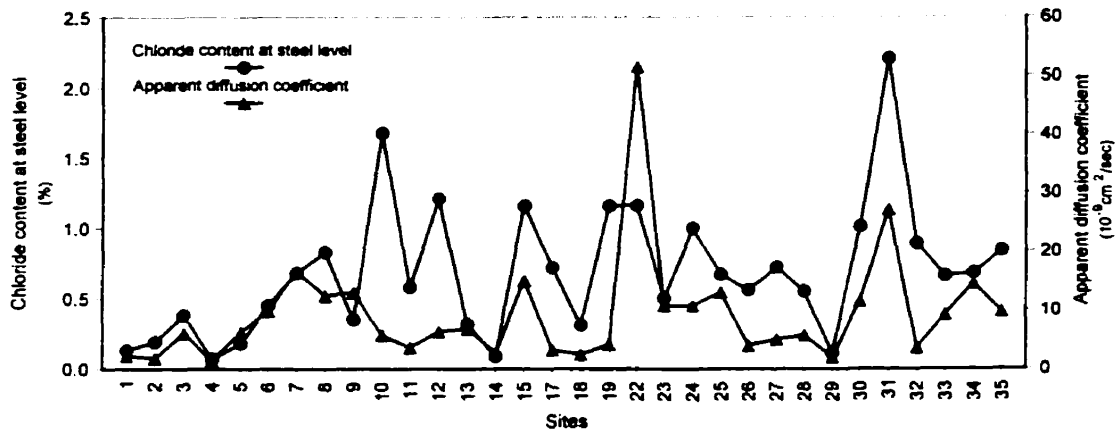
Figure 6-20: *Dependence of chloride content at steel level on apparent diffusion coefficient (entire deck)*
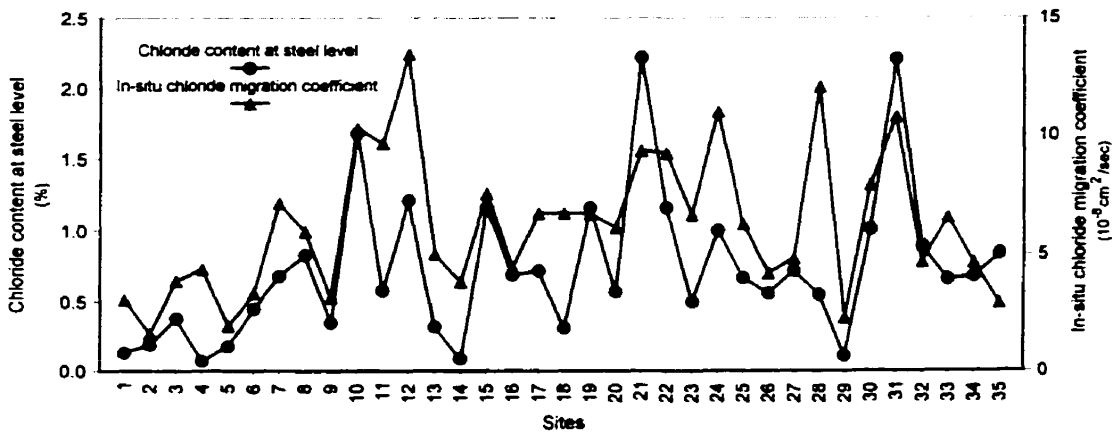
Figure 6-21: *Dependence of chloride content at steel level on in-situ migration coefficient (entire deck)*

163

6.2.7 Discussion: Variations of Test Data

Important trends were detected when comparing variation of the test data, however, no definitive findings can be deduced when correlating between various pairs of the relevant corrosion related parameters, as mentioned earlier. The moisture content at the time of test and the ambient environmental conditions may influence the results, hence, one test method might not be enough to assess the damage or to predict the corrosion rate. No single test method will detect or predict the damage, however, when a combination of test methods are used, it is more likely that any centre of deterioration will not be missed. In the next section, the variables will be correlated using multiple variable regression.

6.3 Prediction of Corrosion Rate Using Statistical Analysis

Much of an engineer's work requires the application of statistical methods to obtain adequate quantitative results[100]. Everything dealing with the collection, analysis, and interpretation of numerical data belongs to the domain of statistics. Measurements of parameters are required to compare performances and predict future performance under the same exposure conditions. Usually, there is a limited amount of data available, and a limited number of observations that can be made, within existing time and budget constraints. The result is that conclusions must be made by analyzing an amount of data (a sample) that is much smaller than the entire body of events (the population or process) to which these conclusions must be applied. In this study, the analysis consists primarily of regressing the variables, individually and in combination, with the dependent/response variable (Y), i.e., the corrosion rate obtained by the method of linear polarization. The corrosion rate was denoted "CR" and was chosen to be the response (dependent) variable and it was considered to be the "true" corrosivity of reinforcement steel in concrete. The relationships of the other variables with CR were derived both individually and with appropriate combinations of variables. Once the relationships between the variables was understood, the importance of the test technique in predicting the corrosion rate was evaluated, and a decision was made, whether or not the variable provided sufficient information to be considered significant.

6.3.1   Scheme of Analysis

A regression model does not imply a cause-effect relationship between the variables. Even though a strong empirical relationship may exist between two or more variables, this cannot be considered evidence that the regressor variables and the response are related in any cause-effect manner[101]. The relationship between the regressors (X_i) and the response (Y) may be suggested by theoretical considerations. Regression analysis can aid in confirming a cause-effect relationship, but it cannot be the sole basis of such a claim. Hence, in this investigation, it is necessary to discuss the results under two titles to deal with the primary objectives presented at the beginning of this thesis, that is: (a) to assess the corrosion induced damage in the bridge concrete deck, and (b) to investigate suitable test techniques for predicting corrosion. In this study, the scheme of the testing program reflected the objectives. The test methods were related to either the mechanisms causing corrosion or properties indicative of the probability of corrosion, hence in this section for the analysis and discussion of the results, it was considered that the condition of the bridge deck and the prediction of the corrosion rate could be classified according to two separate criteria:

- The methods which are generally used to assess corrosion induced damage; and

- The properties of the covercrete.

It is noted that the material properties and the exposure parameters, basically control the susceptibility to deterioration, which is manifested as the damage and is measured with all other available techniques. Therefore, the following definitions could be assigned to the two types of methods to predict the corrosion rate for the Dickson Bridge deck:

- The 'Assessment Methods' are those methods used to assess the symptoms already present and the damage of the structure, viz. delamination, concrete cover thickness, half-cell potentials, chloride content, apparent chloride diffusivity. In this study, there is a total of five independent / regressor variables (X_i), of which four are discrete and one is categorical (i.e. delamination);

- The 'Prediction Methods' are those methods used to measure the material properties of the structure and enable a prediction of the durability. It is a combination of strength, permeability, resistivity and diffusivity (in-situ test). There is a total of four variables (X_i), all of which are discrete.

The D_a parameter is considered to assess the damage and not to be predictive in nature as it is based on the existing chloride profile at this particular exposure. That is, the chlorides need to be present in the concrete to be able to obtain the D_a parameter. On the other hand, the D_{mig} parameter is predictive of the chloride ingress. It can be conducted at any stage of the service life without waiting for the chloride to penetrate into the concrete, however, then it is too late and the damage is already done.

Furthermore, in the previous chapter (Sections 5.3), it was concluded that the west and east sides of the bridge deck behaved differently. The west side displays a high level of deterioration due to the greater extent of delamination, higher corrosion rates and potentials, and much higher chloride content, while the east side is at an earlier point in the process, displaying less delamination and with lower chloride contents. Both sides have surpassed the initiation stage (Figure 2-5). However, the development of corrosion in the propagation period is clearly at different points. Different trends are exhibited in each of the two sides, hence it was decided to split the data in two sets as it is expected that the regression model for the two sides will give two different results. Theoretically, when dividing the bridge in half, a hypothetical maximum tolerated extent of deterioration is established with the two sides having two different residual lives, with the west having a shorter life than the east side.

Many aspects concerning residual service life remain unexplored and the objective of this study is not to predict in any way the residual life of the structure. The main objective is to identify suitable test techniques for the two portions of the bridge. The residual lifetime of the structure depends on the rate of deterioration, hence, the corrosion rate is the determining parameter in calculating the loss in capacity of the structure. The main difficulty is the estimation of the corrosion intensity in a corroding structure. Considerable effort has been directed into the development of on-site techniques to measure the corrosion rate of the reinforcing steel such as the linear polarization resistance. However, these techniques yield no information on the properties of the concrete in the vicinity of the rebar which are instrumental in initiating and sustaining corrosion. Hence, in the following analysis the results of both types of methods, the 'Assessment' and 'Prediction' methods are investigated, and conclusions with recommendations on the adequacy of the type of methods at the two different stages of service life displayed on the Dickson Bridge are stated.

6.3.2 Exploratory Data Analysis

The experimental data for the north side of the bridge deck was presented summarily in the previous chapter. The basic descriptive statistics for each parameter were outlined in Table 5-1. It was noted that the parameters exhibited a large variance, therefore, before undertaking any regression analysis of the various parameters involved, the properties of the distribution for each variable was examined. This was achieved by introducing graphical presentations of the data in order to pinpoint important features, which may not be immediately apparent from the raw data. Hence, preliminary data editing before the regression analysis was conducted to identify outliers, as these can have a serious effect on many of the techniques used in statistical analysis. Appropriate transformations were applied to the parameters when the variance was large, to improve the agreement with normality. These concepts are discussed briefly in the following subsection outlining the scheme of the analysis.

6.3.2.1 Univariate Analysis

Each variable was examined individually and the quantities as the number of data points, the mean, and standard deviation of a variable were easily obtained as introduced earlier in Section 5.2.1. They provided considerable information about the data and are also the values that will be needed for subsequent calculations. It is noted that when dealing with the mean and the standard deviation, the variability of data is often related to the location of the data. The coefficient of variation is suggested as a measure of variability that is free of the location or adjusts for location. The COV is dimensionless and has no units; it is only a numerical ratio[101].

Identification of Outliers

The identification of outliers is extremely important in any statistical analysis. Box and whisker plots and stem-and-leaf diagrams were used to identify observations that might have been outliers (observations in the extremes of the data), which represented inappropriate or incorrect observations[101].

The box and whisker plot uses five numbers to describe a set of data: maximum value, upper hinge or third quartile, Q_3, (approximately equivalent to the 75th percentile), median (the 50th percentile), lower hinge or first quartile, Q_1, (approximately equivalent to the 25th percentile), and the minimum value. In this study, a rectangle was constructed between the lower and the upper

167

hinges, and a plus (+) sign at the location of the median was displayed. The whiskers that extend in either direction indicate the non-outlying data (this is equal to a length 1.5 times the interquartile range to the left of Q_1 and to the right of Q_3)[101, 102]. Extreme values were identified with asterisks (*) or zeros (0) as is demonstrated in the example that will follow.

A stem-and-leaf diagram summarizes the data in a visual manner, which is easy to understand and lists the actual data, hence the stem-and-leaf diagrams were used for each parameter under investigation to identify the values that corresponded to the outliers indicated by the box plots. For example, by studying the box-plot and stem-and-leaf diagram shown in Figure 6-22, it is quite evident that one outlier is present in the lower end, as indicated by the asterisk shown in the box-plot corresponding to the extreme value 13.4×10^{-8} cm^2/sec in the stem-and-leaf diagram. Only one example is presented in this section, while all details are included in Appendix (G).

Stem-and-Leaf diagram for D_m data   Box-and-Whisker plot of D_m

Leaf Unit = 0.10 (x10^{-8}cm^2/sec)

```
 2     1 69
 4     2 39
 9     3 01388
15     4 244668
17     5 09
(7)    6 1256777
11     7 159
 8     8
 8     9 236
 5    10 27
 3    11 0
 2    12 0
 1    13 4
```

```
                    _____
          ——————I   +   I——————————   •

    ———+———————+————————+————————+————————+————————+——————($D_m$x10$^{-8}$cm$^2$/sec)
   2.5      5.0       7.5      10.0     12.5
```
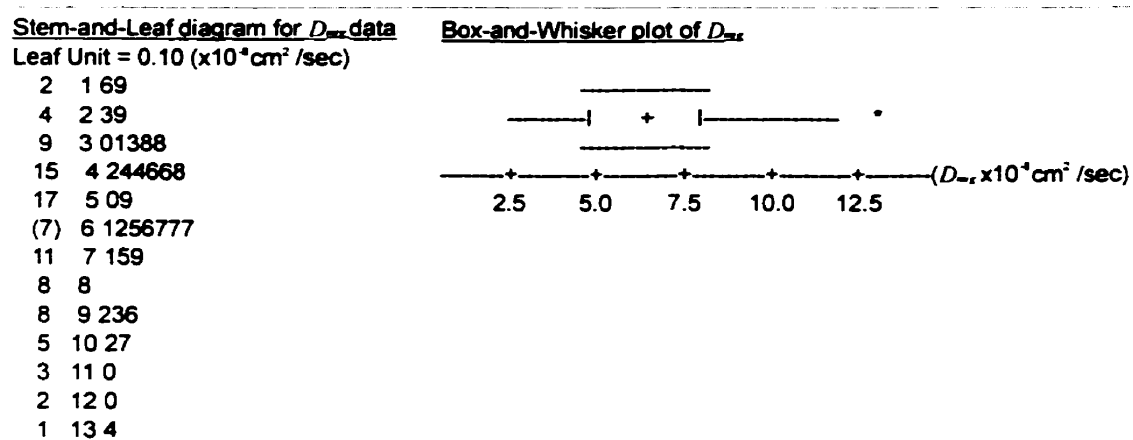
Figure 6-22: *Stem-and-leaf diagram and box-and-whisker plot for D_{mig} (Analysis 1)*

Assessing the Normality Assumption

The normal distribution holds a very special place in statistical analysis. Many of the statistical inference procedures (such as multivariable analysis) assume normality and have optimal properties, if normality holds[102]. A histogram display was used to aid the identification of the sample characteristics such as symmetry, skewness, and general shape. The histogram plot was drawn as an estimate of the probability distribution of the process under investigation. Hence, the proportions of sample observations falling within one, two and three standard deviations of the mean were determined and the frequency distribution graph, that is the histogram was constructed. A smooth frequency curve was drawn superimposing the histogram to estimate the probability distribution as shown in Figure 6-23 for the D_{mig} values. Most of the variables, such as

the corrosion rate, percent chloride at the steel level, resistivity and diffusivity as shown in Figure 6-23 and in Appendix G exhibited a log-normal distribution (positively skewed with a tail of higher values resulting in a high COV) as expected from results of physical measurements at site[101]. This usually occurs in practice whenever a random variable is encountered such that its logarithm has a normal distribution, which will be discussed later. It is noted that it is quite acceptable that the distribution of these variables exhibit log-normal distribution, however, as explained earlier statistical analysis that will follow assumes normality. Hence, normality is a prerequisite of the analysis that will follow and it is the objective in this section.
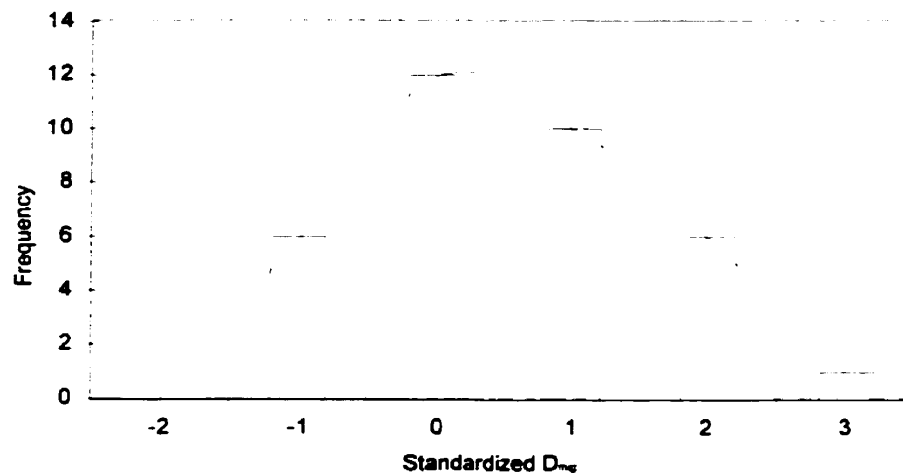
Figure 6-23: *Frequency distribution diagram together with probability curve for D_{mg} values (Analysis 1)*

The histogram and the curve shape for each parameter were analyzed for skewness, that is, if the tail of the curve to one side of the central maximum was longer than the other. The box plot was also used to investigate symmetry. However, these techniques are by nature, subjective. Therefore, it was decided to supplement these displays with more objective statistical procedures[102]. A normal probability plot was used to permit the analyst if the data for each parameter was distributed normally. A straight line of best fit was drawn for the points that estimated the cumulative distribution function for the process derived from the data. The graph resembles the usual form of normal probability paper, with the vertical axis displaying a probability scale and the horizontal axis - a data scale[99, 102]. In addition, the results from the Anderson-Darling normality test (an alternative of the Shapiro-Wilk[102]) are displayed in the lower right corner; these were used to reject or not reject the null hypothesis that the data was normality distributed at a significance level of 0.05 (for example as shown in Figure 6-24). The

plot's p-value is 0.172, therefore, the D_{mg} values are normality distributed at a significance level of 0.05.
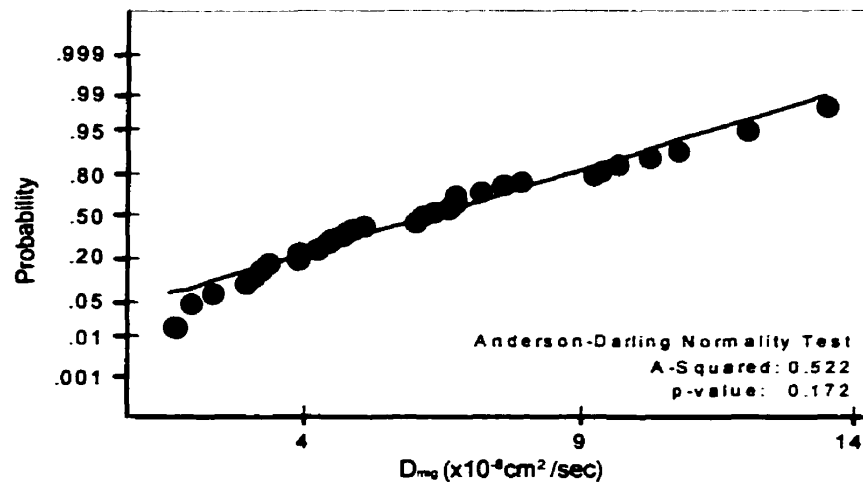
Figure 6-24: *Normal probability plot for D_{mg} values (Analysis 1)*

Transformation to Normality and Variance Stabilizers

Normality is a desirable property and many commonly used statistical procedures, such as multiple variable regression described later in the chapter, require that the probability distribution be nearly normal. In many cases, when the normality condition is not met, an appropriate transformation of the data from the original scale to a different scale can normalize the data[100]. The distribution of the transformed data will be more normal than the original data. This then allows for the valid application of procedures developed for normal populations. The results may then be transformed back to the original scale, as it is difficult to interpret the value of transformed data. These types of transformations are called transformations to normality[99, 100]. The transformations to normality often carry with them another interesting and useful feature: they tend to stabilize the variance of the data. That is, data in the original scale may have the feature that the standard deviation or variance is a function of the mean, but in the transformed scale, there is no relationship. Hence, the COV value usually has a tendency to decrease with the application of a transformation.

There are many different ways to transform the data, using logarithmic, square root, reciprocal and other transformations. Although a transformation can be applied to any variable, each one seems to work best for a particular type of variable. Of all the transformations available, the logarithmic (or log) transformation is useful in applying to variables representing physical

170

characteristics and concentrations. Furthermore, the data must be non-negative, with values, which are not very close to zero[102]. It is possible that a transformation will render the data more tractable, however the key to a simple, effective transformation is the knowledge of the phenomenon being studied.

Results of Univariate Analysis

The first analysis was conducted on the as-collected data (Analysis 1). If the variable showed signs of normality, no additional analysis was conducted. A second analysis was conducted in the case when the frequency distribution plot indicated skewness, the box plot and stem leaf diagrams depicted outliers and the normal probability appeared to be curved. The outliers were removed and the process was repeated analyzing the data for normality. Full details are included in Appendix G, and it is summarized in Table 6-1 (Analysis 2). Furthermore, appropriate transformations were applied to the parameters when the COV was large, to improve the agreement with normality (Table 6-1, Analysis 3).

It is noted that, no transformation was applied for the corrosion potential even though the variable represents the concentration of oxygen in the Nenrst equation. The concentration has already been logged in obtaining the potential ϕ. The potential is not a direct measurement of the concentration, but represents the concentration indirectly given that these concentrations have been logged (see Equation (3-3)). For this reason, it was considered unreasonable to perform a second logarithmic transformation on this variable, which is already the result of a logarithmic transformation. Moreover, no transformation was applied to the percentage chloride content at the level of steel, even though the variable represents a concentration. With the transformation, the distribution ends up normalized (Appendix G); however, the COV increases to 1.41 (might be due to the fact that the values are close to zero), hence, for this reason no transformation was applied. Full details are included in Appendix (G).

Based on the above results, the variables chosen for further investigation are delamination ($Delam$), corrosion potential (ϕ_{corr}) and compressive strength (Str) from Analysis 1, concrete cover ($Cover$) and percentage chloride at the steel level ($\%Cl$) from Analysis 2, and corrosion rate ($LogCR$), apparent diffusion coefficient ($LogD_a$), in-situ chloride migration coefficient ($LogD_{mig}$), resistivity of the concrete ($Log\rho$) and the coefficient of permeability ($Logk_w$) from Analysis 3.

Table 6-1: Results of univariate analysis (Analysis 2 and Analysis 3)

| Quantity measured | Analysis 2: Without outliers | | | | | | | | | Analysis 3: After transformation | | | | | |
| | (a) Entire deck | | | (b) East side of deck | | | (c) West side of deck | | | (a) Entire deck | | (b) East side of deck | | (c) West side of deck | |
	No. of Readings	No. of Outliers	COV	No. of Readings	No. of Outliers	COV	No. of Readings	No. of Outliers	COV	No. of Readings	COV	No. of Readings	COV	No. of Readings	COV
Corrosion potential (mV)	-	-	-	-	-	-	-	-	-	-	-	-	-	-	-
Corrosion rate (µm/year)	129	8	0.48	61	4	0.57	68	4	0.41	137	0.16	65	0.19	72	0.12
Delamination	-	-	-	-	-	-	-	-	-	-	-	-	-	-	-
Concrete cover (mm)	134	3	0.45	63	2	0.52	71	1	0.38	-	-	-	-	-	-
Percentage chloride at steel level	33	2	0.60	17	-	0.79	16	2	0.41	35	1.41	17	1.02	18	2.13
Apparent Cl diffusion coefficient (cm²/sec)	30	2	0.62	16	-	0.69	14	2	0.55	30	0.40	16	0.45	14	0.35
In-situ Cl migration coefficient (cm²/sec)	34	1	0.46	16	1	0.50	18	-	0.40	34	0.30	16	0.35	18	0.24
Electrical resistivity (kΩcm)	118	19	0.43	55	12	0.45	63	7	0.42	137	0.35	67	0.39	70	0.31
Coefficient of permeability (m/sec)	30	4	0.76	15	1	0.79	15	3	0.71	30	0.37	15	0.44	15	0.30
Concrete compressive strength (MPa)	-	-	-	-	-	-	-	-	-	-	-	-	-	-	-

172

6.3.3 Regression of the Individual Variables

Relationships between the variables are often of interest when an association between the variables measured, or alternatively a basis of prediction is needed. Prediction is, of course, important in planning and decision making. One type of analysis primarily concerned with the association between variables is the regression analysis[99, 101]. This section considers the simple linear regression analysis, that is with a single regressor, X, that has a relationship with a response, Y, that is a straight line. The goal is to derive an equation that will link the values of x_i and y_i, with the least amount of error possible. This is better understood graphically. Figure 6-25 shows a plot of Y vs. X. The goal is to find the line which runs through these points such that the vertical distances between the line and the y values are minimized, i.e., the values of e_i are minimized. It follows that the n random variables having the values y_i ($i = 1, ..., n$) are independently normally distributed with the means ($\beta_o + \beta_1 x_i$) and the common variance σ^2. The equation relating the values of each observation of y and x of the following form[100, 101]:

$$y_i = (\beta_o + \beta_1 x_i) + e_i \qquad (6.1)$$

where for any given x, the mean of the distribution of the y_i is given by ($\beta_o + \beta_1 x_i$) (portion of y_i predicted by the straight line) and the e_i is the portion of the y_i that the straight line fails to predict, which is the error or the residual. The terms β_o and β_1 represent the intercept and the slope, respectively.
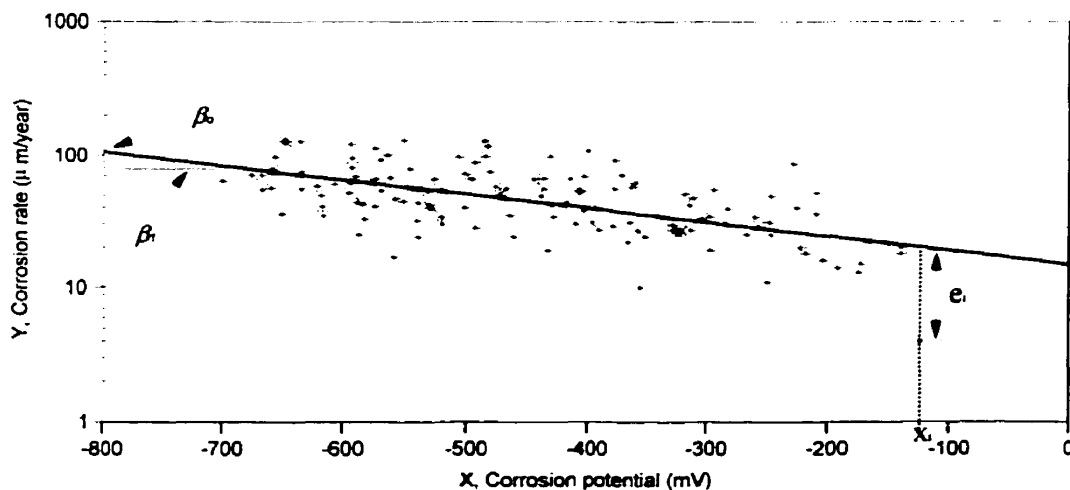
Figure 6-25: Y vs. X plot (Corrosion rate vs. corrosion potential)

However, is it possible to determine if the line represents a good estimate of the relationship between X and Y? The answer lies in the study of the residuals, e_i.

6.3.3.1 Residual Distribution

The distribution of each variable has been studied in an earlier section. The distribution of the residuals arising from the regression of the independent variables with the dependent variable, that is corrosion rate, will be reviewed in this section. It is assumed that the e_i values are independent and are normally distributed random variables having zero mean and the common variance σ^2. Note that this assumption is required to discuss the goodness of predictions based on least-squares equations[99].

Hence, in this study, each independent variable (Xi) was regressed individually, to study the residual distributions for any signs of anomalies, and to keep track of the outliers on Y, that is the corrosion rate values. It is noted that earlier in the previous section, the outliers obtained were outliers on the X variable, while here, the outliers on the residuals are examined, that is the outliers on the model chosen to fit the data. For each variable, the following information was extracted and examined:

- Number of observations N, SSE, R^2, $R^2_{adjusted}$, F-ratio;

- Outliers identified by a z-score > 3;

- Outliers identified by a Cook's Distance (CD) > 1; and

- Normal plot of residuals, histogram of residuals, I-chart of residuals and a residual vs. predicted value of y (residual vs. fits).

These concepts will be briefly described prior to the actual analysis, to get familiar with the meaning of each quantity and graph.

Required Information

The method most commonly used to calculate the magnitude of the error of the equation, is to add the squared values of each of the individual error. This value is referred to as the Error Sum of Squares, or SSE[100]:

$$SSE = \sum e_i^2 \tag{6.2}$$

It should be noted that as the errors are squared, the effect of the larger values are emphasized. The result of this is that outliers, whose residuals are high, can have an enormous effect on the value of the SSE and, consequently, on the best fit line.

It will not always be so obvious that a variable X is insignificant in predicting Y. The significance of X in predicting Y is established by comparing the SSE of the model including X, to the SSE of the model for the mean value of y, y'. This last model is referred as the benchmark model, that is a horizontal line where the slope of the line is zero and the line runs through the y' value. The equation relating X and Y using the benchmark model based on the mean value of y, i.e., the horizontal line, is: $y = \beta_o + e_i$ where β_o is equal to y'. The value of the error sum of squares is referred to this model, as SSY. A measure of fit that is very commonly used is the square multiple correlation, R^2. This value represents how well a model predicts Y in comparison to the benchmark model. The coefficient of determination, R^2, is calculated as follows[100, 101]:

$$R^2 = \frac{SSY - SSE}{SSY} \tag{6.3}$$

The value of R^2 is always positive, and ranges between 0 and 1. The variable X is a good predictor of Y if the value of R^2 is close to unity. However, this model is based on nothing but the mean.

One way to examine the validity of an equation to fit foreign data, that is to fit data, which were not a part of the observations used to create the equation itself, is to compare $R^2_{adjusted}$ (or R^2_{adj}) to R^2. The decrease in R^2 is called the shrinkage, and it represents the decrease in the predictive power of the equation when used on the population as a whole.

The significance of the variable X in the prediction of Y is determined by examining another important parameter in statistics: the F-ratio. It is noted that the benchmark model will be termed the ω-model, and the model being tested as the Ω-model. Hence the value of the F-ratio is calculated as follows[100, 101]:

$$F = \frac{\dfrac{SSE(\omega) - SSE(\Omega)}{DOF(\omega) - DOF(\Omega)}}{\dfrac{SSE(\Omega)}{DOF(\Omega)}} \tag{6.4}$$

The degrees of freedom, DOF is equal to the number of observations, N, minus the number of parameters being fitted by the model. Like R^2, the F-ratio is a measure of the improvement of one

175

model over another, however the F-ratio takes into account the number of variables that were needed to obtain this improvement. This is achieved by including the degrees of freedom (DOF) in the Equation (6.4). The critical values of F that must be obtained in order to consider the Ω-model significant. These critical values are listed in standard tables of the F-distribution, by using $F\{1-\alpha, \upsilon_1, \upsilon_2\}$ where α is the level of significance, and υ_1 and υ_2 are DOF of the numerator and the denominator of the F-ratio, respectively. If the F-ratio calculated is larger than the appropriate critical value, the model Ω-model is considered significant[99, 101].

The measurement of the outliers on the regressor variables have been considered up to this point. The z-scores can be calculated for the residuals obtained when a model is fitted to the data. These standardized residuals are used for finding the observations whose predicted y values are quite different from the actual y value, i.e., they do not fit the model well. If the standardized residuals are approximately normally distributed, then an observation with a standardized residual greater than 3 in absolute, is considered as potential outlier. This is because, in a distribution which is normal, about 99% of the scores should lie within three standard deviations of the mean[102]. Alternatively, an outlier can be defined as a point, which if deleted, can produce a substantial change in at least one of the regression coefficients. That is, the prediction equations, with and without the point, are quite different. A quantity that measures this change is the Cook's Distance (CD). Unlike the z-scores which identify the outliers on Y or on the X's individually, the Cook's Distance measures the combined effect of a point being an outlier on Y and on the set of regressors. Cook and Weisberg indicate that a $CD_i > 1$ would be generally be considered too large, and would therefore identify probable outliers[100, 102].

In addition, the residuals (or standardized residuals) should be plotted in various ways to detect systematic departures. To check the normality assumption, a normal probability plot and a histogram of the standardized residuals can be constructed. In a normal probability plot, a straight line is characteristic of a normally distributed set of values and any non-linear curve would indicate a deviation from normality. The histogram illustrates if any of the observation has a standardized residual value greater than 3 in absolute. Moreover, a plot of the standardized residuals versus the predicted values is a major diagnostic tool to verify the constant variation assumption. A standardized residual vs. fit plot with the appearance of a constant (horizontal) band indicates no violation of the model. The last assumption that the error components are independently distributed is verified using an I-chart of the residuals. A process experiencing only chance variations consistent with an established variability, σ, is said to be in statistical control.

176

Commonly used limits are the so-called 3σ limits, where, in the case of a mean value, or $\overline{X}$, control chart upper (UCL) and lower (LCL) control limits are defined as $\mu \pm 3\sigma/\sqrt{n}$, respectively[99, 102].

Summary of Results from Residual Analysis

The results from the residual analysis are tabulated in Tables 6-2 to 6-4. Separate analyses were conducted on the data of the two sides (east and west) of the deck and on the entire deck as well. The results for the entire deck suggest that the ϕ_{corr} variable performed the best, followed by $LogD_{mig}$, Str, %Cl and $Log\rho$ as indicated by the R^2 results (Table 6-2). On the other hand, in the east side, the $LogD_{mig}$ variable performed the best followed by ϕ_{corr}, %Cl, Str and $Log\rho$, while for the west side the ϕ_{corr} variable performed the best followed by Str, $LogD_a$, $Logk_w$ and Delam. The influence of the chloride content (%Cl) in the west side was negligible, i.e. a $R^2 = 0.1\%$, a figure much higher is found in the east side ($R^2 = 28.9\%$). A similar trend was noticed for $LogD_{mig}$ and $Log\rho$ which is expected as the D_{mig} value is a direct measure of the diffusivity of chloride in concrete while the ρ value is a indirect measure of diffusivity.

The analysis of the entire deck indicated that most of the variables were significant in predicting LogCR as the F-values are greater than the critical value for the corresponding DOF at a 0.05 level of significance with the exception of $LogD_a$ and $Logk_w$ (Table 6-2). The same applies to the east side with the addition of the Str variable to the exceptions (Table 6-3). It is quite different in the west side as the only variables that are significant in predicting LogCR were ϕ_{corr}, Delam and Str. The ϕ_{corr}, Delam, Cover, and $Log\rho$ variables indicated that observation number 17 (Site 5, reading on location 1) may be a possible outlier (Table 6-3). The decrease in R^2, that is the decrease in predictive power of the equation when used on the population as a whole are acceptable with some exceptions as shown in Tables 6-2 to 6-4. Furthermore, the distributions of the standardized residuals were not perfectly normal as illustrated in Figure 6-26 and in Appendix H. The slight deviation from normality suggested that another X variable should be added to the model to account for the variance which was not accounted by the first variable. It is noted that only one example of the plots is included in this section, while the remaining plots can be found in Appendix (H).

Overall single variable analysis is not much of a good tool to correlate the parameters because the data of the various tests are affected by the environmental conditions. Hence, low correlation coefficients (R^2) between the various tests data suggesting no significant relationship was

Table 6-2: *Residual information from regression of the independent variables with the dependent variable (Log(CR))*

Quantity Measured		N	SSE	R^2	R^2_{adj}	Decrease in R^2	F-ratio	$F^*_{critical}$	DOF	Outliers $z > 3$	Outliers $CD > 1$
		(a) Entire bridge deck									
Assessment Methods	Corrosion potential	137	5.83520	36.6%	36.1%	1%	77.80	3.84	136	17	-
	Delamination	137	8.17000	11.2%	10.5%	6%	16.99	3.84	136	17	-
	Concrete cover	134	8.73045	2.6%	1.9%	27%	3.57	3.84	133	17	-
	Percentage chloride at steel level	31	1.68492	16.9%	14.0%	17%	5.88	4.17	30	-	-
	Apparent Cl diffusion coefficient	28	1.79791	10.2%	6.7%	34%	2.95	4.20	27	-	-
Prediction Methods	In-situ Cl migration coefficient	32	1.38563	31.5%	29.2%	7%	13.80	4.17	31	-	-
	Electrical resistivity	134	7.66420	13.5%	12.9%	4%	20.62	3.84	133	17	-
	Coefficient of permeability	29	1.85959	6.5%	3.0%	54%	1.86	4.18	28	-	-
	Concrete compressive strength	32	1.62768	21.0%	18.4%	12%	7.99	4.17	31	-	-

Table 6-3: *Residual information from regression of the independent variables with the dependent variable (Log(CR))*

Quantity Measured		(b) East side of bridge deck									
		N	SSE	R^2	R^2_{adj}	Decrease in R^2	F-ratio	$F^*_{critical}$	DOF	Outliers $z > 3$	Outliers $CD > 1$
Assessment Methods	Corrosion potential	65	3.90380	31.7%	30.6%	3%	29.24	4.00	64	17	-
	Delamination	65	5.33094	6.7%	5.2%	22%	4.54	4.00	64	17	-
	Concrete cover	63	5.15312	7.8%	6.3%	11%	5.15	4.00	62	17	-
	Percentage chloride at steel level	15	1.09042	28.9%	23.4%	19%	5.29	4.60	14	-	-
	Apparent Cl diffusion coefficient	14	1.39790	6.8%	0.0%	100%	0.87	4.67	13	-	-
Prediction Methods	In-situ Cl migration coefficient	14	0.76529	48.8%	44.6%	9%	11.45	4.67	13	-	-
	Electrical resistivity	64	4.58750	19.7%	18.4%	7%	15.17	4.00	63	17	-
	Coefficient of permeability	14	1.42690	5.4%	0.0%	100%	0.68	4.67	13	-	-
	Concrete compressive strength	14	1.18529	20.6%	14.0%	32%	3.12	4.67	13	-	-

Table 6-4: *Residual information from regression of the independent variables with the dependent variable (Log(CR))*

Quantity Measured		(c) West side of bridge deck									
		N	SSE	R^2	R^2_{adj}	Decrease in R^2	F-ratio	$F'_{critical}$	DOF	Outliers z > 3	Outliers CD > 1
Assessment Methods	Corrosion potential	72	1.9142	39.0%	38.1%	2%	44.73	4.41	71	-	-
	Delamination	72	2.78626	11.2%	9.9%	12%	8.82	4.41	71	-	-
	Concrete cover	71	3.05275	0.5%	0.0%	100%	0.33	4.41	70		-
	Percentage chloride at steel level	16	0.44404	0.1%	0.0%	100%	0.01	4.54	15	-	-
	Apparent Cl diffusion coefficient	14	0.36509	17.6%	10.7%	39%	2.56	4.67	13	-	-
Prediction Methods	In-situ Cl migration coefficient	18	0.42397	11.1%	5.6%	50%	2.01	4.45	17	-	-
	Electrical resistivity	70	2.57583	5.7%	4.3%	25%	4.13	4.41	69	2	-
	Coefficient of permeability	15	0.34734	13.4%	6.7%	50%	2.01	4.60	14	-	-
	Concrete compressive strength	18	0.30187	36.7%	32.8%	11%	9.29	4.45	17	-	-
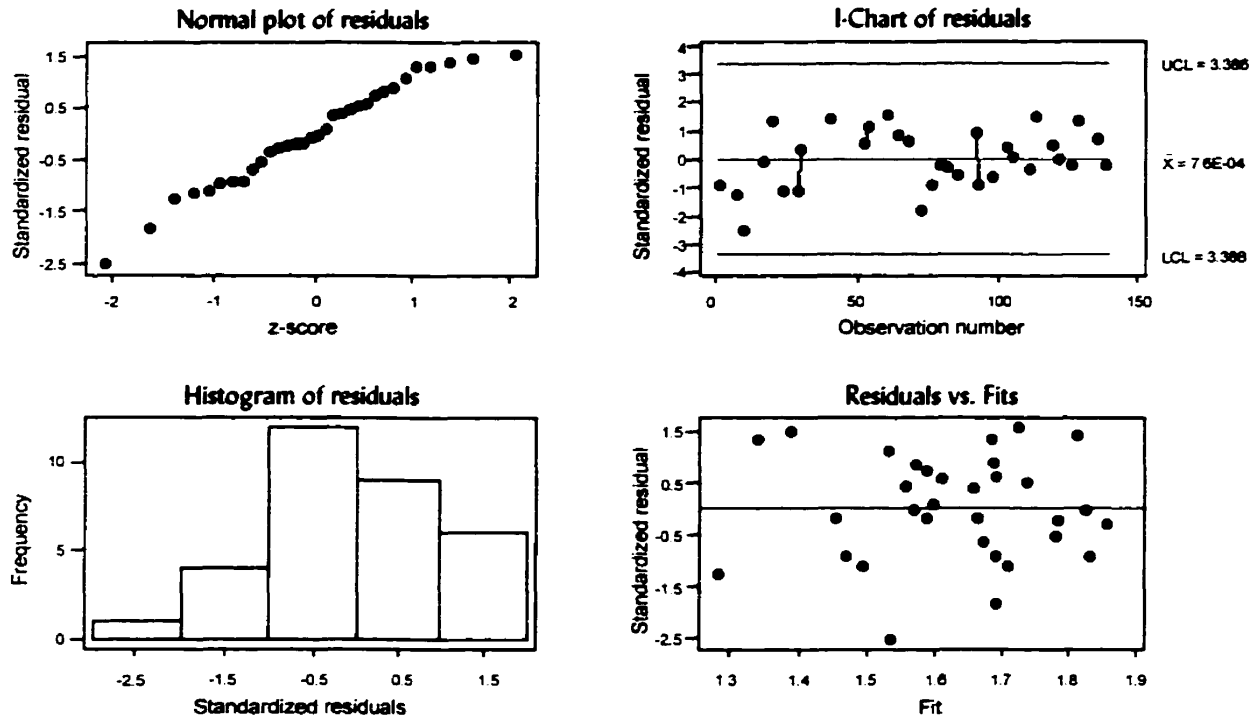
Figure 6-26: *Standardized residual model diagnostics for 'LogD$_{mig}$' (entire bridge deck)*

6.4 Prediction of Corrosion Rate Using Multiple Linear Regression Analysis

Multivariable analysis requires that the probability distribution be nearly normal, hence, the dependent variable and some of the independent variables required transformation to make the data dispersed in a scattergram and normally distributed as indicated earlier. When a dependent variable, Y, relates to two or more independent variables X_1, X_2, ..., X_k, a multiple variable regression analysis may be used. The relationship between these variables is presented as an additive linear model of the form[99, 100]:

$$y_i = \beta_o + \beta_1 x_{i1} + \beta_2 x_{i2} + ... + \beta_k x_{ik} + e_i \qquad (5.5)$$

where β_o, β_1, ..., β_k are constants and are referred to as regression coefficients. The parameters of the equation are obtained easily by making use of certain basic principles of matrix algebra. In the present study, these lengthy calculations were reserved for software packages (Minitab and Data-Analysis application in Excel). Multiple regression can be thought as fitting a line through a set of

181

points in a three dimensional space, or of a higher dimension. The residual, e_i, can be thought of as the distance in the y-direction between a point in space and the line.

6.4.1 Selection of Variables

In the previous section, the relationship between *LogCR* and each of the independent variables was studied. To identify the extent to which the dependant variables are correlated, the correlation matrix of the set of independent variables, plus the dependent one was determined. The correlation matrices for the data under study are presented in Tables 6-5 to 6-7, where the values represent the Pearson[99] correlation coefficients, R ($R= \sqrt{R^2}$). The ideal situation is one in which the correlation factors between the dependent variable (*LogCR*) and each independent variable are high, and the correlation between the independent variables themselves is low. This would result in the least amount of multicollinearity, i.e., redundant information, and it would lead to a situation where each variable that is added to an equation would provide new information and would serve to significantly increase the effectiveness of the equation.

Table 6-5: *Correlation matrix: (a) Entire bridge deck*

(a)	LogCR	φcorr	Delam	Cover	%Cl	LogDs	LogDmig	Logρ	Logkw	Str
LogCR	1.000									
φcorr	-0.605	1.000								
Delam	0.334	-0.635	1.000							
Cover	0.162	-0.300	0.305	1.000						
%Cl	0.411	-0.696	0.602	0.119	1.000					
LogDs	0.319	-0.390	0.240	0.362	0.455	1.000				
LogDmig	0.561	-0.675	0.461	0.169	0.644	0.335	1.000			
Logρ	-0.368	0.422	-0.275	-0.110	-0.386	-0.004	-0.266	1.000		
Logkw	-0.254	0.466	-0.099	-0.042	-0.260	-0.128	-0.161	0.355	1.000	
Str	-0.459	0.447	-0.249	-0.405	-0.070	-0.109	-0.194	0.305	0.333	1.000

Table 6-6: *Correlation matrix: (b) East side of bridge deck*

(b)	LogCR	ϕ_{corr}	Delam	Cover	%Cl	LogD$_a$	LogD$_{mig}$	Logp	Logk$_w$	Str
LogCR	1.000									
ϕ_{corr}	-0.563	1.000								
Delam	0.259	-0.558	1.000							
Cover	0.279	-0.224	0.111	1.000						
%Cl	0.538	-0.838	0.736	0.144	1.000					
LogD$_a$	0.260	-0.404	0.043	0.416	0.454	1.000				
LogD$_{mig}$	0.699	-0.806	0.649	0.009	0.734	0.300	1.000			
Logp	-0.443	0.505	-0.250	-0.011	-0.545	-0.159	-0.416	1.000		
Logk$_w$	-0.232	0.580	-0.070	-0.163	-0.261	-0.243	-0.163	0.401	1.000	
Str	-0.454	0.318	-0.099	-0.203	-0.221	-0.222	-0.091	0.234	0.293	1.000

Table 6-7: *Correlation matrix: (c) West side of bridge deck*

(c)	LogCR	ϕ_{corr}	Delam	Cover	%Cl	LogD$_a$	LogD$_{mig}$	Logp	Logk$_w$	Str
LogCR	1.000									
ϕ_{corr}	-0.624	1.000								
Delam	0.334	-0.646	1.000							
Cover	-0.069	-0.347	0.473	1.000						
%Cl	-0.023	-0.456	0.352	0.039	1.000					
LogD$_a$	0.419	-0.330	0.461	0.266	0.446	1.000				
LogD$_{mig}$	0.334	-0.469	0.131	0.203	0.424	0.351	1.000			
Logp	-0.239	0.330	-0.344	-0.245	-0.170	0.263	-0.155	1.000		
Logk$_w$	-0.366	0.384	-0.132	0.143	-0.257	0.103	-0.115	0.276	1.000	
Str	-0.607	0.637	-0.485	-0.596	-0.084	0.013	-0.374	0.375	0.399	1.000

An examination of the correlation between *LogCR* and the independent variables (Tables 6-5 to 6-7) will quickly reveal that the results are the same as those obtained in Section 6.3.3.1 when comparing the R^2 illustrated in Tables 6-2 to 6-4. However, one important point here is that the sign of correlation between the variables can be investigated. The fact that a linear relationship of negative slope exists between ϕ_{corr} and *LogCR* signifies that the corrosion process was subject to anodic control. This gives rise to the initiation and growth of pits on the surface of the steel[41].

The slope of the lines illustrated in Figure 6-27, which represents the cathodic Tafel coefficient, is reasonably consistent with the value assumed in the calculations of corrosion rate, namely 120 mV per decade.
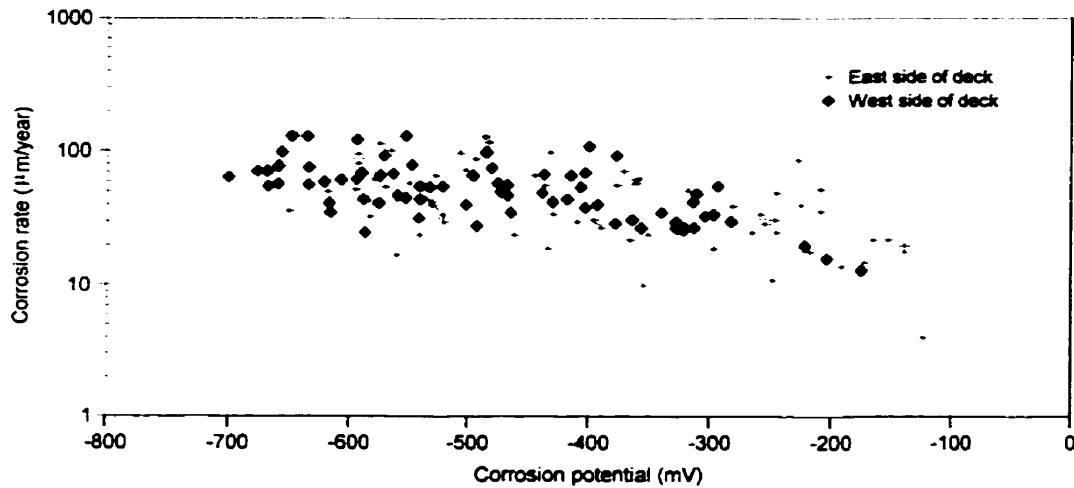
Figure 6-27: *Corrosion rate vs. corrosion potential*

Another correlation of particular interest arises when the $LogD_{mig}$ values are regressed against $LogCR$ and ϕ_{corr} values, a linear relationship of positive slope exists between $LogCR$ and $LogD_{mig}$, and a negative slope between ϕ_{corr} and $LogD_{mig}$. Hence, as the D_{mig} values increase, there is an increase in the corrosion rate and the potential reaches the active zone; the relationship is more pronounced in the east side of the bridge. The relationship between the ϕ_{corr} values and the corresponding $\%Cl$ values show a relatively strong negative correlation as expected (especially in the east side). Moreover, in the east side, the $LogD_{mig}$ values have a relatively strong positive correlation with the $\%Cl$ and *Delam* values, while in the west side, the correlation is poor. The $\%Cl$ and *Delam* values have a similar correlation. As the west side was mostly delaminated (Table 5-2), this indicates that delamination affects both the in-situ and the profile tests.

Another important fact observed from the correlation matrices is the negative and positive relationships that $Log\rho$ has with $LogCR$ and ϕ_{corr}, respectively. This was expected, as resistivity is a rate determining factor once corrosion commences, hence it is encouraging and provides confidence in the data. However, the sign of the correlation that the $Logk_w$ values have with the various variables is opposite to what was expected. For example, one would expect that the correlation would be positive between $LogCR$ and $Logk_w$, i.e. the higher the permeability, the

184

higher the corrosion rate, but this is not the case. This was already noticed in Section 5.2.10.2 when analyzing the results shown in Figure 5-13(a). It must be kept in mind that the variable $Logk_w$ was obtained with an applied pressure that is too small as explained in Sections 3.5.5.3 and 4.9.3, hence, the results should be dealt with caution.

Most importantly, it must be emphasized that the single most important tool in selecting a subset of variables for use in a model is the knowledge of the area under study. Furthermore, it is important for the investigator to be judicious in the selection of predictors. If too many variables are used, the prospects of cross validation may be influenced negatively. In this study, the variables are analyzed under two headings, that is 'Assessment' and 'Prediction' methods as explained in Section 6.3.1. Hence, the interactions between the variables obtained from the two types of methods are investigated. In the east side, the %Cl values have a strong correlation with the ϕ_{corr} and Delam values. Another strong correlation of particular interest is between the ϕ_{corr} and Delam values (on both sides of the bridge). These correlations indicate that the variables essentially provide the same information, hence, this should be kept in mind when choosing the combination of variables amongst the 'Assessment Methods' to predict the corrosion rate values. It is noted that there is no particular correlation amongst the 'Prediction Methods', except the negative correlation between $Log\rho$ and $LogD_{mig}$ values in east side of the bride (Table 6-6).

6.4.2 Determining Significance

When regressing one independent variable (X) against the dependent variable (Y), it is probable that the distribution will not be normal, e.g., as illustrated in Figure 6-26 and in Appendix H. This is because one independent variable (X) is not enough to account for all of the variance, but when another X variable is included in the model it is expected to account for the variance that the first X variable did not. In order to determine if the addition of a variable has a positive influence, the significance of the chosen variables needs to be investigated. A variable is considered significant if the information provided by this variable is sufficiently important, such that its addition to a set of variables increases the ability of the set to explain the phenomenon under consideration. A tool that is used to allow the analyst to quickly calculate the values of R^2, F, SEE, and MS (mean squares) and check all of the relevant information at a single glance is the analysis of variance table, or ANOVA table[99, 100, 101]. Table 6-8 shows a typical ANOVA table indicating the appropriate values needed to construct the table.

185

Table 6-8: *Typical ANOVA table[99]*

SOURCE	DOF	SSE	MS	F	$R^2_{partial}$
Difference	DOF(Diff) [1]	SSE(Diff) [2]	MS(Diff) [3]	F [6]	R^{2} [7]
Ω-model	DOF(Ω)	SSE(Ω)	MS(Ω) [4]		
ω-model	DOF(ω)	SSE(ω)	MS(ω) [5]		

(1) $DOF(Diff) = DOF(\Omega) - DOF(\omega)$

(2) $SSE(Diff) = SSE(\Omega) - SSE(\omega)$

(3) $MS(Diff) = SSE(Diff) / DOF(Diff)$

(4) $MS(\Omega) = SSE(\Omega) / DOF(\Omega)$

(5) $MS(\omega) = SSE(\omega) / DOF(\omega)$

(6) $F = MS(Diff) / MS(\Omega)$

(7) $R^2 = SSE(Diff) / SSE(\omega)$

To determine the significance of a model Ω the following information is entered in the ANOVA table:

- A benchmark model, ω, to which model Ω is compared;

- The error sum of squares, *SSE*, of each of the two models;

- The degrees of freedom, *DOF*, of each of the two models; and

- The critical *F*-ratio with which the calculated *F*-ratio is compared.

An ANOVA table permits rapid calculation of the F-ratio and the correlation coefficient, R^2. Hence, in this study in order to determine the significance of each parameter in predicting *LogCR*, the results of a series of ANOVA tables were studied at each step to check whether the variable added was significant. In addition, the regression equations are valid over the range of the regressor variables contained in the observed data. That is, the equations obtained for one side of the bridge cannot be used to predict the corrosion rate in the other side of the bridge as they both exhibit different trends.

6.4.3 Prediction of Corrosion Rate Using 'Assessment Methods'

The parameters under study in this analysis, first presented in Section 6.3.1, were defined as being able to assess corrosion induced damage. Hence, the goal is to investigate if the 'Assessment Methods' are able to measure the corrosion occurring on the Dickson Bridge deck. The variables

under investigation are only delamination, concrete cover thickness, corrosion potential, chloride content at the steel level and the apparent chloride diffusion coefficient. Table 6-9 summarizes the results of the multiple linear regression analysis for the entire bridge deck and for both sides of the bridge separately. The ANOVA tables used to conclude with the results presented in Table 6-9 are included in Appendix I. It is noted that only the variables significant at a level of $\alpha = 0.05$ were included in the model, that is when the F-value obtained from the ANOVA table satisfied the F-critical value.

6.4.3.1 Entire Bridge Deck

The data from the entire bridge was used in the first model. The corrosion potential (ϕ_{corr}) accounted for 36.6% of the variability of the $LogCR$ values, while $LogD_a$, $\%Cl$, $Delam$ and $Cover$ contributed to 5.2%, 0.5%, 0.5%, and 0.0%, respectively. The total of the explained variability was 42.8%, which is a rather low value.

The $R^2_{adjusted}$ value was computed to measure the shrinkage in the predictive power, that is the decrease in R^2 as it is measured in the sample with the equation derived from it versus what it would be in the population as a whole using the same equation. It resulted in a shrinkage of 31%, hence, the prediction equation derived from the sample data would not work as well on the population sample, that is the theoretical sample consisting of all possible data points.

6.4.3.2 East Side of Bridge Deck

Once again, the corrosion potential (ϕ_{corr}) compared to the other variables accounted for most (31.7%) of the variability in the $LogCR$ values, while $\%Cl$ and $Cover$ contributed to 10.7% and 7.4%, respectively. It is noted that the $Delam$ and $Log\ D_a$ variables were not included in the model as they were not significant at a 0.05 level in the ANOVA tables (Appendix I). The total explained variability was 49.8% with a shrinkage value of 28%. The results indicate that there is quite a high variability (50.2%) in the $LogCR$ which is not accounted by the 'Assessment Methods' and that there is a substantial decrease in the predictive power. The model seems to provide little information.

Table 6-9: Results of the multiple linear regression using 'Assessment Methods'

Analysis	Response variable (Y)	Regressor variable (X)	Intercept (β_0)	Multiplier ($\beta_1...\beta_k$)	Standard error	Explained	Variability Total	Variability Non-explained	R^2	Decrease in R^2
(a) Entire bridge deck	LogCR	ϕ_{curr}	1.0258	-0.0011	0.0005	36.6%				
		$LogD_a$		0.0914	0.1790	5.2%				
		%CI		-0.0753	0.1760	0.5%				
		Delam		0.0552	0.1432	0.5%				
		Cover		0.0004	0.0039	0.0%	42.8%	57.2%	0.428	31%
(b) East side of bridge deck	LogCR	ϕ_{curr}	0.7518	-0.0017	0.0009	31.7%				
		%CI		-0.1087	0.2805	10.7%				
		Cover		0.0069	0.0054	7.4%	49.8%	50.2%	0.498	28%
(c) West side of bridge deck	LogCR	ϕ_{curr}	1.3131	-0.0016	0.0004	39.0%				
		%CI		-0.5388	0.1343	10.0%				
		$LogD_a$		0.3876	0.1236	15.8%				
		Cover		-0.0080	0.0030	17.2%				
		Delam		-0.0378	0.1051	0.3%	82.3%	17.7%	0.823	10%

6.4.3.3 West Side of Bridge Deck

The explained variability in the *LogCR* values accounted by the corrosion potential *(φcorr)* variable was 39.0%, while the *%Cl*, *LogDa*, *Cover* and *Delam* values contributed to 10.0%, 15.8%, 17.2%, and 0.3%, respectively, totaling to 82.3% with a shrinkage of 10%. The unexplained variability (17.7%) and predictive power values are much lower than the value obtained for the east side.

6.4.4 Prediction of Corrosion Rate Using 'Prediction Methods'

In Section 6.3.1, the definition of the 'Prediction Methods' was introduced which included the parameters that quantify the material properties of the concrete structure and enable a prediction of its durability. It is essential that the susceptibility to corrosion damage be determined, hence, the goal of this analysis is to answer the following questions: "Are 'Prediction Methods' able to predict the corrosion rate?", that is "Can material properties be related to the corrosion rate?". Furthermore, "Are in-situ durability test appropriate (reliable) to predict the rate of corrosion on site?". It is noted that the variables under investigation are only in-situ chloride migration coefficient, resistivity of the concrete, coefficient of permeability and the concrete compressive strength. Table 6-10 summarizes the results of the multiple linear regression analysis for the entire bridge deck and for both sides of the bridge separately, where only the variables significant at a level of $\alpha = 0.05$ were included in the model, that is when the *F*-value obtained from the ANOVA table satisfied the *F*-critical value. The ANOVA tables used to conclude with the results presented in Table 6-10 are included in Appendix I.

6.4.4.1 Entire Bridge Deck

The *LogDmig* accounted for 31.5% of the variability of the *LogCR* values, while *Str*, *Logρ*, and *Logkv* accounted for 17.5%, 2.8%, and 1.2%, respectively (Table 6-10). The explained variability in the model totaled to 53.0% with a shrinkage of 17%. The results are pretty much the same to what was obtained from the 'Assessment Methods' in Section 6.4.3.1.

Table 6-10: *Results of the multiple linear regression using 'Prediction Methods'*

Analysis	Response variable (Y)	Regressor variable (X)	Intercept (β_o)	Multiplier ($\beta_1...\beta_k$)	Standard error	Variability Explained	Variability Total	Variability Non-explained	R^2	Decrease in R^2
(a) Entire bridge deck	LogCR	$LogD_{mig}$	1.5970	0.5422	0.1884	31.5%				
		Str		-0.0118	0.0054	17.5%				
		$Log\rho$		0.0221	0.1701	2.8%				
		$Logk_w$		-0.0612	0.1388	1.2%	53.0%	47.0%		0.530	17%
(b) East side of bridge deck	LogCR	$LogD_{mig}$	1.3439	1.1241	0.3257	48.8%				
		Str		-0.0237	0.0083	23.0%				
		$Logk_w$		0.0746	0.1947	4.6%				
		$Log\rho$		0.1746	0.2646	1.3%	77.7%	22.3%		0.777	16%
(c) West side of bridge deck	LogCR	Str	1.7720	-0.0087	0.0035	36.7%				
		$Log\rho$		0.0482	0.1621	5.3%				
		$LogD_{mig}$		0.1500	0.1618	3.6%	45.6%	54.4%		0.456	28%

6.4.4.2 East Side of Bridge Deck

In the east side of the bridge, the $LogD_{mig}$ accounted for 48.8% of the variability of $LogCR$, while the Str, $Logk_w$ and $Log\rho$ values accounted to 23.0%, 4.6%, and 1.3%, respectively, totaling to an explained variability of 77.7% with a shrinkage of 16.0%. The unexplained variability in the $LogCR$ using the 'Prediction Methods' is only 22.3% which is a lot lower than the value (50.2%) obtained from the 'Assessment Methods' in Section 6.4.3.2. The shrinkage is also lower.

6.4.4.3 West Side of Bridge Deck

The variability in the $LogCR$ values explained by $LogD_{mig}$ was found to be marginal (3.6%) compared to the two previous models. On the other hand, the Str value accounted for 36.7% of the variability, where $Log\rho$ contributed to 5.3% totaling to 45.6% with a shrinkage of 28%. It is noted that the unexplained variability is 54.4% which is a lot higher than the unexplained variability obtained from the 'Assessment Methods' in Section 6.4.3.3.

6.4.5 Summary of Multiple Variable Regression Analysis

It is noted that by no means the models presented are suggested to be used to predict service life of existing structures. They represent the importance of the parameters included in the different models and their significance compared to the existing condition of the two parts of this particular bridge deck. The models are only appropriate for this particular case or any other bridge deck with the same exposure conditions and other similar factors such as mix design. Hence, this must be kept in mind. There is too much generalization and this is why every structure needs to be closely monitored because unfortunately every structure is unique.

The measurement of ϕ_{corr} at the surface of concrete is one common and standard method of estimating the corrosion damage in reinforced concrete as also indicated by the results shown in Table 6-9. Although this technique has been used on its own by many investigators, there are advantages in combining it with a survey of the delamination, concrete cover and chloride profiling as shown by the multivariable analysis. This improves the assessment of likelihood of corrosion.

All processes influencing the corrosion of reinforcement are more or less controlled by transport processes (penetration of liquids or gases, diffusion of chlorides and oxygen). Therefore, the major parameter in connection with corrosion and protection of the reinforcement in both uncracked and cracked concrete is the quality of the concrete cover. During their lifetimes, structures are subjected to external actions or agents that in time may alter them from a safe state to failure or a damaged stage. One of the processes that may trigger the onset of corrosion of steel embedded in concrete is the ingress of chloride ions that eventually reach the reinforcement, causing the passive film to rupture or breakdown. Tests that predict the chloride ingress and the resulting corrosion of the reinforcement steel are of immense importance. This was illustrated in the results shown in Table 6-10. The $LogD_{mig}$ values were the most significant in predicting the $LogCR$ values especially for the entire and east side of the bridge.

In addition, it is interesting to note the influence that the compressive strength (Str) values have in the models, especially in the west side of the bridge (6-10). This is not surprising as many researchers in modeling the crack propagation due to the corrosion have used the material strength in the prediction model. Also, the analysis using fracture strength concepts uses strength[32]. Therefore, strength cannot be ignored as is indicated in this investigation. To move away from strength completely would be erroneous as concrete structures are designed to carry a specific loading by using strength criterion of the materials. Therefore, it is not correct to ignore this property and simply use the electrical resistivity and permeation properties when using the 'Prediction Methods'. When internal steel reinforcement corrodes, the strength of the reinforced concrete member is undermined in several ways. Until recently, developments in cement and technology have concentrated on achieving higher and higher strengths. It was assumed that strong concrete is durable concrete, the only special considerations being the effects of alternating freezing and thawing and some forms of chemical attack. It is now known that, for many conditions of exposure of concrete structures, both strength and durability have to be considered explicitly at the design stage. The emphasis is on the word 'both' because it would be a mistake to replace overemphasis on strength by overemphasis on durability. This is illustrated in the obtained models shown in Figure 6-10.

The compressive strength testing, whilst useful in assessing the variations in strength which occur on site, needs to be complemented by permeability, diffusivity and resistivity testing in order to give a much better measure of the likely durability as indicated by the models shown in Table 6-10. The $Logk_w$ values did not contribute much in the models as expected. It was expected because as mentioned previously (Sections 3.5.5.3, 4.9.3, 5.2.10.2 and 6.4.1), the k_w values should be

192

considered with caution. This does not mean that permeability is of less importance than the other properties of concrete. On the contrary, but unfortunately the results in this investigation are not as reliable due to the magnitude of pressure applied during testing. Further research is required and is presently undergoing at The Queen's University of Belfast to make changes in the design of the Autoclam Permeation System. The $Log\rho$ values were of relative importance; the measurements might be influenced by the moisture of the concrete. The most reliable results are obtained from the in-situ chloride migration and strength testing (Table 6-10) when the deterioration is not as advanced. The results of the different types of models are discussed.

Both types of methods, 'Assessment' and 'Prediction' methods, were used to predict the corrosion rate of the east and the west sides of the bridge as well as for the entire bridge. The two sides exhibited two different results as indicated in the previous section, however, what exactly do the results imply. First a summary is given:

- The 'Assessment Methods' were able to assess the symptoms already present and the damage of the structure for the west side of the bridge deck with a correlation coefficient R^2 of 0.823 when including the variables ϕ_{corr}, $\%Cl$, $LogD_a$, Cover, and Delam in the model to predict the corrosion rate. While for the east side, the correlation coefficient was only 0.498 when including the variables ϕ_{corr}, $\%Cl$, and Cover in the model.

- The 'Prediction Methods' were able to measure the material properties of the structure for the east side of the bridge deck with a correlation coefficient R^2 of 0.777 when including the variables $LogD_{mig}$, Str, $Logk_w$ and $Log\rho$ variables in the model to predict the corrosion rate. While for the west side, the correlation coefficient was only 0.456 when including the variables Str, $Log\rho$, and $LogD_{mig}$ variables in the model.

- For the analyses including the data of the entire bridge deck, the correlation obtained is approximately the same, that is 0.428 and 0.530 when using the two different types of methods for predicting the corrosion rate.

The 'Assessment Methods' were more adequate to predict the corrosion rate for a portion of the bridge (the west side) that reached a high level of corrosion damage, while the 'Prediction Methods' were more adequate for the portion of the bridge (the east side) that is at an earlier point of the deterioration process. This is quite an interesting result, because it emphasizes the fact that if a structure is monitored using 'Prediction Methods' at an early stage, preventive measures can be undertaken before the problem becomes excessive. The 'Assessment Methods' are not

adequate to detect damage at an early stage (when the corrosion is at a lower level), as indicated in this study. They do not perform as well, hence methods to predict durability should be included in bridge inspections from the beginning of construction and thereafter. The 'Assessment Methods' are able to detect the problem once the damage is at a point when it cannot be prevented and alternative measures need to be taken. For example, if the two types of methods were used on the Dickson Bridge deck, the damage would have been detected at early stage from the 'Prediction Methods' and maybe the City of Montreal would not have decommissioned the access to the bridge, as preventive measures would have been able to be adopted prior to arriving at such a state.

The actual safety and functional response of a structure in service depends partly on the parameters such as structural dimensioning, detailing, and choice of materials, and partly on the specified or presumed parameters, which in reality depend on the subsequent service conditions. Unfortunately, these service conditions are unpredictable and this also holds true for the ageing of the materials. Hence, there is a need for regular inspection routines in order to maintain confidence in the structural integrity, performance and safety of the structure, and in order to assess the possible needs for safety of the structure, and in order to assess the possible needs for maintenance, repair, strengthening, as the case may require. The findings of the analysis affirm the fact that it is the material properties and the exposure parameters which decide the susceptibility of the concrete to deterioration and it is the damage that it is measured with all other methods. When a structure is at an earlier stage in the deterioration process, measuring the material properties and the exposure parameters is more useful and helps to maintain the structure, while at a later stage the damage can only be assessed. Regular and systematic inspections should be performed in order to identify and quantify possible ongoing deterioration. Inspection constitutes an integral part of structural safety and serviceability by providing a link between the environmental conditions to which the structure is subjected and the manner in which it performs with time. The nature and frequency of the inspection procedures should be determined with this in mind. The strategy towards improved durability should incorporate systematic inspection routines for structures in service, decision models based on forecasting of the rate of degradation (corrosion), and economic consideration of short-term or long-term remedial measures.

7   Conclusions and Recommendations

Based on the detailed tests and the results reported in this thesis, the following conclusions and recommendations have been drawn.

7.1   Conclusions

With regard to the collected data and the analysis of the results, the following conclusions are drawn:

• The on-site measurement of the corrosion state of the concrete reinforcement on the Dickson Bridge deck was conducted using the Linear Polarization technique. The technique was suitable to be applied on-site, however, care had to be taken to refer the R_p value to the steel surface really polarized. The confinement was achieved using a controlled 'guard ring'. By means of this method, the corrosion rate values were obtained. The corrosion rate values indicated that the bridge deck was in a critical condition.

• The existing state-of-health vis-a-vis corrosion damage and concrete quality was determined by having a close examination of the data obtained from the experimental program. Considering all of the data available, it appeared that the corrosion process of reinforcing steel at the Dickson Bridge deck was a result of high level of chlorides enhanced by highly unfavorable environmental conditions prevailing in the region such as high relative humidity and freezing and thawing cycles. Overall, the methods that assess the corrosion damage, such as half-cell potential, corrosion rate, delamination, and chloride content indicated that the top portion of the grid was at high risk of corrosion. In addition, the damage was more pronounced in the west side of the deck. The west side displayed a high level of deterioration due to the greater extent of delamination, higher corrosion rates and potentials, and much higher chloride content, while the east side was at an earlier stage in the process, displaying less delamination and with lower chloride contents. The results of the cover survey seemed to contradict all other results. Lower covers were found at the bottom of the grid suggesting that these particular sites would be more susceptible to deterioration and thicker covers at the top of the grid. However, it was seen that at the bottom of the grid, the damage was less compared

to the top. This suggests that the performance of the cover-zone is dependent on both the cover thickne: , and on the concrete quality of the covercrete.

♦ Moisture is continuously transported in the form of liquid and vapour from the surrounding environment. The rate of water and ion ingress through the concrete depends on the physical structure of the paste. Precise characterization of this physical structure is, however, extremely difficult, if not impossible. Therefore, the average values of permeability, diffusivity, and resistivity have been used to model the transport mechanisms through the complex pore structure. In the present study, the quality of the concrete cover in terms of its permeation properties and electrical resistance proved to be of great importance. The areas of high diffusivity and low resistivity were found to coincide with the locations of significant reinforcement corrosion. The permeability results were not consistent with the other results as the applied pressure used during the testing was too small, hence the permeability results were treated with caution.

● Considerable effort has been directed into the development of on-site techniques to measure the corrosion rate of the reinforcing steel such as the linear polarization resistance. However, measurements of the corrosion rate do not give the complete picture of the problem due to the limited amount of information. They do not provide insight into the quality of the concrete in the vicinity of the rebar which are instrumental in initiating and sustaining corrosion. Hence, in this investigation, the methods used consisted of techniques able to indicate either the causes of deterioration or the extent of the corrosion damage. Quite often methods used to improve the durability of concrete aim at preventing the causes of deterioration, however, occasionally methods which can limit the extent of damage are employed. In this context, and in order to propose which test can assess the durability of existing structures, it was essential that a thorough analysis of the various relationships between the material properties and the corrosion rate was carried out. A multivariable statistical analysis proved to be the most appropriate way of quantifying and correlating the results of the various tests. Both the 'Assessment' and the 'Prediction' methods (measuring damage, and measuring material properties and exposure parameters) have been used to predict the corrosion rate of the east and the west sides as well as for the entire bridge. The adequacy of the two methods at the two different stages of service life displayed on the Dickson Bridge are as follows:

   — Overall, the measurement of the corrosion potential was of important significance in assessing the corrosion damage. However, to improve the assessment of probability of corrosion of the reinforcing steel, it was advantageous to combine this technique with a

survey of the delamination, concrete cover and chloride profiling as shown in the multivariable analysis.

— In relative terms, durability testing is in its infancy, however, in this study it has been demonstrated that the measurement of the permeation properties, in particular the diffusivity, gives an extremely useful insight. The in-situ chloride migration coefficients were the most significant in predicting the corrosion rate values especially for the east side of the bridge. The compressive strength values had a great importance in the models. Hence, strength cannot be ignored as is indicated in this investigation. The steel area decrease, the concrete cracking and the deterioration of bond at the steel-concrete interface, would affect the load carrying capacity of concrete structures. The corrosion in a reinforced concrete structure influences the load carrying capacity of structures, hence, it is not surprising that the compressive strength played such an important role in the models.

— The 'Assessment Methods' were more adequate to predict the corrosion rate for a portion of the bridge (the west side) that reached a high level of corrosion damage, while the 'Prediction Methods' were more adequate for the portion of the bridge (the east side) that is at an earlier stage of the deterioration process.

— The conclusion drawn from the two types of models is that if a structure is monitored using 'Prediction Methods' at an early stage, preventive measures can be undertaken before the problem becomes "excessive". The 'Assessment Methods' are not adequate to detect damage at an early stage (when the corrosion is at a lower level), as indicated in this study. They are able to detect the problem once the damage is at a point when it cannot be prevented and alternative measures need to be taken. Hence, the methods to predict durability should be included in bridge inspection programs from the beginning of construction, and thereafter.

7.2   Recommendations

The overall efforts in this study were directed to gain hands-on knowledge and experience with the in-situ durability tests. The results are consistent and these in-situ testing techniques are promising. However, with regard to the actual tests carried out on the bridge, some other information would have been beneficial and most probably stronger correlations would have resulted. The following recommendations are made:

- It has to be taken into account that electrochemical measurements are "instantaneous", thus in order to get meaningful corrosion rates they have to be related to the climatic conditions at the time of measurement. Thus the relation between instantaneous and average corrosion rate has to be studied. This applies to all of the parameters. Data needs to be collected with different intervals for at least one year in order to get information on seasonal, weekly and daily changes.

- To expose the reinforcing steel underneath the sites where the corrosion rate was measured and to obtain the weight loss of the cross section of the bar in order to compare the two quantities. Thus the accuracy of the corrosion rate would have been established.

- In addition to the concrete compressive strength, it would have been beneficial to know the constituents of the original concrete mix design, such as the water/cement ratio, cement content, etc... A petrographic examination would have provided a complete assessment of the quality of the concrete and its constituents, thus revealing the causes for concrete distress or poor performance. The variations in the constituents would have provided a more appropriate criterion to classify the concrete. The variations of the tests results would have been better interpreted, thus allowing a complete analysis of the results.

- Reliable testing techniques for determining the in-situ strength of concrete have been available for many year, however, experienced users have found it best not to rely on a single test. Hence, a combination of non-destructive testing such as the pullout test and coring should have been used.

The research program was fundamental and unique in nature. The scope of the project was not only to do a post-mortem of the Dickson Bridge deck, but to illustrate that on-site monitoring is important, even though there are still uncertainties in the techniques. Further work needs to be invested in on-site monitoring as it is the only manner that researcher and engineers can interact with the real problems encountered in reinforced concrete structures. The initial concrete quality to protect the steel should not be taken for granted once the structure is in use. This protective quality is an important factor that makes it possible for concrete structures to be built and this needs to be assured on site. The only way to know is to monitor structures on site. Modelling and accelerated corrosion research work in the laboratory needs to be correlated to the field work. However, laboratory work can never replace what is happening in a real structure as there are so many unknown factors. There have been some attempts in the past to propose specification criteria based on laboratory tests, however, proposals are needed which are based on in-situ methods. The structure and physical characteristics of the concrete change with time, hence its

sustenance in service environment needs careful consideration rather than simplistic approaches currently been used. The durability of concretes is not a static property, i.e., it is not constant with time. The continuous change of the microstructure of the concrete due to its response to the service environment may increase or decrease the properties (permeation properties, electrical resistivity and strength) of the concrete.

There are many new concrete mixes and new techniques available to the researchers for use in their investigations. Corrosion engineers spend much of their time trying to find ways of stopping corrosion of steel by applying protective coatings. Metals such as zinc or polymers, and acrylics or epoxies are used to stop corrosive conditions from reaching the steel surface. The passive layer is the corrosion engineer's dream coating as it forms, maintains and repairs itself as long as the passivating (alkaline) environment is there to regenerate it if it gets damaged. If the passivating environment can be maintained, it is far better than any artificial coatings that can be consumed or damaged, allowing corrosion to proceed in damaged areas. Measurement of chloride ion diffusion is by far the most important concern, as it is the chloride ion that promotes depassivation of the reinforcing steel, resulting in the initiation of corrosion. Diffusivity is a parameter that can be used to assess the present condition of a concrete structure and also to predict the future risk. Because both engineers and researchers need a rapid method to evaluate existing structures and new materials and treatments, the new in-situ chloride migration test appears to satisfy the engineering requirements. The main challenge is for the practicing engineers to work in tandem with those involved in the relevant research. Thus, practicing engineers, and especially those in the industry involved in testing, are encouraged to increase the use of in-situ testing for durability so as to build up an essential pool of knowledge and experience. This will ultimately lead to the realization of the full potential for the in-situ test methods.

There is a need to foster collective agreement and thinking to develop an integrated approach to research and development for rational and intelligent infrastructure renewal. Good management and maintenance of steel reinforced concrete structures requires frequent monitoring of the risk of reinforcement corrosion as it is essential that every concrete structure must continue to perform its intended functions in terms of the required strength and serviceability conditions, during the specified expected service life. Visual evaluation techniques and a few assessment methods are used in inspection programs. However, it is very difficult to make long-term recommendations based on these techniques because none of these methods can suggest future needs of repair and maintenance. Therefore, the owner (different levels of government or owners from the private sector) might not be able to prioritize bridges with the present level of information about the

durability of bridges. On the other hand, if tests such as the in-situ chloride tests (after further research to standardize the apparatus and testing procedure) would be included in the inspection program, it would enable the future maintenance needs to be established.

A benefit of monitoring reinforced concrete structures is that information on the in-situ performance of the concrete in the service environment can be collected, used to verify whether the original specifications have been met, or whether it was appropriate, and then fed back into the design process. The use of these modern in-situ tests will mean less reliance on destructive testing which are expensive and limited because it can weaken the structure and, if testing on a periodic basis, it is unacceptable to remove cores frequently. Long term durability monitoring is technically valid, and it can be a cost effective method of maintaining the structures in good regime by evaluating repair options and monitoring the structure and its environment with respect to corrosion. The prediction of the corrosion rate is very important for timely implementation of preventive maintenance strategies that slow down the deterioration processes thereby extending the service life of reinforced concrete structures. The preventive actions are generally much more cost effective when implemented in the early stages of the deterioration life cycle, as compared to waiting until deterioration problems become quite advanced and visible. At this stage, they are extremely costly to repair or rehabilitate; in some case the system or a part may have to be replaced at a much high cost. Hence, it is recommended to measure the 'state of health' of the structure upon its completion and then check it regularly during its 'life' by further routine tests to monitor the progress of condition changes. It is necessary to update the database of the bridge record with the information from the inspections so that the condition of the bridges can be ranked and priorities for repair and rehabilitation can be developed.

References

[1]   Portland Cement Association, *Infrastructure: Investing in Our Future.*, Portland Cement Association, Stokie, Il, 1992.

[2]   Organization of Economic Cooperation and Development, *Urban Infrastructure in Canada.*, Canada Mortgage and Housing Corporation, Canada, 1989.

[3]   Kurtis, K.E. and Mehta, P.K., 'A Critical Review of Deterioration of Concrete Due to Corrosion of Reinforcing Steel', *Durability of Concrete Proceedings - Fourth CANMET/ACI International Conference.*, Vol. I, Sydney, Australia, 1997, pp. 535-55.

[4]   Woodward, R.J. and Williams, F.W., 'Collapse of Ynes-y-Gwas Bridge, West Glamorgan', *Proceedings of the Institution of Civil Engineers Part I.*, Vol. 84, pp. 635-69.

[5]   Grigg, N.S., *Infrastructure Engineering and Management.*, John Wiley & Sons, New York, 1988.

[6]   'High Performance Concrete: Improving Canada's Infrastructure and International Competitiveness', *Concrete Canada.*, Vol.1, October 1993.

[7]   U.S. General Accounting Office. *Deteriorating Highways and Lagging Revenues: A Need to Reassess the Federal Highway Program: Report No. CED-81-42.*, Washington, DC: US General Accounting Office, 1981.

[8]   Federal Highway Administration. *1991 Status of the Nation's Highways and Bridges: Conditions, Performance, and Capital Investment Requirements.*, July 2, 1991.

[9]   Page, C.L., Bamforth, P. and Figg, J.W., *Corrosion of Reinforcement in Concrete Construction.*, Turnip, London, 1996.

[10]   Comité Euro-International du Béton, *CEB Durable Concrete Structures.*, Thomas Telford Ltd., London, 1992.

[11]   Sommerville, G., 'The Interdependence of Research, Durability and Structural Design', *Institution of Civil Engineers, Proceedings of Symposium on design Life of Buildings.*, Thomas Telford Ltd., London, 26-27 November 1984, pp. 233-50.

[12]   Basheer, P.A.M., Chidiac, S.E. and Long, A.E., 'Predictive Models for Deterioration of Concrete Structures', *Construction and Building Materials.*, Vol. 10, no. 1, February 1996, pp. 27-37.

[13]   Gannon, E.J. and Cady, P.D., 'State of the Art of Existing Methods', *Condition Evaluation of Concrete Bridges Relative to Reinforcement Corrosion*, Vol.1, National Research Council, SHRP-S-323, Washington, DC, 1993.

[14]   Basheer, P.A.M., 'Clam Permeability Tests for Assessing the Durability of Concrete', *Ph.D. Thesis.*, The Queen's University of Belfast, 1991.

[15]   Dewar, J.D., 'Testing of Concrete for Durability', *Proceedings of a One Day Symposium: Developments in Testing Concrete for Durability.*, The Concrete Society, London, September 26, 1984.

[16]   Tonias, D.E., *Bridge Engineering: Design, Rehabilitation, and Maintenance of Modern Highway Bridges.*, McGraw-Hill, New York, 1995.

[17]   Mirza, M.S., Shao, Y. and Collinge, J.P., 'Post-Mortem of the Abandoned Dickson Bridge', *1998 CSCE Annual Conference - Structural Specialty.*, Halifax, Canada, June 1998.

[18]   Mirza, M.S., *Proposal for a Joint University-Industry Program for Research and Development on Dickson Bridge.*, March 1995.

[19]   McCarter, W.J., Emerson, M. and Ezirim, H., 'Properties of Concrete in the Cover Zone: Developments in Monitoring Techniques', *Magazine of Concrete Research.*, Vol. 47, no. 172, September 1995, pp. 243-51.

[20]   Rodriguez, J., Ortega, L.M. and Casal, J., 'Load Carrying Capacity of Concrete Structures with Corroded Reinforcement', *Construction and Building Materials*, Vol. 11, no. 4, June 1997, pp. 239-48.

[21]   Rosenberg, A., Hansson, C.M. and Andrade, C., 'Mechanisms of Corrosion of Steel in Concrete', *Material Science of Concrete I.*, The American Ceramic Society, Westerville, OH, 1989, pp. 285-313.

[22]   Tuutti, K., *Corrosion of Steel in Concrete.*, Swedish Cement and Concrete Institute, Stockholm, 1982.

[23]   Schiessl, P., 'Influence of the Composition of Concrete on the Corrosion Protection of the Reinforcement', *Concrete Durability Katharine and Bryant Mather International Conference.*, American Concrete Institute, ACI SP-100, Vol. 2, Detroit, 1987, pp. 1633-50.

[24]   Andrade, C. and Alonso, M.C., 'Values of Corrosion Rate of Steel in Concrete to Predict Service Life of Concrete Structures', *Application of Accelerated Corrosion Tests to Service Life Prediction of Materials, ASTM STP-1194.*, American Society for Testing and Materials, Philadelphia. 1994, pp. 282-94.

[25]   ACI Committee 222. *Corrosion of metals in concrete - ACI 222R-89.*, American Concrete Institute, 1989, pp. 3-32.

[26]   Suzuki, K., Ohno, Y., Praparntanatorn, S. and Tamura, H., 'Mechanism of Steel Corrosion in Cracked Concrete', in Page, C.L., Treadaway, K.W.J. and Bamforth, P.B., *Proceedings Corrosion of Reinforcement in Concrete.*, London: Elsevier, SCI-2, 1990, pp. 19-28.

[27]   The Concrete Society. *Permeability Testing of Site Concrete – A Review of Methods and Experience.*, Report of a Concrete Society Working Party, Concrete Society Technical Report No. 31, London, August 1988.

[28]   Brown, P.W., Shi, D. and Skalny, W.R., 'Porosity/Permeability Relationships', *Materials Science of Concrete II.*, The American Ceramic Society, Westerville, OH, 1991, pp. 83-109.

[29]   Cady, P.D. and Weyers, R.E., 'Chloride Penetration and the Deterioration of Concrete Bridge Decks', *Cement, Concrete and Aggregates.*, CCAGDP, Vol. 5, no. 2, Winter 1983, pp. 81-7.

[30]   Manning, D., 'A Rational Approach to Corrosion Protection of the Concrete Components of Highway Bridges', *Concrete Durability Katharine and Bryant Mather International Conference*, American Concrete Institute, ACI SP-100, Vol. 2, Detroit, 1987, pp. 1527-47.

[31]   Glass, G.K. and Buenfeld, N.R., 'Chloride Threshold Levels for Corrosion Induced Deterioration of Steel in Concrete', *Proceedings International RILEM Workshop on Chloride Penetration into Concrete.*, Saint-Rémy-Les-Chevreuse, October 15-18, 1995.

[32]   Neville, A.M., *Properties of Concrete.*, Longman Group Ltd., London, 1995.

[33]   Broomfield, J.P., *Corrosion of Steel in Concrete – Understanding, Investigation and Repair.*, E & FN Spon, London, 1997.

[34]   ACI 318 Committee. *Building Code Requirements for Reinforced Concrete (ACI 318M-89) and Commentary (ACI 318RM-89).*, American Concrete Institute, June 1990.

[35]   CSA Standards A23.1-94. *Concrete Materials and Methods of Concrete Construction.*, Canadian Standard Association, June 1994.

[36]   Kropp and Hilsdorf. 'Performance criteria for concrete durability', *RILEM Report 12.*, 1995.

[37]   Poulsen, E., 'The Chloride Diffusion Characteristics of Concrete: Approximative Determination by Linear Regression Analysis', *Nordic Concrete Research.*, No. 9, Nordic Concrete Federation, 1990, pp. 124-33.

[38]   Glass, G.K., Wang, Y., Buenfeld, N.R., 'An Investigation of Experimental Methods Used to Determine Free and Total Chloride Contents', *Cement and Concrete Research.*, Vol. 26, no. 9, 1996, pp. 1443-9.

[39]   Nilsson, L.O. et al, 'Chloride Penetration into Concrete', *HETEK.*, State of the Art, Report No. 53, 1996.

[40]   Hausmann, D.A., 'Steel Corrosion in Concrete – How Does it Occur?', *Materials Protection.*, Vol. 6, no. 11, 1967, pp. 96-106.

[41]   Lambert, P., Page, C.L. and Vassie, P.R.W., 'Investigations of reinforcement Corrosion. 2. Electrochemical Monitoring of Steel in Chloride-Contaminated Concrete', *Materials and Structures.*, Vol. 24, 1991, pp. 351-8.

[42]   ACI 201 Committee. *Guide to Durable Concrete.*, American Concrete Institute, ACI 201.2R-77, Detroit, 1982. 37 pp.

[43]   British Standards Institution. *Structural use of Concrete.*, BS 8110: Part 1: Code of Practice for Design and Construction, London, 1989.

[44]   Parrott, L.J., *A Review of Carbonation in Reinforced Concrete.*, Cement and Concrete Association, July 1987.

[45]   Richardson, M.G., *Carbonation of Reinforced Concrete: Its Causes and Management.*, Citis Ltd., Dublin, 1991.

[46]   Venuat, M., 'Relationship Between Concrete Carbonation and the Corrosion of Reinforcement', *Recemtres.*, CEFRACOR-77, JTBTP, October 1977.

[47]   Johnson, C.D., 'Deicer Salt Scaling Resistance and Chloride Permeability', *Concrete International: Design and Construction.*, Vol. 16, no. 8, August 1994, pp. 48-55.

[48]   Mehta, P.K. and Montiero, P.J.M., *Concrete: Structure. Properties, and Materials.*, Prentice Hall, New Jersey, 1993.

[49]   Basheer, P.A.M., Long, A.E. and Montgomery, F.R., 'An Interaction Model for Causes of Deterioration and Permeability of Concrete', *Malhotra Symposium on Concrete Technology.*, San Francisco, CA, 21-25 March 1994, SP 144, ACI, Detroit, 1994, pp. 213-33.

[50]   Rasheeduzzafar, 'Influence of Cement Composition on Concrete Durability', *ACI Materials Journal.*, Vol. 89, no. 6, 1992, pp. 574-85.

[51]   12-CRC Committee (Rilem Technical Committee – Corrosion of Reinforcing Steel in Concrete). 'Corrosion of Reinforcement and Prestressing Tendons', A State of the Art, *Matériaux et Constructions.*, in Concrete., Vol. 9, no. 51, 1976, pp. 187-206.

[52]   Rasheeduzzafar, Al-Saadoum, S.S., and Al-Gahtani, A.S., 'Corrosion Cracking in Relation to Bar Diameter, Cover, and Concrete Qulaity', *Journal of Materials in Civil Engineering.*, Vol. 4, no. 4, 1992.

[53]   Alekseev, S.N., Ivanov, F.M., Modry, S. and Schiessl, P., *Durability of Reinforced Concrete in Aggressive Media.*, Oxford & IBH Publishing CO. PVT Ltd., New Dehli, India, 1993.

[54]   Page, C.L., 'Basic Principles of Corrosion', in Schiessl, P., *Corrosion of Steel in Concrete – RILEM Report.*, Chapman and Hall, London, 1988, pp. 3-21.

[55]   Uhlig, H.H. and Revie, R.W., *Corrosion and Corrosion Control – An Introduction to Corrosion Science and Engineering.*, John Wiley & Sons, Toronto, Canada, 1985.

[56]   Fontana, M.G., *Corrosion Engineering.*, McGraw-Hill, Toronto, Canada, 1986.

[57]   Franczek, J., 'A Review of Elecrochemical Principles as Applied to Corrosion of Steel in a Concrete or Grout Environment', in Gibson, F.W., *Corrosion, Concrete, and Chlorides*

- *Steel Corrosion in Concrete: Causes and Restraints.*, American Concrete Institute, Detroit, SP-102-2, 1987, pp. 13-24.

[58] Trethewey, K.R. and Chamberlain, J., *Corrosion for Science and Engineering.*, Longman Acientific & Technical, Essex, England, 1995.

[59] Gonzalez, J.A., Lopez, W. and, Rodriguez, P., 'Effects of Moisture Availability on Corrosion Kinetics of Steel Embedded in Concrte', *Corrosion.*, December 1993, pp. 1004-10.

[60] Sagoe-Crentsil, K.K. and Glasser, F.P., Steel in Concrete: Part 1 – A Review of the Electrochemical and Thermodynamic Aspect', *Magazine of Concrete Research.*, Vol. 41, no. 149, 1989, pp. 205-12.

[61] Cady, P.D. et al, 'Method for Measuring the Corrosion Rate of Reinforcing Steel', *Condition Evaluation of Concrete Bridges Relative to Reinforcement Corrosion.*, Vol.2, National Research Council, SHRP-S-/FR-92-104, Washington, DC, 1992.

[62] Bungey, H.H. and Millard, S.G., *Testing of Concrete in Structures.*, Blackie Academic & Professional, London, 1995.

[63] Vassie, P.R., 'The Half-Cell Potential Method of Locating Corroding Reinforcement in Concrete Structures', *Transport Research Laboratory Application Guide AG9.*, Crowthorne, Berkshire, UK, 1991.

[64] ASTM C876. *Standard Test Method for Half-Cell Potentials of Uncoated Reinforcing Steel in Concrete.*, American Society for Testing and Materials, Philadelphia, PA, 1991.

[65] Clear, K.C., 'Measuring the Rate of Corrosion of Steel in Field Concrete Structures', *Transportation Research Record 1211.*, Transportation Research Board, National Research Council, Washington, DC, 1989, pp. 28-37.

[66] Jones, D.A, *Principles and Prevention of Corrosion.*, Prentice Hall, Englewood Cliffs, NJ, 1996.

[67] Stern, M.S. and Geary, A.J., 'A Method for Determining Corrosion Rates from Linear Polarization Data', *Journal of the Electrochemical Society.*, Vol. 105, 1958.

[68] Feliu, S., Gonzalez, J.A., Feliu Jr., S. and Andrade, M.C., 'Confinement of the Electrical Signal for In-Situ Measurement of Polarization Resistance in Reinforced Concrete', *ACI Materials Journal.*, Vol. 87, no. 5, 1990, pp. 457-60.

[69] Feliu, S., Gonzalez, J.A. and Andrade, C., 'Electrochemical Methods for On-Site Determinations of Corrosion Rates of Rebars', *Techniques to Assess the Corrosion Activity of Steel Reinforced Concrete Structures, ASTM STP 1276.*, American Society for testing and Materials, 1996, pp. 107-18.

[70] Millard, S.G., 'Corrosion Rate Measurement of In-Situ Reinforced Concrete Structures', *Proceedings Institution of Civil Engineers, Structures & Buildings.*, Vol. 99, 1993, pp. 84-8.

[71] Berke, N.S. and Hicks, M.C., 'Electrochemical Methods of Determining the Corrosivity of Steel in Concrete', *ASTM 25th Anniversary Symposium.*, STP 1000, Philadelphia, 1990, pp. 425-40.

[72] Miyuki, H., Ohno, T., Yokota., M. and Yoshida, M., 'Corrosion Monitoring of Steel Rebars in Concrete Structures by AC Impedance Method', *Proceedings of International Symposium on Plant Aging and Life Predictions of Corrodible Structures.*, May 15-18, 1995, Sapporo, Japan, pp. 447-51.

[73] Millard, S.G., 'Reinforced Concrete Resistivity Measurement Techniques', *Proceedings of the Institution of Civil Engineers, Part 2: Research and Theory.*, Vol. 91, 1991, pp. 59-63.

[74] Buenfeld, N.R. and Newman, J.B., 'Examination of Three Methods for Studying Ion Diffusion in Cement Pastes, Mortars and Concrete', *Materials and Structures.*, Vol. 20, 1987, pp. 3-10.

[75] Streicher, P.E. and Alexander, M.G., 'A Critical Evaluation of Chloride Diffusion Test Methods for Concrete', *Third CANMET/ACI International Conference on Durability of Concrete.*, Nice, France, 1994, pp. 517-29.

[76] Crank, J., *The Mathematics of Diffusion.*, Clarendon, Oxford, 1975.

[77] Basheer, P.AM., Gillece, P.R.V., Andrews, R.J. and Long, A.E. 'Feasibility study of the development of an in-situ chloride migration test', *ACI Special Publication on Innovations in Non-destructive Testing of Concrete.*, Nov. 1995, Montreal, Canada, 1995.

[78] Herald, S.E., Henry, M., Al-Qadi, I., Weyers, R.E., Feeney, M.A., Howlum, S.F. and Cady, P.D., 'Method of field determination of total chloride', *Condition Evaluation of Concrete Bridges Relative to Reinforcement Corrosion.*, Vol. 6, National Research Council, SHRP-S-/FR-92-108, Washington, DC, 1992.

[79] Sergi, G., Yu, S.W. and Page C.L., 'Diffusion of Chloride and Hydroxyl Ions in Cementitious Materials Exposed to a Saline Environment', *Magazine of Concrete Research.*, Vol. 44, no. 158, 1992, pp. 63-9.

[80] Whiting, D., 'Rapid Measurement of the Chloride Permeability of Concrete', *Report No. FHWA/RD-81/119, Federal Highway Administration.*, Washington, D.C., August 1981.

[81] Whiting, D., 'In-Situ Measurement of the Permeability of Concrete to Chloride Ions', *In-Situ Nondestructive Testing of Concrete.*, ACI SP-82, American Concrete Institute, Michigan, 1984, pp. 501-24.

[82] Andrade, C., 'Calculation of Chloride Diffusion Coefficients in Concrete from Ionic Migration Experiments', *Cement and Concrete Research.*, Vol. 23, no. 3, 1993, pp. 724-42.

[83] AASHTO T 277-93., 'Standard Method of Test for Electrical Indication of Concrete's Ability to Resist Chloride', *American Association of State Highway and Transportation Officials (AASHTO)*, Standard Specifications for Transportation Materials and Methods of Sampling and Testing., Part II-Tests, Washington, D.C., 1993.

[84]   ASTM C 1202-94, 'Standard Test Method for Electrical Indication of Concrete's Ability to Resist Chloride Ion Penetration', *American Society for Testing and Materials, Book of ASTM Standards.*, Vol. 04.02-Concrete and Aggregates, Philadelphia, PA, 1994, pp. 623-8.

[85]   Gillece, P.R.V., 'An Investigation of Chloride Penetration into Modified Concrete', *Ph.D. Thesis.*, The Queen's University of Belfast, U.K., 1997.

[86]   Andrews, R.J. 'The Design and Development of an In-Situ Chloride Migration Test', *Ph.D. Thesis.*, The Queen's University of Belfast, U.K., To be submitted in May 1999.

[87]   Basheer, P.AM. 'A Brief Review of Methods for Measuring the Permeation Properties of Concrete In-Situ', *Proceedings of the Institution of Civil Engineers, Structures and Buildings.*, 1993, pp. 74-83.

[88]   Rilem Recommendations CPC-18., 'Measurement of Hardened Concrete Carbonation Depth', *Materials and Structures.*, Vol. 21, no. 26, 1988, pp. 453-5.

[89]   British Standards Institution. *Testing Concrete.*, BS 1881: Part 122: Method for Determination of Water Absorption, London, 1983, pp. 1737-41.

[90]   British Standards Institution. *Methods of Testing Concrete.*, BS 1881: Part 5: Method for Testing Hardened Concrete for Other than Strength, BSI, London, 1970.

[91]   Montgomery F.R. and Adams A., 'Early Experience with a New Concrete Permeability Apparatus', *Proceedings of the 2nd International Conference of Structural Faults and Repair, Institution of Civil Engineers.*, Edinburgh, April 30 – May 2, 1985, pp. 359-63.

[92]   Basheer, P.A.M., Montgomery, F.R. and Long, A.E., 'Clam Tests for Measuring In-Situ Permeation Properties of Concrete', *Nondestructive Testing Evaluation.*, Vol. 12, 1995, pp. 53-73.

[93]   Alldred, J.C., 'Quantifying the Losses in Cover-meter Accuracy Due to Congestion of Reinforcement', *Proceedings of the Fifth International Conference on Structural Faults and Repair.*, Vol. 2, Engineering Technics Press, Edinburg, pp. 125-30.

[94]   ASTM G 102-89. *Standard Practice for Calculation of Corrosion Rates and Related Information from Electrochemical Measurements.*, American Society for Testing and Materials, Philadelphia, PA, 1989, pp. 404-12.

[95]   McCafferty, E., 'Relationship Between Permeation Properties and Concrete Deterioration on the Dickson Bridge', *M.Sc. Dissertation.*, The Queen's University of Belfast, U.K., 1998.

[96]   Fazio, R. and Andrews, R.J., ''Permeability and Chloride Migration Tests on Dickson Street Overpass Deck', *Preliminary Report.*, McGill University, Montreal and The Queen's University of Belfast, October 1997.

[97]   ASTM C39-93a. *Standard Test Method for Compressive Strength of Cylindrical Concrete Specimens.*, American Society for Testing and Materials, Vol. 4.02, 1994, pp. 17-21.

[98]   Pigeon, M. and Pleau, R., *Durability of Concrete in Cold Climates.*, E & FN Spon, London, 1995.

[99]   Montgomery, D.C. and Peck, E.A., *Introduction to Linear Regression Analysis.*, John Wiley & Sons, New York, 1992.

[100]   Schiff, D. and D'Agostino, R.B., *Practical Engineering Statistics.*, John Wiley & Sons, New York, 1996.

[101]   Kennedy, J.B. and Neville, A.M., *Basic Statistical Methods for Engineers and Scientists.*, Harper & Row, New York, 1986.

[102]   Ostle, B., Turner, K.V., Hicks, C.R. and McElrath, G.W., Engineering Statistics: The Industrial Experience., Duxbury Press, London, 1996.

208

Appendix A: Bar Charts of Experimental Results

The following are supplementary graphs for Chapter 4 and Chapter 5. The corresponding parameters calculated from the experimental data as indicated in Chapter 4 are plotted showing the values obtained for each site at the location where the test was conducted. These values were used in Chapter 5 to plot Figures 5-8 to 5-13.
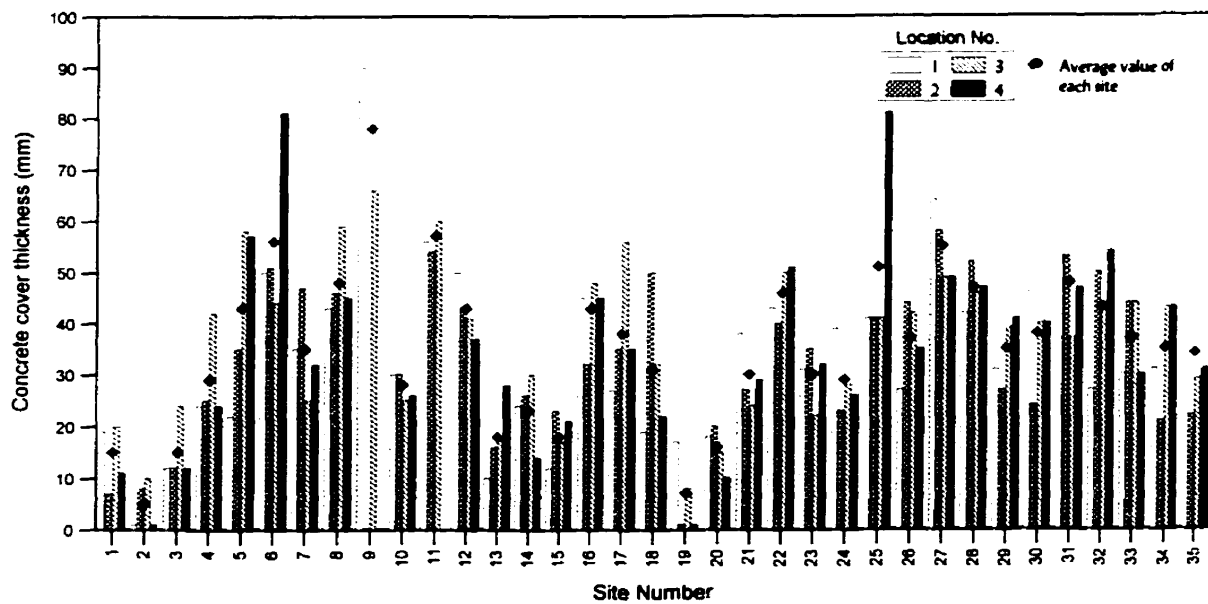

Figure A-1: *Concrete cover thickness survey*
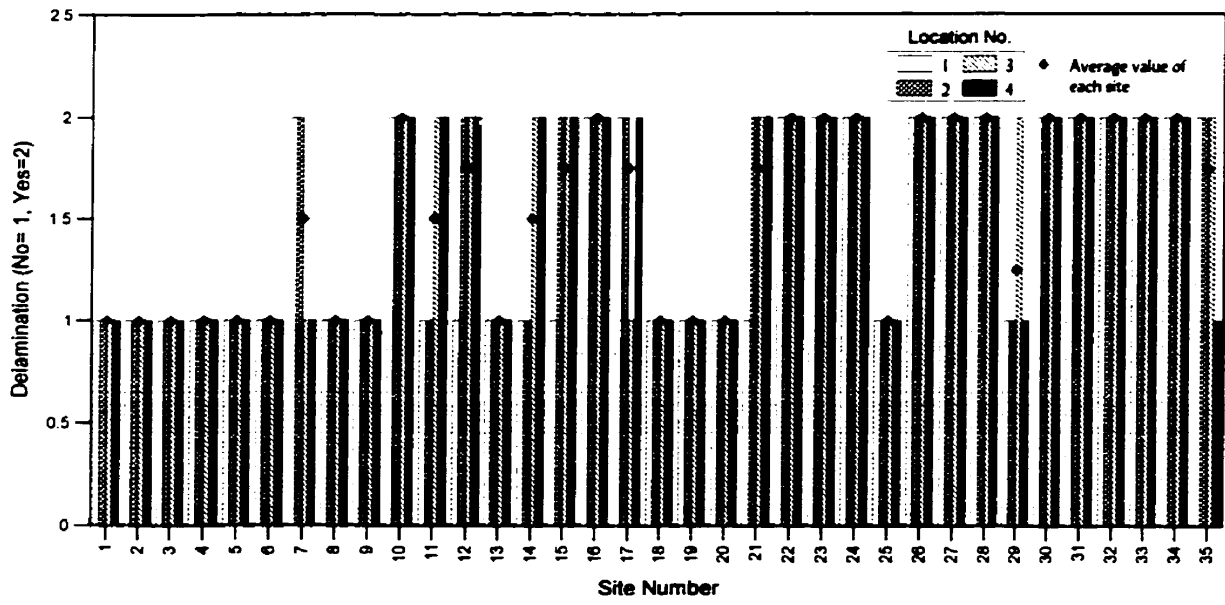
Figure A-2: *Delamination survey*
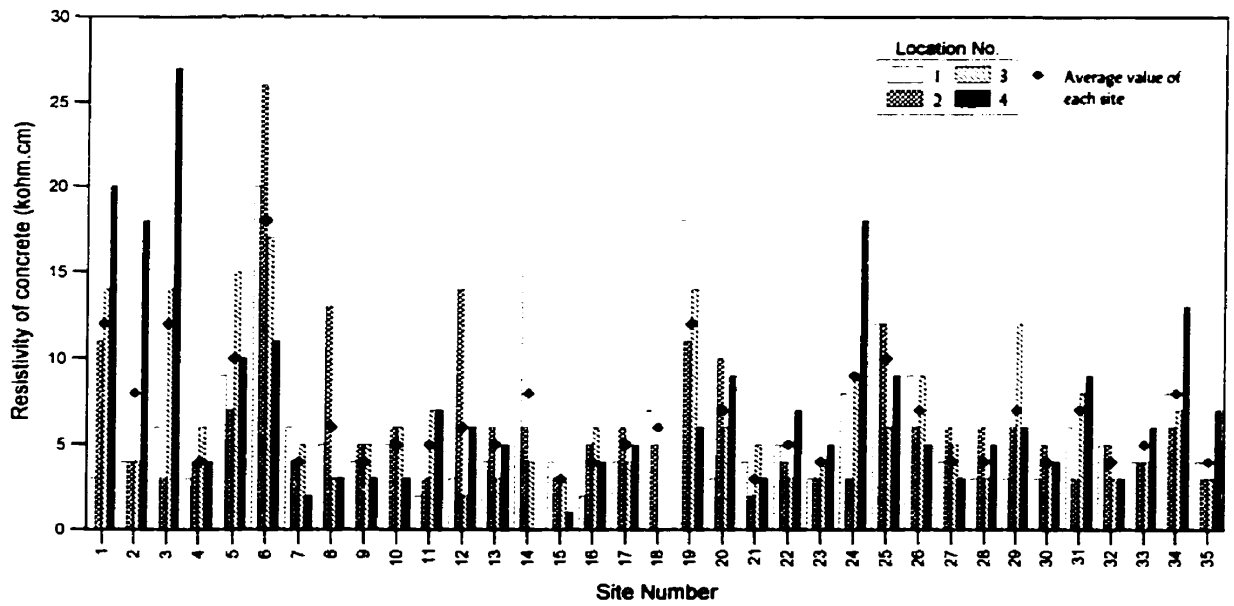
Figure A-3: *Resistivity of concrete readings*

Figure A-4: *Corrosion potential values*

Figure A-5: *Corrosion rate values*

211
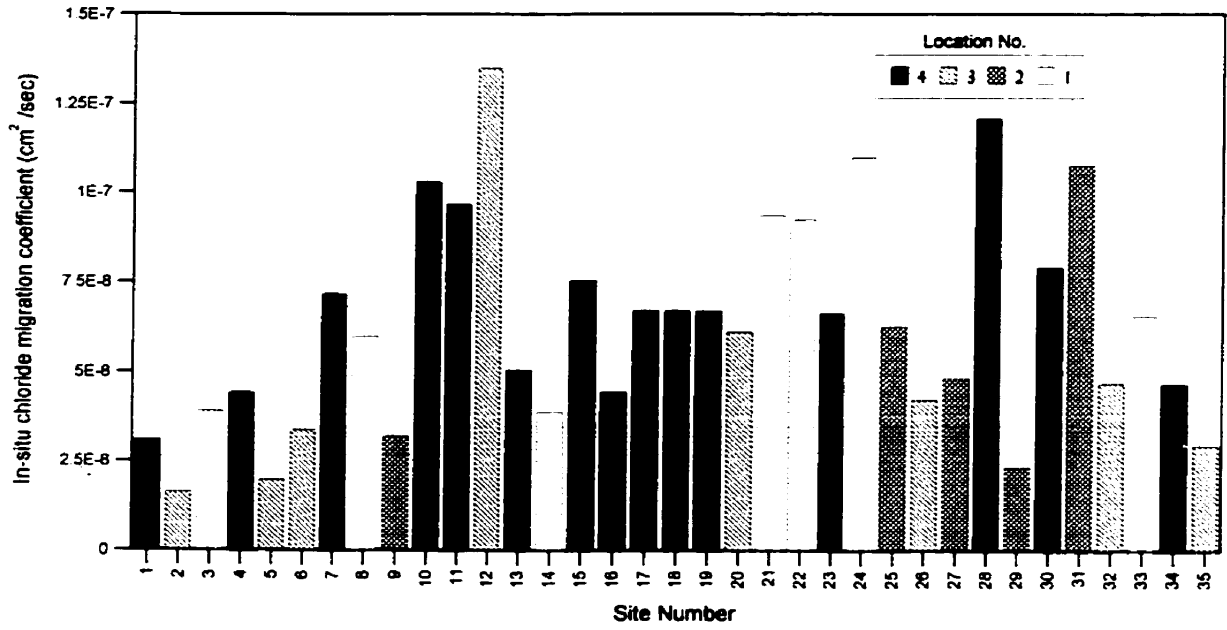
Figure A-6: *In-situ chloride migration coefficient values*
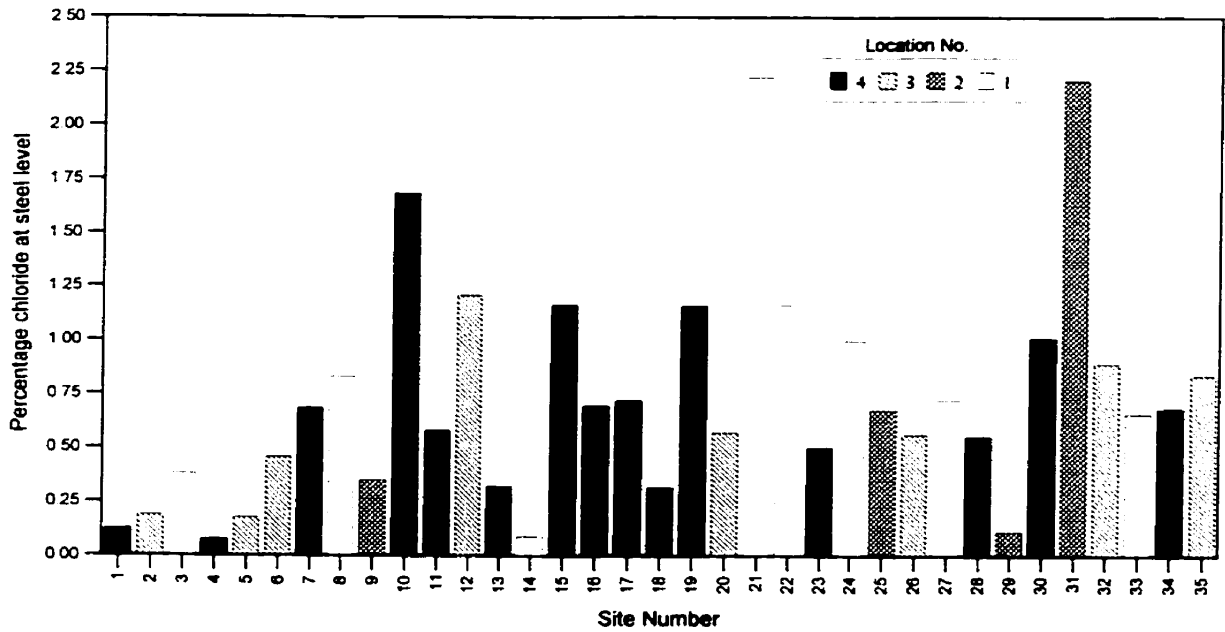
Figure A-7: *Percentage chloride at steel level*

212
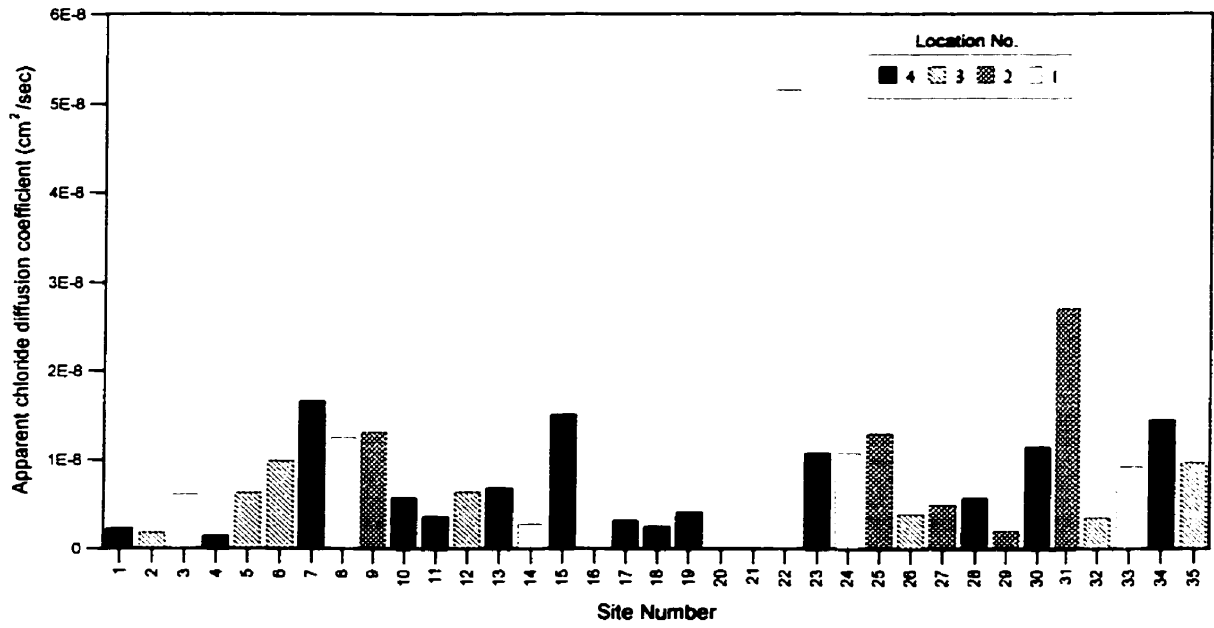
Figure A-8: *Apparent chloride diffusion coefficient values*
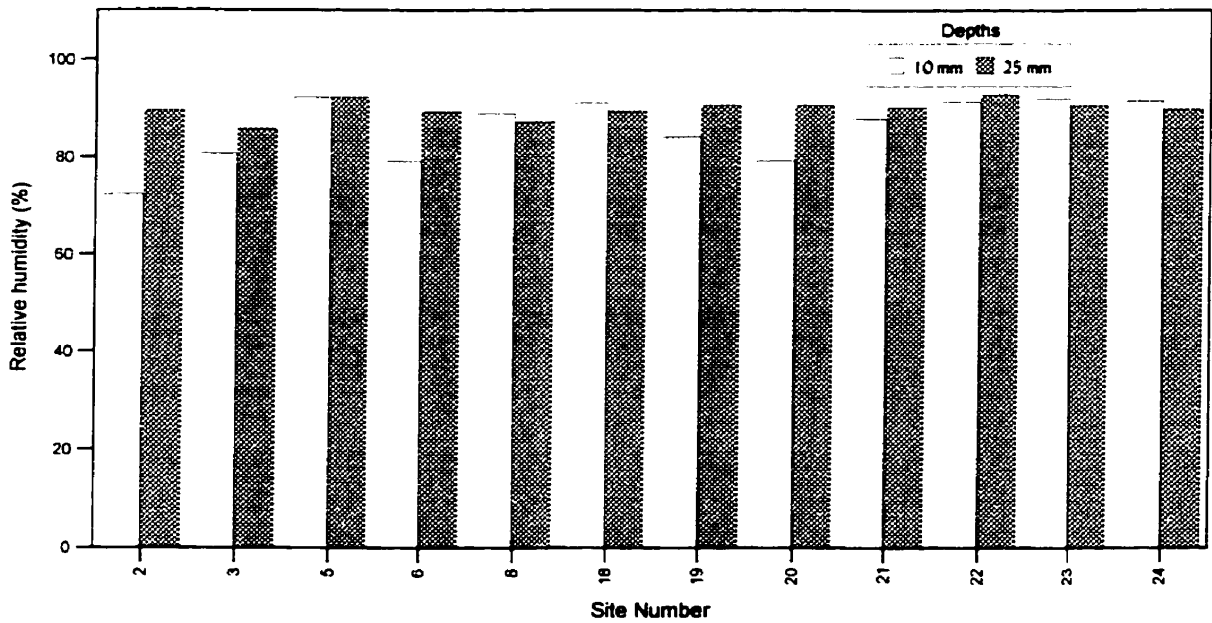
Figure A-9: *Relative humidity readings*

213
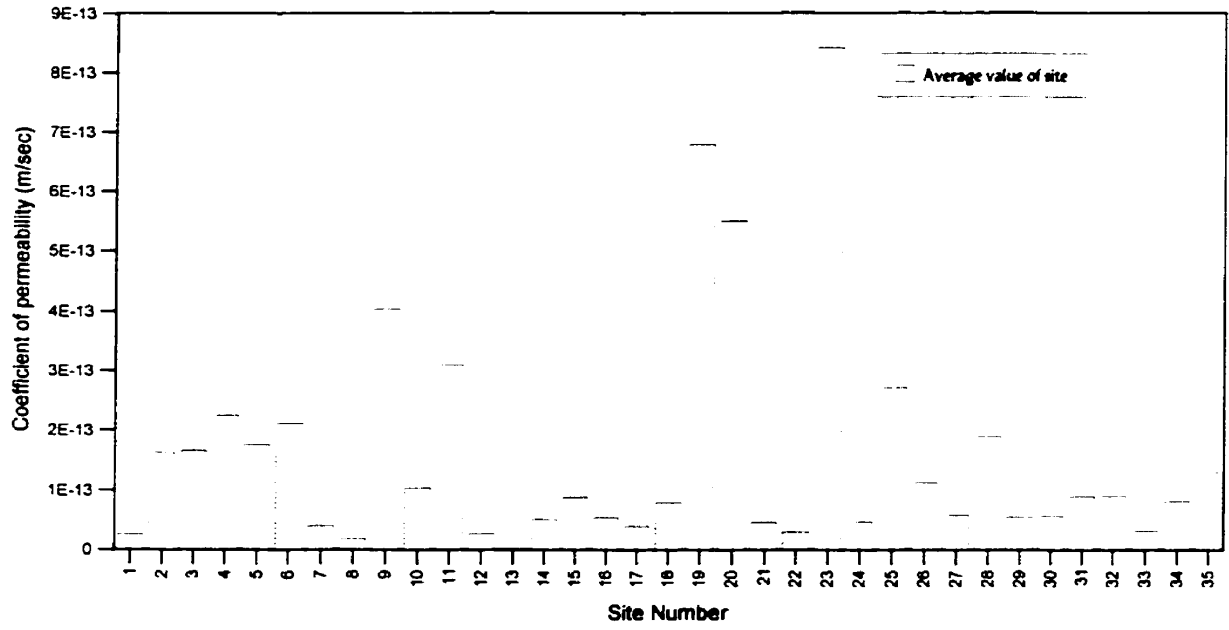
Figure A-10: *Coefficient of permeability values*
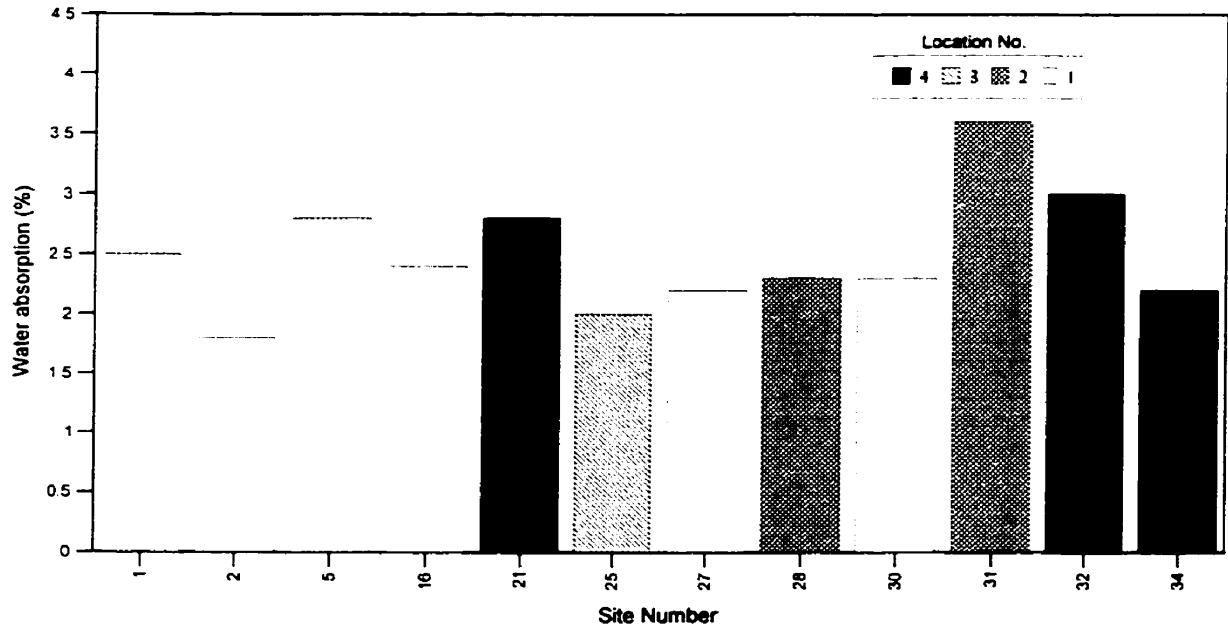
Figure A-11: *Water absorption values*
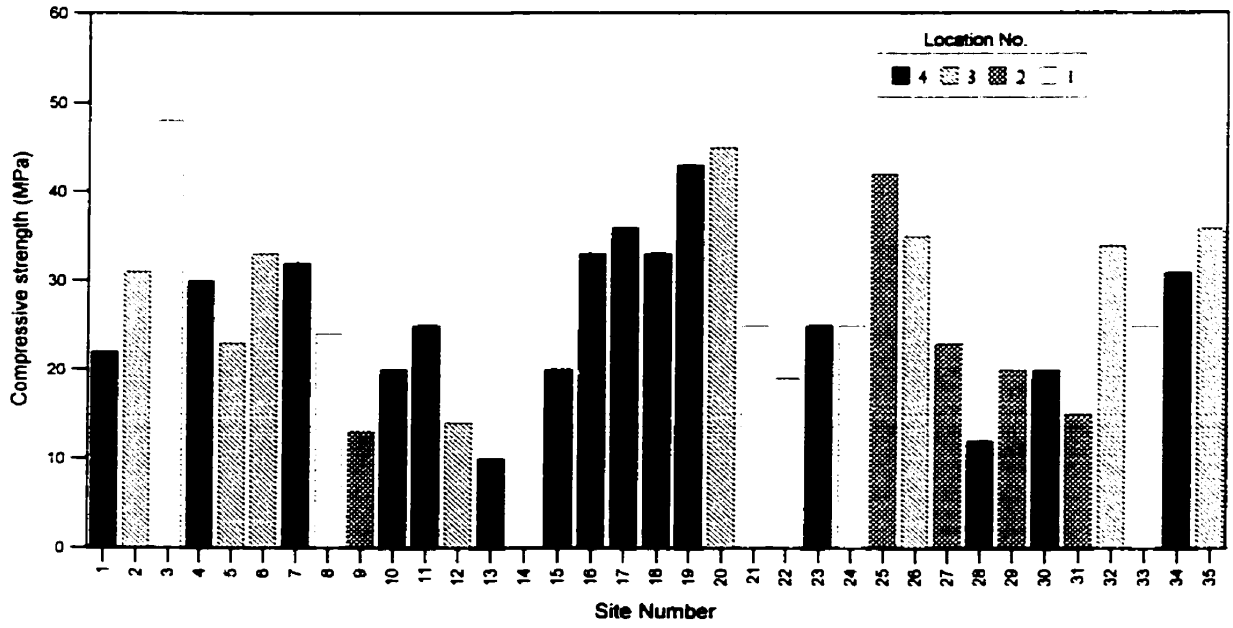
Figure A-12: *Concrete compressive strength values*

Appendix B: Linear Polarization Curves

Due to the large amount of readings (a total of 140 LPR tests), only a sample of the polarization resistance curves are included in the present appendix to illustrate the consistency of the readings in the achievement of the linear relationship between the potential and the current density values, which made it possible to calculate the polarization resistance, R_p (Equation (3.11)).

Figure B-1: *Polarization resistance plot (Site 24, location 1)*

Polarization Resistance
'pols24_2.dta' 6/29/1998-7:29:32

Pstat #1
Scan: -0.02 V to 0.02 V, 0.125 mV/s, 2 s/pt
ϕ_{oc}: -0.65682 V
Area: 55.359 cm^2
Electrode: 7.87 gm/cm^3, 27.92 g/Equiv
Conditioning: OFF
Delay: ON, 500 s
IR Comp.: ON

NOTES:

POLRES RESULTS
Region = -19.9 mV to 20.1 mV
β_c = 120.0 mV/decade
β_a = 120.0 mV/decade
ϕ_{corr} = -658.9 mV
I_{corr} = 6.670E-06 A/cm^2
R_p = 3.907E+03 Ohm cm^2
CR = 0.077 mm/yr

Potential (V) vs ϕ_{oc} / Current Density (A/cm^2)

Figure B-2: *Polarization resistance plot (Site 24, location 2)*

Polarization Resistance
'pols24_3.dta' 6/29/1998-7:43:11

Pstat #1
Scan: -0.02 V to 0.02 V, 0.125 mV/s, 2 s/pt
ϕ_{oc}: -0.60489 V
Area: 55.359 cm^2
Electrode: 7.87 gm/cm^3, 27.92 g/Equiv
Conditioning: OFF
Delay: ON, 500 s
IR Comp.: ON

NOTES:

POLRES RESULTS
Region = -20.1 mV to 19.9 mV
β_c = 120.0 mV/decade
β_a = 120.0 mV/decade
ϕ_{corr} = -606.9 mV
I_{corr} = 5.225E-06 A/cm^2
R_p = 4.987E+03 Ohm cm^2
CR = 0.061 mm/yr

Potential (V) vs ϕ_{oc} / Current Density (A/cm^2)

Figure B-3: *Polarization resistance plot (Site 24, location 3)*

Polarization Resistance
'pols24_4.dta' 6/29/1998-8:6:42

NOTES:

0.020
0.015
0.010
0.005
0.000
-0.005
-0.010
-0.015
-0.020
-0.025

Potential (V) vs ϕ_{oc}

-1.5E-05   -1.0E-05   -5.0E-06   0.0E+00   5.0E-06   1.0E-05

Current Density (A/cm²)

POLRES RESULTS
Region = -20.1 mV to 19.9 mV

β_c = 120.0 mV/decade
β_a = 120.0 mV/decade
ϕ_{corr} = -647.7 mV
I_{corr} = 1.110E-05 A/cm²
R_p = 2.348E+03 Ohm cm²
CR = 0.129 mm/yr
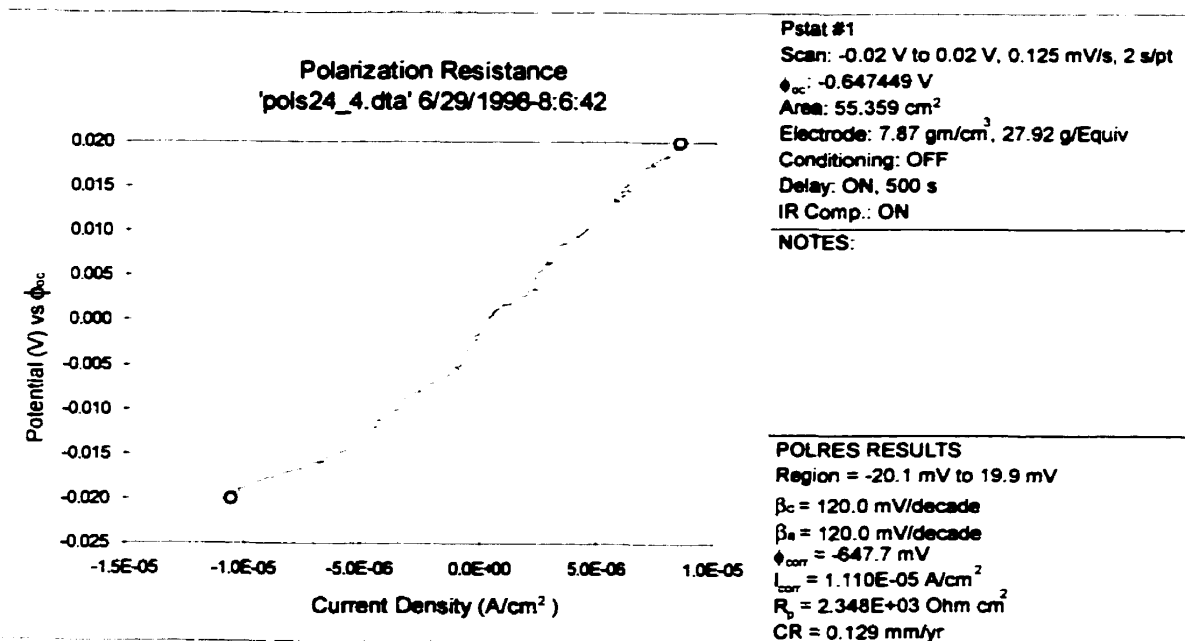
Figure B-4: *Polarization resistance plot (Site 24, location 4)*

Polarization Resistance
'pols25_1.dta' 6/30/1998-11:47:5

NOTES:

0.020
0.015
0.010
0.005
0.000
-0.005
-0.010
-0.015
-0.020
-0.025

Potential (V) vs ϕ_{oc}

-2.5E-06   -1.5E-06   -5.0E-07   5.0E-07   1.5E-06   2.5E-06

Current Density (A/cm²)

POLRES RESULTS
Region = -20.1 mV to 19.9 mV

β_c = 120.0 mV/decade
β_a = 120.0 mV/decade
ϕ_{corr} = -303.8 mV
I_{corr} = 2.824E-06 A/cm²
R_p = 9.226E+03 Ohm cm²
CR = 0.033 mm/yr

Figure B-5: *Polarization resistance plot (Site 25, location 1)*

Polarization Resistance
'pols25_2.dta' 6/30/1998-11:57:25

Pstat #1
Scan: -0.02 V to 0.02 V, 0.125 mV/s, 2 s/pt
ϕ_{oc}: -0.293153 V
Area: 55.359 cm^2
Electrode: 7.87 gm/cm^3, 27.92 g/Equiv
Conditioning: OFF
Delay: ON, 500 s
IR Comp.: ON

NOTES:

POLRES RESULTS
Region = -20.1 mV to 19.9 mV
β_c = 120.0 mV/decade
β_a = 120.0 mV/decade
ϕ_{corr} = -297.0 mV
I_{corr} = 2.916E-06 A/cm^2
R_p = 8.935E+03 Ohm cm^2
CR = 0.034 mm/yr

Potential (V) vs ϕ_{oc}

Current Density (A/cm^2)

Figure B-6: *Polarization resistance plot (Site 25, location 2)*

Polarization Resistance
'pols25_3.dta' 6/30/1998-12:9:2

Pstat #1
Scan: -0.02 V to 0.02 V, 0.125 mV/s, 2 s/pt
ϕ_{oc}: -0.351617 V
Area: 55.359 cm^2
Electrode: 7.87 gm/cm^3, 27.92 g/Equiv
Conditioning: OFF
Delay: ON, 500 s
IR Comp.: ON

NOTES:

POLRES RESULTS
Region = -19.9 mV to 20.1 mV
β_c = 120.0 mV/decade
β_a = 120.0 mV/decade
ϕ_{corr} = -356.7 mV
I_{corr} = 2.353E-06 A/cm^2
R_p = 1.107E+04 Ohm cm^2
CR = 0.027 mm/yr

Potential (V) vs ϕ_{oc}

Current Density (A/cm^2)

Figure B-7: *Polarization resistance plot (Site 25, location 3)*

Polarization Resistance
'pols25_4.dta' 6/30/1998-13:9:36

Potential (V) vs ϕ_{oc} — Current Density (A/cm^2)

Pstat #1
Scan: -0.02 V to 0.02 V, 0.125 mV/s, 2 s/pt
ϕ_{oc}: -0.318018 V
Area: 55.359 cm^2
Electrode: 7.87 gm/cm^3, 27.92 g/Equiv
Conditioning: OFF
Delay: ON, 500 s
IR Comp.: ON

NOTES:

POLRES RESULTS
Region = -20.0 mV to 20.0 mV
βc = 120.0 mV/decade
βa = 120.0 mV/decade
ϕ_{corr} = -321.3 mV
I_{corr} = 2.353E-06 A/cm^2
R_p = 1.107E+04 Ohm cm^2
CR = 0.027 mm/yr

Figure B-8: *Polarization resistance plot (Site 25, location 4)*

Polarization Resistance
'pols27_1.dta' 6/30/1998-19:44:40

Potential (V) vs ϕ_{oc} — Current Density (A/cm^2)

Pstat #1
Scan: -0.02 V to 0.02 V, 0.125 mV/s, 2 s/pt
ϕ_{oc}: -0.574073 V
Area: 55.359 cm^2
Electrode: 7.87 gm/cm^3, 27.92 g/Equiv
Conditioning: OFF
Delay: ON, 500 s
IR Comp.: ON

NOTES:

POLRES RESULTS
Region = -19.9 mV to 20.1 mV
βc = 120.0 mV/decade
βa = 120.0 mV/decade
ϕ_{corr} = -574.6 mV
I_{corr} = 3.559E-06 A/cm^2
R_p = 7.322E+03 Ohm cm^2
CR = 0.041 mm/yr

Figure B-9: *Polarization resistance plot (Site 27, location 1)*

Polarization Resistance
'pols27_2.dta' 6/30/1998-19:52:41

Potential (V) vs φₒc — (y-axis values: 0.025, 0.020, 0.015, 0.010, 0.005, 0.000, -0.005, -0.010, -0.015, -0.020)

Current Density (A/cm²) — (x-axis values: -3.0E-06, -2.0E-06, -1.0E-06, 0.0E+00, 1.0E-06, 2.0E-06, 3.0E-06)

Pstat #1
Scan: -0.02 V to 0.02 V, 0.125 mV/s, 2 s/pt
ϕ_{oc}: -0.615292 V
Area: 55.359 cm²
Electrode: 7.87 gm/cm³, 27.92 g/Equiv
Conditioning: OFF
Delay: ON, 500 s
IR Comp.: ON

NOTES:

POLRES RESULTS
Region = -20.0 mV to 20.0 mV
β_c = 120.0 mV/decade
β_a = 120.0 mV/decade
ϕ_{corr} = -617.4 mV
I_{corr} = 3.536E-06 A/cm²
R_p = 7.370E+03 Ohm cm²
CR = 0.041 mm/yr

Figure B-10: *Polarization resistance plot (Site 27, location 2)*

Polarization Resistance
'pols27_3.dta' 6/30/1998-20:0:35

Potential (V) vs φₒc — (y-axis values: 0.020, 0.015, 0.010, 0.005, 0.000, -0.005, -0.010, -0.015, -0.020, -0.025)

Current Density (A/cm²) — (x-axis values: -4.0E-06, -2.0E-06, 0.0E+00, 2.0E-06, 4.0E-06)

Pstat #1
Scan: -0.02 V to 0.02 V, 0.125 mV/s, 2 s/pt
ϕ_{oc}: -0.631428 V
Area: 55.359 cm²
Electrode: 7.87 gm/cm³, 27.92 g/Equiv
Conditioning: OFF
Delay: ON, 500 s
IR Comp.: ON

NOTES:

POLRES RESULTS
Region = -20.1 mV to 19.9 mV
β_c = 120.0 mV/decade
β_a = 120.0 mV/decade
ϕ_{corr} = -634.4 mV
I_{corr} = 4.837E-06 A/cm²
R_p = 5.388E+03 Ohm cm²
CR = 0.056 mm/yr

Figure B-11: *Polarization resistance plot (Site 27, location 3)*

Polarization Resistance
'pols27_4.dta' 6/30/1998-20:8:42

Potential (V) vs φoc

0.020
0.015
0.010
0.005
0.000
-0.005
-0.010
-0.015
-0.020
-0.025

-8.0E-06 -6.0E-06 -4.0E-06 -2.0E-06 0.0E+00 2.0E-06 4.0E-06 6.0E-06

Current Density (A/cm²)

Pstat #1
Scan: -0.02 V to 0.02 V, 0.125 mV/s, 2 s/pt
φoc: -0.656499 V
Area: 55.359 cm²
Electrode: 7.87 gm/cm³, 27.92 g/Equiv
Conditioning: OFF
Delay: ON, 500 s
IR Comp.: ON

NOTES:

POLRES RESULTS
Region = -20.0 mV to 20.0 mV
βc = 120.0 mV/decade
βa = 120.0 mV/decade
φcorr = -656.2 mV
Icorr = 8.451E-06 A/cm²
Rp = 3.083E+03 Ohm cm²
CR = 0.098 mm/yr

Figure B-12: *Polarization resistance plot (Site 27, location 4)*

Polarization Resistance
'pols32_1.dta' 6/30/1998-8:42:42

Potential (V) vs φoc

0.020
0.015
0.010
0.005
0.000
-0.005
-0.010
-0.015
-0.020
-0.025

-4.0E-06 -3.0E-06 -2.0E-06 -1.0E-06 0.0E+00 1.0E-06 2.0E-06 3.0E-06 4.0E-06

Current Density (A/cm²)

Pstat #1
Scan: -0.02 V to 0.02 V, 0.125 mV/s, 2 s/pt
φoc: -0.667985 V
Area: 55.359 cm²
Electrode: 7.87 gm/cm³, 27.92 g/Equiv
Conditioning: OFF
Delay: ON, 500 s
IR Comp.: ON

NOTES:

POLRES RESULTS
Region = -20.0 mV to 20.0 mV
βc = 120.0 mV/decade
βa = 120.0 mV/decade
φcorr = -666.7 mV
Icorr = 4.737E-06 A/cm²
Rp = 5.501E+03 Ohm cm²
CR = 0.055 mm/yr

Figure B-13: *Polarization resistance plot (Site 32, location 1)*

Figure B-14: *Polarization resistance plot (Site 32, location 2)*
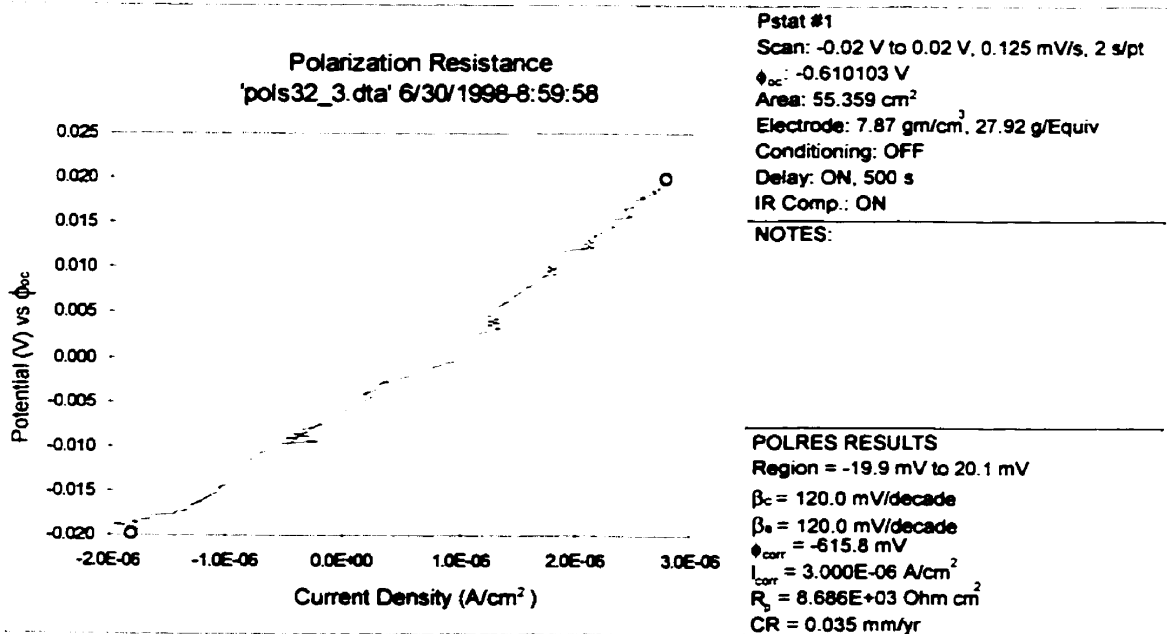
Figure B-15: *Polarization resistance plot (Site 32, location 3)*
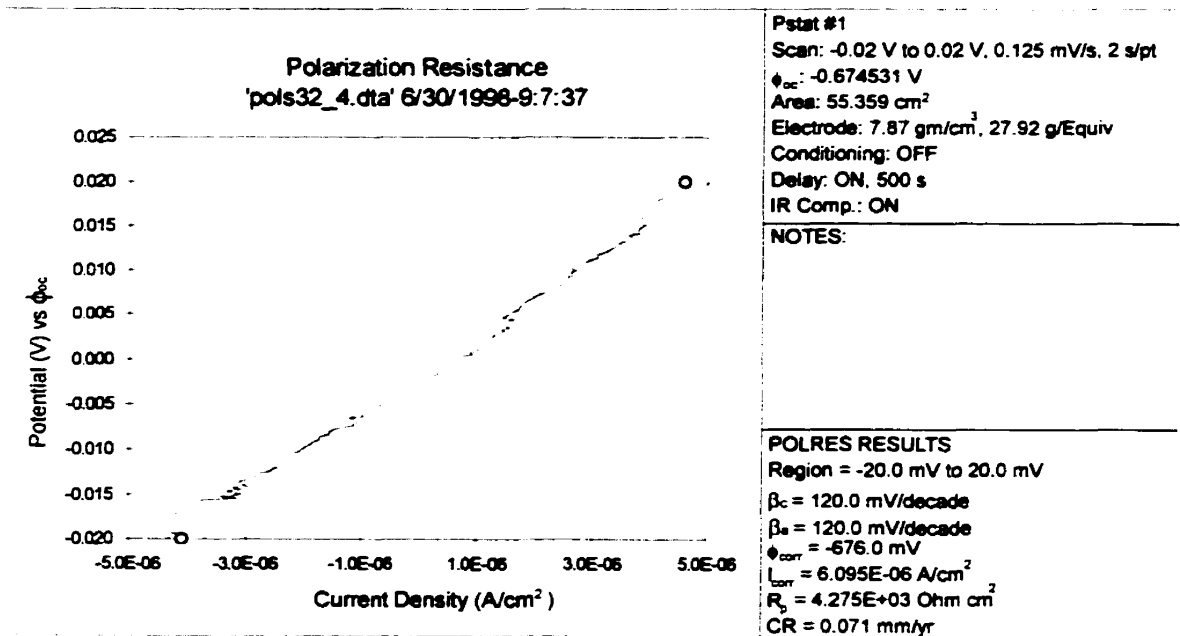
Figure B-16: *Polarization resistance plot (Site 32, location 4)*

Appendix C: Calculation of Chloride Migration Coefficient

Equation (3-29) was required to calculate the flux, J, from the test results. The value dc/dt (ppm/hour) was obtained from the linear portion of the concentration versus time graphs (Figures C-1 to C-3). The J values were converted ($mol.cm^{-2}.s^{-1}$) using appropriate conversions. Table C-1 includes all the above mentioned calculations and also the calculation of the in-situ chloride migration coefficients (D_{mig}) using Equation (3.28).

Table C-1: *Calculation of chloride migration coefficient (D_{mig})*

Site No.	dc/dt (ppm/hr)	J (mol.cm^{-2}.s^{-1})	T (K)	D$_{mig}$ (cm^2.s^{-1})
1	65	3.15E-06	307.0	3.09E-08
2	35	1.70E-06	299.3	1.62E-08
3	81	3.93E-06	310.5	3.90E-08
4	92	4.46E-06	306.2	4.37E-08
5	42	2.04E-06	302.0	1.97E-08
6	72	3.49E-06	301.8	3.37E-08
7	151	7.32E-06	306.0	7.16E-08
8	127	6.16E-06	303.8	5.98E-08
9	68	3.30E-06	302.8	3.19E-08
10	215	1.04E-05	308.8	1.03E-07
11	271	1.31E-05	305.4	1.28E-07
12	289	1.40E-05	300.8	1.35E-07
13	90	4.36E-06	303.8	4.24E-08
14	81	3.93E-06	308.0	3.87E-08
15	157	7.61E-06	310.4	7.55E-08
16	95	4.61E-06	302.4	4.45E-08
17	130	6.30E-06	303.8	6.12E-08
18	137	6.64E-06	316.8	6.73E-08
19	136	6.59E-06	318.3	6.71E-08
20	128	6.21E-06	308.6	6.12E-08
21	195	9.45E-06	309.6	9.36E-08
22	192	9.31E-06	310.7	9.25E-08
23	143	6.93E-06	300.5	6.66E-08
24	234	1.13E-05	303.6	1.10E-07
25	133	6.45E-06	305.0	6.29E-08
26	92	4.46E-06	296.2	4.22E-08
27	104	5.04E-06	300.6	4.85E-08
28	257	1.25E-05	303.4	1.21E-07
29	49	2.38E-06	306.3	2.33E-08
30	167	8.10E-06	306.0	7.92E-08
31	227	1.10E-05	306.6	1.08E-07
32	99	4.80E-06	306.2	4.70E-08
33	139	6.74E-06	304.8	6.57E-08
34	108	5.24E-06	304.6	5.10E-08
35	64	3.10E-06	296.6	2.94E-08
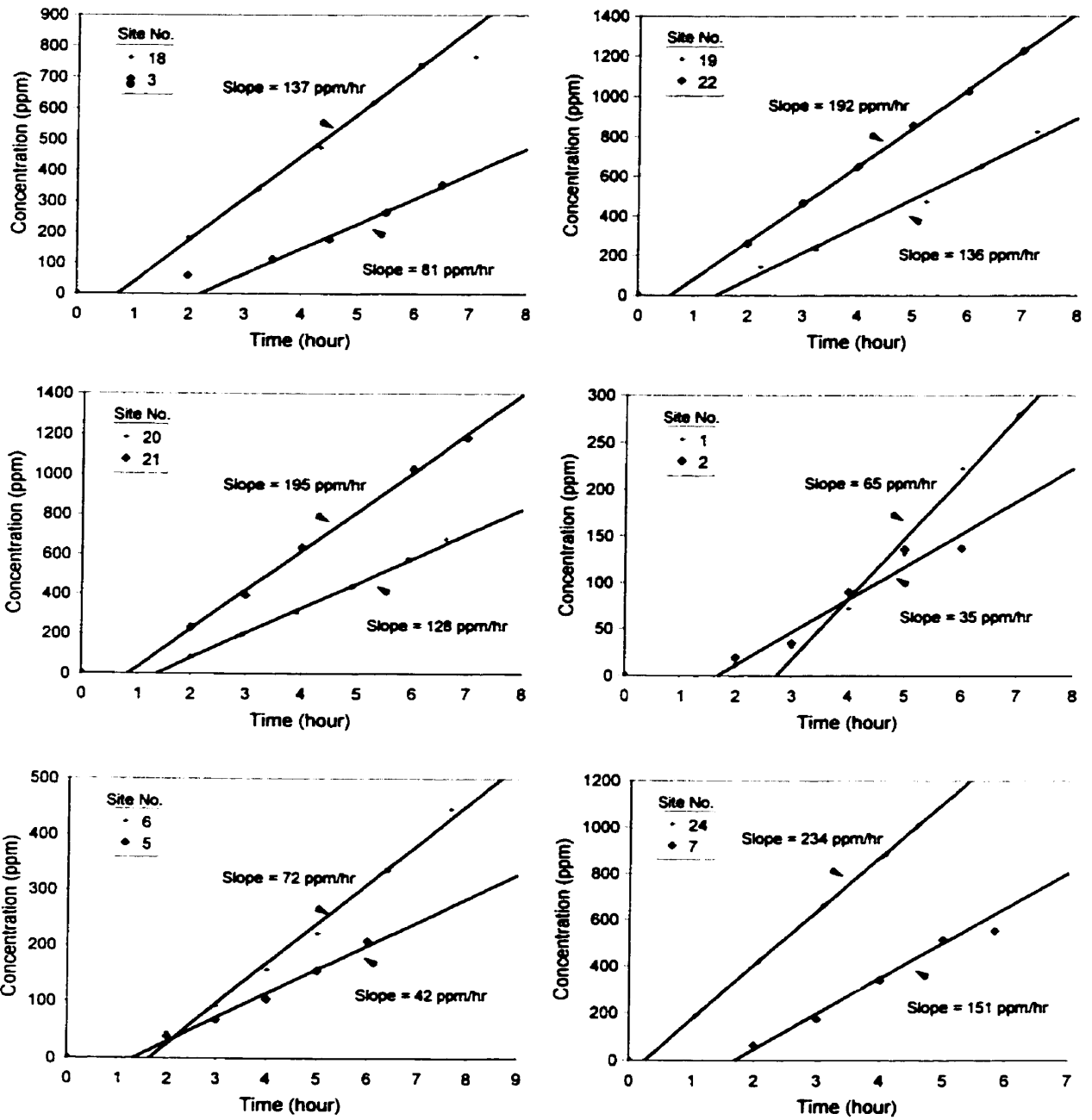
Figure C-1: *Steady state slope of concentration vs. time graphs (Sites 1-3, 5-7, 18-22 and 24)*
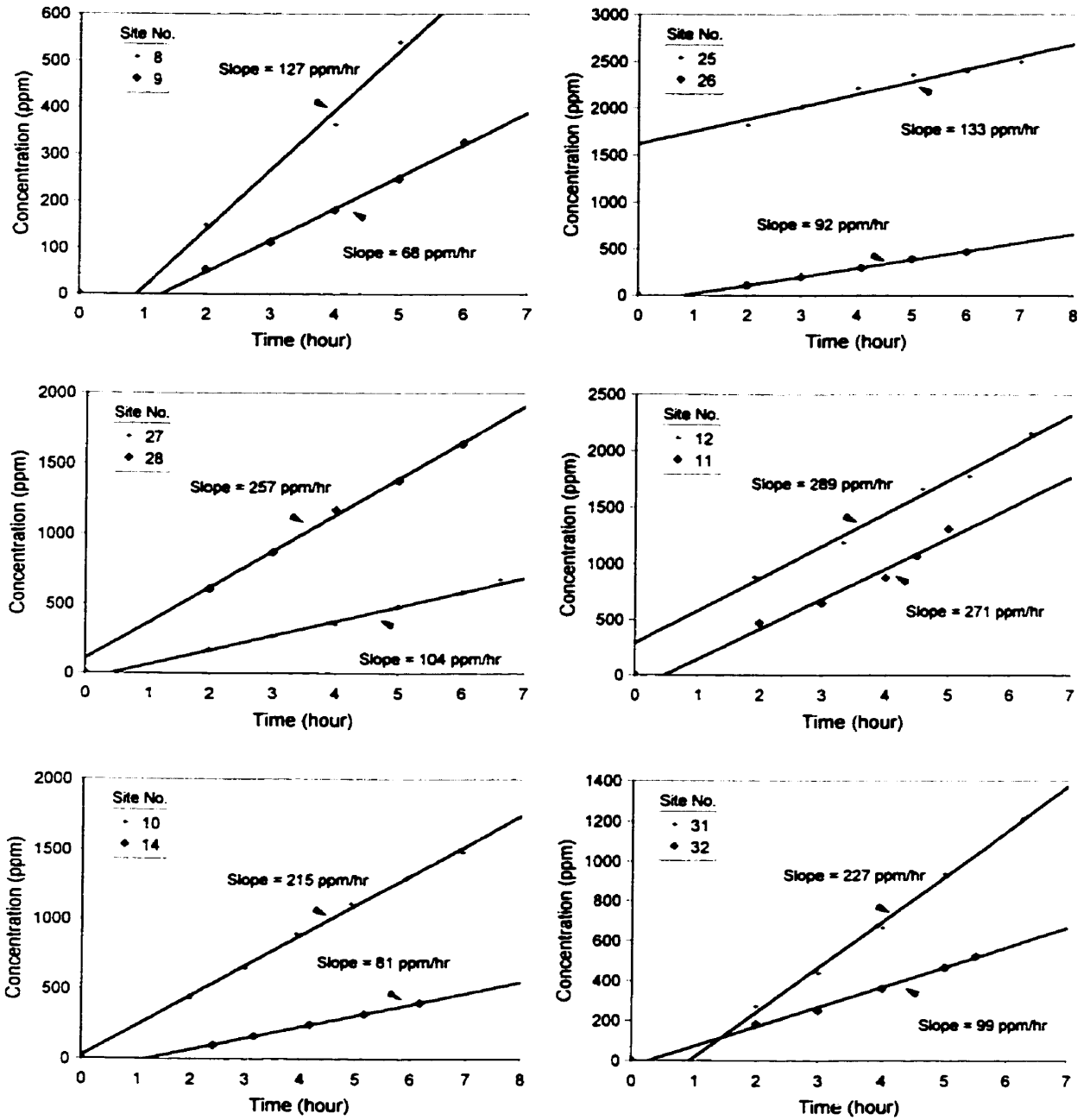
Figure C-2: *Steady state slope of concentration vs. time graphs (Sites 8-12, 14, 25-28, 31 and 32)*
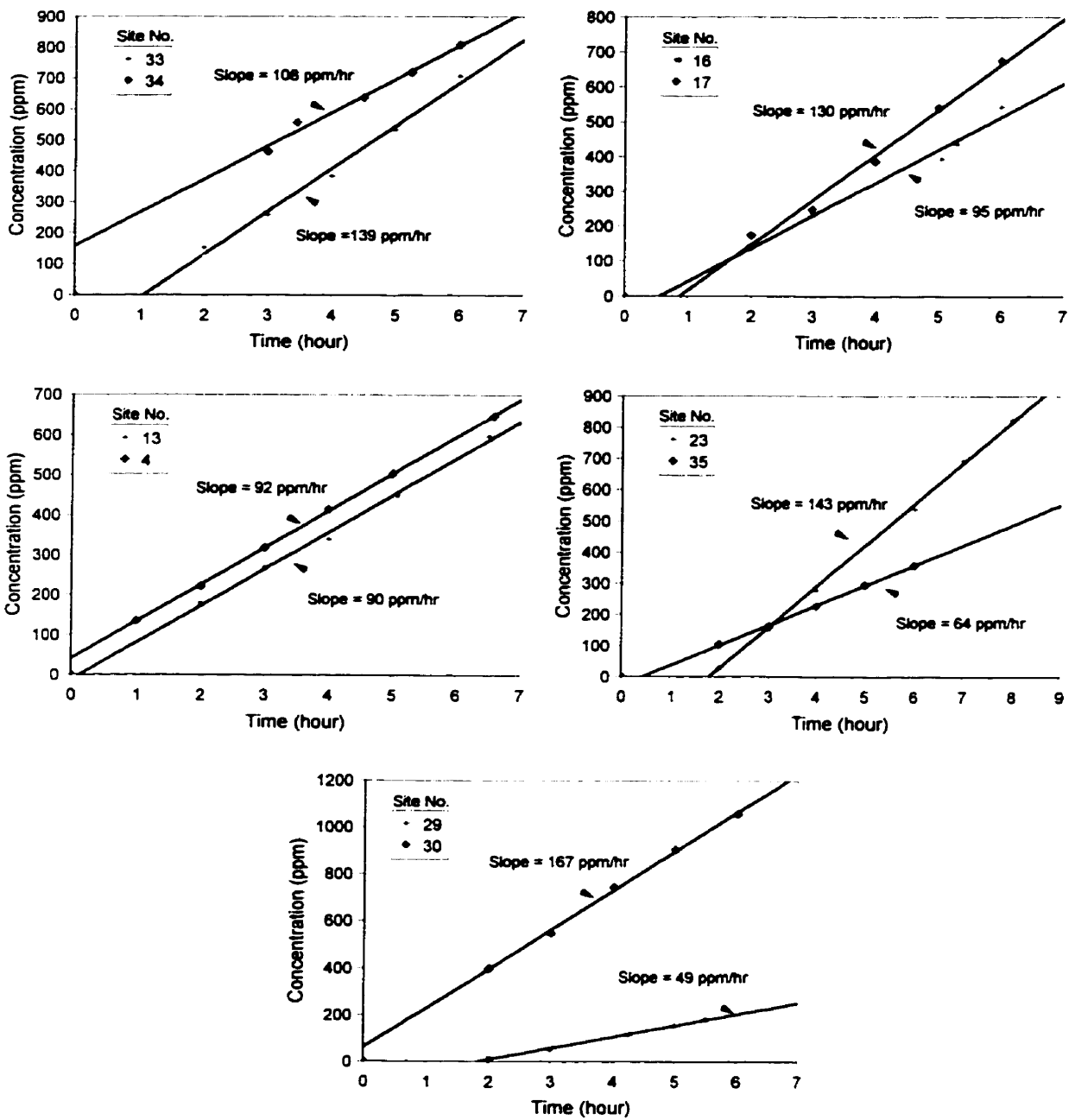
Figure C-3: *Steady state slope of concentration vs. time graphs (Sites 4, 13, 16, 17, 23, 29, 30 and 33-35)*

228

Appendix D: Chloride Profile Evaluation

The objective of this appendix is to illustrate an example of the calibration series (Figure D-1) conducted to plot the chloride profiles. Also, supplementary chloride profiles to those included in Section 4.8.2.4 are included in the present appendix (Figures D-2 to D-5). Lastly, details of the calculation of the apparent chloride diffusion coefficient from the profiles are provided in Table D-1.

SERIES 1

Date: August 7, 1998

Calibration table: **Samples:** 1, 2, 3, 6, 18 and 19

Chloride Concentration	3PPM		9PPM		90PPM		180PPM		374PPM	
	Potential	Deviation	Potential	Deviation	Potential	Deviation	Potential	Deviation	Potential	Deviation
Trials										
1	220.8	1.2	201.7	1.4	143.6	0.2	126.9	0.1	108.6	0.1
2	219.0	0.6	200.5	0.2	143.5	0.1	127.1	0.1	108.8	0.1
3	219.8	0.2	200.4	0.1	143.3	0.1	127.0	0.0	108.3	0.4
4	218.8	0.8	200.2	0.1	143.2	0.2	126.7	0.3	108.7	0.0
5	218.8	0.8	200.4	0.1	143.2	0.2	127.0	0.0	108.2	0.5
6	219.1	0.5	199.5	0.8	143.2	0.2	126.9	0.1	108.6	0.1
7	220.7	1.1	200.5	0.2	143.6	0.2	127.0	0.0	108.8	0.1
8	220.0	0.4	200.1	0.2	143.2	0.2	127.1	0.1	109.3	0.6
9	220.7	1.1	199.4	0.9	143.5	0.1	127.1	0.1	109.0	0.3
10	218.3	1.3	200.0	0.3	143.4	0.0	127.4	0.4	109.1	0.4
AVERAGE (mV)	219.6		200.3		143.4		127.0		108.7	
Max DEVIATION (mV)		1.3		1.4		0.2		0.4		0.6
Max ALLOWABLE (mV)		1.5		1.5		1.5		1.5		4.5

Checks: It is noted that the maximum deviations are less or equal to the maximum allowable deviations, therefore, the average of the ten readings listed below with the corresponding logarithm of the chloride concentrations were used to plot calibration curve shown in Figure 4-19 (Section 4.8.2.2).

Values plotted:

Potential (mV)	Log (ppmCl)
219.6	0.477
200.3	0.954
143.4	1.954
127.0	2.255
108.7	2.573

Figure D-1: *Potentials obtained for calibrating solutions: Series 1*
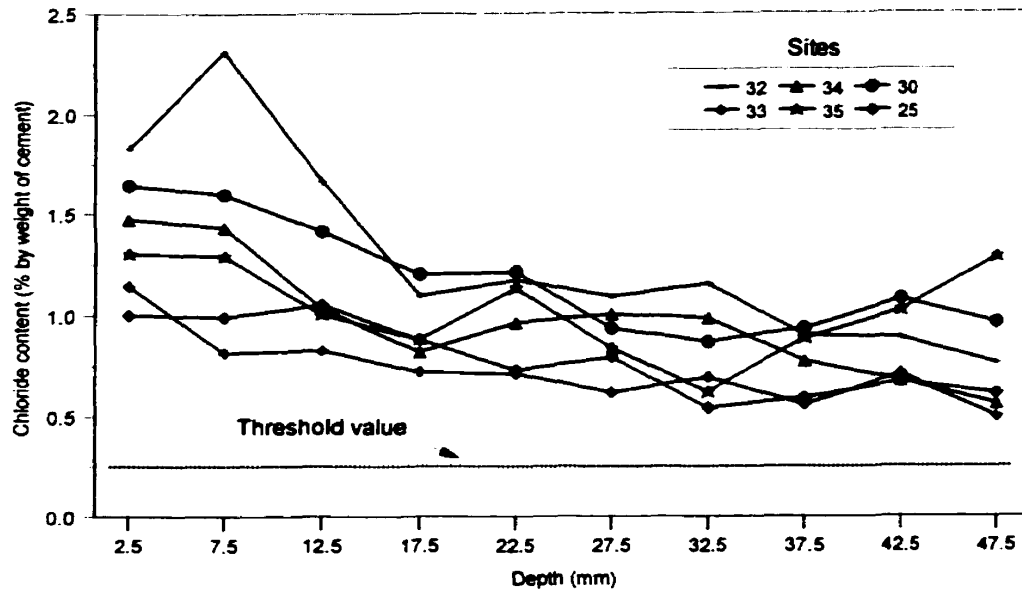
Figure D-2: *Chloride profiles (Sites 25,30 and 32-35)*
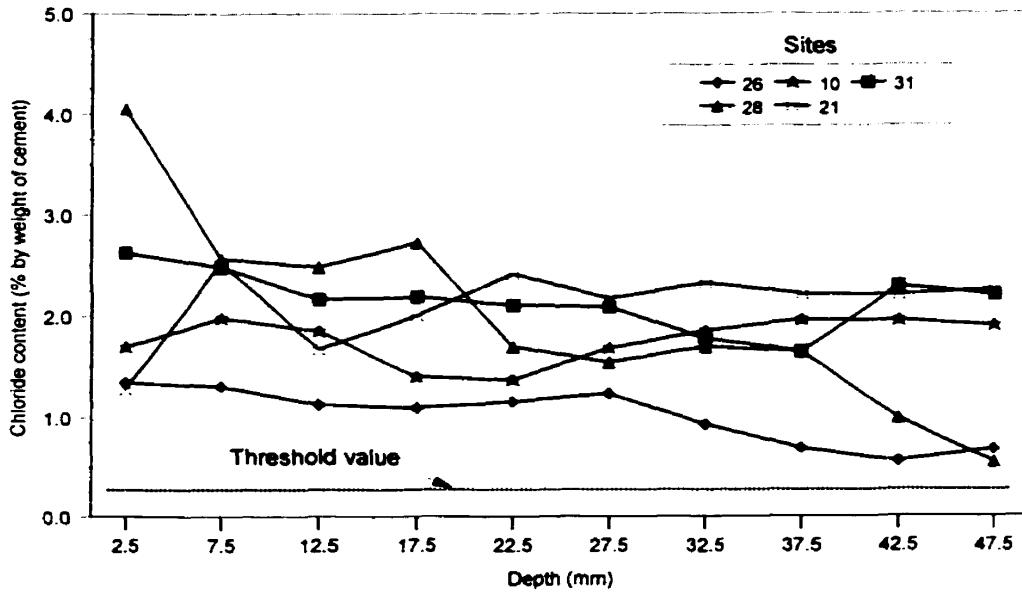
Figure D-3: *Chloride profiles (Sites10, 21, 26, 28 and 31)*

230
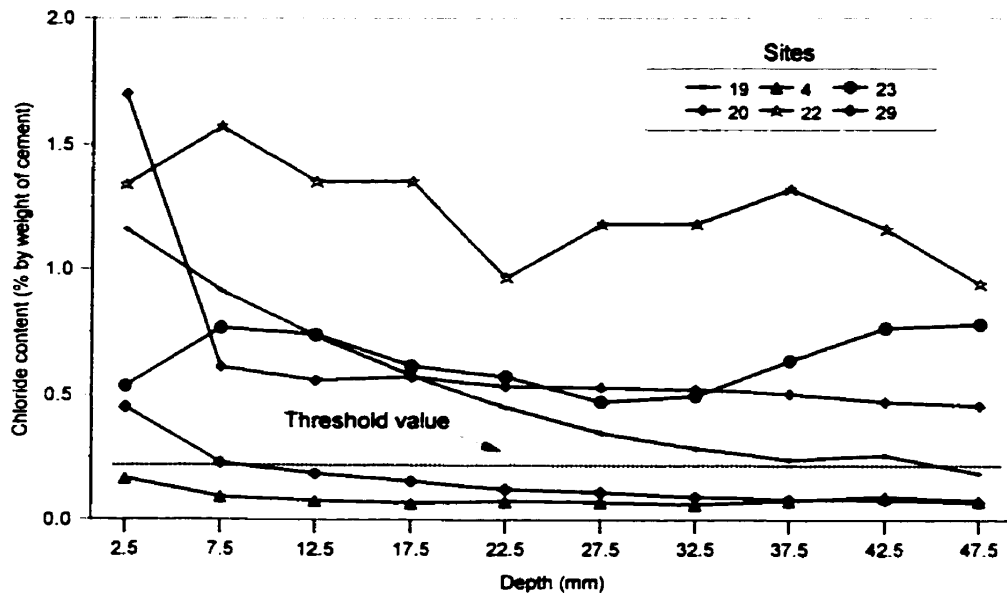
Figure D-4: *Chloride profiles (Sites 4, 19, 20, 22, 23 and 29)*
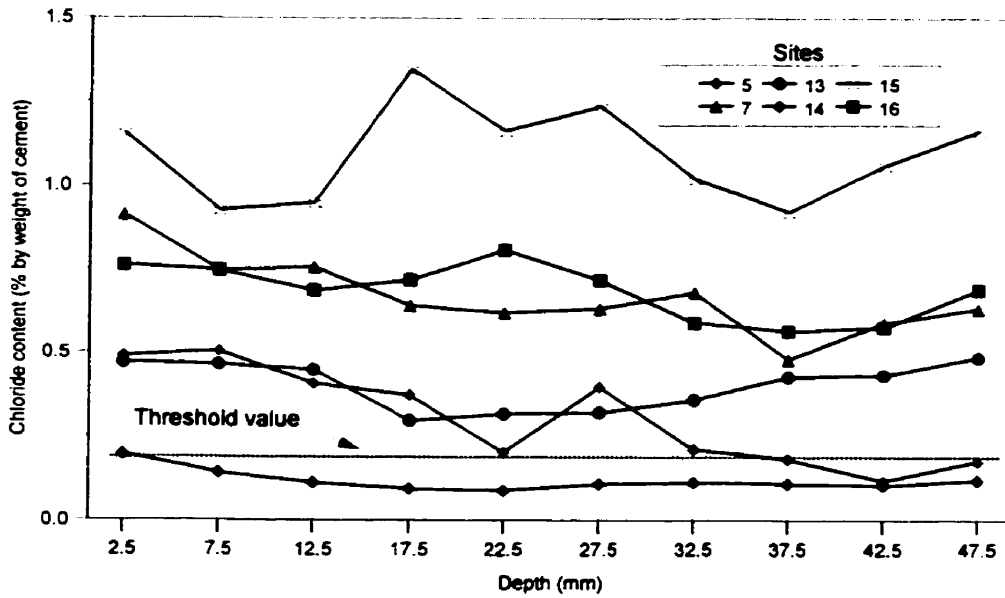
Figure D-5: *Chloride profiles (Sites 5, 7 and 13-16)*

231

Calculation of Apparent Chloride Diffusion Coefficient

A linear regression analysis of the transformed variables (y values obtained from Equation (3.22) against depth, x) was required to calculate the q and α values (the y-intercept and the slope of the straight line (Equation (3-21)). Table D-1 includes the values of q and α and the calculation of the apparent diffusion coefficient using Equation (3.25), assuming a chloride exposure period, t, of 35 years (Section 4.8.3.2).

Table D-1: *Calculation of apparent diffusion coefficient (D_a)*

Site No.	t (year)	q	α	D_a (cm^2/sec)
1	35	0.1811	0.0033	2.27E-09
2	35	0.2245	0.0046	1.80E-09
3	35	0.2877	0.0032	6.10E-09
4	35	0.1607	0.0037	1.42E-09
5	35	0.2920	0.0032	6.29E-09
6	35	0.4348	0.0038	9.88E-09
7	35	0.3713	0.0025	1.67E-08
8	35	0.5143	0.0040	1.25E-08
9	35	0.3554	0.0027	1.31E-08
10	35	0.6112	0.0070	5.76E-09
11	35	0.5909	0.0085	3.65E-09
12	35	0.6157	0.0067	6.38E-09
13	35	0.2861	0.0030	6.87E-09
14	35	0.1750	0.0029	2.75E-09
15	35	0.5221	0.0037	1.50E-08
16	35	-	-	-
17	35	0.5222	0.0080	3.22E-09
18	35	0.3677	0.0064	2.49E-09
19	35	0.4089	0.0055	4.17E-09
20	35	-	-	-
21	35	-	-	-
22	35	0.4965	0.0019	5.16E-08
23	35	0.3703	0.0031	1.08E-08
24	35	0.5851	0.0049	1.08E-08
25	35	0.4203	0.0032	1.30E-08
26	35	0.6994	0.0097	3.93E-09
27	35	0.4634	0.0057	4.99E-09
28	35	0.7596	0.0087	5.76E-09
29	35	0.2475	0.0048	2.01E-09
30	35	0.5194	0.0042	1.15E-08
31	35	0.6445	0.0034	2.71E-08
32	35	0.6333	0.0092	3.58E-09
33	35	0.4093	0.0037	9.24E-09
34	35	0.4718	0.0034	1.45E-08
35	35	0.4654	0.0041	9.73E-09

Appendix E: Calculation of Coefficient of Permeability

Due to the large amount of readings (a total of 105 water permeability tests, that is three per site), only a sample of the volume of water versus time graphs are included in the present appendix to illustrate the consistency of the readings in the achievement of steady state (second portion of the graphs), which made it possible to calculate the rate of flow (Figures E-1 and E-2).

In order to obtain a representative value of the whole site, the rate of flow of the three locations for each site were averaged as shown in Figure E-3. It is noted that readings for sites 19, 20 and 23 at location one are much larger than the values obtained for the other locations in the same site. The presence of cracks under the testing area might have been the cause even though when cross-checked with the delamination survey (Figure A-2), sites 19 and 20 were not delaminated while site 23 was delaminated. During testing, water might have escaped through the cracks in the concrete into the delamination voids underneath, instead of penetrating through the pores. The values were kept in the analysis, that is when calculating the average of each site, however, they were carefully studied when conducting the univariate analysis in Section 6.3.2.1. This average value was used to obtain an average coefficient of permeability for each site as shown in Table E-1 using Equation (3.30) and a calibration factor of 0.207×10^{-3} (Section 4.9.3).
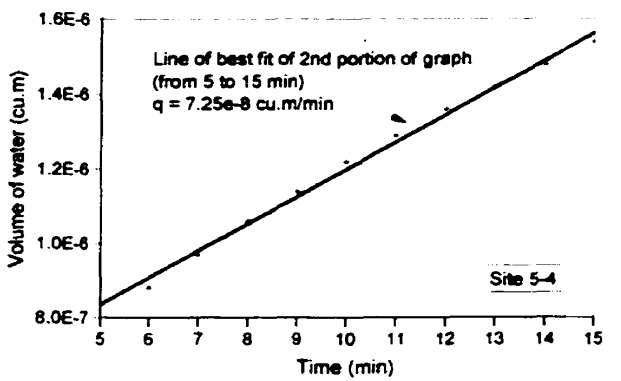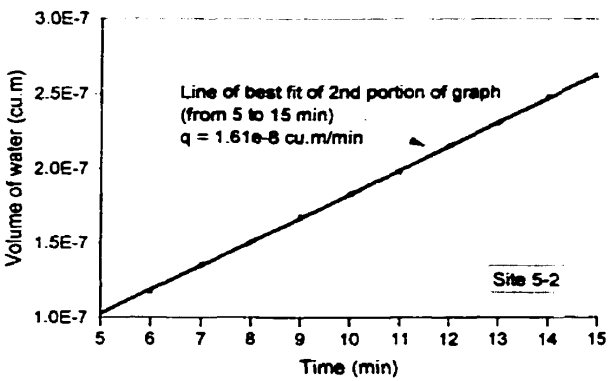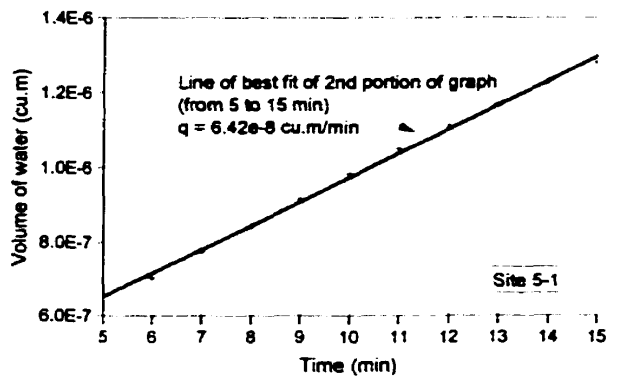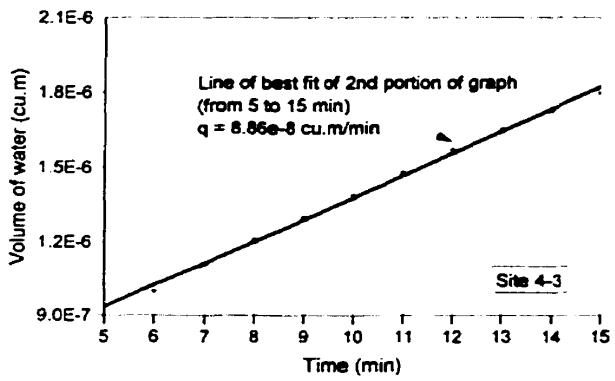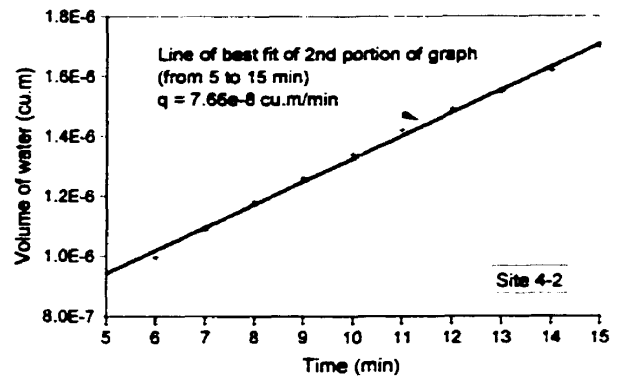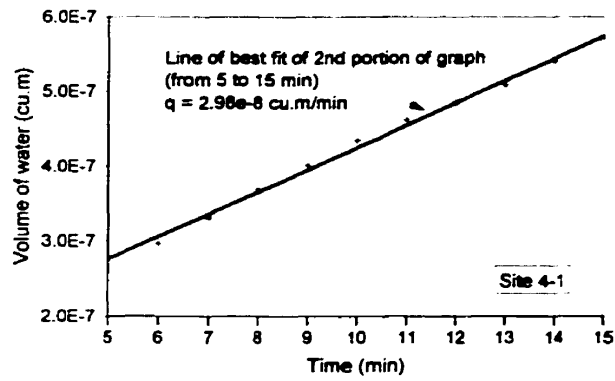
Figure E-1: *Steady state slope of volume of water vs. time graphs for Sites 4 and 5*
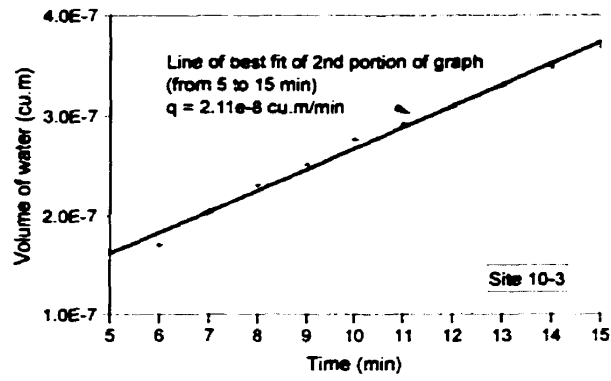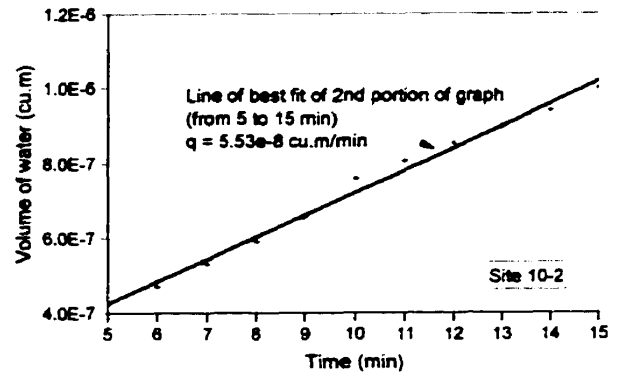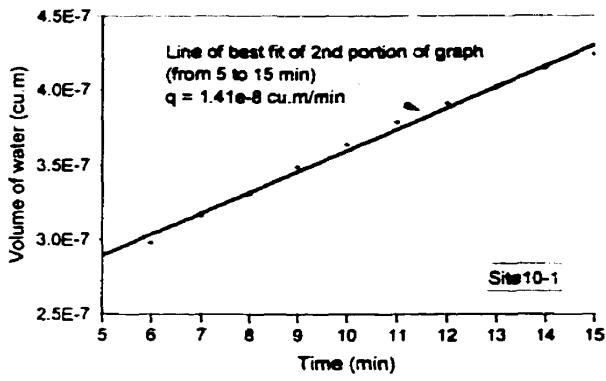
Figure E-2: *Steady state slope of volume of water vs. time graphs for Site10*
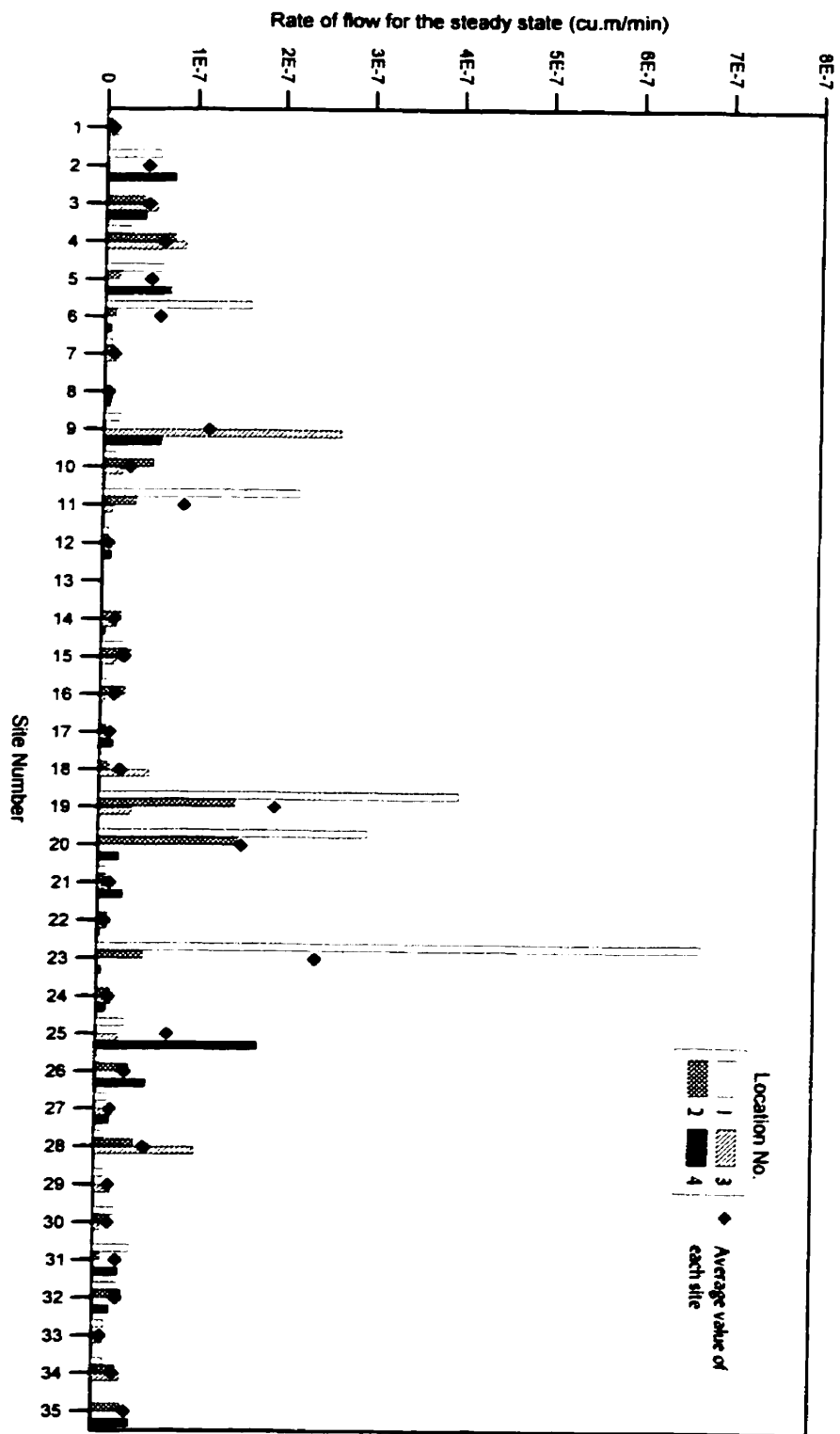
Figure E-3: *Rate of flow values for steady state condition*

Table E-1: *Calculation of coefficient of permeability (k_w)*

Site No.	$q_{average}$ (m^3/min)	k_w (m/sec)
1	7.49E-09	2.58E-14
2	4.69E-08	1.62E-13
3	4.81E-08	1.66E-13
4	6.50E-08	2.24E-13
5	5.09E-08	1.76E-13
6	6.12E-08	2.11E-13
7	1.16E-08	3.99E-14
8	5.12E-09	1.77E-14
9	1.17E-07	4.04E-13
10	3.02E-08	1.04E-13
11	8.99E-08	3.10E-13
12	7.78E-09	2.69E-14
13	-	-
14	1.48E-08	5.11E-14
15	2.56E-08	8.82E-14
16	1.58E-08	5.45E-14
17	1.15E-08	3.97E-14
18	2.31E-08	7.97E-14
19	1.97E-07	6.80E-13
20	1.60E-07	5.51E-13
21	1.34E-08	4.63E-14
22	8.72E-09	3.01E-14
23	2.44E-07	8.42E-13
24	1.37E-08	4.74E-14
25	7.89E-08	2.72E-13
26	3.26E-08	1.13E-13
27	1.72E-08	5.92E-14
28	5.50E-08	1.90E-13
29	1.61E-08	5.54E-14
30	1.66E-08	5.73E-14
31	2.60E-08	8.99E-14
32	2.62E-08	9.04E-14
33	9.21E-09	3.18E-14
34	2.37E-08	8.19E-14
35	3.75E-08	1.30E-13

Appendix F: Presentation of Force versus Displacement Plots

Supplementary force versus displacement plots to the one included in Section 4.11.2 are included in the present appendix (Figures F-1 to F-5).
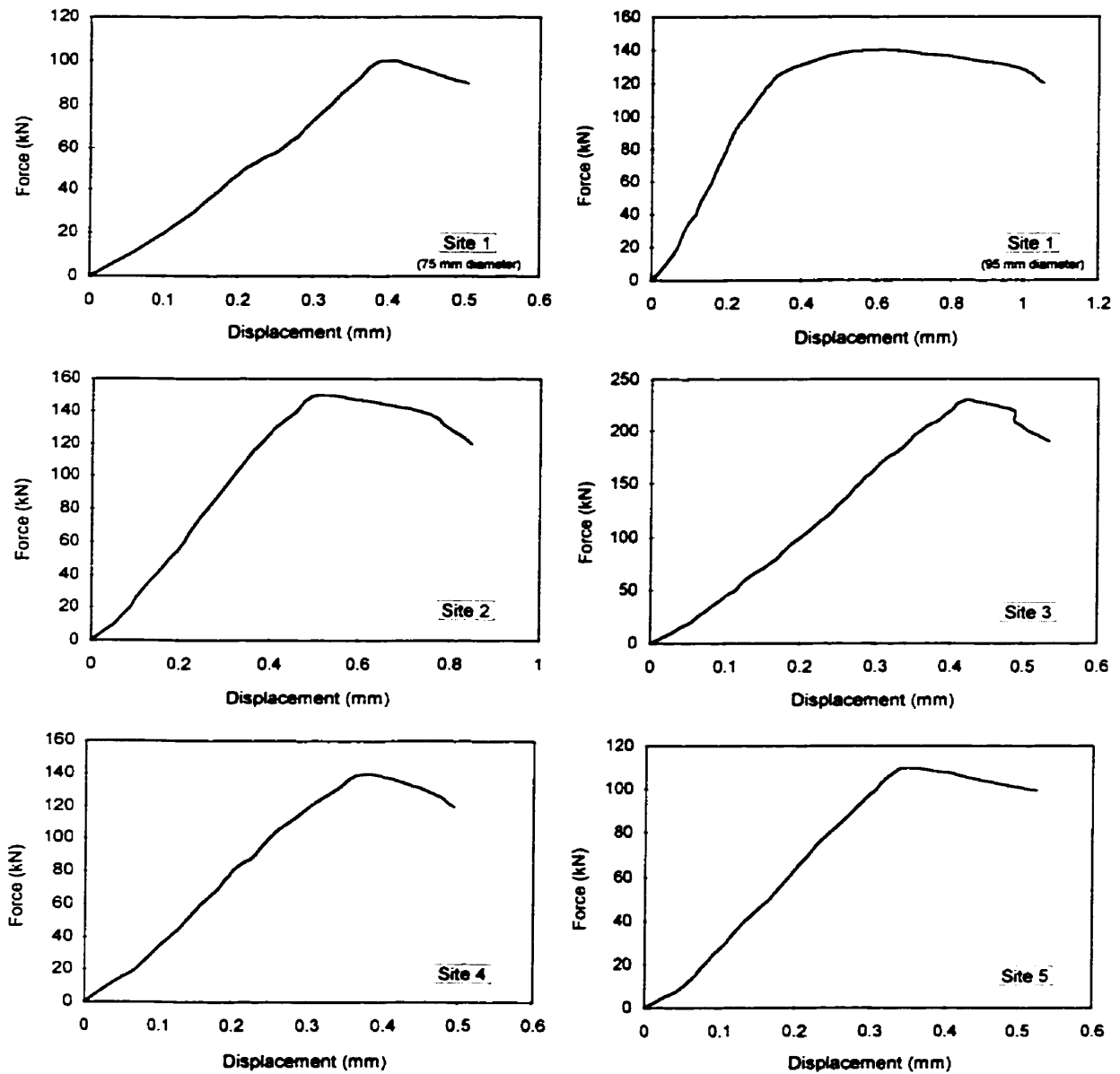
Figure F-1: *Force versus displacement plot (Sites 1-5)*

238
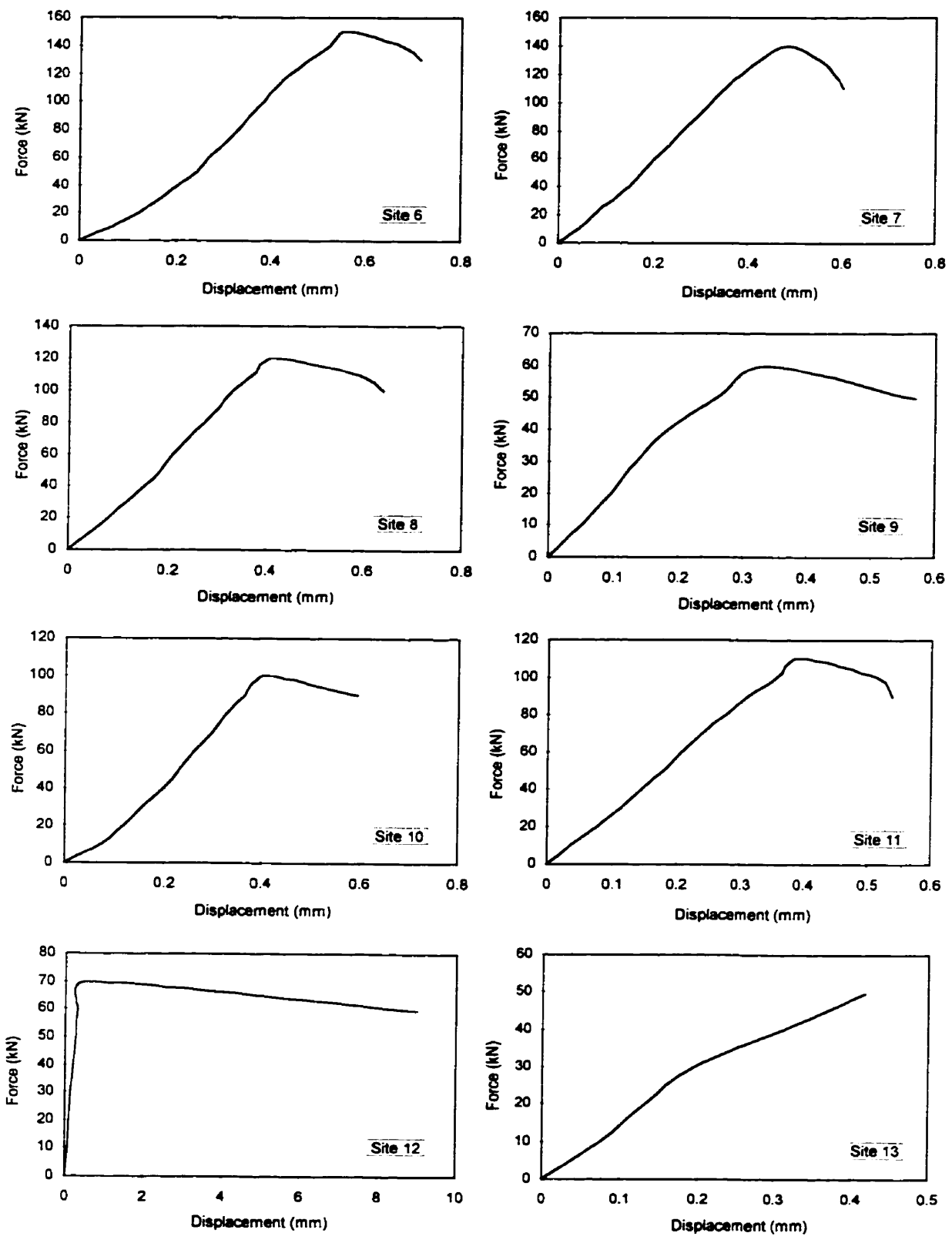
Figure F-2: *Force versus displacement plot (Sites 6-13)*
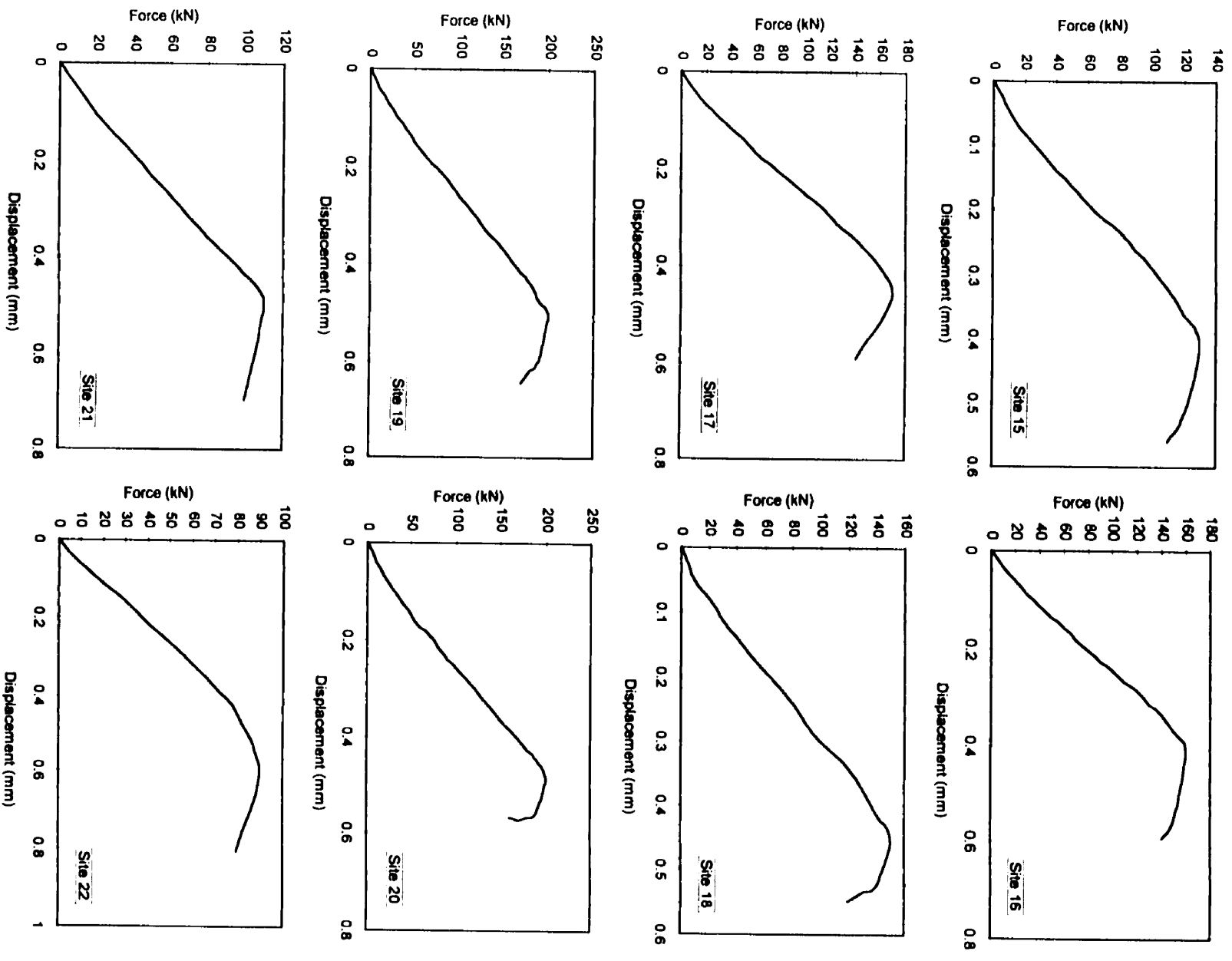
Figure F-3: *Force versus displacement plot (Sites 15-22)*
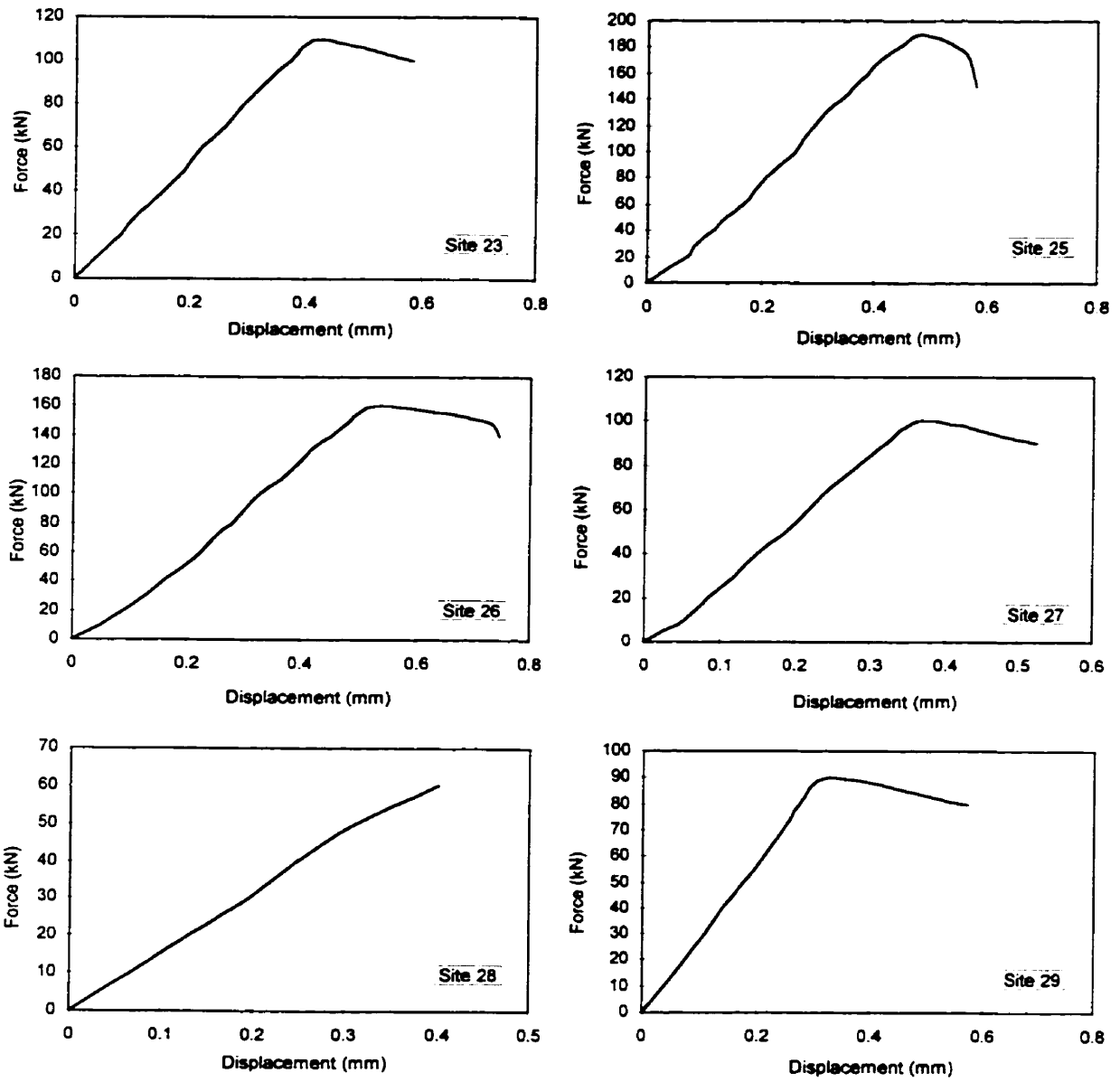
Figure F-4: *Force versus displacement plot (Sites 23-29)*
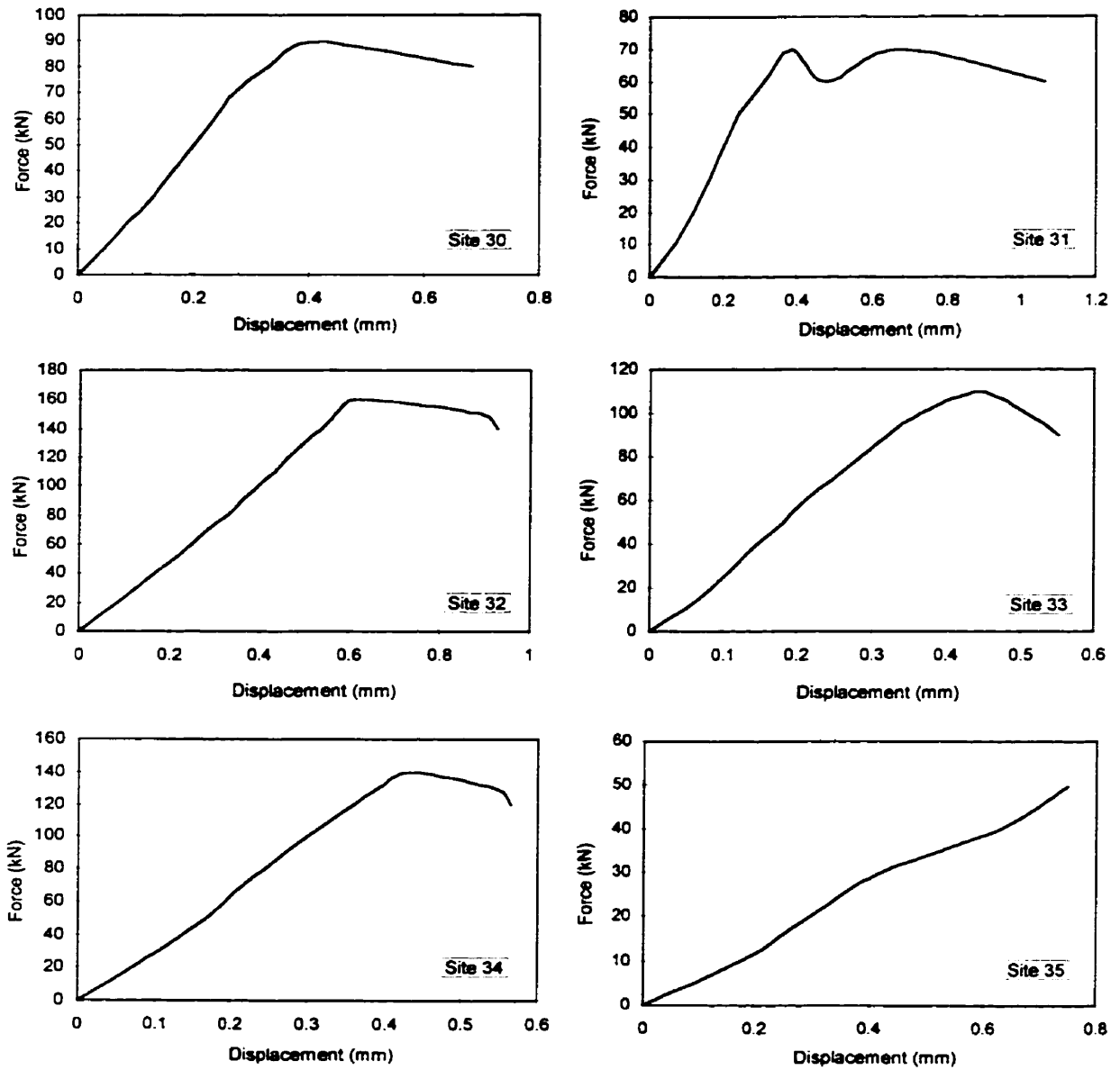
Figure F-5: *Force versus displacement plot (Sites 30-35)*

Appendix G: Univariate Analysis

The objective of this appendix is to illustrate supplementary details for Section 6.3.2. Stem-and-leaf diagrams, box-and-whisker plots, frequency distribution diagrams, and normal probability plots are included for all of the various parameters under investigation. It is noted that only the analysis for the entire bridge deck is included in the present appendix. The same procedure was performed for the east and the west sides of the bridge and the results are summarized in Tables 5-1 and 6-1. As indicated in Chapter 6, Analyses 1, 2 and 3 are the analyses undertaken to the as-collected data, without outliers and after application of transformation, respectively.

Corrosion Potential

The frequency distribution plot indicates that the data is skewed slightly negatively (log-normal distribution). However, no outliers are present. The normal probability plot is slightly curved. No transformation is applied as the ϕ_{corr} variable represents the concentration of oxygen in the Nernst equation and it has already been logged in obtaining the potential ϕ_{corr}.

Stem-and-Leaf diagram for ϕ_{corr} data
Leaf Unit = 10

```
  1  -7 0
  8  -6 7665555
 19  -6 44433321110
 41  -5 9999998888777776665555
 57  -5 4444433322222000
(13) -4 9998888776666
 67  -4 433333321100000
 52  -3 9999777766665555
 37  -3 4222211110
 27  -2 99988655
 19  -2 44442221000
  8  -1 97765
  3  -1 442
```

Box-and-Whisker plot of ϕ_{corr}

-720   -600   -480   -360   -240   -120

Frequency distribution diagram

Normal probability plot

Average: -443.6
Std Dev: 147.3
N of data: 137

Anderson-Darling Normality Test
A-Squared: 1.411
p-value: 0.001

Figure G-1: *Analysis 1 for corrosion potential (entire deck)*

Corrosion Rate

The frequency distribution plot indicates that the data is negatively skewed. This generally indicates the presence of outliers in the lower end of the distribution, and this is quite evident when the stem-and-leaf diagram and box-plot are studied (Figure G-2). There are eight outliers in the lower end. The normal probability appears to be curved. Besides the outliers, the data points seem to give a log-normal distribution.
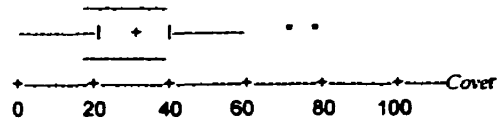
In order to determine the normality of the variable, the eight extreme values are removed and the process is repeated. The COV reduces to 0.48, but it is still high (Analysis 2 in Table 6-1). The normal probability plot is not linear and it appears still to be slightly curved. The data points seem to give a log-normal distribution (Figure G-3).
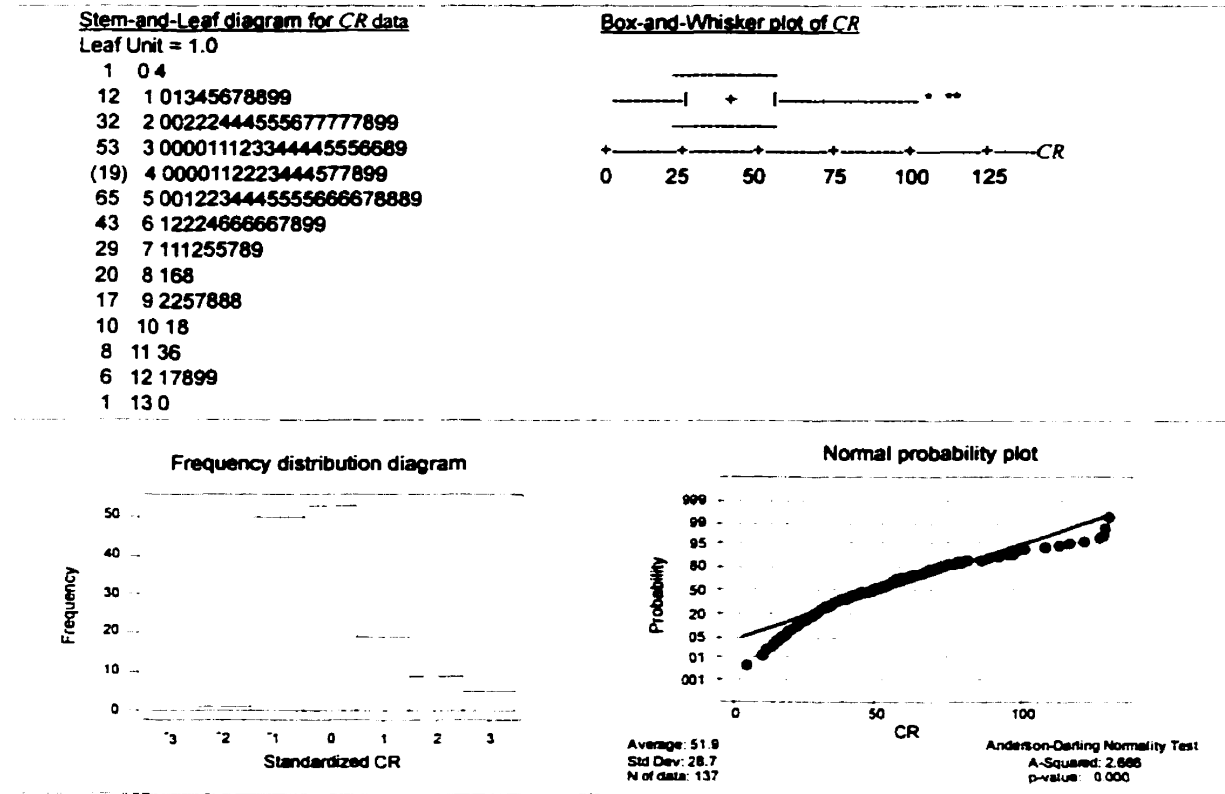
Figure G-2: *Analysis 1 for corrosion rate (entire deck)*
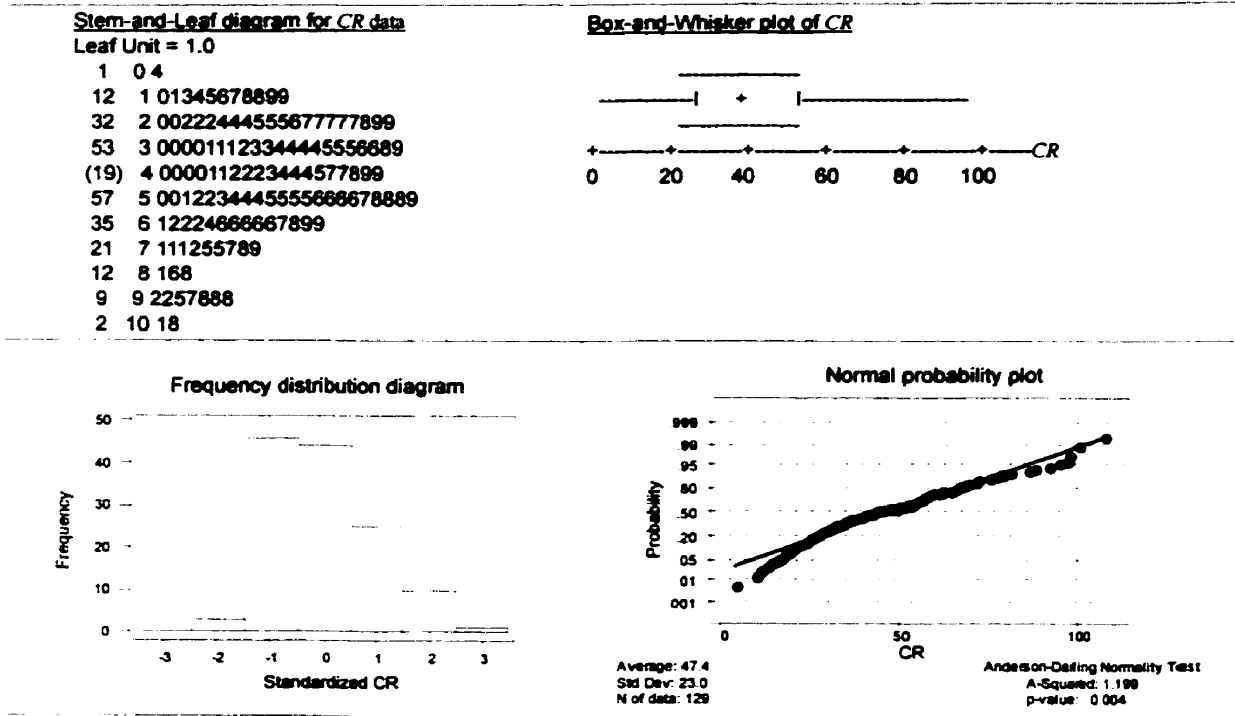
Figure G-3: *Analysis 2 for corrosion rate (entire deck)*

Even though it is accepted that corrosion rate exhibits a log-normal distribution, for later analysis (multivariate analysis), it is better to apply a logarithmic transformation to the variable in order to make the data dispersed and normally distributed. The transformation is applied and the process is repeated. The COV reduces to 0.16 (Analysis 3 in Table 6-1), which shows the transformation contributes to a great improvement (Figure G-4). The normal probability plot is now linear and the data points seem to give a normal distribution (Figure G-4).

245

Stem-and-Leaf diagram for LogCR data
Leaf Unit = 0.010

```
 1    6 0
 1    7
 1    8
 1    9
 3   10 04
 6   11 147
12   12 035577
23   13 00444888999
39   14 13333346677777999
53   15 011333334445579
(21) 16 000011222344457789999
63   17 0112333444444444566678999
39   18 01111112333555577899
20   19 0346678999
10   20 03568
 5   21 00111
```

Box-and-Whisker plot of LogCR

Frequency distribution diagram

Normal probability plot

Figure G-4: *Analysis 3 for corrosion rate (entire deck)*

Concrete Cover Thickness

Presence of outliers in the lower end of the distribution is quite evident when the stem-and-leaf diagram and box-plot are studied (Figure G-5). There are two outliers in the lower end. The normal probability plot is linear and besides the outliers, the data points seem to give a nearly normal distribution.

The two extreme values are removed and the process is repeated. The *COV* reduces to 0.45 (Analysis 2 in Table 6-1). The normal probability plot is linear. The data points seem to be slightly positive skewed (Figure G-6).

Stem-and-Leaf diagram for _Cover_ data
Leaf Unit = 1.0
```
   7   0 1111788
  24   1 00012222456778899
  55   2 0011222233444444555666777778899
 (24)  3 000001111222255555577899
  58   4 000111111222333334444445556666777899
  25   5 00000011234445667889
   6   6 046
   3   7
   3   8 11
   1   9 0
```
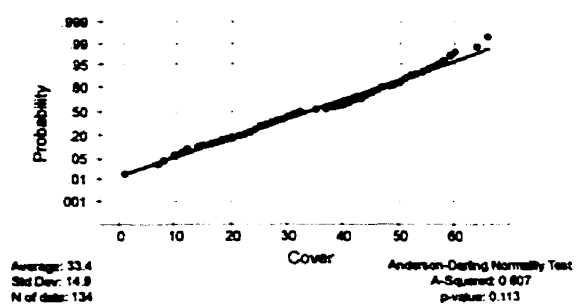
Box-and-Whisker plot of _Cover_

Frequency distribution diagram

Normal probability plot

Average: 34.5
Std Dev: 16.5
N of data: 137

Anderson-Darling Normality Test
A-Squared: 0.447
p-value: 0.277
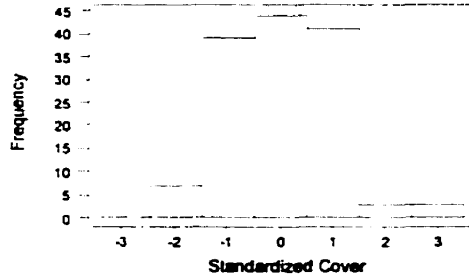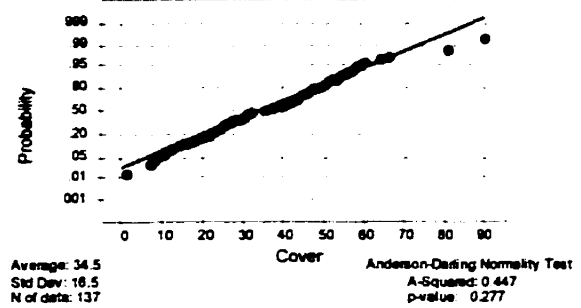
Figure G-5: _Analysis 1 for concrete cover thickness (entire deck)_

Stem-and-Leaf diagram for _Cover_ data
Leaf Unit = 1.0
```
   4   0 1111
   7   0 788
  16   1 000122224
  24   1 56778899
  40   2 0011222233444444
  55   2 555666777778899
 (13)  3 0000011112222
  66   3 55555577899
  55   4 000111111222333333444444
  34   4 555666777899
  22   5 000001123444
  10   5 5667889
   3   6 04
   1   6 6
```

Box-and-Whisker plot of _Cover_

Frequency distribution diagram

Normal probability plot

Average: 33.4
Std Dev: 14.9
N of data: 134

Anderson-Darling Normality Test
A-Squared: 0.807
p-value: 0.113
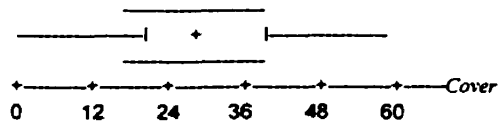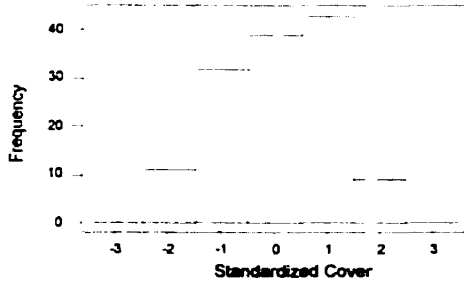
Figure G-6: _Analysis 2 for concrete cover thickness (entire deck)_

247

Percentage Chloride at Steel Level

The frequency distribution plot indicates that the data is negatively skewed. This generally indicates the presence of outliers in the lower end of the distribution, and this is quite evident when the stem-and-leaf diagram and box-plot are studied (Figure G-7). There are two outliers in the lower end.

The two extreme values are removed and the process is repeated. The COV reduces to 0.60, but it is still high (Analysis 2 in Table 6-1). The normal probability plot improved, in fact it appears to be linear (Figure G-8). The data points seem to give a log-normal distribution. No transformation is applied even though the $\%Cl$ variable represents the concentration of chloride ions at the steel level. With the transformation, the distribution becomes normalized, however, the COV increases to 1.41, therefore, for this reason no transformation is applied.
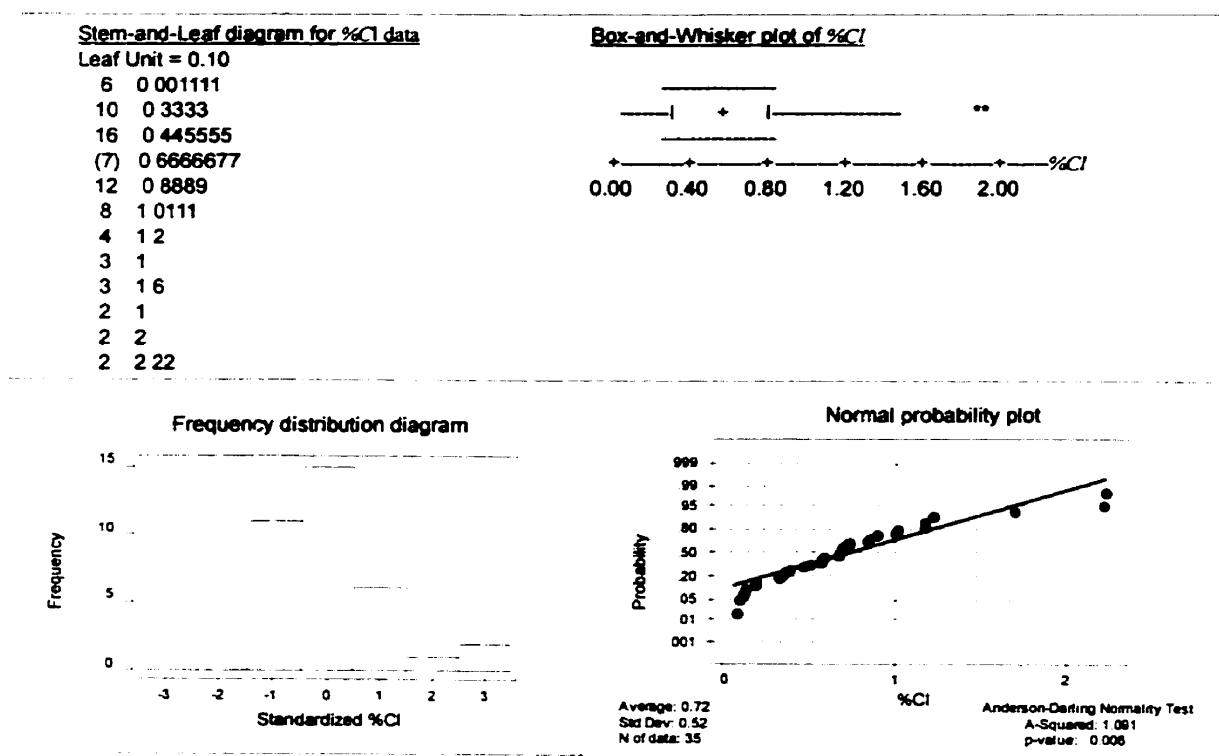
Figure G-7: *Analysis 1 for percentage chloride at steel level (entire deck)*

Stem-and-Leaf diagram for %Cl data
Leaf Unit = 0.010
```
 2   0 78
 6   1 1278
 6   2
10   3 1257
12   4 59
16   5 5667
(5)  6 57889
12   7 11
10   8 339
 7   9 9
 6  10 0
 5  11 666
 2  12 0
 1  13
 1  14
 1  15
 1  16 8
```

Box-and-Whisker plot of %Cl

Frequency distribution diagram

Normal probability plot

Average: 0.63
Std Dev: 0.38
N of data: 33

Anderson-Darling Normality Test
A-Squared: 0.347
p-value: 0.460
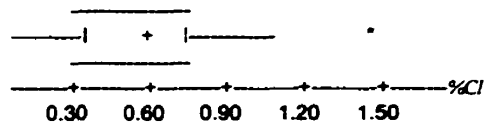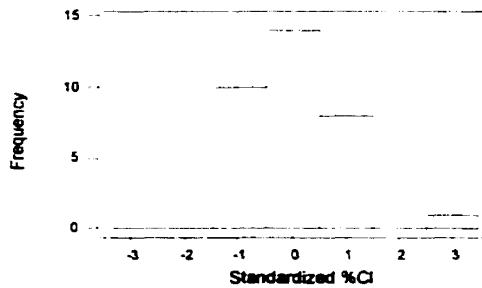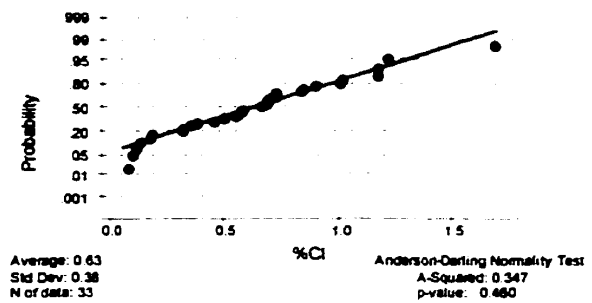
Figure G-8: *Analysis 2 for percentage chloride at steel level (entire deck)*

Apparent Chloride Diffusion Coefficient

The frequency distribution plot indicates that the data is negatively skewed indicating the presence of outliers in the lower end of the distribution shown in the stem-and-leaf diagram and the box plot (Figure G-9). There are two outliers in the lower end.

The two extreme values are removed and the process is repeated. The COV reduces to 0.62 (Analysis 2 in Table 6-1), but it is still high. The normal probability plot is still not linear (Figure G-10).

A common transformation used for physical properties is the logarithmic transformation to ensure normality. The transformation is applied and the process is repeated. The COV reduces to 0.40, which shows the transformation contributes to an improvement. The normal probability plot is linear and the data points seem to give a positively skewed distribution, which is common for diffusivity (Figure G-13).
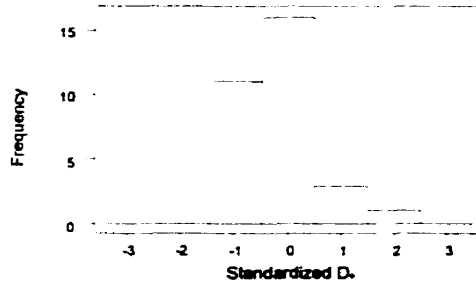
Stem-and-Leaf diagram for _Da_ data
Leaf Unit = 1.0 ($\times 10^{-9}$)

```
12    0 112222333344
(9)   0 556666999
11    1 0012334
 4    1 56
 2    2
 2    27
 1    3
 1    3
 1    4
 1    4
 1    51
```
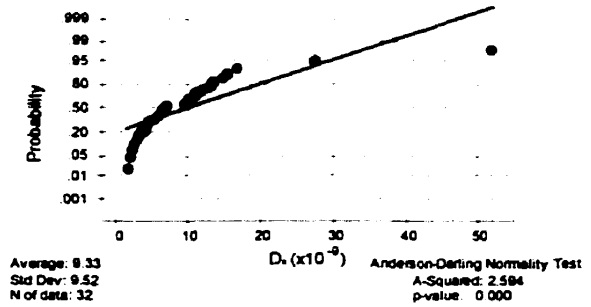
Box-and-Whisker plot of _D_

$D_a (\times 10^{-9})$

0   10   20   30   40   50

Frequency distribution diagram

Frequency

Standardized D_a

Normal probability plot

Probability

$D_a (\times 10^{-9})$

Average: 8.33
Std Dev: 9.52
N of data: 32

Anderson-Darling Normality Test
A-Squared: 2.594
p-value: 0.000
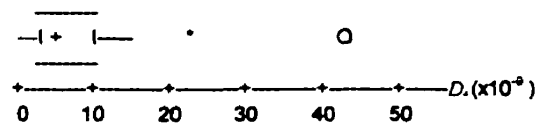
Figure G-9: *Analysis 1 for apparent chloride diffusion coefficient (entire deck)*

Stem-and-Leaf diagram for _D_ data
Leaf Unit = 0.10 ($\times 10^{-9}$)

```
 2    1 48
 6    2 0247
10    3 2569
12    4 19
14    5 77
(4)   6 1238
12    7
12    8
12    9 278
 9   10 77
 7   11 5
 6   12 4
 5   13 00
 3   14 5
 2   15 0
 1   16 6
```
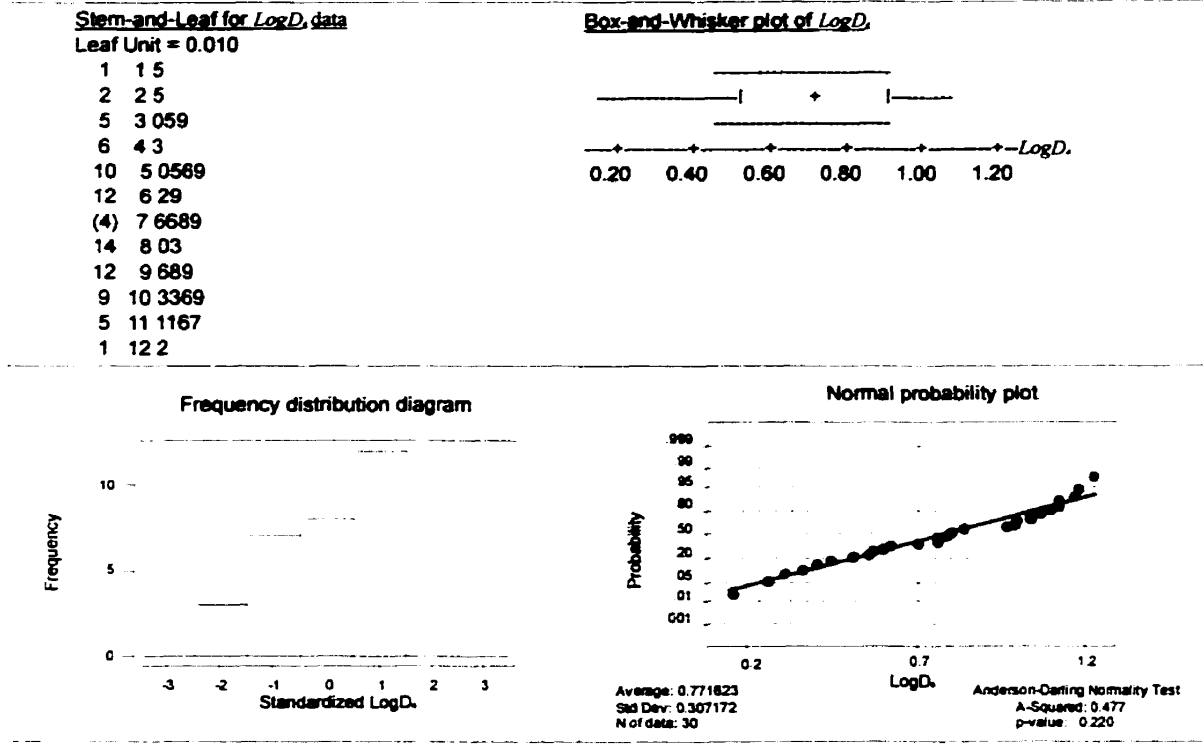
Box-and-Whisker plot of _D_

$D_a (\times 10^{-9})$

3.0   6.0   9.0   12.0   15.0

Frequency distribution diagram

Frequency

Standardized D_a

Normal probability plot

Probability

$D_a (\times 10^{-9})$

Average: 7.33
Std Dev: 4.51
N of data: 30

Anderson-Darling Normality Test
A-Squared: 0.775
p-value: 0.039
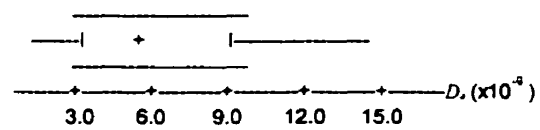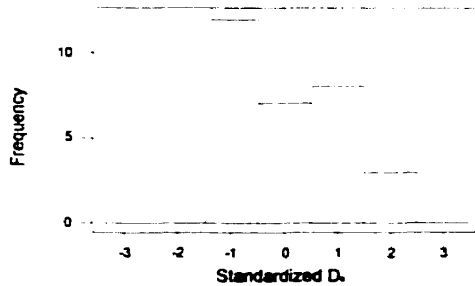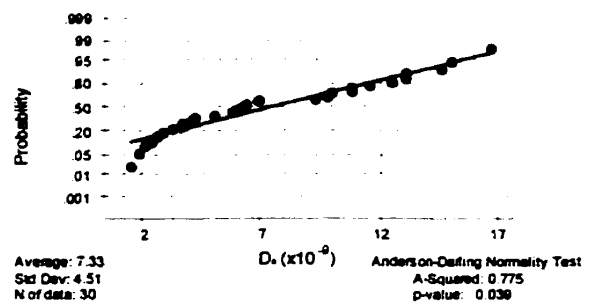
Figure G-10: *Analysis 2 for apparent chloride diffusion coefficient (entire deck)*

250

Stem-and-Leaf for LogD, data
Box-and-Whisker plot of LogD,

Leaf Unit = 0.010

```
 1    1 5
 2    2 5
 5    3 059
 6    4 3
10    5 0569
12    6 29
(4)   7 6689
14    8 03
12    9 689
 9   10 3369
 5   11 1167
 1   12 2
```

```
                  ———————————
     —————————|    +    |————
                  ———————————

  —+———————+———————+———————+———————+———————+—LogD.
 0.20    0.40    0.60    0.80    1.00    1.20
```

Frequency distribution diagram

Normal probability plot

```
        .999
         99
         95
         80
         50
         20
         05
         01
        .001
```

```
10 —

 5 —

 0 —
   -3   -2   -1    0    1    2    3
        Standardized LogD.
```

```
     0.2         0.7        1.2
                 LogD.
```

Average: 0.771823
Std Dev: 0.307172
N of data: 30

Anderson-Darling Normality Test
A-Squared: 0.477
p-value: 0.220

Figure G-11: *Analysis 3 for apparent chloride diffusion coefficient (entire deck)*

In-Situ Chloride Migration Coefficient

The frequency distribution plot indicates that the data is negatively skewed indicating the presence of one outlier in the lower end of the distribution as shown in the stem-and-leaf diagram and box-plot (Figure G-12).

The extreme value is removed and the process is repeated. The COV reduces to 0.46 (Analysis 2 in Table 6-1). The normal distribution plot is linear and the data points seem to give a log-normal distribution (Figure G-13).

The COV is quite high (0.46), hence the transformation is applied and the process is repeated. The COV reduces to 0.30, which shows that the transformation contributes to a great improvement. The normal distribution plot is linear and the data points give a nearly normal distribution (slightly positively skewed), which is common for diffusivity (Figure G-14).
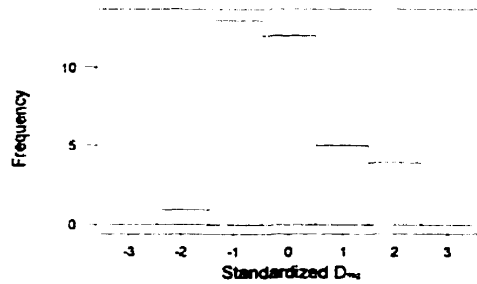
Stem-and-Leaf diagram for D_{nx} data
Leaf Unit = 0.10 (x10⁻⁶)

```
  2    1 69
  4    2 39
  9    3 01388
 15    4 244668
 17    5 09
(7)    6 1256777
 11    7 159
  8    8
  8    9 236
  5   10 27
  3   11 0
  2   12 0
  1   13 4
```
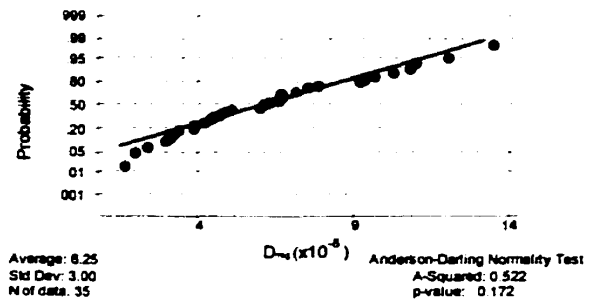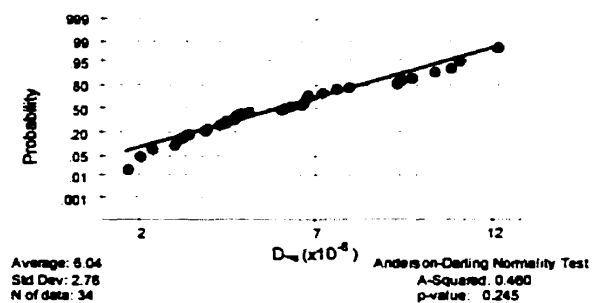
Box-and-Whisker plot of D_{nx}

D_{nx} (x 10⁻⁶)

2.5   5.0   7.5   10.0   12.5

Frequency distribution diagram

Frequency

10

5

0

-3 -2 -1 0 1 2 3

Standardized D_{nx}

Normal probability plot

Probability

999
99
95
80
50
20
05
01
001

4   9   14

D_{nx}(x10⁻⁶)

Average: 6.25
Std Dev: 3.00
N of data: 35

Anderson-Darling Normality Test
A-Squared: 0.522
p-value: 0.172
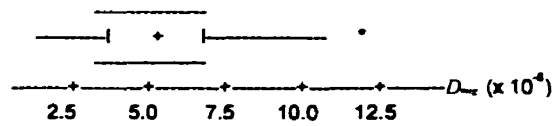
Figure G-12: *Analysis 1 for in-situ chloride migration coefficient (entire deck)*

Stem-and-Leaf diagram for D_{nx} data
Leaf Unit = 0.10 (x10⁻⁶)

```
  2    1 69
  4    2 39
  9    3 01388
 15    4 244668
 17    5 09
 17    6 1256777
 10    7 159
  7    8
  7    9 236
  4   10 27
  2   11 0
  1   12 0
```

Box-and-Whisker plot of D_{nx}

D_{nx} (x10⁻⁶)

2.0   4.0   6.0   8.0   10.0   12.0

Frequency distribution diagram

Frequency

10

5

0

-3 -2 -1 0 1 2 3

Standardized D_{nx}

Normal probability plot

Probability

999
99
95
80
50
20
05
01
001

2   7   12

D_{nx}(x10⁻⁶)

Average: 6.04
Std Dev: 2.78
N of data: 34

Anderson-Darling Normality Test
A-Squared: 0.460
p-value: 0.245
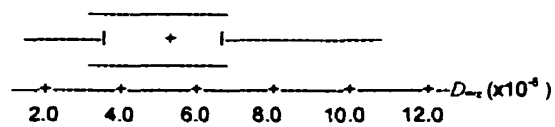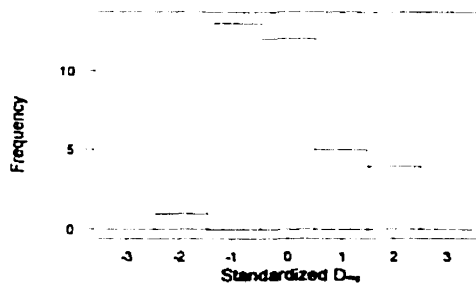
Figure G-13: *Analysis 2 for in-situ chloride migration coefficient (entire deck)*

252

Stem-and-Leaf diagram for _LogD_ data
Leaf Unit = 0.010

```
 1    2 1
 2    2 9
 2    3
 3    3 6
 3    4
 5    4 69
 7    5 02
 9    5 89
12    6 244
15    6 678
16    7 0
(3)   7 789
15    8 12222
10    8 579
 7    9
 7    9 678
 4    10 134
 1    10 8
```
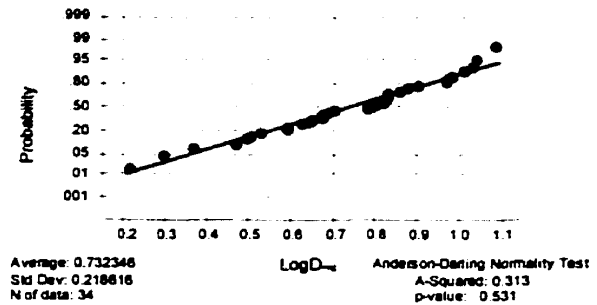
Box-and-Whisker plot of _LogD_

```
                                        LogD
   0.32   0.48   0.64   0.80   0.96
```

Frequency distribution diagram

Normal probability plot

Average: 0.732346
Std Dev: 0.218816
N of data: 34

LogD

Anderson-Darling Normality Test
A-Squared: 0.313
p-value: 0.531
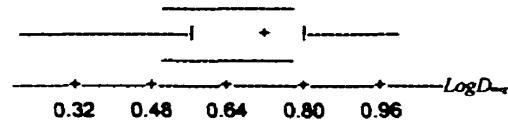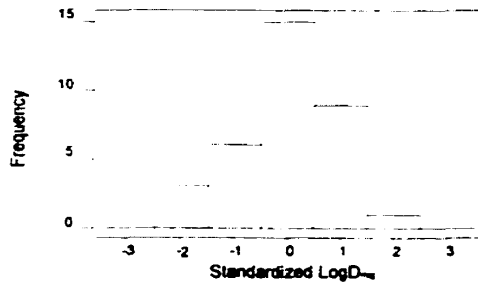
Figure G-14: *Analysis 3 for in-situ chloride migration coefficient (entire deck)*

Electrical Resistivity of Concrete

The frequency distribution plot indicates that the data is negatively skewed indicating the presence of 19 outliers in the lower end of the distribution (Figure G-15). The normal distribution plot is very much curved.

The 19 extreme values are removed and the process is repeated. The COV reduces to 0.43 (Analysis 2 in Table 6-1), but it is still high. The normal distribution plot is still not linear and the data points seem to give a log-normal distribution (Figure G-16).

The COV is quite high, hence the transformation is applied and the process is repeated. The COV reduces to 0.35 indicating that the transformation contributes to some improvement. The normal distribution plot is nearly linear and the data points seem to give a slightly positively skewed distribution, which is common for resistivity (Figure G-17).

253

Stem-and-Leaf diagram for ρ data
Leaf Unit = 1.0
```
   2   0 11
  45   0 222222222222222222222233333333333333333333333
 (42)  0 444444444444444444444444444555555555555555555555
  50   0 6666666666666667
  34   0 8888899999
  24   1 00111
  19   1 222233333
  10   1 45
   8   1 677
   5   1 89
   3   2 0
   2   2
   2   2 5
   1   2 6
```

Box-and-Whisker plot of ρ

Frequency distribution diagram

Normal probability plot

Average: 6.5
Std Dev: 4.7
N of data: 137

Anderson-Darling Normality Test
A-Squared: 9.932
p-value: 0.000

Figure G-15: *Analysis 1 for resistivity of concrete (entire deck)*

Stem-and-Leaf diagram for ρ data
Leaf Unit = 0.10
```
   2   1 48
  22   2 12355568888888888899
  45   3 012233333334667777789999
 (24)  4 011111223334577777888899
  49   5 0011124555555558899
  31   6 011123333566669
  16   7 2
  15   8 03359
  10   9 11223
   5  10 22
   3  11 001
```

Box-and-Whisker plot of ρ

Frequency distribution diagram

Normal probability plot

Average: 4.9
Std Dev: 2.1
N of data: 118

Anderson-Darling Normality Test
A-Squared: 2.885
p-value: 0.000

Figure G-16: *Analysis 2 for resistivity of concrete (entire deck)*

```
Stem-and-Leaf diagram for Logρ data
Leaf Unit = 0.010
    1   1 4
    2   2 4
    6   3 1469
   24   4 013333333333346678
   45   5 001111111235566668889999
  (26)  6 0111111222224577777778888999
   66   7 00124444444446677888889999
   42   8 01112235
   34   9 0113556666
   24  10 00444999
   16  11 01333368
    8  12 15569
    3  13 0
    2  14 12
```

Box-and-Whisker plot of Logρ
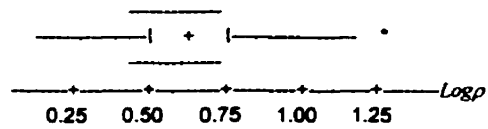
Frequency distribution diagram
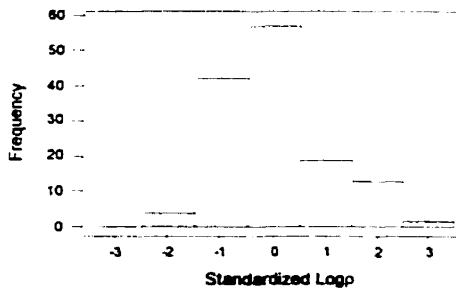
Normal probability plot
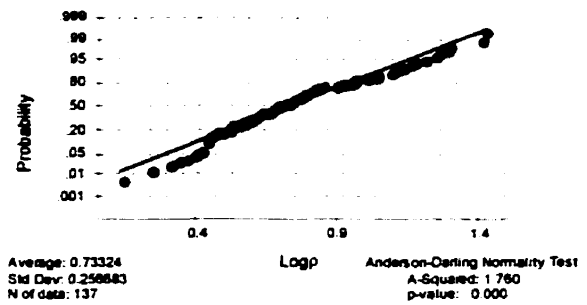
Figure G-17: *Analysis 3 for resistivity of concrete (entire deck)*

Coefficient of Permeability

The frequency distribution plot indicates that the data are negatively skewed indicating the presence of four outliers in the lower end of the distribution as shown by the stem-and-leaf diagram and box plot (Figure G-18). The normal probability plot is very much curved (Figure G-18).

The four extreme values are removed and the process is repeated. The COV reduces to 0.76 (Analysis 2 in Table 6-1). The normal distribution plot is still not linear and the data points seem to give a log-normal distribution (Figure G-19).

A logarithmic transformation is applied and the process is repeated and the COV reduces to 0.37, which shows that the transformation contributes to a great improvement. The normal distribution plot is nearly linear and the data points seem to give a slightly positively skewed distribution, which is common for permeability (Figure G-20).

255
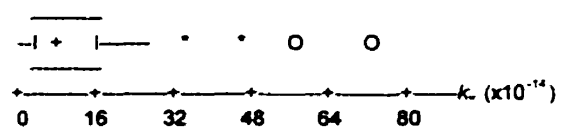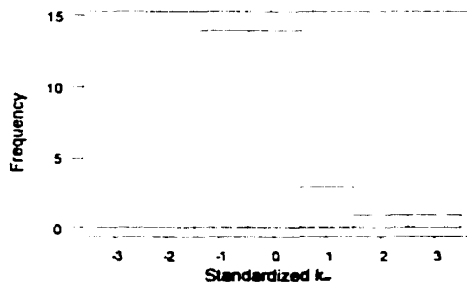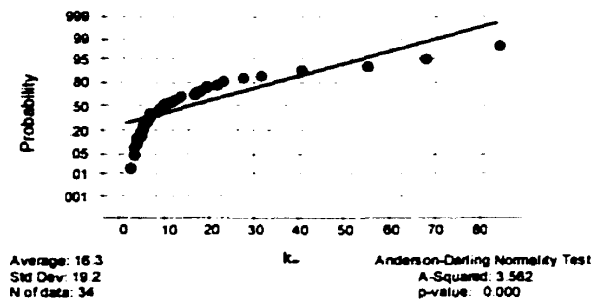
Figure G-18: *Analysis 1 for coefficient of permeability (entire deck)*

Stem-and-Leaf diagram for *k* data
Leaf Unit = 1.0 (x10⁻¹⁴)
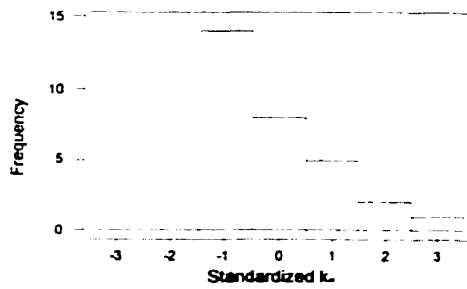
```
  1   0 1
  7   0 223333
 14   0 4455555
 15   0 7
 15   0 8889
 11   1 01
  9   1 2
  8   1
  8   1 667
  5   1 8
  4   2 1
  3   2 2
  2   2
  2   2 7
  1   2
  1   3 1
```
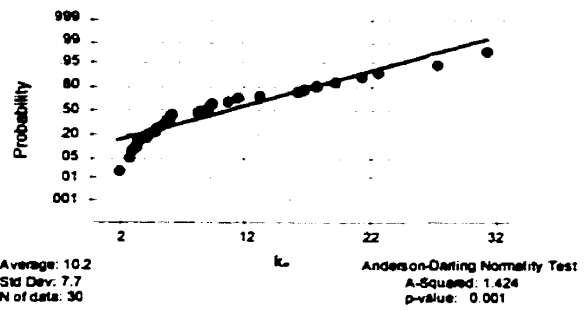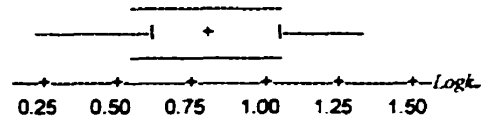
Box-and-Whisker plot of *k*

k (x10⁻¹⁴)

```
0.0   6.0   12.0   18.0   24.0   30.0
```

Frequency distribution diagram

Frequency

```
15
10
 5
 0
      -3  -2  -1   0   1   2   3
         Standardized k
```

Normal probability plot

Probability

```
999
 99
 95
 80
 50
 20
 05
 01
001
      2      12      22      32
                 k
```

Average: 10.2
Std Dev: 7.7
N of data: 30

Anderson-Darling Normality Test
A-Squared: 1.424
p-value: 0.001
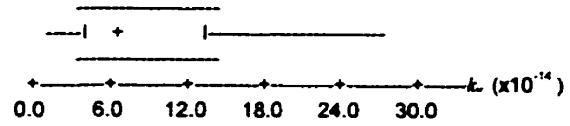
Figure G-19: *Analysis 2 for coefficient of permeability (entire deck)*

257
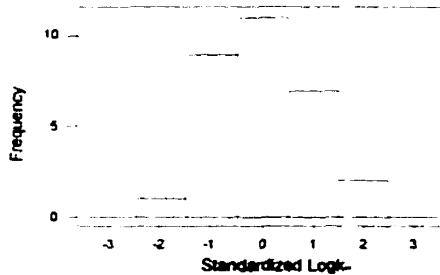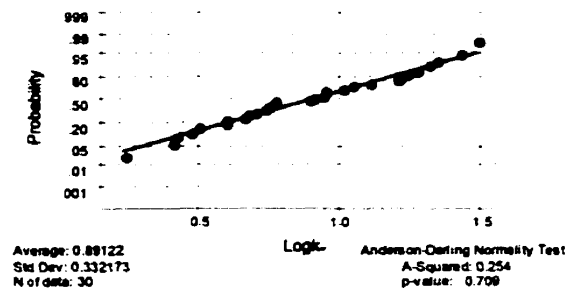
Figure G-20: *Analysis 3 for coefficient of permeability (entire deck)*

Compressive Strength

The frequency distribution plot indicates that the data is normal. This generally indicates absence of outliers, and this is quite evident when the stem and leaf diagram and box plot are studied (Figure G-21). The normal probability plot is linear and the data points seem to give a normal distribution. No transformation is required.
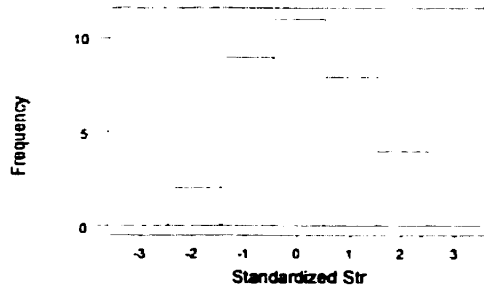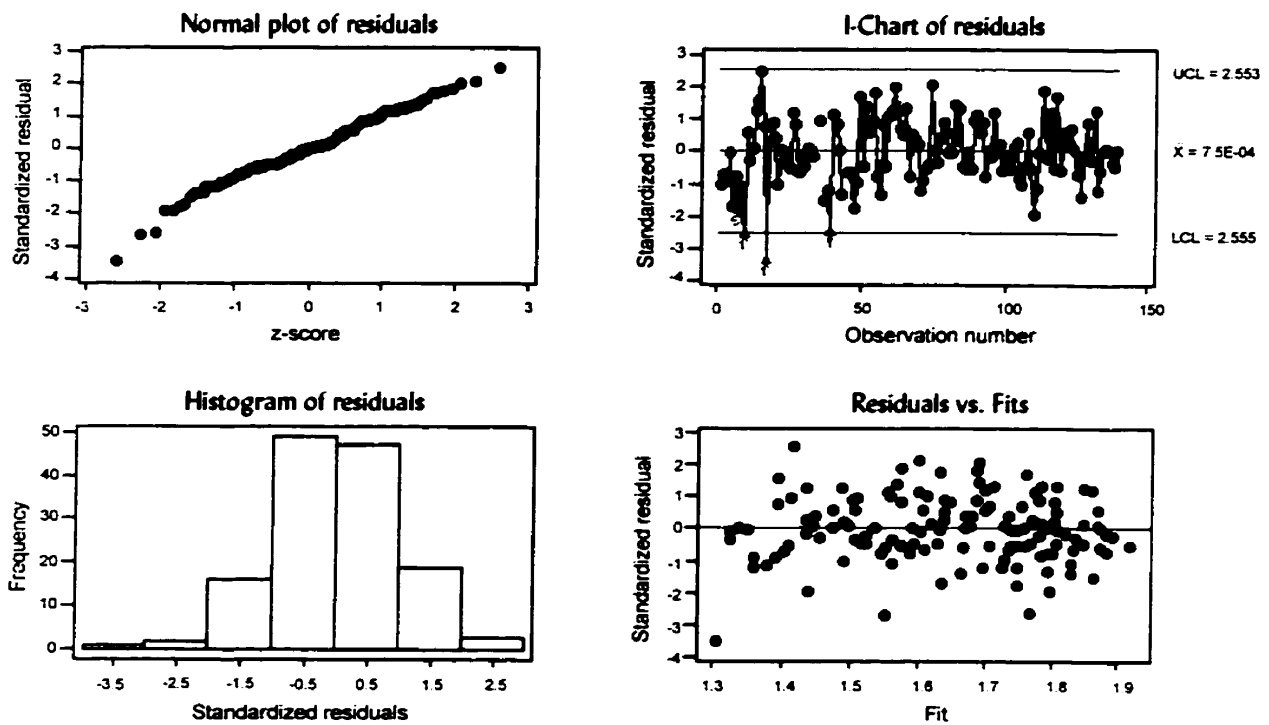
Stem-and-Leaf diagram for _Str_ data
Leaf Unit = 1.0

```
 4    1 0234
 6    1 59
14    2 00002334
(5)   2 55555
15    3 01123334
 7    3 566
 4    4 23
 2    4 58
```

Box-and-Whisker plot of _Str_


```
14.0   21.0   28.0   35.0   42.0   49.0
```

Frequency distribution diagram

Normal probability plot

Average: 27.1
Std Dev: 9.6
N of data: 34

Anderson-Darling Normality Test
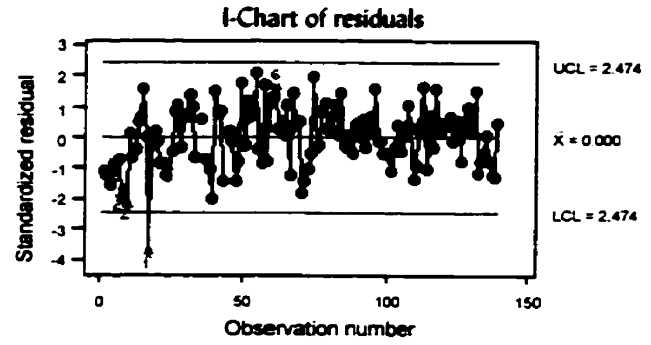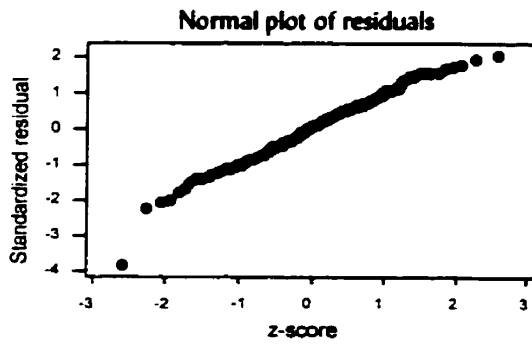A-Squared: 0.344
p-value: 0.466
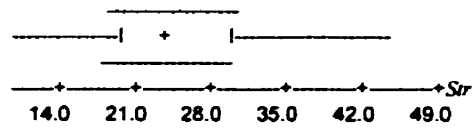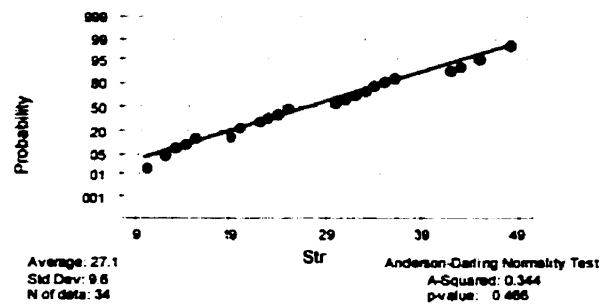
Figure G-21: *Analysis 1 for compressive strength (entire deck)*
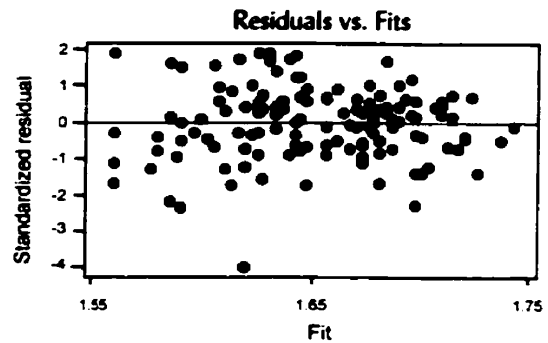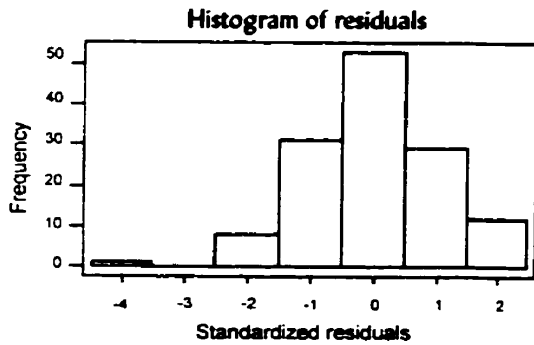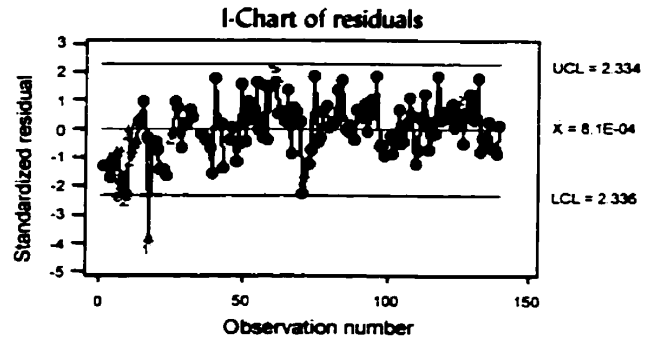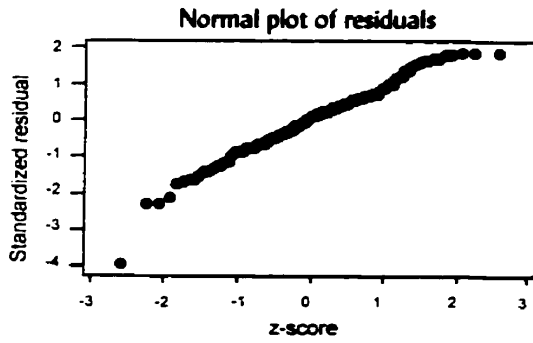
259

Appendix H: Residual Model Diagnostics

The objective of this appendix is to illustrate supplementary details for Section 6.3.3.1. Normal plot of residuals, histogram of residuals, I-chart of residuals, and residual versus fits plot are included for all of the various parameters under investigation. It is noted that only the analysis for the entire bridge deck is included in the present appendix. The same procedure was undertaken for the east and west sides of the bridge and the results are summarized in Tables 6-2 to 6-4.

Figure H-1: *Standardized residual model diagnostics for 'ϕ_{corr}' (entire deck)*

Normal plot of residuals

Standardized residual vs z-score

I-Chart of residuals

Standardized residual vs Observation number

UCL = 2.474
X = 0.000
LCL = 2.474

Histogram of residuals

Frequency vs Standardized residuals

Residuals vs. Fits

Standardized residual vs Fit
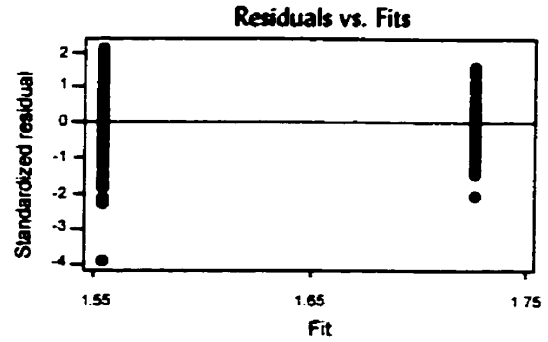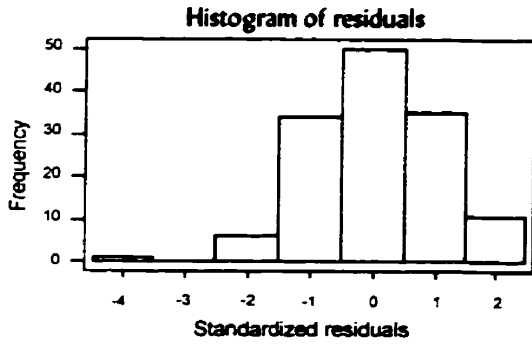
Figure H-2: *Standardized residual model diagnostics for 'Delam' (entire deck)*

Normal plot of residuals

Standardized residual vs z-score

I-Chart of residuals

Standardized residual vs Observation number

UCL = 2.334
X = 8.1E-04
LCL = 2.336

Histogram of residuals

Frequency vs Standardized residuals

Residuals vs. Fits

Standardized residual vs Fit

Figure H-3: *Standardized residual model diagnostics for 'Cover' (entire deck)*
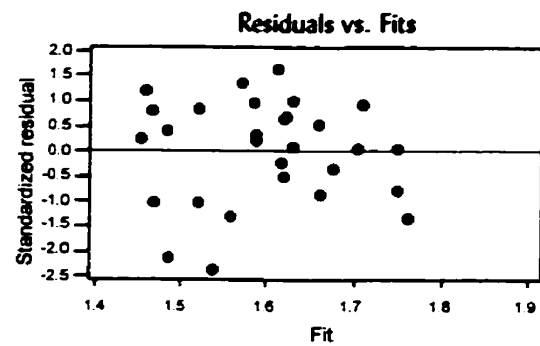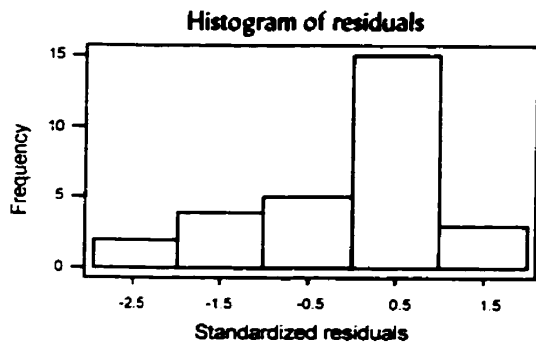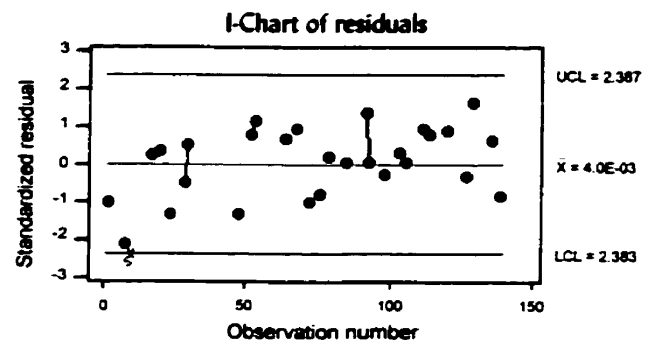
261

Figure H-4: *Standardized residual model diagnostics for '%Cl' (entire deck)*

Figure H-5: *Standardized residual model diagnostics for 'LogD$_a$' (entire deck)*
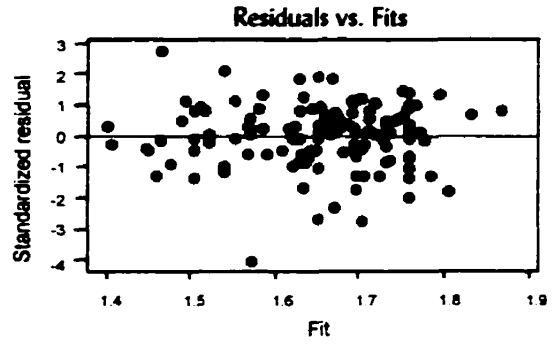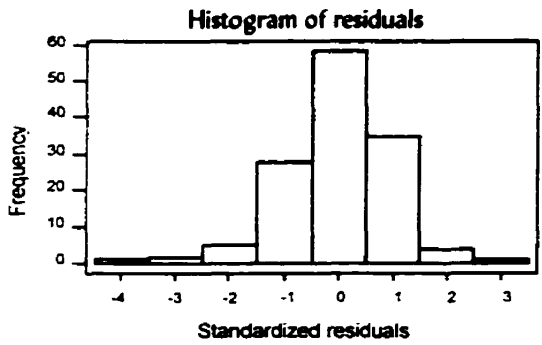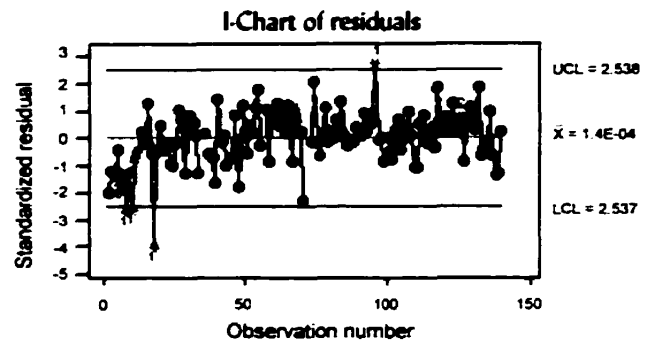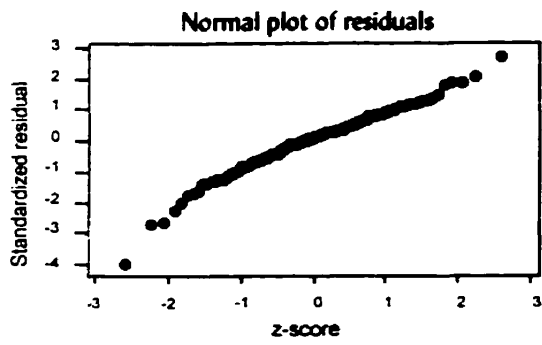
Figure H-6: *Standardized residual model diagnostics for 'Logp'(entire deck)*
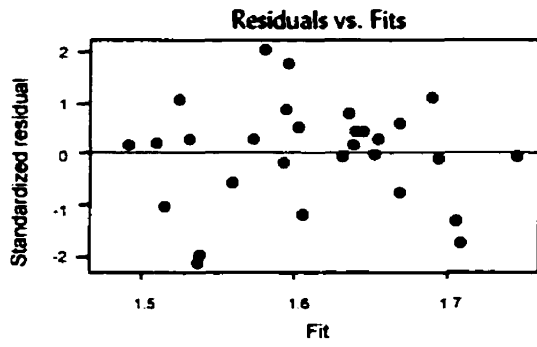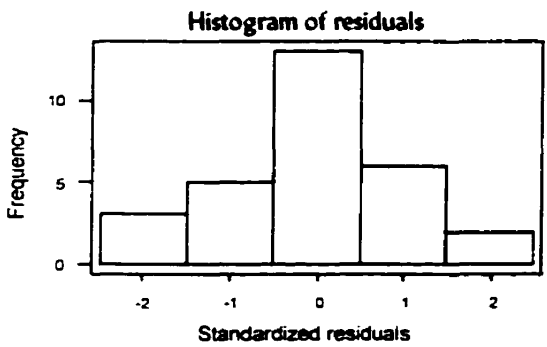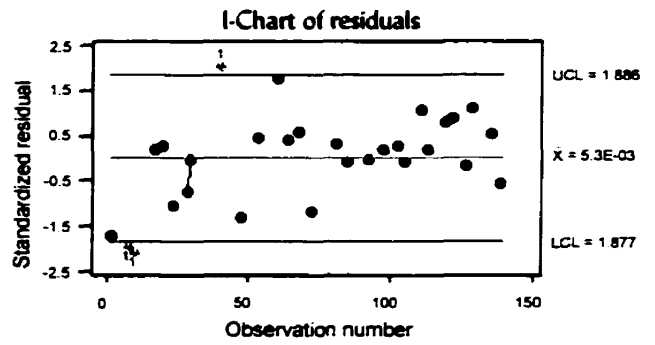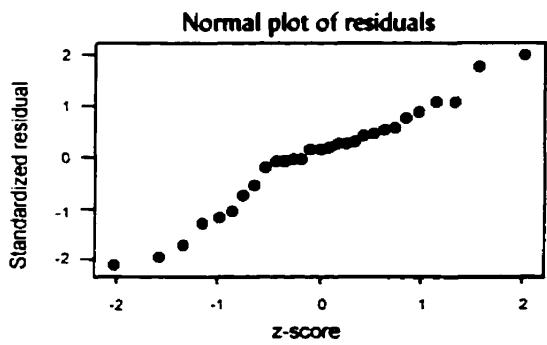
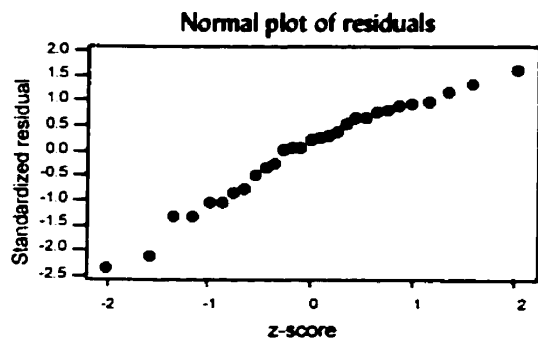
Figure H-7: *Standardized residual model diagnostics for 'Logk_w'(entire deck)*
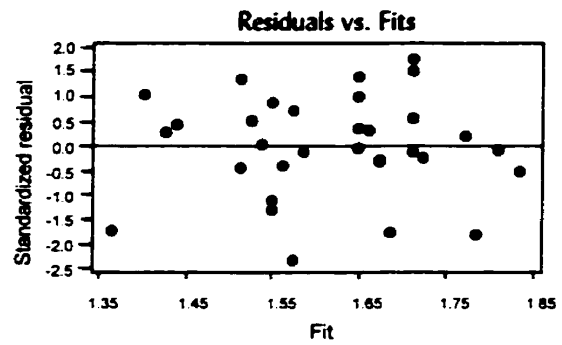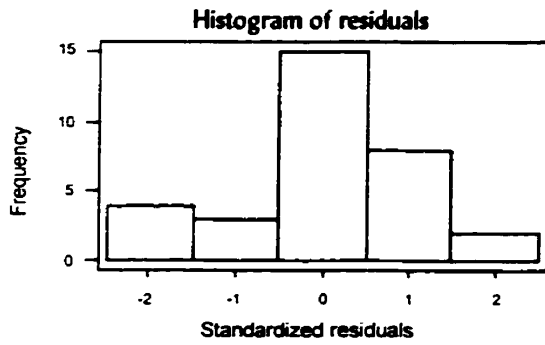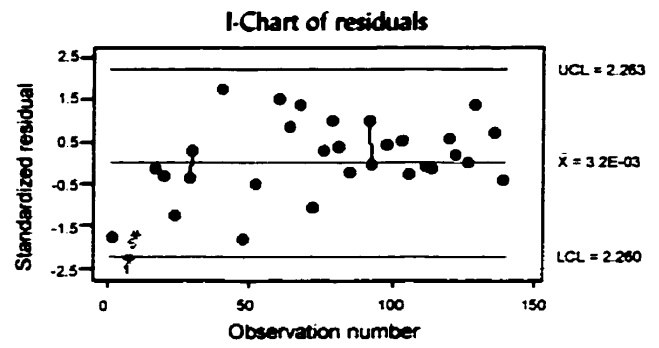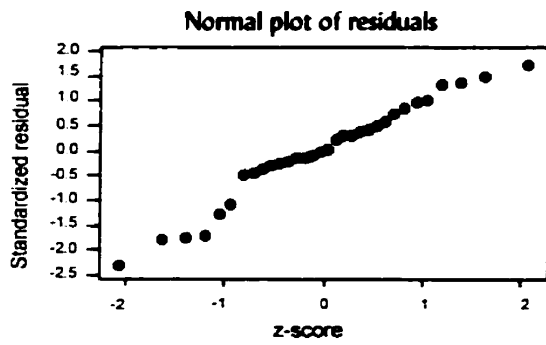
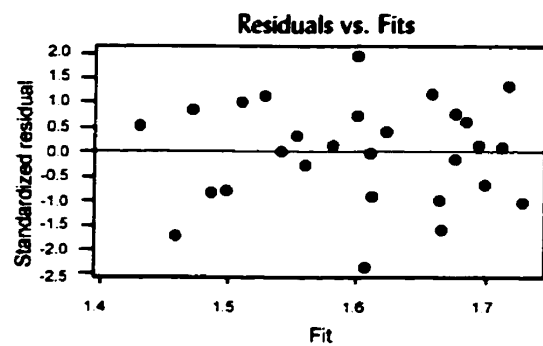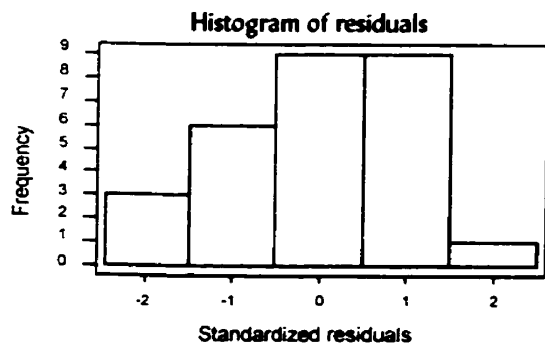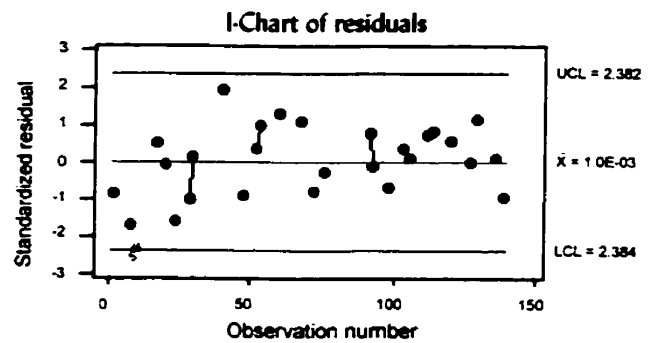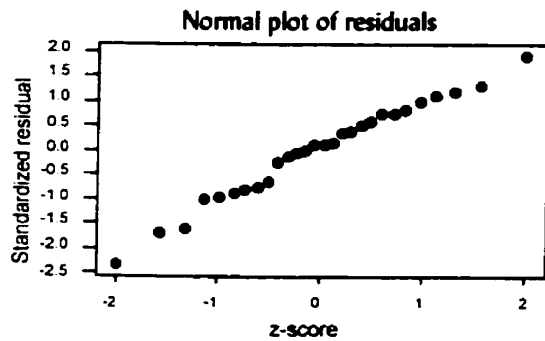**Figure H-8:** *Standardized residual model diagnostics for 'Str'(entire deck)*

Appendix I: Multivariate Statistical Analysis

The objective of this appendix is to illustrate supplementary details for Section 6.4. A list of ANOVA tables is included to determine the significance of the addition of a variable in a model. The summary of these results are listed in Tables 6-9 and 6-10. The analysis is subdivided in two as explained in Section 6.3.1, that is using the 'Assessment' and the 'Prediction' methods separately. Three models are obtained i.e. (a) the entire bridge deck, (b) the east side of the bridge deck, and (c) the west side of the bridge deck.

The procedures most commonly used to select a model are the forward, backward and stepwise selection. The forward selection procedure is used in this study. The first predictor that enters the equation is the one with the highest simple correlation with y. If this predictor is significant, the remaining variables are tested in turn and the F-ratio and R^2 are calculated to consider if the addition of the variable is significant (at an $\alpha = 0.05$ level of significance). At some point, a given predictor is not significant and the procedure is terminated. It is noted that in the forward selection procedure, once a variable enters the equation, it is not removed[102]. There are an infinite number of ANOVA tables, which can be constructed from these variables, but only the tables considered relevant are presented here. The model tested (Ω) and the model against which it was tested (ω) are presented along with F-ratio and the result of the significance test, i.e., whether it is significant or not.

Multiple Linear Regression Using 'Assessment Methods' (Entire Bridge Deck)

The first step of the analysis is to determine if the variable with the highest simple correlation with $LogCR$ is significant. The results (Table I-1) indicate that the ϕ_{corr} variable is indeed significant in predicting $LogCR$ as the F-ratio value is much greater than the $F_{critical}$ value (3.84).

Table I-1: *One variable (entire bridge deck)*

SOURCE	DOF	SSE	MS	F	R^2
Difference	1	3.3628	3.3628	77.080	0.366
Intercept + ϕ_{corr} (Ω)	135	5.8352	0.0432		
Intercept (ω)	136	9.1980			

The next step is to determine which variable can be added to ϕ_{corr} significantly. Each variable is tested in turn (Table I-2), and the results indicate that $LogD_a$, %Cl and Delam can be added to the model, with variable $LogD_a$ performing best. There is an increase in R^2 of 5.2% and the F-value is greater than the acceptable $F_{critical}$ value (3.38 with a DOF of 28).

Table I-2: Two variables (entire bridge deck)

VARIABLE	R^2	ΔR^2	F-VALUE	SSE	DOF
Delam	37.8%	+1.2%	40.69	5.7226	134
Cover	35.1%	-1.5%	35.35	5.8238	131
%Cl	39.8%	+3.2%	9.24	1.2207	28
$LogD_a$	41.8%	+5.2%	8.97	1.1656	25

The next step consists of determining which variables can be added to ϕ_{corr} and $LogD_a$ significantly. Each of the remaining variables was tested in turn (Table I-3), and the results indicate that all three variables can be added to the model, with variable %Cl performing best.

Table I-3: Three variables (entire bridge deck)

VARIABLE	R^2	ΔR^2	F-VALUE	SSE	DOF
Delam	42.1%	+0.3%	5.82	1.15872	24
Cover	42.1%	+0.3%	5.81	1.15921	24
%Cl	42.3%	+0.5%	5.86	1.15559	24

Each of the remaining variables was tested in turn (Table I-4), and the results indicate that Delam performs the best when be added to ϕ_{corr}, $LogD_a$ and %Cl.

Table I-4: Four variables (entire bridge deck)

VARIABLE	R^2	ΔR^2	F-VALUE	SSE	DOF
Delam	42.8%	+0.5%	4.30	1.14578	23
Cover	42.4%	+0.1%	4.23	1.15304	23

The last step is to determine if the last variable, *Cover*, can be added to ϕ_{corr}, $LogD_a$, %*Cl* and *Delam* significantly. The results indicate that there is no improvement in the correlation coefficient when adding the variable to the model (Table I-5). However, the *F*-value is larger than the critical value of 2.66, indicating that the *Cover* variable is significant when added to the model.

Table I-5: *Proposed 'Assessment Methods' model (entire bridge deck)*

SOURCE	DOF	SSE	MS	F	R²
Difference	5	0.85647	0.17129	3.29	0.428
Intercept + ϕ_{corr} +$LogD_a$ + %*Cl* + *Delam* + *Cover* (Ω)	22	1.14532	0.05206		
Intercept + ϕ_{corr} +$LogD_a$ + %*Cl* + *Delam* (ω)	27	2.00179			

Multiple Linear Regression Using 'Prediction Methods' (Entire Bridge Deck)

To determine the significance of a model Ω, the same procedure as in the previous section is followed using ANOVA tables. The first step of the analysis is to determine the first variable to be included in the model. The $LogD_{mig}$ variable was selected as it performed the best in the regression of the individual variables. The following ANOVA table results:

Table I-7: *One variable (entire bridge deck)*

SOURCE	DOF	SSE	MS	F	R²
Difference	1	0.63737	0.63737	13.80	0.315
Intercept + $LogD_{mig}$ (Ω)	30	1.38563	0.04619		
Intercept (ω)	31	2.02300			

The results indicate that the $LogD_{mig}$ variable is indeed significant (Table I-7). Each variable is tested in turn (Table I-8), and the results indicate that *Str*, *Logρ* and *Logk_v* can be added significantly to $LogD_{mig}$, with the variable *Str* performing best.

Table I-8: *Two variables (entire bridge deck)*

VARIABLE	R^2	ΔR^2	F-VALUE	SSE	DOF
Logp	35.9%	+4.4%	7.83	1.22664	28
Logk$_w$	36.0%	+4.5%	7.02	1.23715	25
Str	49.0%	+17.5%	13.45	1.02190	28

Each of the remaining variables was tested in turn (Table I-9), and the results indicate that both variables can be added to $LogD_{mig}$ and *Str* significantly, with variable *Logp* performing best.

Table I-9: *Three variables (entire bridge deck)*

VARIABLE	R^2	ΔR^2	F-VALUE	SSE	DOF
Logp	51.8%	+2.8%	9.30	0.91475	26
Logk$_w$	50.7%	+1.7%	7.88	0.94264	23

The last step consists of determining if the last variable, *Logk$_w$*, can be added to $LogD_{mig}$, *Str* and *Logp* significantly. The results indicate that there is an improvement in correlation coefficient when adding the variable and the F-value is larger than the critical value of 2.84, hence, the addition is significant (Table I-10).

Table I-10: *Proposed 'Prediction Methods' model (entire bridge deck)*

SOURCE	DOF	SSE	MS	F	R^2
Difference	4	0.95935	0.23984	5.93	0.530
Intercept + $LogD_{mig}$ + *Str* + *Logp* + *Logk$_w$* (Ω)	21	0.84938	0.04045		
Intercept + $LogD_{mig}$ + *Str* + *Logp* (ω)	25	1.80873			

Multiple Linear Regression Using 'Assessment Methods' (East Side of Deck)

The first step of the analysis is to determine the first variable to be included in the model. The ϕ_{corr} variable was selected as it performed the best in the regression of the individual variables. The results indicate that the ϕ_{corr} variable is indeed significant (Table I-11).

Table I-11: *One variable (east side of deck)*

SOURCE	DOF	SSE	MS	F	R²
Difference	1	1.8116	1.8116	29.24	0.317
Intercept + ϕ_{corr} (Ω)	63	3.9038	0.0620		
Intercept (ω)	64	5.7155			

The next step is to determine which variable can be added to ϕ_{corr} significantly. Each variable is tested in turn (Table I-12), and the results indicate that all four variables can be added, with variable %Cl performing best.

Table I-12: *Two variables (east side of deck)*

VARIABLE	R²	ΔR²	F-VALUE	SSE	DOF
Delam	32.1%	+0.4%	14.68	3.87872	62
Cover	35.1%	+1.0%	14.59	3.75958	60
%Cl	42.4%	+10.7%	4.42	0.88312	12
LogD$_a$	42.2%	+10.5%	4.01	0.86722	11

Each of the remaining variables was tested in turn (Table I-13), and the results indicate that only the *Cover* variable ($F_{critical}$ = 3.59) can be added to ϕ_{corr} and %Cl significantly.

Table I-13: *Three variables (east side of deck)*

VARIABLE	R^2	ΔR^2	F-VALUE	SSE	DOF
Delam	45.0%	+2.6%	3.00	0.84342	11
Cover	49.8%	+7.4%	3.63	0.77046	11
LogD$_a$	42.2%	-0.2%	2.43	0.86685	10

Each of the remaining variables was tested in turn (Table I-14), and the results indicate that neither of the two variables add significance to the ϕ_{corr} and %*Cl* and *Cover* model. Even though the correlation coefficient increases with the addition of *Delam* or *LogD$_a$*, the F-ratio is smaller than the $F_{critical}$ (3.48 and 3.63, respectively). Hence, the proposed model is without the addition of *Delam* and *LogD$_a$* (Table I-15).

Table I-14: *Four variables (east side of deck)*

VARIABLE	R^2	ΔR^2	F-VALUE	SSE	DOF
Delam	51.5%	+1.7%	2.66	0.74325	10
LogD$_a$	49.9%	+0.1%	2.24	0.75201	9

Table I-15: *Proposed 'Assessment Methods' model (east side of deck)*

SOURCE	DOF	SSE	MS	F	R^2
Difference	3	0.76351	0.25450	3.63	0.498
Intercept + ϕ_{corr} + %*Cl* + *Cover* (Ω)	11	0.77046	0.07004		
Intercept + ϕ_{corr} + %*Cl* (ω)	14	1.53397			

Multiple Linear Regression Using 'Prediction Methods' (East Side of Deck)

The first step of the analysis is to determine the first variable to be included in the model. The *LogD$_{mig}$* variable was selected as it performed the best in the regression of the individual variables. The following ANOVA table results:

270

Table I-16: *One variable (east side of deck)*

SOURCE	DOF	SSE	MS	F	R^2
Difference	1	0.73047	0.73047	11.45	0.488
Intercept + $LogD_{mig}$ (Ω)	12	0.76529	0.06377		
Intercept (ω)	13	1.49576			

The results indicate that the $LogD_{mig}$ variable is indeed significant (Table I-16). Each variable is tested in turn (Table I-17), and the results indicate that Str, and $Log\rho$ can be added significantly to $LogD_{mig}$, with variable Str performing best.

Table I-17: *Two variables (east side of deck)*

VARIABLE	R^2	ΔR^2	F-VALUE	SSE	DOF
$Log\rho$	50.5%	+1.7%	5.62	0.73972	11
$Logk_w$	48.7%	-0.1%	4.75	0.75561	10
Str	71.8%	+23.0%	12.70	0.41247	10

Each of the remaining variables was tested in turn (Table I-18), and the results indicate that both variables can be added to $LogD_{mig}$ and Str significantly, with variable $Logk_w$ performing best.

Table I-18: *Three variables (east side of deck)*

VARIABLE	R^2	ΔR^2	F-VALUE	SSE	DOF
$Log\rho$	72.6%	+0.8%	7.93	0.40069	9
$Logk_w$	76.4%	+4.6%	8.61	0.33909	8

The last step consists of determining if the last variable, $Log\rho$, can be added to $LogD_{mig}$, Str and $Logk_w$ significantly. The results indicate that it is indeed significant (Table I-19).

Table I-19: *Proposed 'Prediction Methods' model(east side of deck)*

SOURCE	DOF	SSE	MS	F	R^2
Difference	4	1.11506	0.27876	6.11	0.777
Intercept + $LogD_{mig}$ + Str + $Logk_w$ + $Logp$ (Ω)	7	0.31922	0.04560		
Intercept + $LogD_{mig}$ + Str + $Log\,k_w$ (ω)	11	1.43428			

Multiple Linear Regression Using 'Assessment Methods' (West Side of Deck)

To determine the significance of a model Ω, the same procedure as in the previous section is followed using ANOVA tables. The first step of the analysis is to determine the first variable to be included in the model. The ϕ_{corr} variable was selected as it performed the best in the regression of the individual variables. The following ANOVA table results:

Table I-20: *One variable (west side of deck)*

SOURCE	DOF	SSE	MS	F	R^2
Difference	1	1.2230	1.2230	44.73	0.390
Intercept + ϕ_{corr} (Ω)	70	1.9142	0.0273		
Intercept (ω)	71	3.1372			

Each of the remaining variables was tested in turn (Table I-21), and the results indicate that all four variables can be added significantly to ϕ_{corr} model, with variable %Cl performing best.

Table I-21: *Two variables (west side of deck)*

VARIABLE	R^2	ΔR^2	F-VALUE	SSE	DOF
Delam	38.1%	+0.8%	22.81	1.88853	69
Cover	47.0%	+8.0%	30.20	1.62439	68
%Cl	49.0%	+10.0%	6.26	0.22639	13
$LogD_a$	45.0%	+6.0%	4.50	0.24365	11

Each of the remaining variables was tested in turn (Table I-22), and the results indicate that all three variables can be added significantly to ϕ_{corr} and $\%Cl$, with variable $LogD_a$ performing best.

Table I-22: *Three variables (west side of deck)*

VARIABLE	R^2	ΔR^2	F-VALUE	SSE	DOF
Delam	49.1%	+0.1%	3.85	0.22631	12
Cover	57.6%	+8.6%	5.43	0.18836	12
LogD_a	64.8%	+15.8%	6.15	0.15579	10

The next step consists of determining which variables can be added to ϕ_{corr}, $\%Cl$ and $LogD_a$ significantly. Each of the remaining variables was tested in turn (Table I-23), and the results indicate that both variables can be added, with the variable *Cover* performing best.

Table I-23: *Four variables (west side of deck)*

VARIABLE	R^2	ΔR^2	F-VALUE	SSE	DOF
Delam	66.6%	+1.8%	4.48	0.14808	9
Cover	82.0%	+17.2%	10.23	0.079851	9

The last step consists of determining if the last variable, *Delam*, can be added to ϕ_{corr}, $\%Cl$, $LogD_a$ and *Cover* significantly. The results indicate that it is indeed significant as the F-ratio is greater than the critical value (Table I-24).

Table I-24: *Proposed 'Assessment Methods' model (west side of deck)*

SOURCE	DOF	SSE	MS	F	R^2
Difference	5	0.364493	0.072899	7.42	0.823
Intercept + ϕ_{corr} +$LogD_a$ + $\%Cl$ + *Cover* + *Delam* (Ω)	8	0.078579	0.009822		
Intercept + ϕ_{corr} +$LogD_a$ + $\%Cl$ + *Cover* (ω)	13	0.443072			

Multiple Linear Regression Using 'Prediction Methods' (West Side of Deck)

The first step of the analysis is to determine the first variable to be included in the model. The *Str* variable was selected as it performed the best in the regression of the individual variables. The results indicate that the *Str* variable is indeed significant in predicting *LogCR* (Table I-25).

Table I-25: *One variable (west side of deck)*

SOURCE	DOF	SSE	MS	F	R²
Difference	1	0.17526	0.17526	9.29	0.367
Intercept + *Str* (Ω)	16	0.30187	0.01887		
Intercept (ω)	17	0.47713			

The next step is to determine which variable can be added to *Str* significantly. Each variable is tested in turn (Table I-26), and the results indicate that all three can be added, with the variable *Logρ* performing best.

Table I-26: *Two variables (west side of deck)*

VARIABLE	R²	ΔR²	F-VALUE	SSE	DOF
LogD_{mig}	38.1%	+1.4%	4.61	0.29549	15
Logρ	42.0%	+5.3%	5.06	0.19667	14
Logk_w	41.6%	+4.9%	4.27	0.23445	12

Each of the remaining variables was tested in turn (Table I-27), and the results indicate that the variable *LogD_{mig}* can be added significantly to the model.

Table I-27: *Three variables (west side of deck)*

VARIABLE	R²	ΔR²	F-VALUE	SSE	DOF
LogD_{mig}	45.6%	+3.6%	3.63	0.18447	13
Logk_w	46.5%	+4.5%	2.90	0.13976	10

The last step consists of determining if the last variable, $Logk_w$, can be added to Str, $Log\rho$ and $LogD_{mig}$ significantly. The results indicate that it is not significant (Table I-28).). Hence, the proposed model is without the addition of $Logk_w$ (Table I-29).

Table I-28: *Four variables (west side of deck)*

SOURCE	DOF	SSE	MS	F	R²
Difference	4	0.13220	0.03305	2.30	0.506
Intercept + Str + $Log\rho$ + $LogD_{mig}$ + $Logk_w$ (Ω)	9	0.12921	0.01436		
Intercept + Str + $Log\rho$ + $LogD_{mig}$ (ω)	13	0.26141			

Table I-29: *Proposed 'Prediction Methods' model (west side of deck)*

SOURCE	DOF	SSE	MS	F	R²
Difference	3	0.15446	0.05149	3.63	0.456
Intercept + Str + $Log\rho$ + $LogD_{mig}$ (Ω)	13	0.18447	0.01419		
Intercept + Str + $Log\rho$ (ω)	16	0.33893			